Lappeenrannan teknillinen yliopisto
Lappeenranta University of Technology

Mikko Kuisma

MINIMIZING CONDUCTED RF-EMISSIONS IN SWITCH MODE POWER SUPPLIES USING SPREAD-SPECTRUM TECHNIQUES

Thesis for the degree of Doctor of Science (Technology) to be presented with due permission for public examination and criticism in the auditorium 1382 at Lappeenranta University of Technology, Lappeenranta, Finland on the 12th of March, 2004, at noon.

Acta Universitatis
Lappeenrantaensis
177

ISBN 951-764-874-X
ISBN 951-764-875-8 (PDF)
ISSN 1456-4491

Lappeenrannan teknillinen yliopisto
Digipaino 2004

Abstract

Mikko Kuisma

Minimizing Conducted RF-emissions in Switch Mode Power Supplies Using Spread-Spectrum Techniques

Lappeenranta 2004

190 p.

Acta Universitatis Lappeenrantaensis 177

Diss. Lappeenranta University of Technology

ISBN 951-764-874-X, ISBN 951-764-875-8 (PDF), ISSN 1456-4491

Switching power supplies are usually implemented with a control circuitry that uses constant clock frequency turning the power semiconductor switches on and off. A drawback of this customary operating principle is that the switching frequency and harmonic frequencies are present in both the conducted and radiated EMI spectrum of the power converter. Various variable-frequency techniques have been introduced during the last decade to overcome the EMC problem.

The main objective of this study was to compare the EMI and steady-state performance of a switch mode power supply with different spread-spectrum/variable-frequency methods. Another goal was to find out suitable tools for the variable-frequency EMI analysis. This thesis can be divided into three main parts: Firstly, some aspects of spectral estimation and measurement are presented. Secondly, selected spread spectrum generation techniques are presented with simulations and background information. Finally, simulations and prototype measurements from the EMC and the steady-state performance are carried out in the last part of this work.

Combination of the autocorrelation function, the Welch spectrum estimate and the spectrogram were used as a substitute for ordinary Fourier methods in the EMC analysis. It was also shown that the switching function can be used in preliminary EMC analysis of a SMPS and the spectrum and autocorrelation sequence of a switching function correlates with the final EMI spectrum.

This work is based on numerous simulations and measurements made with the prototype. All these simulations and measurements are made with the boost DC/DC converter. Four different variable-frequency modulation techniques in six different configurations were analyzed and the EMI performance was compared to the constant frequency operation. Output voltage and input current waveforms were also analyzed in time domain to see the effect of the spread spectrum operation on these quantities.

According to the results presented in this work, spread spectrum modulation can be utilized in power converter for EMI mitigation. The results from steady-state voltage measurements show, that the variable-frequency operation of the SMPS has effect on the voltage ripple, but the ripple measured from the prototype is still acceptable in some applications. Both current and voltage ripple can be controlled with proper main circuit and controller design.

Keywords: Variable-frequency, conducted EMI, switching frequency modulation, power supply

UDC 621.391.823 : 621.314.69 : 621.311.62

Acknowledgements

This work is the conclusion of four years of research at the Laboratory of Applied Electronics, Lappeenranta University of Technology. Many people have helped me over the past years both in research work and in teaching, and it is my great pleasure to take this opportunity to express my gratitude to them all.

I would first like to thank my family and friends for their warm support and patience during the research and writing of this thesis and throughout my career path. This includes all my friends, school and work colleagues and managers. Especially I wish to thank my friend and supervisor, professor Pertti Silventoinen for his help and companionship during these years we have spent at Lappeenranta. I would also like to thank professor Juha Pyrhönen and professor Teuvo Suntio for giving me the opportunity to take part in the project from which this work has been originated. Compliments also to the project team participants at Salcomp, Fincitec/National Semiconductor and the University of Oulu.

I wish to express my sincere thanks to the pre-examiners of this work, professor Pekka Eskelinen from the Institute of Digital Communication, Helsinki University of Technology and professor Jorma Kyyrä from the Power Electronics Laboratory, Helsinki University of Technology. Both pre-examiners spent many hours with my thesis and gave valuable comments, which improved my work in many ways.

I would also like to acknowledge my other colleagues, Tony Vesterinen, Tero Järveläinen, Janne Heinola and Mohammad Ahmed, for the help that they rendered to me during various stages of my study. Special thanks to Kimmo Tolsa for his valuable theoretical and practical advises during the last ten years.

The National Technology Agency (TEKES) and the Graduate School of Electric Engineering have supported this research financially, which is gratefully acknowledged. In addition, the grants received from IVO-foundation, SKR– Etelä-Karjalan rahasto and Elektroniikkainsinöörien säätiö are also gratefully acknowledged.

My parents, Kaija ja Pentti, have supported and encouraged me during the years, which I highly appreciate. Unfortunately, my father who led me to the world of electronics cannot share this joy with us, but his memory will live with me.

Special appreciation to Marjut for her care and understanding – "…no more lonely nights…".

Lappeenranta, February 2004 *Mikko Kuisma*

Contents

Abstract
Acknowledgements
Contents
Symbols and Abbreviations
1 INTRODUCTION....15
1.1 Power Supplies and EMI....15
1.2 Motivation and Background....17
1.2.1 Authors Publications in the Scope of This Work....18
1.3 Spread Spectrum Techniques in EMI Mitigation....19
1.3.1 Spread Spectrum in the Power Supply....20
1.4 Literature survey....23
1.5 Some Aspects on Spectrum Estimation and Measurement....24
1.6 EMI-Standards....25
1.7 Outline of the Thesis....28
1.8 Key results....29
2 SWITCHING POWER CONVERTERS....31
2.1 General Background....31
2.2 Distributed Power Systems....32
2.3 Control of the Power Converter....34
2.4 Case study: The Boost (step-up) DC/DC Converter....37
2.4.1 The Prototype Converter and Simulation Model....41
2.5 Practical Aspects and Limitations in Variable Frequency Power Converters....43
2.6 Summary....45
3 SPECTRUM ESTIMATION, SIGNAL ANALYSIS AND EMI-MEASUREMENTS....46
3.1 Fourier Analysis of Periodic and Aperiodic Signals....47
3.1.1 Fourier Spectrum of a Periodic Signal....47
3.1.2 Fourier Spectrum of an Aperiodic Signal....49
3.2 Random Signals and Random Process Characterization....51
3.3 Power Spectrum Estimation....54
3.3.1 Welch Power Spectrum Estimate....60
3.4 Spectrogram in EMI-Analysis....63
3.5 Few Aspects in EMC Measurements....68
3.5.1 Detectors in EMI-Measurements....70
3.5.2 Sweep of the Test Instrument....72
3.5.3 Stabilizing Network....76
3.6 The Relation between Calculated and Measured Spectrum....76

3.7 Summary 78
4 SELECTED SPREAD SPECTRUM MODULATION METHODS WITH SIMULATION 79
4.1 Simulations with the Constant-Frequency Reference Converter 83
4.2 Angle Modulation 84
4.2.1 Theoretical Background of Angle Modulation 84
4.2.2 The Spectrum of the Angle Modulated Signal 87
4.2.3 Simulation with Selected FM-Signals 89
4.2.4 CASE 1: Single-Tone Frequency Modulation 89
4.2.5 CASE 2: Modulation with Sinusoidal Wave + Added Random Noise 91
4.2.6 CASE 3: Modulation with Triangular Wave + Added Random Noise 92
4.3 Frequency-Hopping 93
4.3.1 CASE 4: Simulations with a Frequency-Hopping Switching Function 96
4.4 Chaotic Peak Current Mode Controlled Boost-Converter 98
4.4.1 Chaos in a Power Converter 100
4.4.2 Case 5: Chaotic Peak Current Control 103
4.5 Sigma-Delta Modulation 105
4.5.1 Basic Operation of the ΣΔ-Converter 106
4.5.2 A Sigma-Delta Modulator in a Power Converter 109
4.5.3 Case 6: Chaotic Sigma-Delta Controller 110
4.6 Summary of Spectral Results 111
4.7 Summary 112
5 THE TEST SETUP AND TEST RESULTS 113
5.1 The Test Setup 113
5.2 Analysis of the Converter Steady-state Performance 119
5.2.1 Constant-frequency Reference Converter 119
5.2.2 Voltage Ripple in Different VF-techniques 121
5.2.3 Current Waveforms in VF-converter 123
5.2.4 Summary of Voltage and Current waveforms 128
5.3 EMC Simulations and Measurements 129
5.3.1 Constant-frequency Reference Converter 131
5.3.2 Simulated Input Current Spectrograms 132
5.3.3 Simulated and Measured Input Current Spectra 133
5.3.4 Measured Spectra Compared to the Reference 136
5.3.5 Summarized EMI Test Results 140
5.4 Discussion 143
5.4.1 Output Voltage and Input Current Ripple 143

5.4.2 EMI-Measurements in CISPR Conducted RF-Emission Band 150 kHz to 30 MHz 146
5.4.3 Implementation Complexity in Different Cases 147
5.4.4 How Disturbing is the Spread Spectrum Noise, [P4] 148
5.5 Summary 149
6 CONCLUSIONS AND FUTURE WORK 151
6.1. Usability of the Results 152
6.2. Suggestions for Future Research 153
REFERENCES 155

APPENDIX A – SIMULATION MODELS AND MATLAB™-SCRIPTS 167
APPENDIX B – MEASUREMENTS FROM THE INPUT FILTER AND LOAD RESISTOR 173
APPENDIX C – COMPONENT LIST, SCHEMATIC DIAGRAM AND ASSEMBLY DRAWING OF THE PROTOTYPE 175
APPENDIX D – MEASURED BACKGROUND NOISE 182
APPENDIX E – MEASURED EMI-SPECTRUM 9 KHZ – 30 MHZ 183
APPENDIX F – EMI MEASUREMENT UNCERTAINTY 189

Symbols

A	Amplitude
A_c	Amplitude of the carrier wave
A_m	Amplitude of the modulating wave
b	Number of bits in AD/DA converters
c_k	Arbitrary complex constant in Fourier series
D	Average duty cycle
D	Deviation ratio, diode in schematic diagram
$d(t)$	Duty cycle
D_{xx}	Power spectral density function
$E[\ ]$	Expectation value
E_x	Energy of a signal
$e(n)$	Quantization noise
$F_X(x)$	Probability distribution function
$f(x)$	Function
$f_x(x)$	Probability density function
f, F	Frequency
f_c	Frequency of the carrier wave
f_i	Instantaneous frequency
f_m	Frequency of the modulating wave
f_s	Switching frequency
f_{SA}	Sampling frequency
Δf	Maximum frequency deviation
Δf_D	Spectral resolution in DFT
$\Delta f_{D,H}$	Efficient spectral resolution with Hamming window
$G_c(s)$	Dynamic compensator in a feedback controller
G_i	Gain of a current loop in a feedback controller
G_n	Gain
G_v	Gain of a voltage loop in a feedback controller
G_{vf}	Gain of a voltage feedback loop in a feedback controller
h_i	Periodic function
I, i	Current
i_{in}	Input current
I_L, i_L, $i_L(t)$	Inductor current
Δi_L	Inductor current ripple
I_{ref}	Current reference of the converter controller
K	Parameter in definition of voltage conversion ratio
k	Index
k_f	Frequency deviation constant
L	Inductance
L	Number of sampled data segments
M	Discrete sample sequence
$m(t)$	Modulating signal
N	Sample/data segment length
n	Time (discrete), index
P	Average power
$P(\ )$	Probability
P_x	Harmonic average power
P_{xx}	Power spectrum estimate
P_{xx}^W	Welch power spectrum estimate
$P_{S,loss}$	Average power dissipated in the switching device

$q(t)$	Switching function (power switch drive signal)
r_{xx}	Autocorrelation function
R	Resistor
R_L	Parasitic resistor of the inductance
R_{DSON}	Conduction loss of a power switch
S	Apparent power, switch in schematic diagram
S_{xx}	Energy density spectrum
$s(t)$	Angle modulated signal
$STFT(t_i,f)$	Short-time Fourier transform
T_D	Dwell time
T_s, T_{sn}	Switching time (instantaneous)
T_{sa}	Sampling time
T_{set}	Settling time
T_{off}	Switch off-time
t, t_n	Time
Δt	Time resolution
U	Normalization factor of the window function
U_{CM}	Common mode noise voltage
U_D	Diode forward voltage drop
U_{DM}	Differential mode noise voltage
U_{in} , u_{in}	Input voltage
U_{out}	Output voltage
U_{ref}	Reference voltage
u, u_n, $u(y)$	Uncertainty
u_L, $u_L(t)$	Inductor voltage
u_C	Capacitor voltage
u_c	Control voltage in a pulse width modulator
u_{saw}	Saw-tooth wave in a pulse width modulator
u_{tot}	Combined (standard) uncertainty
Δu_{out}	Output voltage ripple
$W_{S(on)}$, $W_{S(off)}$	Turn-on and turn-off energy required in power switch drive
w	Bandwidth of the hop channel in frequency-hopping
$w(k)$	Window function
$X(F)$	Continuous-time Fourier transform
$X(\omega)$	Discrete-time Fourier transform
X, $X(t)$, $X(n)$	Random process
x_{eq}	Equilibrium point
x, $x(t)$	Unknown variable
$x(n)$	Discrete unknown variable
$y(n)$	Quantized signal

β	Modulation index
β_n	Modulation index of a n:th harmonic
$\phi(t)$	Angular function of a modulating signal in angle modulation
$\phi_t(x_0)$	Trajectory
$\theta(t)$	Angle argument in angle modulation
δ	S kin depth
λ, λ_i	Outcome from sample space
μ, μ_x	Expectation value, mean
μ	Permeability
Ω	Sample space
σ	Conductivity
τ	Time (delay)

ω	Angular frequency
ω_c	Angular frequency of the carrier wave
ω_i	instantaneous angular frequency
ω_0	Fundamental angular frequency
$\Delta\omega$	Maximum (angular) frequency deviation
$\Re^n$	Vector field

Acronyms

AC	Alternating current
ADC	Analog to digital converter
AJ	Anti-jam
AN	Artificial network
AR	Autoregressive
ASIC	Application specific integrated circuit
BW	Bandwitdh
CENELEC	European Committee for Electrotechnical Standardization
CISPR	*Comité International Spécial des Perturbations Radioélectriques* (The International Special Committee on Radio Interference)
CM	Common mode
CCM	Continuous conduction mode
DAC	Digital to analog converter
DC	Direct current
DCM	Discontinuous conduction mode
DFT	Discrete Fourier transform
DTFS	discrete-time Fourier series
DM	Differential mode
DS	Direct sequence
DPS	Distributed power system
DTC	Direct torque control
EMC	Electromagnetic compatibility
EMI	Electromagnetic interference
ESD	Electrostatic discharge
ETSI	European Telecommunication Standards Institute
EUT	Equipment under test
FCC	Federal Communications Commission
FFT	Fast Fourier transform
FM	Frequency modulation
FH	Frequency-hopping
IC	Integrated circuit
IEC	International Electrotechnical Commission
IF	Intermediate frequency
ITE	Information technology equipment
LISN	Line impedance stabilization network
LPI	Low probability of intercept
PAM	Pulse amplitude modulation
PCB	Printed circuit board
PF	Power factor
PFC	Power factor correction
PI	Proportional-integral (in controller)
PM	Phase modulation
PN	Pseudo-noise
PPU	Power processing unit

PR	Pseudo-random
PWM	Pulse width modulation
PSD	Power spectral density
QP	Quasi-peak (detector)
RBW	Resolution bandwidth
RF	Radio frequency
$\Sigma\Delta$	Sigma-delta
SA	Spectrum analyzer
SMPS	Switch mode power supply
SS	Spread spectrum
SSM	Spread spectrum modulation
SSS	Strict-sense stationary
STFT	Short-time Fourier transform
SQNR	Signal to quantization noise ratio
EU	European Union
EUT	Equipment under test
VLSI	Very large scale integration
VF	Variable frequency
WSS	Wide-sense stationary

1 Introduction

1.1 Power Supplies and EMI

Different kinds of power supplies are used everywhere in normal daily routines both in the home, office work or in an industrial environment. This is due to the progress in electronic components and equipment development that has been achieved in the last few decades. Electronic and electric apparatus are everywhere, and all these devices need electrical power to work. For example, in a normal office room there are numerous power converters in different electronic equipments: battery chargers, computer power supplies, display units, lighting, printers, consumer electronic equipment are just a few to mention. Even in one personal computer there are several power supplies inside the cover. Most of them are switching power converters. The reason behind the popularity of switching power converters is due to the efficiency, size, capability to operate at different current and voltage levels, control features and price compared to the linear power supply.

Conducted Electromagnetic Interference (conducted EMI) from switch mode power supplies (SMPS) has become a major problem due to the dramatically increased use of these devices in both industrial and consumer applications. When these converters are connected to a distribution network, the distribution network operates as an efficient propagation path to the EMI generated by the converter. The power distribution network and noise propagation path can be the common electrical distribution network or local power supply arrangement inside the device or system. High frequency electromagnetic noise can also propagate via air when some part of the circuit acts as an antenna. This *Radiated Electromagnetic Interference* (radiated EMI) has to be taken into consideration when frequencies used in the converter are high or the electrical length of some part, i.e. wire, is long compared to the wavelength of the used maximum frequency. Usually the electrical length is considered long when the maximum dimension of the electrical part exceeds 1/16 – 1/10 of the wavelength, [Paul 1992].

Man-made electromagnetic interference was spotted in the early 1930s, when unintentional electrical interference in the radio reception was recognized. The first steps in the engineering discipline of the electromagnetic compatibility (EMC) were made in 1933, when the *Comité International Spécial des Perturbations Radioélectriques* (CISPR) was founded, [Redl 1997].

Nowadays, products planned to be sold on the open market must first fulfill general requirements set by local and international standards and regulations. The product must fulfill EMC requirements, which means the ability of the electrical equipment to function in its electromagnetic environment satisfactorily, without impermissibly influencing this environment to which other equipments also belong. EMC requirements of the equipment can be divided in two important parts:

- The equipment has some limits on the electromagnetic noise generated (*EMISSIONS*)
- The equipment must withstand some level of electromagnetic noise generated by the equipment itself and also other equipments (*SUSCEPTIBILITY - IMMUNITY*)

Other definitions of basic terms used in EMC engineering according to [Ott 1988], [Paul 1992], [Redl 1996], [Perez 1995] are summarized as:

- *Electromagnetic disturbance*: any electromagnetic phenomenon, which can degrade the performance of the system under investigation.
- *Electromagnetic interference* (EMI): the degradation in performance of a system caused by electromagnetic disturbance.
- *Radio frequency interface* (RFI): the degradation in performance of a system caused by electromagnetic disturbance having components in the radio frequency range.

Switching power supplies are usually implemented with a control circuitry that uses some constant clock frequency. For example, one common control principle utilizes pulse width modulation (PWM). This pulse width modulator operates at a constant clock frequency turning the power electronic switches of the converter on and off. A drawback of this common operation principle is that this switching frequency and harmonic frequencies are present in both the conducted and radiated EMI spectrum of the power converter. SMPS that have a periodic switching pattern, have an EMI spectrum that contains a switching frequency and its harmonic frequencies with significant amplitude at least up to the 20^{th} harmonic [P1]. These periodic noise components may be very harmful because they are repeating continuously - even if they have low amplitude and energy content.

There are two main areas of switching noise generation in a switch mode power supply. The first area is associated with the switching frequency of the power supply. Obviously, the power supply switching frequency is an integral part of its operation, and there are limited possibilities in noise suppression at this frequency and its harmonics. The second aspect of SMPS noise is associated with the fast switching edges of voltages and currents. These edges will generate high-frequency interference that is dependent on the transition ratio of the signal, [Paul 1992].

The switching noise is both common mode (CM) and differential mode (DM). Common mode noise is injected into the earth of the power supply via the parasitic capacitance between the switching devices, circuit components and wires. The CM noise can be measured between the earth ground and input connectors of the converter. The CM voltage or current cannot be measured between the input connectors of the converter because it is in-phase. Differential-mode noise is present between the input connectors of the converter in the same way as the supplying voltage and current, see Figure 1.1. Usually, a filter is placed on the input line of the power supply to deal with both the common- and differential mode noise.

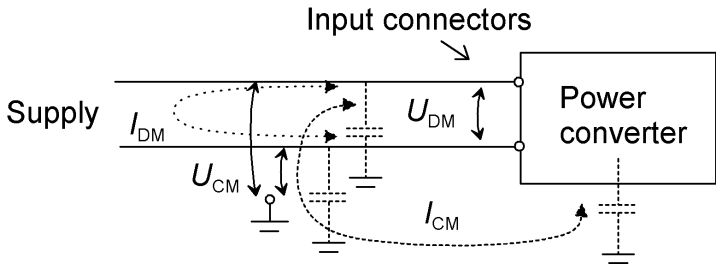

Figure 1.1. Differential-mode noise voltage U_{DM} can be measured between normal power input connectors. Normal supply leads also provide current loop for DM current I_{DM}. Common mode current I_{CM} propagates via stray capacitances (here dotted capacitors) and CM voltage U_{CM} can be measured between input connector(s) and earth ground.

Various EMI reduction schemes have been proposed over the last decades, [Bolden 2001]. These techniques include filtering, random modulation, frequency modulation and soft switching. The principal method in power converter noise reduction has been so far filtering, which also has its limitations: size, weight, design complexity, efficiency, sometimes cost, etc., [Caponet 2002]. Modern, modulation based, EMI reduction techniques have been under intensive research to overcome the problems faced in filter-solutions. With the help of these *spread spectrum* (SS) modulation techniques emissions can be reduced, [Lin 1994], [Stankovic 1993-1], [Bolden 2001], [Stone 1995-1], [Stone 1995-2], [Zigliotto 1998], [Mihalic 1999-1] and [Chan 2002].

1.2 Motivation and Background

EMI-control in switch mode power supplies was one of the project objectives when the co-operation between Lappeenranta University of Technology, University of Oulu, Fincitec (later National Semiconductor), Salcomp and The National Technology Agency of Finland, Tekes, begun in 1999. The work presented in this dissertation originates from this project “Optimizing of Design Methods for High-Volume Power Supplies – Part I”, which took place from January 1, 1999 to September 30, 2000, [Tekes 2002, pages 181-183].

The area of interest in part I of the project was mainly addressed on AC/DC converters used in charger applications such as cellular phones, notebooks etc. The market of these kinds of power supplies is growing continuously, and the competition is heavy. To survive in the market, the manufacturer must be able to reduce the cost of their products. This means that the existence of every single component must be well reasoned, thus emphasizing the importance of the design phase. The general goal of this project has been to formulate a proper design philosophy that automatically optimizes the product, with a minimal number of components and sufficient product quality.

The theoretical and experimental work was carried out at Lappeenranta University of Technology and at the University of Oulu. The main topics covered in Lappeenranta were general design methodology and EMI, while research in Oulu concentrated on system dynamics and EMI. It was noticed, that the main problem areas were EMI and controller design. These problems are typically solved by trial-and-error methods, thus increasing the development time and generating an uncertainty in the timetable of the product design flow.

The EMI design consideration started with a study of the usability of spread spectrum techniques to reduce conducted EMI. It was also noticed that the variable frequency (VF) operation had not been successfully modeled earlier. This started the development of general analysis methods, presented partly in this dissertation, to evaluate different variable frequency methods in power supply applications.

As a result of this project, two topologies were selected for further studies in later projects coordinated by professor Teuvo Suntio, [Tekes 2002]. These were a single-stage AC/DC converter with integrated power factor correction (PFC) and a peak-current controlled variable frequency AC/DC flyback converter. It was also concluded that further studies on switching frequency modulation needed to be carried out. The work presented in this dissertation is a general study on variable frequency techniques in power supply applications. The power supply topology selected for this work is a derivation of generally used topology used in PFC-converters, thus linking this work also to the application area of the original project goals.

1.2.1 Authors Publications in the Scope of This Work

The author has published five publications in the field of spread spectrum techniques and control of power converter during this research work. These publications are referred to as P1, P2, P3, P4 and P5 in the text. The text in this dissertation is partly based on these papers. A brief summary of these papers is as follows:

[P1] Kuisma, M., Järveläinen, T., Silventoinen, P, Vesterinen, T. 2000. *Effects of Nonperiodic and Chaotic Switching on the Conducted EMI Emissions of Switch Mode Power Supplies.* Proceedings of the 2000 IEEE Nordic Workshop on Power and Industrial Electronics. Aalborg, Denmark. 13-16 August 2000. pp. 185-190.

This paper presents two controller based spread spectrum methods for EMI harmonic reduction. The first method is based on hysteresis control and the other one utilizes chaotic peak current control in a boost converter. The most important aspects in EMI measurements with experimental results are also presented.

[P2] Kuisma, M., Ahmed, M., Silventoinen, P. 2003. *Comparison of Conducted RF-Emissions between PID and Sliding Mode Controlled DC-DC Converter*. 10th European Conference on Power Electronics and Applications, EPE 2003. September 2 - 4 2003. Toulouse, France, on CD-ROM.

This paper proposes a sliding mode control for EMI mitigation of a SPMS. A comparison between EMI-noise effects at a fixed frequency, PID-controlled PWM and sliding mode–controlled converter has been done. Both simulation and experimental results are presented.

[P3] Kuisma, M. 2003-2. *Variable Frequency Switching in Power Supply EMI-control: An Overview*. IEEE Aerospace and Electronic Systems Magazine. Vol. 18, No 12. pp. 18 – 22.

This paper summarizes different types of spread spectrum techniques in switch mode power supply applications. Modulation based methods, randomized system clock and controller based methods are presented with experimental results.

[P4] Silventoinen, P., Kuisma, M., Pyrhönen, J., Huppunen, J. 2002. *Effects of the Modulation Technique on the Conducted RF-Emissions of an Adjustable Speed Motor Drive*. 15th International Conference on Electrical Machines, ICEM2002. 25-28 August 2002. Bruges, Belgium.

In this paper a comparison between fixed frequency PWM, hysteresis controlled converter and frequency modulated switching is presented. The test setup used in this dissertation was presented in this paper. Applicability of spread spectrum techniques is discussed from a motor drive point of view. Also a general discussion on the disturbing effect of spread spectrum noise was presented.

[P5] Ahmed, M., Kuisma, M., Tolsa, K., Silventoinen, P. 2003. *Implementing sliding mode control for buck converter*. IEEE 34th Annual Conference on Power Electronics Specialist, PESC '03. Acapulco, Mexico. 15-19 June 2003. pp. 634-637, Vol. 2.

In this paper sliding mode control, a nonlinear control method for SMPS was presented. Theoretical analysis and an experimental study with a buck converter prototype is presented.

Publications [P2-P3] were mainly contributed by the author of this thesis. In [P1] and [P4-P5], the author's contribution is shared with the other authors.

1.3 Spread Spectrum Techniques in EMI Mitigation

In digital communication, spread-spectrum signals are distributed over a wide range of frequencies for the transmission. These signals are so inconspicuous that they almost seem to be transparent to other receivers that are not part of the signal chain. This transparency gained the interest at military applications of SS-communication in 1960’s, and SS-communication was widely adapted in service. The main properties of SS-communication in military use are the harder signal tracking, information security and strength against jamming, [Kosola 2000], [MCWP 3-40.5 2001]. Just as SS-signals are unlikely to be intercepted by a military opponent, so are they unlikely to interfere with other signals intended for industrial and consumer users.

The aim of the use of spread spectrum techniques in power electronics is to reduce both the measurable and effective noise content of the switch mode power supply. The question “Is the spread spectrum technique just an another trick to fool the measurement equipment and fulfill the requirements of the standardization?” often rises when the topic of the work is discussed about. The answer to this question is two-folded: *No*, because the power of the disturbing signal is actually spread over the wider frequency range. Therefore, the *level of the power at different frequency components is lower than in the case of a single frequency component because the total transferable power is constant*, Figure 1.2. In addition, wideband disturbance does not act like a periodic excitation to a possible victim system and the possibility of electrical or mechanical resonance is lower, [P4], [Bech 2000-1]. *Yes*, because the EMI-spectrum of a continuously changing signal is very hard to measure, and therefore the test measurements may give far too optimistic results with some specific modulation methods, or with different equipments, different operators, different days, etc. Also, the spectrum is not so unambiguous as it may first sound.

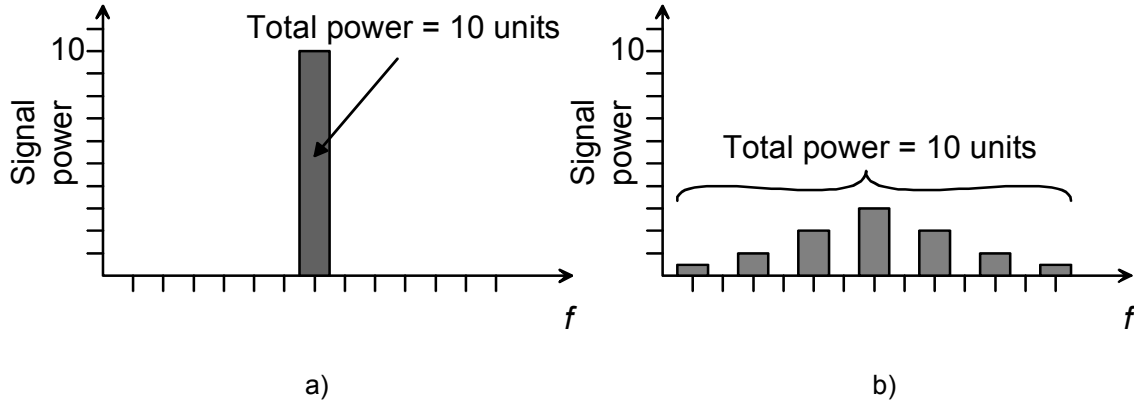

Figure 1.2. Spectral distribution of the signal power in single frequency (a) and in a spread spectrum signal (b). The total signal power is the same in both cases, though the peak level is reduced in (b).

In this work, the term *spread spectrum* has been used in a wide sense. Strictly speaking, in modern communication an SS signal has to meet the following two technicalities:

- The signal bandwidth must be much wider than the information bandwidth
- Some code or pattern, other than the data to be transmitted, determines the actual on-the-air transmit bandwidth

In this work SS means, that the signal power is transmitted at the power converter in the wide-band mode compared to fixed frequency operation at several frequencies that are constantly changing. Frequency modulation (FM), for example, is not considered as an SS technique in modern communication. In power supply applications, however, FM can be utilized in system clock modulation. The signal power is then transmitted at a wider bandwidth that is controlled with the modulating pattern, thus fulfilling formal requirements for an SS-system - at least from the power converter point of view.

1.3.1 Spread Spectrum in the Power Supply

Figure 1.3 shows a system diagram of traditional implementation of an SMPS control system with a pulse width modulator. The switching function $q(t)$ denotes the time varying waveform, which drives the power switch of the converter. Usually, like in Figure 1.3, the switching function is generated with the aid of the feedback from voltages and currents of the power supply. Normally there is also a system clock, which operates at constant frequency. The frequency of the system clock can be seen in the switching function and also the EMI spectrum of the converter. The switching function $q(t)$ is defined as follows:

$$q(t) = \begin{cases} 0, \text{ for the switch off - state} \\ 1, \text{ for the switch on - state} \end{cases} \tag{1.1}$$

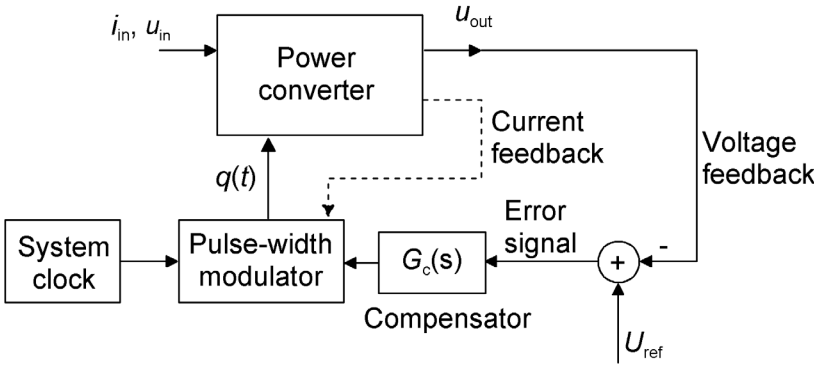

Figure 1.3. Simplified block diagram of a typical switching converter feedback control. The pulse-width modulator turns the power switch of the circuit on and off and makes the required actions to keep the output voltage at a set level U_{ref}. The control section may have a dynamic compensation network, here $G_c(s)$, and multiple feedback loops to affect on the system dynamics.

The power supply control presented in Figure 1.3 has a feedback from the output voltage u_{out} and from some current of the converter, for example the power switch current. The controller has typically dynamic compensation circuits to improve the dynamic behavior of the converter. Of course, a more conventional voltage feedback controlled converter would be constructed by removing the inner current feedback loop. Some applications don't require feedback at all if the quality and regulation of the output voltage is not crucial. However, even in the simplest configuration there is still some kind of a system clock or oscillation frequency, which affects the EMI-spectrum of the converter.

One method for spreading the EMI-spectrum of the converter is to use random frequency in the system clock. In this approach, the instantaneous frequency of the switching function is continuously changing, Figure 1.4.

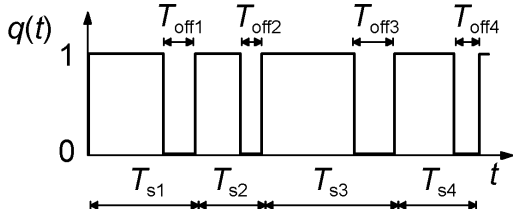

Figure 1.4. Example of a switching function waveform when a randomized, variable frequency clock generation is used in the pulse width modulator.

The duty cycle $d(t)$ of the converter is defined as the ratio of the on and off periods, $T_{s1} - T_{s4}$ and $T_{off1} - T_{off4}$ in Figure 1.4, respectively. Normally, the controller of the power converter affects on the duty cycle $d(t)$ to control the state variables (i.e. voltage, current, power) of the converter. If the duty cycle stays constant in an ideal converter, the output voltage or current will stay at a set value. This also applies to a practical converter and allows using normal control strategies in the converter feedback design with variable system clock frequency converters. A variable switching frequency converter can be implemented easily with normal power supply control circuits with an additional variable system clock.

Next, a general classification of different variable frequency techniques is presented, [P3].

System Clock Modulation

One possible method in the VF-clock generation is the modulation of the system clock. Frequency modulation is one of the most suitable methods for this scheme. FM has been used in communication for many decades and therefore the spectral effects of frequency-modulated signal are well known. Usually, in practical power supply applications, the modulated clock signal is fed to the clock input of a PWM-modulator circuit. This makes it possible to use commercial power supply control circuits with proven control settings with a modulated system clock.

Randomization of the System Clock

Another typical method for spreading the EMI-spectrum is to use random frequency in the system clock. Pseudo-random or pseudo-noise (PN) generators used in telecommunication applications can be utilized in a system clock generation. With this additional PN-clock signal, the variable frequency (VF) converter can be constructed from a traditional SMPS with traditional control design. Discrete digital components can be used for PN generation, but the VF clock generation circuit could be easily integrated into the same chip with the power supply converter control IC, or even with the whole power system chip.

Controller-based Methods

Third common VF-method utilizes nonlinearities of the control system. Peak current, hysteresis, sigma-delta and sliding mode control are the most commonly used nonlinear control techniques used in the field of power electronics. These nonlinear control techniques generate a non-harmonic switching spectrum when controller parameters are correctly chosen. The advantage of the nonlinear control design approach is the simplicity of the circuit: even basic switch mode power supply control circuits, made by many IC manufacturers, can be used with only a few additional passive components. The main drawback of this approach is that the designer has to study carefully the circuit performance at all load conditions and parameter variations to ensure the spread spectrum operation and system overall stability in all possible operation modes.

Usually these controller-based methods require the system to operate in *chaotic mode*. Chaos can be loosely defined as apparently random behavior in a nonlinear system. Since all switch mode power electronic circuits are nonlinear, chaotic behavior can be expected in power electronic circuits with some specific component and parameter values.

1.4 Literature survey

In the literature there are several SS-based methods proposed for EMI mitigation in power supplies. These include:

- quasi-random system clock generation
- random or quasi-random modulation of the system clock frequency
- frequency modulation (FM) of the system clock
- sigma-Delta ($\Sigma\Delta$)–modulation
- chaotic control
- hysteresis control

The operation of all methods mentioned above share a common principle of altering the periodic nature of the switching function $q(t)$. The spectrum of the switching function changes from the one peak frequency and harmonics (in ideal case line spectrum) to the wider band, noise like, spectrum, [Shrivastava 1997]. The periodic nature has been changed by altering directly the system clock frequency or by using some nonlinear function in the generation of the switching function $q(t)$. For example, chaotic peak current control and sigma-delta modulation utilize the constant system clock frequency. However, the switching function generated contains non-periodic signals caused by the nonlinear modulation method.

The growing interest in spread spectrum techniques in power supply applications started at the beginning of the nineties. Not very much literature can be found before 1990. Maybe the first reported random switching scheme is the patent "*Switching Regulator with Random Noise Generator*" by Clarke [Clarke 1969]. Then it took two decades before scientific papers from this area were published. Tanaka et al. [Tanaka 1989] was probably the first in the field of switching power supplies reporting random switching methods in EMI-reduction. Another early paper concerning random and programmed PWM in DC/DC power supplies was from Wang and Sanders, [Wang 1990].

Stankovic was among the first to study SS techniques in power supplies, he also made his doctoral studies on random pulse applications in power converters, [Stankovic 1993-2]. In another paper Stankovic et al. [Stankovic 1993-1] proposed a generation of randomized modulation schemes via Markov chains. Numerical solutions for the random signal analysis are also presented in this paper. Another paper from Stankovic et al. [Stankovic 1992] uses the Monte-Carlo method on the power spectrum estimation in random modulation.

Randomization of the computer clock signal for reduction of EMI was proposed by Stone et al. [Stone 1995-1]. Randomization of the system clock in the power converter control can also be used to reduce the EMI of the SMPS [Stankovic 1992]. In another paper from Stone et al. [Stone 1995-2], randomized carrier frequency modulation of a power supply is presented.

Tse et al. [Tse 2000] proposes random carrier frequency approach generating a randomized system clock for the controller. This paper has also a quite detailed theoretical analysis of the spectral characteristics of randomized signals in power supplies. Rigorous spectral analysis of the random pulse width modulation (RPWM)

and random pulse positioning modulation (RPPM) are presented in [Shrivastava 2000].

In the field of motor drive systems interest on spread spectrum modulation has also arisen. In the beginning of the nineties, the main interest of random modulation in drive systems was to minimize the torque ripple. Also acoustic noise and mechanical oscillations of the drive system can be reduced with SS modulation. Acoustic properties of the SS drive system has been reported in [Boys 1992] and [Habetler 1991]. Another paper from Boys et al. [Boys 1993] focuses on implementation of random PWM control in a three-phase inverter. Bech et al. [Bech 2000-1] presents measured results from inverter voltage, current and acoustic spectra, also giving a nice overview on the SS topic in the inverter systems. Zigliotto et al. [Zigliotto 1998] analyzed the EMI spectrum of a bi-frequency vector-controlled inverter drive. Some other modern control methods, such as direct torque control (DTC), [Takahashi 1985], generate also a non-periodic switching pattern, [Silventoinen 2001]. However, the main interest in literature considering the SS drive system applications was rarely on the EMC-properties of the system.

Bech in his dissertation [Bech 2000-2] covers quite comprehensively two variable frequency techniques, random pulse position and random carrier frequency techniques. The main goal in his work was on spectral estimation and acoustic noise reduction in a three-phase converter, although some part of his work deals with low-frequency EMI in close-loop DC/DC-converter applications.

Chaos is a well-known phenomenon in a peak current controlled boost converter and widely studied in the literature, [Poddar 1995], [Marrero 1996], [Deane 1996], [P1], for example. The chaotic mode of the converter operation is proposed for EMI reduction in many references. Peak current mode control is not the only chaotic converter mode. Sigma-Delta converter operation discussed later is also one form of chaotic operation. The author also proposed chaotic sliding mode control for EMI reduction in the paper [P2].

Wong et al. [Wong 2002] proposed different applications of chaos in SS SMPS. The paper presented a chaotic frequency modulator to generate a chaotic clock signal to the converter. They reported significant improvement on both conducted and radiated EMI properties of the converter proven with measurements. A 10 dB reduction in noise level was mentioned in the paper.

Paramesh and Jouanne [Paramesh 2001] reported the use of a Sigma-Delta controller in switch mode power supply EMI-reduction. Also Chan et al. [Chan 2002] proposed a Sigma-Delta scheme for harmonic reduction of the power converter.

More detailed literature survey is presented in Chapter 4 where different techniques are introduced.

1.5 Some Aspects on Spectrum Estimation and Measurement

The spectrum of the signal cannot be defined analytically if the signal is a purely random signal and thus unknown. The use of conventional FFT (Fast Fourier Transform), [Cooley 1965], is not acceptable in spectrum estimation because the

spectrum calculated directly from random signal sequence is a random signal itself, [Mihalic 1999-1], [Stankovic 1993-1], [Aumala 1998]. An estimation method that is more acceptable is the use of *power spectral density* (PSD, power spectral density function), which can be defined as a Fourier transform of the *autocorrelation function* of the random signal, [Kay 1988]. The PSD is a good *estimate* of the spectrum of a random or quasi-random signal.

Analytical methods in spectrum estimation are presented for example by Nagel [Nagel 1997]. These analytical methods meant for periodic standard signals (non-symmetric square wave, trapezoid wave etc) are unusable when dealing with constantly changing SS signals. A few applicable methods are proposed by Lev-Ari and Stankovic [Lev-Ari 2002] where the derivation of the average autocorrelation and the average power spectrum has been presented. Analytical methods are usually not suitable for analysis of arbitrary SS-signals. A Welch algorithm is proposed in this work as a universal spectrum estimation tool in the practical analysis of the power converter design. Mihalic et al. [Mihalic 1999-1] and [Bech 2000-2] also propose the Welch method in analysis of random modulation.

In several standards, the EMI measurements are suggested to be done with an EMI test receiver or a spectrum analyzer (SA), [CISPR 16-2 1999] [CISPR 22 2003], [FCC CFR 47-15. 2002]. The test instrument, *per se,* is designed for periodic signal measurements. These analyzers have several components that have finite settling times, so the reliable result of the input signal amplitude is not available without some delay, [Schaefer 1998], [Southwick 1989], [Silventoinen 2001], [P1]. This will cause variation in the reading with a variable-frequency test signal.

1.6 EMI-Standards

The primary purpose of the EMC design in product design flow is to ensure that an electronic system can reliably operate in its intended electromagnetic environment without either responding to electrical noise or generating unwanted electrical interference. Another main interest is to ensure, that the product will comply with national and international regulations. The leading idea in all EMC related standards and regulations is that the product must have a certain level of immunity and the emitted interference level of the product must be below some certain limit. There are a great number of different standards covering all aspects of EMC: conducted or radiated emissions, electrostatic discharge (ESD), electromagnetic field, electrical fast transients, line harmonics and mains dips are just a few to mention. In Europe, the requirement for emissions and for immunity derives from the EMC Directive, which delegates the actual limits to specific standards. The area of interest in the scope of this study is illustrated in Figure 1.5.

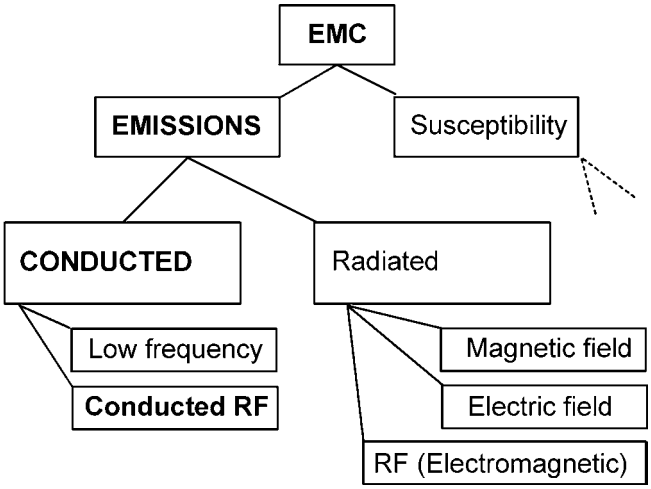

Figure 1.5. Simplified diagram of the EMC standards in the scope of this work. The area of interest is on conducted RF-emissions.

In European Union (EU), the European EMC Directive 89/336/EEC sets out the legal requirements on EMC for practically all electric and electronic equipment to be sold or used in the common market. There are baseline, generic standards as well as product specific standards. The general idea in European EMC standards is, that the basic standards describe the test procedures, and in some cases test instrumentation and calibration techniques, while more specific product or application standards usually define limits, severity levels, and compliance criteria, [Björklöf 1999]. This EMC standardization field utilizes a range of standards produced by various national and international standard bodies, for example IEC (International Electrotechnical Commission), CISPR (International Special Committee on Radio Interference) and ETSI (European Telecommunications Standards Institute).

In generic EMC standards, only two types of environments are defined: 1) residential, commercial, and light industrial and 2) industrial. In the EU, the generic standards include:

- EN 55081-1: Emissions standard for residential, commercial, and light industrial environments.
- EN 55081-2: Emissions standard for industrial environments.
- EN 55082-1: Immunity standard for residential, commercial, and light industrial environments.
- EN 55082-2: Immunity standard for industrial environments.

Product family standards and product specific standards override generic requirements if such standards exist. If there is no product family standard, one must follow the suitable generic or general standard, which in turn refers to different basic standards. Some of the product family standards are also referred to in other standards. The hierarchy of EU EMC standards is presented in Table 1-1.

Table 1-1. Hierarchy of standards in EMC directive, [Benitez 1997].

First priority	Use of product specific standards, if available
Second priority	Use of product family standards, if available
Third priority	Use of *generic standard*, if no product specific or product family standards are applicable.

Typical product family standards concerning also power supplies are:

- EN 55011: Industrial, scientific, and medical (ISM) radio-frequency equipment—Radio disturbance characteristics—Limits and methods of measurement;
- EN 55022: Information technology equipment—Radio disturbance characteristics—Limits and methods of measurement.

Examples of product specific standards in the field of this study are:

- ETSI EN 300 132-2: Environmental Engineering (EE); Power supply interface at the input to telecommunications equipment; Part 2: Operated by direct current (dc).
- EN 300 386: Electromagnetic compatibility and radio spectrum matters (ERM); Telecommunication network equipment; Electromagnetic compatibility (EMC) requirements.

For telecommunication applications, compliance are demonstrated via product standards developed by ETSI and the European Committee for Electrotechnical Standardization (CENELEC).

One standard that is closely related to the area of power supplies is EN 61000-3-2. This standard applies to all electrical and electronic equipment that is connected to the public low-voltage AC distribution network and that has an input current of up to 16A per phase. This standard considers low frequency line harmonic measurements.

Important standards for EMC measurements are CISPR 16-1 and CISPR 16-2. These standards describe the general test setup, measuring instruments and test procedures for EMC measurements. These standards are also utilized in this work.

Information technology equipment is classified as Class A or Class B, the distinction again being on industrial (class A) or domestic (class B) use. Again the more stringent regulations apply to equipment intended for domestic use.
Measurements for information technology equipment are defined in CISPR 22.

In general, the frequency ranges are defined as [CISPR 16-1]:

- Band A, 9 kHz to 150 kHz
- Band B, 0.15 MHz to 30 MHz
- Band C, 30 MHz to 300 MHz
- Band D, 300 MHz to 1000 MHz

Conducted RF-emission measurements defined in different generic and product family standards are made in Band B. There are also differences in conducted emission regulatory frequency ranges. The most important general emission standards, FCC [FCC CFR 47-15 2002] (United States) and IEC CISPR 22 (Europe) define the range of conducted RF emissions from 150 kHz to 30 MHz. The former version of FCC defined the conducted emission frequency range from 450 kHz to 30 MHz. Some product standards have different frequency ranges. For example, products specified in EN 300386-2 standard [EN 300386-2 1997], the conducted emissions range is from 20 kHz to 30 MHz in DC power supply ports.

1.7 Outline of the Thesis

This thesis can be divided into three main parts: Firstly, some aspects of spectral estimation and measurement are covered in Chapter 3. Secondly, selected spread spectrum generation techniques are presented with simulations and background information in Chapter 4. Finally, simulations and prototype measurements from EMC and steady-state performance are presented in Chapter 5.

Main goals of this thesis are:

- Find suitable EMI analysis tools for random switching in a switch mode power supply
- Compare the EMI and steady-state performance of selected spread spectrum switching methods in the prototype switching converter

This work is based on numerous simulations and measurements made with the prototype. All these simulations and measurements are made with the boost converter. The study is focused on the steady-state operation of the converter without the voltage feedback control loop. The generated EMI content has been calculated and measured from input current at low frequencies (*conducted differential emissions,* 9kH-1MHz) in a non-standard frequency range. This frequency range was selected for evaluation of highlight special characteristics of different modulation methods. These features would have been buried in the results if for example a 150 kHz to 30 MHz measuring range was used. The number of uncertainty factors and non-idealities in the circuit will also rise if the frequency range is increased. Although the test set up and the converter operation is not practical from a compliance testing point of view, it provides a *uniform platform for comparison* of different types of switching patterns and their effect on the EMI content generated by the converter.

Many theoretical studies have been made in the literature considering the spectral characteristics and the generation of randomized switching patterns of one selected topology. However, there exists no universal analysis method in the literature or practical engineering for the comparative analysis of variable EMI signals. The objective of this work is not to give fully detailed analytical solutions and analysis methods for every different type of power supplies. The scope is on a practical study of the differences and possibilities of selected spread spectrum modulation methods with analysis tools covered in Chapter 3

The EMI properties are also analyzed from the switching function $q(t)$ of the boost converter. The reason behind the use of the switching function in this work is the general applicability of the results presented. It will be shown, that the spectrum of the switching function correlates with the simulated and measured EMI spectrum of the boost converter.

The contents of the thesis are divided into six chapters. Besides this introductory chapter, the following chapters are:

Chapter 2 treats the basic theory of power supplies and control in the scope of this work. The prototype boost converter is presented and the simulation model of the

converter is derived. Practical aspects and limitations are discussed in the end of this chapter.

Chapter 3 deals with the analysis and measurement of the EMI spectrum. Limitations of basic Fourier theory are illustrated and numerical spectrum estimation methods are presented. Time-frequency analysis is proposed for EMI analysis of an SMPS. In addition, important aspects of the EMI test receiver in time variant EMI spectrum measurements are discussed.

Chapter 4 reviews selected spread spectrum techniques with theoretical background information. Preliminary analysis is made with a simulated power spectrum, spectrogram and autocorrelation sequence of the switching function.

Chapter 5 presents the simulation and experimental results. Both EMC and steady-state voltage and current waveforms are presented. The laboratory test setup is described in the beginning of this chapter.

Chapter 6 concludes the results and makes some suggestions for future work.

1.8 Key results

This work combines the theory of signal analysis and measurement, communication theory, nonlinear control theory and EMC, which are applied in power electronics. This kind of combination in comparative analysis is believed to be novel.

According to the results presented in this work, spread spectrum modulation can be utilized in a power converter for EMI mitigation. Several tests were made with different spread spectrum modulation techniques and the results show, that reduction can be achieved in conducted EMI-disturbance levels.

The spectrogram has been proposed as a design and analysis tool when selecting a spread spectrum modulation method for the power converter and characterizing the variable frequency EMI of a converter in general. The spectrogram can also be used in compliance testing when characterizing the signal under investigation thus reducing the total testing time. The spectrogram is a well-known time-frequency analysis tool in different applications, but the use of the spectrogram in SMPS EMI analysis has not been proposed or analyzed in the literature.

Voltage and current ripple has been considered as a major problem with spread spectrum modulated power supplies, but comparative analysis of different spread spectrum techniques has not been made. Results from the steady state voltage measurements show, that the variable-frequency operation of the SMPS has an effect on the voltage ripple, but the ripple measured from the prototype is still acceptable in several applications. This voltage fluctuation caused by the modulation can be reduced with a normal voltage feedback control and proper main circuit design.

Preprogrammed spread spectrum techniques, such as frequency modulation and frequency hopping (FH), give reliable and predictable results in EMI mitigation. Frequency hopping is one of the most suitable methods for power supply

applications. The frequency range and the hopping sequence can be tailored for maximum spectral efficiency with a PN-sequence with known statistical properties. In addition, requirements and limitations from power supply components and controller design can be taken into account. A drawback of this solution is that practical implementation needs an extra circuitry or an application specific integrated circuit.

Controller-based EMI-reduction techniques have been left out of the scope when different SS techniques have been compared in recent publications. However, controller-based spread spectrum techniques, such as a peak current controlled chaotic converter or Sigma-Delta controller, can be applicable to some applications where the operation conditions of the converter are constant or all operation conditions can be taken into account at the design phase. The main advantage of these types of spread spectrum generation methods is the simplicity of the additional circuitry needed: usually there is no need for extra components because of the inherent spread spectrum property of the converter control operation. The main drawback is the dependence on the system parameters – even a little change in the load may force the system into periodic operation thus modifying the spectral performance.

2 Switching Power Converters

2.1 General Background

In general, switching power converters are used in control and conversion of power by shaping currents and voltages by means of power semiconductor devices. This shaping means that there is a change in characteristics, voltage, current, and/or frequency, of the electrical power to suit a particular application. Typically, this means changing the

- voltage and current form, AC or DC,
- voltage and current level (magnitude),
- voltage and current frequency.

Generally, these converters are classified as, [Erickson 1997]:

- a ***rectifier,*** converting an AC voltage to a DC voltage,
- a ***switch-mode DC/AC converter*** or ***inverter,*** converting a DC voltage to an AC voltage,
- a ***switch-mode DC/DC converter*** that converts a DC voltage to another DC voltage, and
- a ***cycloconverter*** converting an AC voltage to another AC voltage.

Rectifiers can be classified as uncontrolled and controlled rectifiers. In uncontrolled rectifiers, the main semiconductor switching component is a diode. Controlled rectifiers use components like thyristors, and the DC output voltage of these rectifiers can be controlled. In more complicated rectifiers, the input current waveform can be controlled. Rectifiers are broadly used in different kinds of power converter applications. The power range is very wide, from milliwatt range to megawatts. Small power range devices operate mainly from a single-phase supply while high-power rectifiers are mainly used in a three-phase configuration.

The converter that changes a DC voltage to an alternating voltage is called an inverter. Usually a rectifier is used as an inverter system front-end in the generation of a DC voltage. The output of the inverter is typically one- or three-phase AC, depending on the application. The main applications of inverter systems are AC variable speed motor drives, uninterrupted power supplies and frequency converters.

Switch mode DC/DC converters are mainly used in applications, where the regulated DC output is needed. Typical applications for a switch-mode power supply are regulated DC power supply, battery charger and DC motor drive. Usually the unregulated input is fed for example from a rectifier, a battery or a solar cell and then converted to a desired, controlled voltage level. The DC voltage output level can be either lower or higher than the input voltage, possibly with opposite polarity and galvanic isolation.

Cycloconverters are mainly used in variable frequency AC motor drive systems when a very high power output is needed. The output frequency range of a cycloconverter

is limited because of the operation principle of the converter [Mohan 1989]. A typical application for a cycloconverter is to use it for controlling the speed of an AC traction system.

The power factor (*PF*) is an important measure in power electronics. It represents the real power utilization in the converter, thus closely relating to the efficiency of the system. It also represents the measure in the distortion of line voltage and line current and phase shift between them. The power factor is defined as the ratio of the average power *P* divided by the apparent power *S:*

$$PF = \frac{P}{S} \quad . \tag{2.1}$$

PF can be easily defined for purely sinusoidal current and voltage waveforms. In this simple case, the power factor is equal to the cosine of the phase-angle between the current and voltage. However, in switching power converters, due to the switching of active power devices, voltage and current waveforms are distorted, and the phase-angle representation alone is not valid. Harmonic analysis in line voltage and current is needed.

As mentioned in Chapter 1.2, the power factor correction was one of the project objectives. Power factor correction (PFC) is a technique where the line current/voltage distortion and the power factor of the converter are controlled by means of the control of a switching power converter. Practically this means that the input current is forced to follow the supply voltage waveform. The power factor is, however, out of the scope of this work, although the converter topology selected in this work is generally used in power factor correction applications.

2.2 Distributed Power Systems

The design of power systems is moving towards a modular building-block approach, where the overall power system is based on a combination of different power modules, [Watson 1998]. Modularity is one of the main characters in a distributed power system (DPS). Distributed power systems in general consist of front-end modules and load modules. The architecture and the design philosophy are different when comparing a DPS to a traditional central power supply approach. Several basic DPS structures can be identified according to the way the power processing units (PPU) are combined in the power system, Figure 2.1.

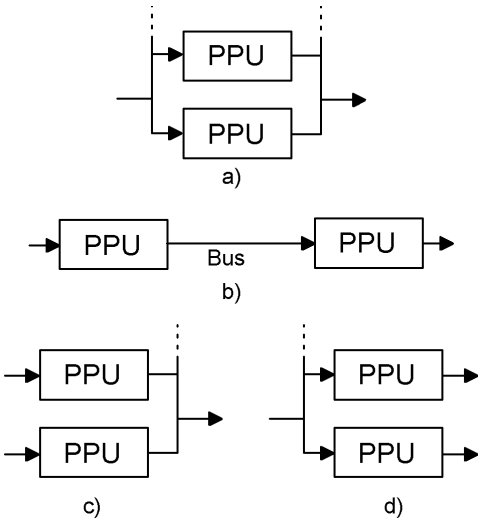

Figure 2.1. Basic DPS structures: a) Paralleling. b) Cascading. c) Source splitting. d) Load splitting, [Tabisz 1992].

Most DPS architectures are combinations of these basic structures. Typically, there is an intermediate distribution bus (either DC or AC) and various combinations of cascading and load splitting. The most important benefits of the DPS are thermal management, modularity, size reduction, efficiency, regulation in load points, handling of large line variations and reduction of noise coupling between different loads, [Tabisz 1992].

Examples of different types of power supply arrangement are presented in Figure 2.2 and in Figure 2.3. The first example (Figure 2.2) represents a customary power supply, where a central power supply produces two regulated DC outputs. This kind of a power supply contains a rectifier part to convert the AC line input to a DC link voltage and a DC/DC converter part to regulate unregulated DC link voltage to a regulated output voltage. In this case, the DC/DC converter-part is more complicated because the power supply has two different outputs. Load blocks may even have their own linear regulators to adjust the voltage level thus decreasing the overall efficiency.

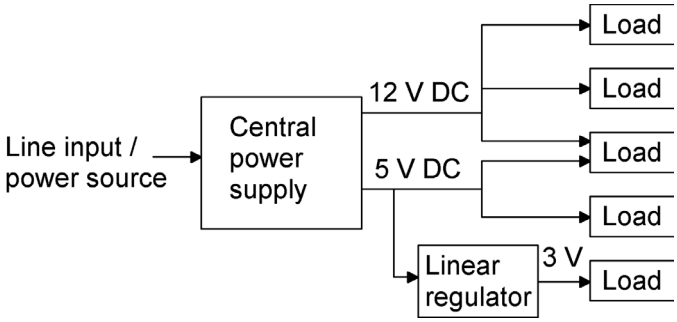

Figure 2.2. An example of conventional implementation of power distribution in a system with different loads. A bulky central power supply is utilized to generate different regulated outputs. All loads with the same voltage level are electrically connected.

The DPS approach to the same example is presented in Figure 2.3. A simple front-end power supply generates an intermediate DC voltage to the distribution bus. With a higher voltage level the power transfer from the front-end is more efficient, especially if the system is physically large and the load(s) is heavy. At the load-end, every load has its own DC/DC converter which regulates the intermediate bus voltage to the desired level. With this arrangement the load regulation is better and

more efficient. Also the noise coupling via a power bus impedance between different loads is much lower than in a conventional system.

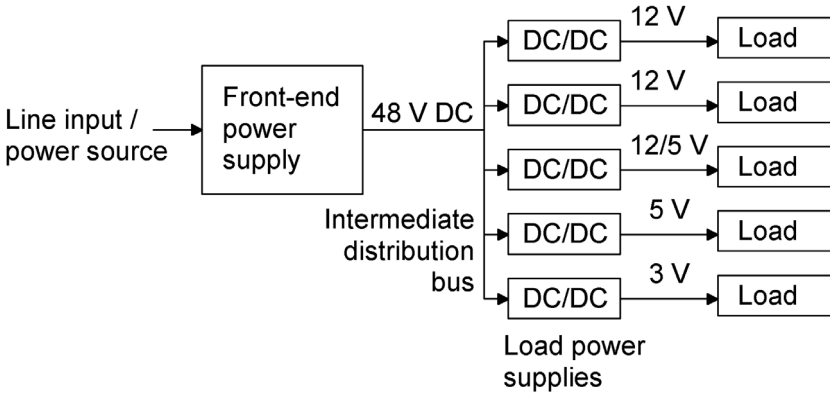

Figure 2.3. An example of a distributed power system approach. A simple front-end power supply is used to generate intermediate output and the load points have their own DC/DC regulators.

The front-end PPU performs one or all of the following tasks, [Tabisz 1992],

- Line rectification and filtering
- Power factor correction and input line current harmonic reduction
- DC/DC conversion
- Energy storage

In this dissertation, the scope is on the DC/DC part of a front-end power supply. The power source is taken from a lead acid battery and 48 V DC intermediate output voltage is generated.

2.3 Control of the Power Converter

Usually the average output of the switching converter must be controlled to the desired level. Regulation of output voltage or current is normally required in many power converter applications. Some kind of a controller is invariably required, Figure 2.4. Only some very primitive applications, such as electrical heating, can operate without control.

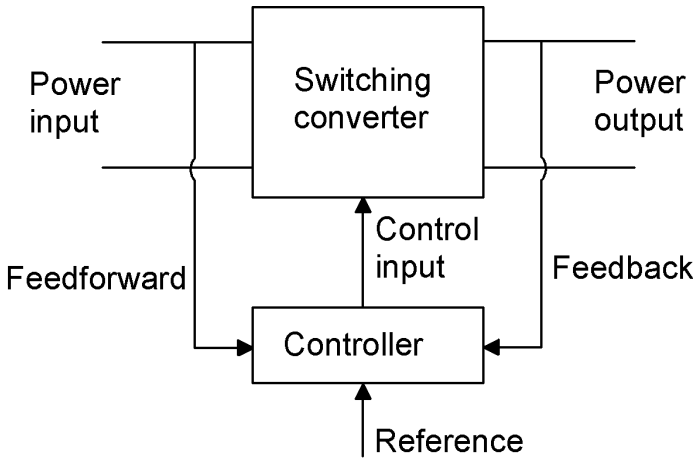

Figure 2.4. A controller is generally required in a switching converter, [Erickson 1997].

The controller can have feedback from the output and feedforward from the input of the converter to have better regulation of the power and immunity to load and line variations. The main purpose of this controller is to keep the output and/or input at

some desired level set by the reference. The basic form of a closed loop control system utilizes the measured feedback signal and compares it to the desired reference.

Normally the output voltage of the DC/DC converter is regulated with some control circuitry, which ensures that the average DC output voltage is constant and almost independent of the input voltage and load fluctuations. Usually this is done by controlling the duty cycle $d(t)$ of the switching converter. The controller typically utilizes one or two feedback signals from the converter state variables, which are then fed to the controller. An example of a boost converter controller is presented in Figure 2.5. The controller in this example has two feedback loops: the outer loop is a voltage feedback loop from the output voltage of the converter and inner loop is a current feedback loop from the input current of the converter.

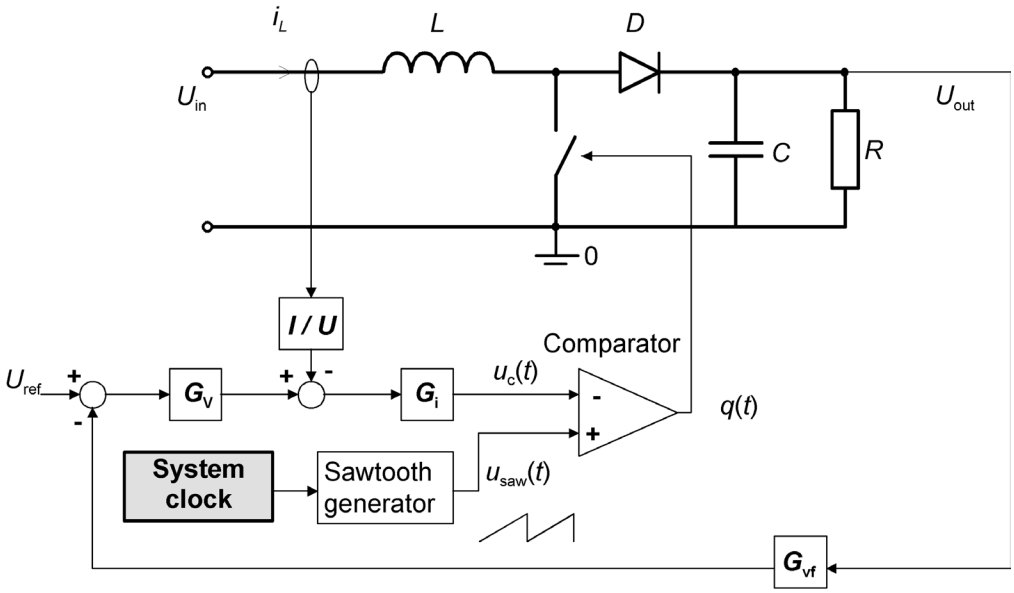

Figure 2.5. A block diagram of a boost converter controller. The controller circuit in this example uses two control feedback loops.

The PWM-controller presented in Figure 2.5 adjusts the duty cycle $d(t)$ to commit required actions to keep the output voltage at a desired level. A measured feedback signal is used to monitor the output voltage and the desired output voltage is set by the reference signal U_{ref}. Some other feedback signals may also be used, this example uses feedback from the input current.

The controller also has dynamic properties, and these system dynamics can be analyzed with system functions. Here system functions are presented in the block diagram as G_{vf}, G_v and G_i. System dynamics can be linear or nonlinear. If the differential equations describing the system operation can be linearized, then the Laplace transform can be utilized to simplify the method of solution and transfer functions can be used in the system description, [Dorf 1995].

One customary method for the SMPS control is pulse width modulation. PWM was already presented in Figure 2.5. The main parts of the pulse width modulator are presented in Figure 2.6 a). Figure 2.6 b) shows waveforms of the modulator: saw-tooth wave $u_{saw}(t)$ is compared to the analog control input $u_c(t)$ and the switching

function $q(t)$ is generated according to these waveforms. The control signal of the modulator comes from the controller of the power converter. The linear control system with voltage feedback is traditionally used in power converter control. Basic linear control strategies are presented for example in [Dorf 1998], [Mohan 1989] and [Erickson 1997].

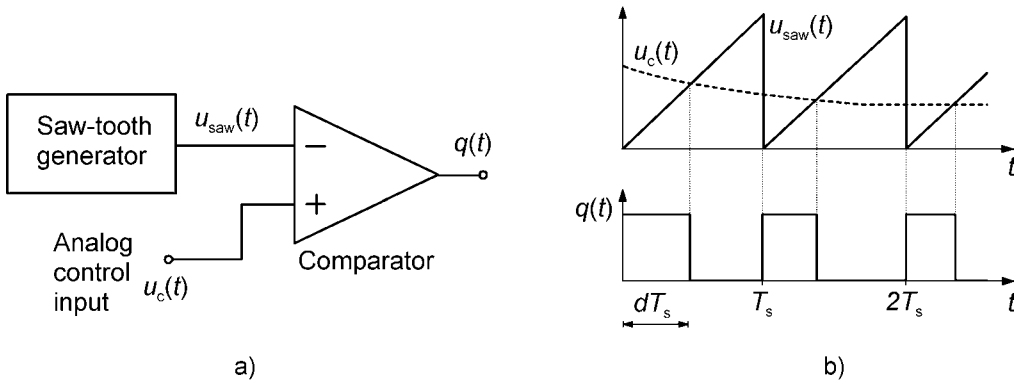

Figure 2.6. a) Main components of the PWM-modulator. b) Waveforms in a PWM-modulator.

If the control input of the modulator is kept constant, the duty cycle of $q(t)$ remains constant. The basic PWM also operates at a constant switching frequency f_s used in the saw-tooth generator. The relation between the switching frequency f_s and switching period T_s is

$$T_s = \frac{1}{f_s} \tag{2.2}$$

Current mode control (or current programmed control) is another control technique used in SMPS control. The motion rate of the current is much faster than the motion rate of the output voltage for most DC/DC converters used in practice, [P5]. This fact can be utilized to improve system dynamics and to realize faster controller response to disturbances. The main advantage of current programmed control is its simpler dynamics, [Erickson 1997].

Usually there is a voltage feedback loop in current mode control in order to regulate the output voltage. The cascaded control structure of a DC/DC converter consisting of an inner current feedback loop and outer voltage feedback loop was already presented in Figure 2.5. However, the block diagram of a current mode controller presented in Figure 2.7 does not contain a pulse width modulator to control the duty cycle. The switch current is directly controlled with feedback measurement and it is forced to follow the current reference.

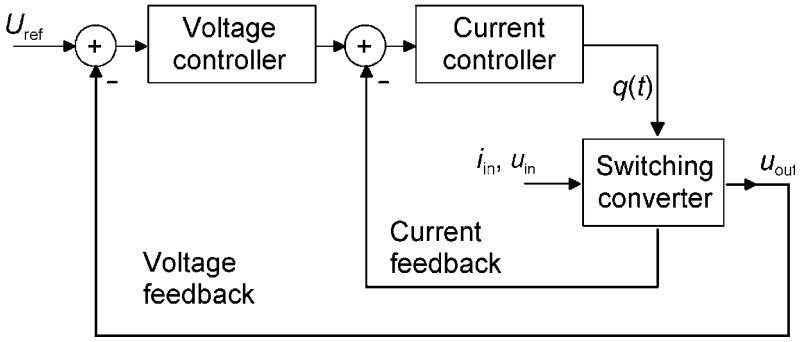

Figure 2.7. Cascaded control structure of a current mode control. The current controller used in this control method differs from PWM. The current controller block uses the nonlinear mode in the switching function generation, for example peak current control. The linear voltage feedback controller is used as part of this controller to regulate the output voltage, [P5].

An example of current mode control is presented in Figure 2.8, where operation of the peak current control is presented. In current-mode control, a DC/DC converter controller has a peak inductor current limit. This limit controls the power switch and sets the constantly changing duty cycle. In constant frequency operation, the switch is turned on at a constant time interval. The switch is turned off when the current reaches the limit set by the controller.

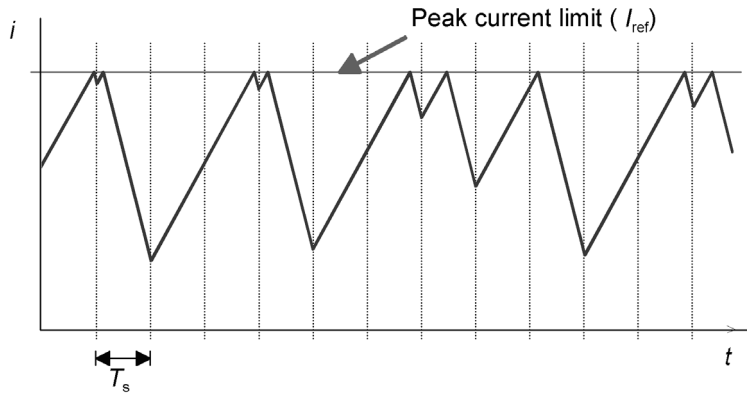

Figure 2.8. An example of a current waveform in a peak current controlled converter. The power switch is turned off when the current reaches the peak current limit. The switch is turned on again at constant frequency (vertical lines).

With some parameters like in the previous example, the system operates at varying frequency, and the converter operation is said to be in subharmonic or chaotic mode, [P1], [Banerjee 2001]. This happens when the average duty cycle $D > 0.5$, [Erickson 1997]. Although generally regarded as an unstable and unwanted operation point of the power converter, it will be shown that this chaotic operation mode can be used in power converter control.

2.4 Case study: The Boost (step-up) DC/DC Converter

The boost converter was selected as a prototyping platform for the study of SSM in this thesis. Any other basic converter topology could also have been adopted for this purpose, but the boost converter was selected to be studied in the beginning of the work. This was because of the applicability of the boost converter for power factor correction (PFC).

The boost converter is one of the DC/DC converters capable of producing an output voltage greater than the input voltage. Figure 2.9 shows the main circuit of the boost converter.

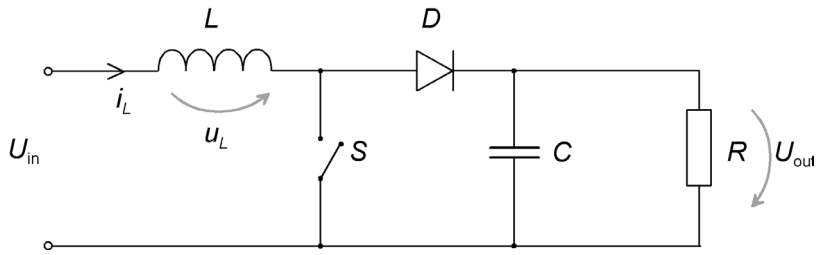

Figure 2.9. Schematic diagram of the boost converter main circuit.

Simplified analysis of the steady-state operation is described next. When the switch *S* is conducting (switch on), current i_L flows through the inductor *L*. The inductor current i_L is also the input current i_{in} of the converter, supplied from the voltage source U_{in}. In this case, when the switch is on, the diode *D* is reverse biased, thus isolating the capacitor *C* and the load *R* from the input stage. In this subinterval, the capacitor supplies the load current and the capacitor is partly discharged. When the switch is turned off, the output stage is connected to the input stage because the diode is operating forward biased. The inductor current supplies the load and charges the capacitor during this subinterval. Energy stored in the magnetic field of the inductor during the switch on phase plays an important role in the voltage rising feature of the boost converter.

Figure 2.10 shows steady state waveforms of the inductor in continuous conduction mode (CCM). In CCM, the inductor current $i_L(t) > 0$.

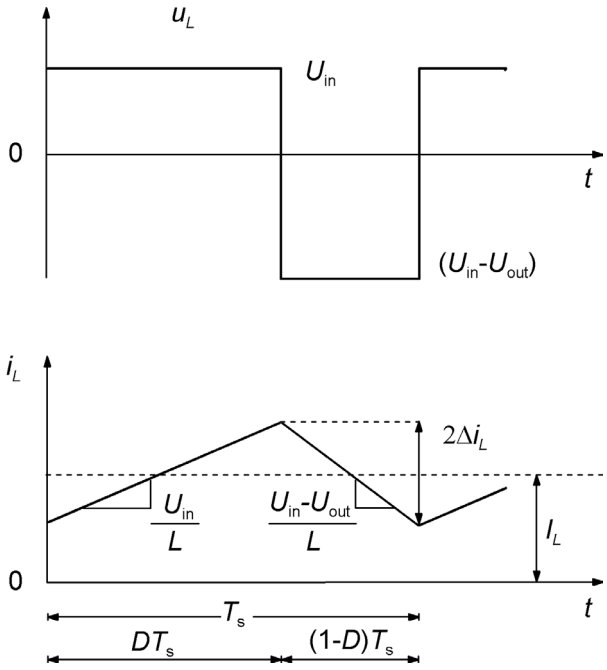

Figure 2.10. Theoretical inductor voltage u_L and inductor current i_L waveforms of a boost converter operating in continuous conduction mode. The dashed line represents the average inductor and input current I_L.

In general, the inductor voltage u_L is

$$u_L(t) = L\frac{di_L(t)}{dt} \ . \tag{2.3}$$

During the first subinterval when the switch is conducting, the slope of the inductor current is

$$\frac{di_L(t)}{dt} = \frac{u_L(t)}{L} = \frac{U_{\text{in}}}{L}. \tag{2.4}$$

During the second subinterval of the converter operation when the switch is turned off, the slope of the inductor current is

$$\frac{di_L(t)}{dt} = \frac{u_L(t)}{L} = \frac{U_{\text{in}} - U_{\text{out}}}{L}. \tag{2.5}$$

If the inductor current slope is assumed linear during the subintervals, the current ripple of the inductor can be obtained. This was also presented in Figure 2.10. Over one switching period T_s, the peak to peak inductor current $2\Delta i_L$, sketched in Figure 2.10, is equal to the slope multiplied by the length of the subinterval, [Erickson 1997],

$$2\Delta i_L = \frac{U_{\text{in}}}{L} DT_s. \tag{2.6}$$

Equation (2.6) is very important in converter design. Firstly, it can be used in selection of the right inductor value for the converter with specified current ripple. Secondly, it can be used to calculate the maximum current ripple in the variable frequency operation of the converter or vice versa, to calculate maximum switching period such that the given value of peak to peak current is not exceeded.

Another important variable in converter design is the average duty cycle D. Since the inductor volt-second balance or actually the time integral of the inductor voltage over one steady-state time period is zero, [Mohan 1989],

$$U_{\text{in}}DT_s + (U_{\text{in}} - U_{\text{out}})(1-D)T_s = 0 \, . \tag{2.7}$$

Dividing both sides by switching period T_s and rearranging the terms, the voltage conversion ratio of the boost converter operating in CCM can be obtained:

$$\frac{U_{\text{out}}}{U_{\text{in}}} = \frac{1}{1-D} \tag{2.8}$$

In addition to the CCM, there is another possible operation mode for the boost converter, namely the discontinuous conduction model (DCM). In this DCM-mode, the inductor current i_L goes to zero for some part of the switching period, Figure 2.11.

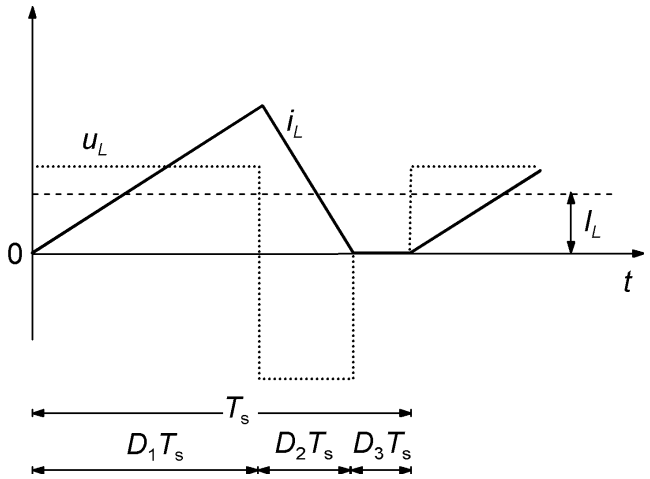

Figure 2.11. Theoretical inductor current i_L (solid line) and inductor voltage u_L (dotted) waveforms of a boost converter operating in discontinuous conduction mode. The dashed line represents the average inductor and input current I_L.

The inductor current i_L is zero during the third subinterval D_3T_s of the converter operation in DCM. During D_3T_s, no current is drawn from the input source and the capacitor partly discharges and provides the current to the load. According to Erickson, [Erickson 1997], the voltage conversion ratio in DCM is

$$\frac{U_{out}}{U_{in}} = \frac{1+\sqrt{1+\frac{4D^2}{K}}}{2}\ , \qquad (2.9)$$

where parameter $K = 2L/(RT_s)$. For a more detailed analysis and derivation of the equations, see references [Erickson 1997] and [Mohan 1989].

The average DC output voltage of the boost converter can be calculated with Equations (2.8) and (2.9). The output voltage ripple is assumed to be zero in previous analysis. However, the output voltage ripple is not zero and the ripple is one of the main design parameters of a practical converter. Figure 2.12 shows an approximation for a boost converter output voltage waveform.

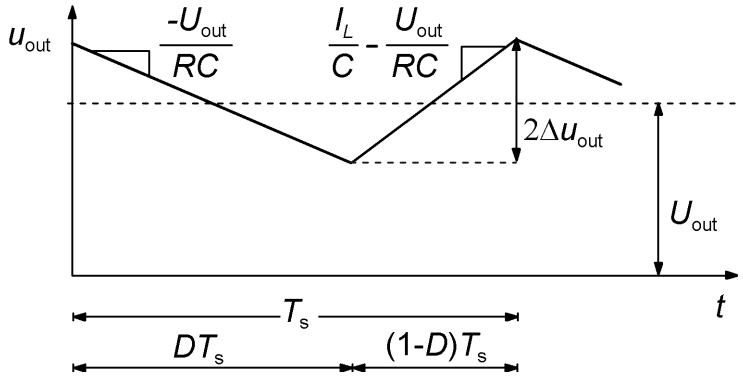

Figure 2.12. Theoretical output voltage waveform of a boost converter. The slope of the voltage is approximated to be linear. The instantaneous output voltage varies around the nominal output voltage U_{out}.

In general, the output voltage ripple of the boost converter is dependent mainly on the output capacitor, load and the switching frequency. To be more specific, the ripple is, [Erickson 1997],

$$\Delta u_{out} = \frac{U_{out}}{2RC} D T_s . \qquad (2.10)$$

This equation can be used in the selection of the output capacitor value. This equation also relates the switching frequency $f_s = 1/T_s$ to the voltage ripple.

2.4.1 The Prototype Converter and Simulation Model

The prototype of a boost converter was designed for empirical analysis of different spread spectrum techniques. Nominal values for the main design parameters of the prototype converter are presented in Table 2-1.

Table 2-1. The main parameters of the prototype boost converter.

Parameter	Value
Input voltage U_{in}	12 V
Output voltage U_{out}	48 V
Nominal output power P_O	50 W
Nominal switching frequency f_s	50 kHz
Inductor, L	100 μH
Capacitor, C	220 μF

The calculated nominal duty cycle D for nominal operation according to Equation (2.8) is 0.75. The nominal input current ripple is 1.8 A and the output voltage ripple is 37 mV according to Equations (2.6) and (2.10). These calculations assume ideal components and operation conditions. The inductor and capacitor values were selected from simulations for the purpose to achieve chaotic operation in peak current control. An example of chaotic current waveform was presented in Figure 2.8. Detailed simulations results will be presented in a later part of this study.

The main circuit of the prototype boost converter is presented in Figure 2.13. State variables, inductor current i_L and capacitor voltage u_C, used in the circuit analysis are marked with arrows.

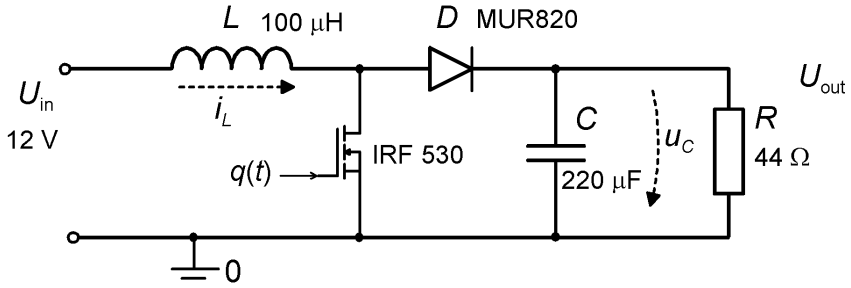

Figure 2.13. Simplified schematic diagram of the boost converter. State variables i_L and u_C used in circuit analysis are marked with dashed arrows.

A more detailed description of the prototype converter with a schematic diagram, printed circuit board layout and control circuit is presented in Appendix C.

For the creation of the simulation model the operation of the converter is divided into three different modes, switch off (1°), switch conducting (2°) and DCM switch off (3°), Figure 2.14. There are also additional loss-components in the model. These are

diode forward voltage drop U_D (0.7 V), inductor coil resistance R_L (0.1 Ω) and power switch conduction loss R_{DSON} (0.12 Ω). Losses in the capacitor C are assumed negligible for the simplicity of the simulation model: the output voltage U_{out} equals the capacitor voltage u_C in the simulation model. Capacitor non-idealities effect mainly on the voltage feedback controller performance and stability analysis, [Erickson 1997]. The controller used in this work does not use voltage feedback and accurate modeling of the capacitor is therefore unnecessary.

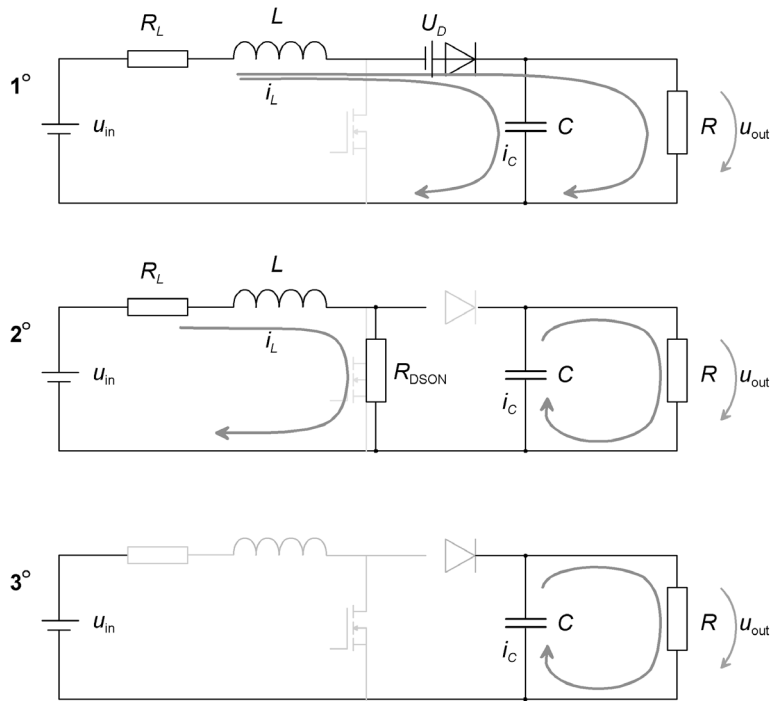

Figure 2.14. Converter equivalent circuit and operation in different power switch positions.

Based on the model presented in Figure 2.14, equations describing the system can be written as follows in different states of the switch:

1° - Switch off :

$$i_L = \frac{1}{L}\int (u_{in} - u_{out} + i_L R_L + U_D)dt \qquad (2.11)$$

$$u_{out} = \frac{1}{C}\int i_C\, dt = \frac{1}{C}\int (i_L - \frac{u_{out}}{R})\, dt$$

2° - Switch on :

$$i_L = \frac{1}{L}\int (u_{in} - (R_{DSON} + R_L) i_L)\, dt \qquad (2.12)$$

$$u_{out} = -\frac{1}{RC}\int u_{out}\, dt$$

$3° - \text{Switch off, DCM}:$

$$i_L = 0 \tag{2.13}$$

$$u_{\text{out}} = -\frac{1}{RC}\int u_{\text{out}}\,dt$$

Straigthforward implementation of a previous equation set is presented in Figure 2.15. Inputs of the boost converer model are (1): input voltage U_{in}, (2): gate signal for the power switch and (3): value for the load resistance. Outputs are (1): output voltage u_{o} and (2): inductor current i_L.

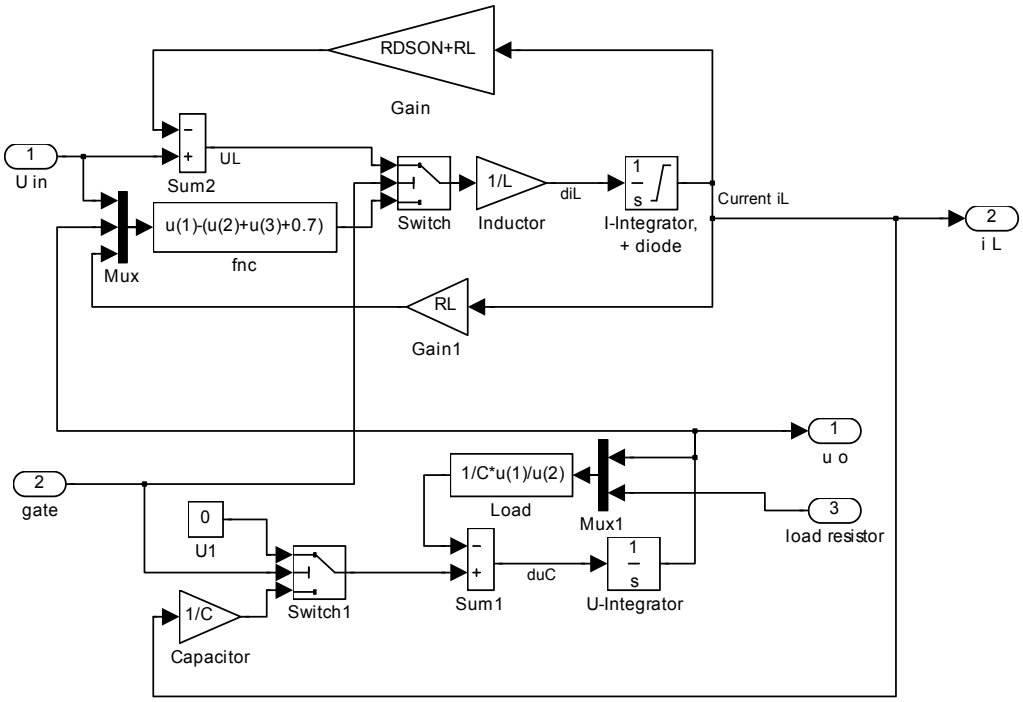

Figure 2.15. Simulink™ model for the main boost power circuit. This model was used in all simulations with a different control circuit in each case.

2.5 Practical Aspects and Limitations in Variable Frequency Power Converters

Use of a ferromagnetic core is general practice in power supply design to reduce the size of the inductor compared to the size of an air-cored inductor. Transformers especially require the use of a magnetic core because of the operation principle of the transformer. Magnetic saturation may occur in ferromagnetic material if the inductor design uses ferromagnetic core and the current exceeds certain, material dependent level, [Erickson 1997]. This limiting factor must be taken into account in variable frequency power converter design. As presented in Equation (2.6) when describing the operation of the boost converter, the peak current of the inductor is dependent on the voltage and the on-time of the switch. This means that if the instantaneous switching frequency of the converter becomes low, the on-time of the switch will increase thus increasing the peak current of the inductor. In addition to the possible core saturation, the hysteresis losses of the core material will increase along with increased flux density (current ripple), [Ferroxcube 2003]. Therefore, the

magnetic parts, in this case inductor, set one limitation at the low frequency limit in the VF converter operation.

Magnetic parts set some limitations also on the upper limit of the converter frequency range. Losses in the coil can be categorized as follows, [Ferroxcube 2003]:

- Winding losses, due to the DC resistance of the wire and eddy-current losses in the wire, dielectric losses in insulation.
- Core losses, due to hysteresis losses in the core material, eddy-current and residual losses in the core material.

The most important frequency dependent loss mechanism in the core material is eddy current losses. This will also limit the maximum usable frequency of the power converter. Eddy current losses, the skin effect and the proximity effect, [Erickson 1997], will increase losses in coil windings because of the non-uniform current density in the cross-section of the conductor. The high frequency current in round wire can be assumed concentrated in the annulus at the wire surface of thickness equal to skin depth δ, [Paul 1992]

$$\delta = \frac{1}{\sqrt{\pi f \mu \sigma}} \quad , \tag{2.14}$$

where f is frequency, μ is permeability [H/m] and σ is conductivity [S/m]. Above the frequency, when the skin depth is equal to the wire radius, the AC-resistance of the wire increases as a square root of the frequency, [Paul 1992]. Dielectric losses in the winding insulation also increase when the frequency increases.

Turn-on and turn-off transients of semiconductor devices require tens of nanoseconds to microseconds. During these transitions, very high instantaneous power losses can occur. To switch the semiconductor device on or off, the controlling charge has to be inserted or removed, since semiconductor devices can be regarded as charge-controlled devices. Charge and energy is also stored in the capacitances of the device and in the leakage inductances in the circuit. In most converter circuit, these stored energies are lost during the switching transients, [Erickson 1997]. The average power $P_{S,loss}$ dissipated in the switching device can be formulated with turn-on energy $W_{S(on)}$ and turn-off energy $W_{S(off)}$:

$$P_{S,loss} = f_s (W_{S(on)} + W_{S(off)}) \tag{2.15}$$

The most important loss mechanisms, [Erickson 1997], [Mohan 1989], [Ferroxcube 2003], of the power converter are summarized next:

- Switching losses.
- Losses in magnetic materials.
- Resistive losses.

All of above are dependent on frequency. Switching losses are linearly dependent on the switching frequency. Losses in magnetic materials are dependent on the specific material characteristics. This will reflect on the selection of the maximum allowable switching frequency of the converter.

2.6 Summary

A general overview on power converters was made in the beginning of this chapter. Power factor correction and distributed power supply arrangement were introduced as a background and possible applicability of this work. The main control principles of switching converters were introduced. The boost converter was selected as a prototyping platform and nominal values of the prototype with the main component selection and analysis was presented. A simulation model of the boost converter was derived for simulation analysis of the converter with different modulation and control methods. In addition, some practical aspects of power supply losses and other limitations were discussed in the scope of this work.

3 Spectrum Estimation, Signal Analysis and EMI-Measurements

EMC regulations are based on the measured spectral content of the emissions generated by the equipment under test (EUT). Methods for defining the spectrum of a device have remained the same for many decades. Of course, development of microprocessors and other semiconductor devices have made measurement apparatus more comfortable to use and gained the accuracy of the test results. However, modern EMI test equipments are still using an analog front end in the spectrum analysis. We are still waiting for the arrival of digital spectrum analyzers capable of standardized EMI test measurements.

Modern computers and powerful mathematical and simulation programs have made the routine tasks of a design engineer much easier compared to the design work of an engineer two decades ago. Even the EMC-problems and the EMI-spectrum of an apparatus can be approximated with simulations in the beginning of a design flow. The design engineer has to, anyhow, know the basics of the theory behind the simulations. This chapter deals with the theory of signal analysis, especially the spectrum estimation, which is essential in the performance and EMI analysis of a spread spectrum system.

The spectrum can be estimated by calculations or by measurements. When using calculations, the spectrum can be calculated either analytically or numerically. Analytical methods for spectrum estimation are not suitable for the analysis of a non-stationary signal (i.e. spread spectrum signal), because the exact signal waveform can be very complex and partly unknown. For numerical spectrum estimation, many different methods have been developed during the last four decades. The most common method is Fast Fourier Transform (FFT), introduced in the mid 1960's by Cooley and Tukey, [Cooley 1965].

Analytical methods can be utilized in spectrum estimation for simple, a well-defined periodic signal. The spectrum of a sinusoidal signal is a well-defined quantity. However, practical signals rarely are sinusoidal or even periodical. Non-stationary signals in particular do not lend themselves well to decomposition into sinusoidal components, [Boashash 1992-1]. Analytical methods are covered in the literature [Boashash 1992-2], [Nagel 1997], [Stankovic 1995], [Tse 1999], but the analysis has been limited to waveforms like square and triangle wave with specific rise and fall times. Fourier transform based analytical solutions for periodic signals (non-symmetrical square wave, non-symmetrical trapezoid, sinusoidal PWM) are presented in the study by Nagel et al., [Nagel 1997], and Bech, [Bech 2000]. These idealized methods are still unsuitable for the analysis of spread spectrum signals. Analytical analyses with a spread spectrum power converter signal are made in papers [Tse 2000] and [Shrivastava 2000]. Calculation of spectral spikes in a chaotic boost converter with simplified mapping is presented in reference [Banerjee 2001].

Numerical methods are effective with modern computers and widely adopted in practice. Although very common, the direct FFT-method is not a universal spectrum estimation method. For example, use of FFT in EMI-spectrum estimation of a spread spectrum modulated converter leads to a random spectral estimate, [Stankovic 1995], [Mihalic 1999-1], [Mihalic 1998]. Results vary with time and parameters and may lead to wrong assumptions of the spectral content of the signal, as mentioned in [Stankovic 1993].

In next few pages, the problem in defining the spectrum is reviewed and some possible methods for defining the spectrum of a SS system are presented. First, the analytical approach with suitable numerical methods is presented. Secondly, performance and operation of a typical EMI-measurement system is analyzed. Finally, practical aspects on EMI-measurement techniques are discussed.

3.1 Fourier Analysis of Periodic and Aperiodic Signals

Spectrum estimation in general is quite demanding and a parameter depending task. Even from a simple, periodic sample signal, one can get rather different results only by changing slightly the calculation parameters. The process of obtaining the spectrum of a signal using basic mathematical tools is known as spectral analysis. In contrast, the process of obtaining the spectrum from a practical, measurement signal is called spectrum estimation. When non-stationary spread spectrum signals should be analyzed, statistical signal analysis tools are needed. Selected statistical tools are covered in the next pages to clarify the problems faced in the spectrum estimation of a non-stationary signal. First, the main properties of the Fourier series and the Fourier transform in the scope of this study are presented without rigorous mathematical derivation. A more detailed analysis and derivation of the equations can be found in basic textbooks, for example [Kay 1987], [Oppenheim 1997], [Aumala 1998] and [Proakis 1992].

3.1.1 Fourier Spectrum of a Periodic Signal

The signal is periodic [Oppenheim 1997], if

$$x(t) = x(t + T_P) \qquad \text{for all } t \tag{3.1}$$

The fundamental period of $x(t)$ is the minimum, nonzero positive value of T_P which satisfies Equation (3.1).

A periodic signal can be expressed as harmonically related complex exponents [Kay 1987], [Oppenheim 1997], [Proakis 1992]:

$$x(t) = \sum_{k=-\infty}^{\infty} c_k e^{jk\omega_0 t} = \sum_{k=-\infty}^{\infty} c_k e^{jk2\pi F_0 t}, \tag{3.2}$$

$$c_k = \frac{1}{T_P} \int_{T_P} x(t) e^{-jk\omega_0 t} dt = \frac{1}{T_P} \int_{T_P} x(t) e^{-jk2\pi F_0 t} dt, \tag{3.3}$$

where c_k and $k = \pm 1, \pm 2, \ldots$, are arbitrary complex constants. It can be noted that $x(t)$ is a periodic with a fundamental period of $T_P = 1/F_0$. Other harmonic components

have a period of T_P/k. Since the signal that is a periodic with period T_P/k, is also a periodic with period $k(T_P/k) = T_P$, which is the fundamental period. Generally, Equation (3.2) is known as the *Fourier series* expansion of $x(t)$. To be valid, the signal must fulfill so-called *Dirichlet conditions*[1], which can be summarized as follows:

1. The signal $x(t)$ has a finite number of finite discontinuities.
2. The signal $x(t)$ has a finite number of maxima and minima.
3. The signal $x(t)$ is absolutely integrable.

The exponential signals $e^{jk\omega_0 t}$, $k = \pm 1, \pm 2, \ldots$, can be considered as basic building blocks from which the periodic signal can be constructed with coefficients c_k. ω_0 defines the fundamental frequency and coefficients c_k define the shape of the waveform, [Proakis 1992].

A periodic signal has infinite energy and a finite average power. Average power P of a periodic signal can be obtained from the square of the signal. According to the *Parseval's relation* for power signal, [Proakis], the signal power is given as

$$P_x = \frac{1}{T_P} \int_{T_P} |x(t)|^2 dt = \sum_{k=-\infty}^{\infty} |c_k|^2 . \tag{3.4}$$

The left-hand side of the equation (3.4) presents the average power (i.e. energy per unit time) in one period of the signal. The total average power in the periodic signal is the sum of average powers in all the harmonics. If the resulted power obtained from the right-hand side of Equation (3.4) is plotted as a function of frequencies kF_0, $k = \pm 1, \pm 2, \ldots$, the resulting graph, spectrum, represents the *power distribution* of the signal in different frequency components. The term power can be used here, because the square of signal amplitude presents the signal power. The spectral unit in the periodic spectrum is in terms of power, for example volts^2 or watts if the power is normalized to a 1 Ω system.

Since the power exists only at *discrete values of frequencies with equidistant lines*, the spectrum of the periodic signal based on the Fourier series is said to have a *line spectrum*. The spacing Δf between two adjacent spectral lines is equal to the reciprocal of the fundamental period T_P, whereas the shape of the spectrum depends on the time-domain characteristics of the signal, [Proakis 1992]. The spectrum of a periodic signal can have values at discrete frequency intervals $n\Delta f$, where the frequency increment Δf can be obtained as

$$\Delta f = \frac{1}{T_P} . \tag{3.5}$$

As the continuous time signal has a frequency range from - ∞ to ∞, a discrete-time signal $x(n)$ has a frequency range from $-\pi$ to π (or from 0 to 2π). If the discrete-time

[1] For rigorous mathematical derivation of Dirichlet conditions and Fourier theory, refer for example [Proakis 1992] or [Oppenheim 1997]

has a fundamental period of N, the frequency-domain representation consists of frequency components separated $2\pi/N$ radians or $f = 1/N$ cycles. The discrete-time Fourier series pair is, [Proakis 1992]:

$$x(n) = \sum_{k=0}^{N-1} c_k e^{j2\pi kn/N} \tag{3.6}$$

$$c_k = \frac{1}{N} \sum_{n=0}^{N-1} x(n) e^{-j2\pi kn/N} \tag{3.7}$$

Equation (3.6) is called the discrete-time Fourier series (DTFS). According to Parseval's relation for a discrete-time periodic signal, the sequence $|c_k|^2$ for $k = 0, 1,\ldots, N - 1$ is the distribution of the power as a function of the frequency in the discrete time periodic signal.

3.1.2 Fourier Spectrum of an Aperiodic Signal

Whereas for periodic signals the complex exponentials are harmonically related, for a continuous time *aperiodic* signals they are infinitesimally close in frequency. The representation in terms of linear combinations takes the form of an integral rather than a sum, [Oppenheim 1997]. In other words, if the fundamental period of the signal approaches infinite, the line spacing in the spectrum tends towards zero. The Fourier transform pair for an aperiodic continuous-time signal $x(t)$ is

$$x(t) = \int_{-\infty}^{\infty} X(F) e^{j2\pi Ft} dF \tag{3.8}$$

$$X(F) = \int_{-\infty}^{\infty} x(t) e^{-j2\pi Ft} dt \tag{3.9}$$

$X(F)$ is a function of the continuous frequency variable F. The inverse Fourier transform provides information needed for describing $x(t)$ as an integral of sinusoidal signals. With this pair of functions the frequency properties of the signal, commonly referred to the spectrum of signal $x(t)$, can be obtained. The key difference between the Fourier series and Fourier transform representation of the signal spectrum is that the latter has *continuous spectrum*.

The Parseval's relation for aperiodic, finite energy signal can be expressed as, [Proakis 1992],

$$E_x = \int_{-\infty}^{\infty} |x(t)|^2 dt = \int_{-\infty}^{\infty} |X(F)|^2 dF\,, \tag{3.10}$$

where the quantity

$$|X(F)|^2 = S_{xx}(F) \tag{3.11}$$

represents the *energy distribution* of the signal as a function of frequency. S_{xx} is called the energy density spectrum of the signal, and the integral of S_{xx} over all frequencies gives the total energy of the signal. Here the spectral units are in the form of power distribution over the frequency range, i.e. V^2/Hz, W/Hz.

Like in the case of continuous-time Fourier transform, the frequency analysis of a discrete-time signal is made with a Fourier transform of the time-domain signal $x(n)$. The discrete-time Fourier transform (DTFT) pair for aperiodic signal is, [Oppenheim 1997]:

$$x(n) = \frac{1}{2\pi} \int_{2\pi} X(\omega) e^{j\omega n} d\omega \tag{3.12}$$

$$X(\omega) = \sum_{n=-\infty}^{\infty} x(n) e^{-j\omega n} \tag{3.13}$$

$X(\omega)$ presents the frequency content of the signal $x(n)$, and is a periodic function with period of 2π. Thus, the signal spectrum has a frequency range from $-\pi$ to π or equivalently from 0 to 2π. Again, Dirichlet conditions must be fulfilled to guarantee the existence of the Fourier transform.

The energy of a discrete-time signal x(n) is defined as

$$E_x = \sum_{n=-\infty}^{\infty} |x(n)|^2 = \frac{1}{2\pi} \int_{-\pi}^{\pi} |X(\omega)|^2 d\omega \,. \tag{3.14}$$

This is the Parseval's relation for discrete-time aperiodic signal with finite energy. As in the case of the continuous-time signal, the quantity

$$|X(\omega)|^2 = S_{xx}(\omega) \tag{3.15}$$

represents the energy distribution of the signal $x(n)$, [Proakis 1992].

Table 3-1 summarizes the continuous-time and discrete-time Fourier series and Fourier transform.

Table 3-1. Summary of Fourier series and Fourier transform, [Oppenheim 1997], [Proakis 1992].

	Continuous time	
	Time domain	**Frequency domain**
Fourier series	$x(t)=\sum_{k=-\infty}^{\infty} c_k e^{jk2\pi F_0 t}$	$c_k=\frac{1}{T_P}\int_{T_P} x(t)e^{-jk2\pi F_0 t}dt$
	Continuous time Periodic in time	Discrete frequency Aperiodic in frequency
Fourier transform	$x(t)=\int_{-\infty}^{\infty} X(F)e^{j2\pi Ft}dF$	$X(F)=\int_{-\infty}^{\infty} x(t)e^{-j2\pi Ft}dt$
	Continuous time Aperiodic in time	Continuous frequency Aperiodic in frequency
	Discrete time	
	Time domain	**Frequency domain**
Fourier series	$x(n)=\sum_{k=0}^{N-1} c_k e^{j2\pi kn/N}$	$c_k=\frac{1}{N}\sum_{n=0}^{N-1} x(n)e^{-j2\pi kn/N}$
	Discrete time Periodic in time	Discrete frequency Periodic in frequency
Fourier transform	$x(n)=\frac{1}{2\pi}\int_{2\pi} X(\omega)e^{j\omega n}d\omega$	$X(\omega)=\sum_{n=-\infty}^{\infty} x(n)e^{-j\omega n}$
	Discrete time Aperiodic in time	Continuous frequency Periodic in frequency

As a conclusion, only well-defined signals with infinite length can be analyzed with Fourier series or with Fourier transform. There is also a difference when the signal is periodic and when it is aperiodic. Periodic signals have line spectrum defined at discrete frequencies whereas aperiodic signals have continuous spectrum. The spectral units are also different when the signal spectral power is analyzed. Periodic signal produces a power distribution/density and aperiodic signal produces an energy distribution/density spectrum. This generates a mathematical dilemma with spectral units when the spectrum of a signal containing both periodic and aperiodic parts is presented.

The Fourier series and Fourier transform thus allow us to view nonrandom time series as the weighted sum or integral of sinusoidal functions. Fourier series and Fourier transform basically involve the decomposition of the signal in terms of sinusoidal components, [Proakis 1992]. For the class of periodic signals the decomposition is called Fourier series and for the class of aperiodic signals the decomposition is called the Fourier transform. These traditional Fourier estimation methods have limitations when dealing with (quasi-) random or non-periodic waveforms. However, the principle of a time series as being composed of sinusoidal components is useful for random signal analysis.

3.2 Random Signals and Random Process Characterization

Random and unknown pseudo-random signals cannot be explicitly described before their occurrence. However, when observing such a signal over a long period, a

random signal or noise may exhibit certain regularities that can be described in terms of statistical values and probabilities. Analysis of a random signal is based on statistical methods. One important property of a random signal is that it cannot be predicted exactly. Nevertheless, the signal can be expressed in terms of its statistical properties such as the average, autocorrelation function or the spectral content of the signal power.

A random (*stochastic*) signal is defined as an output from a stochastic process. The instant value of such a signal can depend on one or many random variables. There exist no algorithm that can describe the random process or signal. The random signal can have any value in theory. Usually the possible output of the random system is limited, and can have some instant value from some particular set. In Figure 3.1, the limit set is presented as the sample space Ω, and symbol λ stands for the outcomes. If a real-value time function $X(t,\lambda)$ is assigned to every outcome $\lambda \in \Omega$, the system is a random process, [Hsu 1993].

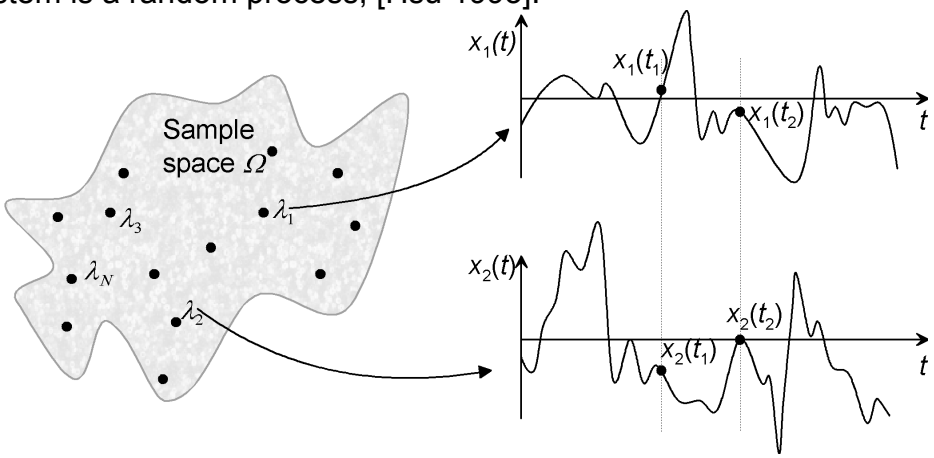

Figure 3.1 A random process $X(t,\lambda)$ is a function of the time t and the outcome λ. With a different outcome, the behavior of the process is different, although usually bounded.

When a measurement is performed from the output of a random process, it is natural to be aware of the various outcomes that are likely to arise. For example, in an SSM power converter, when measuring the current in normal operation, we usually know the upper and lower limit of the current. In addition, the *probability* or the *probability density function* plays an important role in signal analysis, and is usually somehow predictable in SMPS-signals.

Next, we simplify the analysis and concentrate on a single variable, one-dimensional random variable functions, $X(t)$ or simply X, the output denoted as $x_i(t)$ or $x(t)$. Therefore, the sample space is one-dimensional representing, for example, the input current at different time events. The probability with which different values are taken by the random variable is defined by the probability distribution function $F_x(x)$. The probability distribution function of X is

$$F_X(x) = P(X \le x), \tag{3.16}$$

where $P(\ )$ stands for the probability of the occurrence, and the function is defined for every x_i, i from $-\infty$ to ∞. The probability density function is

$$f_X(x) = \frac{dF_X(x)}{dx}. \tag{3.17}$$

Random processes (signals) are often characterized by using statistical averages. The *expectation value* $E[X(t)]$ or *mean* $\mu_x(t)$ of the sample record is, [Hsu 1993]:

$$\mu_x(t) = E\left[X(t)\right] = \int_{-\infty}^{\infty} x f_X(x) dx \tag{3.18}$$

Equation (3.18) assumes, that all possible outputs of the stochastic process are measured, which is not possible in practice. More often, there is a discrete, limited, set of sample values for the stochastic signal. With this limited sample record, or *sequence*, the whole system is analyzed and characterized. Of course, the data record is chosen to be long enough to fully describe the nature of the random system. One limit is also set by the discrete nature of the sequence; Rarely the data is analyzed with continuous time operations.

If the probability density function of all different signal sample sets are the same or can be approximated to be the same, the expectation value, or the mean $\mu_x(t_i)$, at time t_i can be estimated [Aumala 1998]. In practice, this means that the sample size M needs to be long enough to get a reliable estimate of the signal properties. When the sample set is limited, the mean can be estimated as

$$\mu_x(t_i) = \lim_{M\to\infty} \frac{1}{M} \sum_{p=1}^{M} x_p(t_i). \tag{3.19}$$

The autocorrelation of the of $X(t)$ is defined as

$$r_{xx}(\tau) = E\left[x(t)x(t+\tau)\right], \tag{3.20}$$

where τ is time delay (time shift). The expectation value of the autocorrelation function can be also estimated from a limited number of samples, [Aumala 1998]:

$$r_{xx}(t_i, t_i+\tau) = \lim_{M\to\infty} \frac{1}{M} \sum_{p=1}^{M} x_p(t_i) x_p(t_i+\tau) \tag{3.21}$$

Random signals can be classified in *stationary* and *non-stationary* signals by their nature. Stationary random signals behave more regularly and predictable than non-stationary signals. To be specific, if both the deterministic and probabilistic structures of the signal are constant in time, the signal is called stationary. A random process is called *wide-sense stationary* (WSS), if the mean of the system output is constant, [Leon-Garcia 1993],

$$E\left[X(t)\right] = \mu_x \ , \tag{3.22}$$

and the autocorrelation of the sequence depends only on time delay τ:

$$E[X(t)X(t+\tau)] = r_{XX}(\tau). \tag{3.23}$$

By setting $\tau = 0$, the following is obtained:

$$E[X^2(t)] = r_{XX}(0). \tag{3.24}$$

The equation represents the average power of the WSS process. Power is independent of time *t* and equals $r_{xx}(0)$.

If a random process is *strict-sense stationary* (SSS), its statistics are invariant to a shift of origin. Proper proof[2] of this statement is beyond the interest of this thesis because of the statistical nature of the power supply signals. Most of the statistical methods are valid only for stationary processes. Therefore, it is necessary to ensure that the process (signal) is stationary before employing statistical signal analysis tools. Usually, if the process is WSS, we can use statistical tools in the signal analysis, [Leon-Garcia 1993].

ASSUMPTION: Power converter with the spread spectrum modulation is a WSS – process.

This assumption is very important when statistical methods (e.g. power spectrum estimation) are used in mathematical analysis. This also sets limits on the signal under observation.

3.3 Power Spectrum Estimation

The finite-energy signals are characterized in the spectral domain by their energy density spectrum. Signals characterized as stationary random processes do not have finite energy and hence do not possess a Fourier transform (not fulfill Dirichlet condition 3). Such signals have finite average power and are characterized by a power density spectrum, [Proakis 1992]. The power spectral density (PSD), or the power spectral density function, can be utilized for estimating the signal *power* distribution at different frequencies. Search of periodic components from random-like signals is one typical application of power spectrum estimation, especially in the case of this study.

According to [Kay 1988], the PSD can be estimated with:

- Fourier transform of the autocorrelation function (Blackman – Tukey estimate).
- Fourier transform of the signal (periodogram or averaged periodogram, the Welch –method).
- Filtering with (infinite number of) narrow band band-pass filters.
- The frequency response of the parametric model made for the signal (so called modern spectrum estimation methods, for example autoregressive (AR) spectrum estimation).

[2] For rigorous analysis of stochastic system, see for example [Leon-Garcia 1993]

All methods mentioned above give the same result in theory. In practice, calculated spectrum estimates can be quite different even for exactly the same signal. Different methods have numerous different parameters that affect on the spectrum estimate. There is no universal approach or method for spectrum estimation, especially not in SSM-signals.

The autocorrelation function $r_{xx}(\tau)$ of a random process is a valuable statistical average characterizing the signal in the time domain. Since a sample function of a random process can be viewed as being selected from an ensemble of allowable time series, the spectrum for a random process must refer in some way to the average rate of change of the ensemble of allowable time functions, [Leon-Garcia 1994]. The rate of change in a random process can be analyzed with an autocorrelation function $r_{xx}(\tau)$. If the random process changes slowly with time, it remains correlated with itself for a long period of time and $r_{xx}(\tau)$ decreases slowly as a function of the time delay τ. A rapidly changing random signal quickly becomes uncorrelated with itself, and $r_{xx}(\tau)$ decreases rapidly.

One particular property of the correlation function is that the periodic nature of the signal can be analyzed and visualized with the autocorrelation function, thus linking autocorrelation to frequency analysis. The autocorrelation of the signal may also be needed when estimating the power spectral density of the signal (Blackman-Tukey method). To illustrate the use of the autocorrelation function in search of the periodicity of the signal, simulation was made with Matlab™. In Figure 3.2 a), there is a square-wave signal, which is mixed with the noise presented (b), and the resulting sum is presented in Figure 3.2 c). The period of the square-wave is buried under the noise, and it cannot be seen clearly in Figure 3.2 c). The normalized autocorrelation sequence is estimated from the wave in Figure 3.2 c) and the period of the original wave is clearly detectable in the plotted autocorrelation presented in Figure 3.2 d).

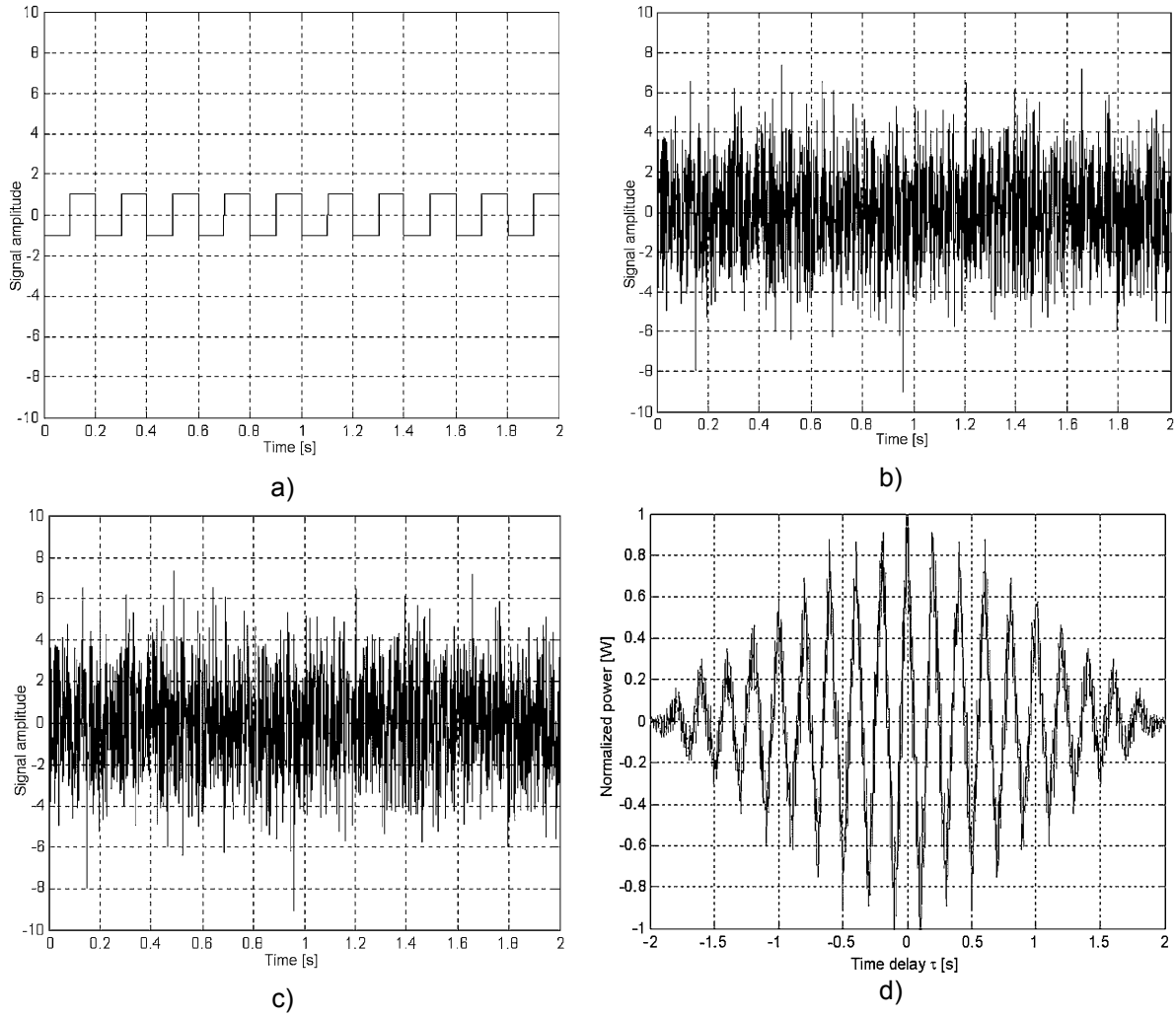

Figure 3.2. Use of an autocorrelation function estimate to find out periodicity in a test signal. Original signal (a), noise (b) and the sum of a) and b) is presented in c). The period of the original square-wave signal cannot be seen in (c), but the period is clearly detectable in estimated autocorrelation (d) of the periodic noisy signal presented in (c).

Fourier transform of the autocorrelation function represents the power distribution of the signal in the frequency domain. If the autocorrelation function of a random process is known, the power spectrum or the power spectral density can be obtained according to Wiener-Khintchine theorem, [Kay 1988]. Wiener-Khintchine theorem states, that the PSD of a WSS random process is given by the Fourier transform of the autocorrelation function:

$$D_{xx}(f) = \int_{-\infty}^{\infty} r_{xx}(\tau) e^{-j2\pi f\tau} d\tau \,. \tag{3.25}$$

The resulted PSD-function is two-sided including negative frequencies. The Wiener-Khintchine theorem can be applied also to a discrete-time WSS system. The PSD of the discrete random process $X(n)$ is defined as the Fourier transform of the autocorrelation sequence $r_{xx}(n)$, [Leon-Garcia 1994]:

$$D_{XX}(f) = \sum_{n=-\infty}^{\infty} r_{xx}(n) e^{-j2\pi fn} \tag{3.26}$$

Since the autocorrelation sequence used in spectrum estimation is a truncated version from a long, actual autocorrelation sequence, there exists a distortion in the shape of the spectrum estimate. However, after the invention and development of FFT-algorithms, the importance of this Blackman-Tukey-method has decreased, and the power spectrum estimation is commonly made with direct utilization of Fourier transform to the data itself, [Aumala 1998].

Since the continuous time signal can have in theory an infinite sample length, it is possible to have signals that contain an infinite number of frequency components. However, there is always a finite signal sample length in a practical measurement. Many signal analysis tools, including Fourier transform, have defined for an infinite sample length. To overcome this limitation, the measured signal is assumed periodic with the period of sample length N. Practical data analysis is usually made with a computer, which means that the analysis is made with a discrete-time signal. Owing to this, the theory presented next is limited to a discrete-time signal $x(n)$ with sample length $N \in M$ and a sampling frequency of f_{SA}.

The *periodogram estimate* of the power spectral density is defined as the Fourier transform of the signal itself. This can be calculated by the use of discrete Fourier transform (DFT), which is an efficient FFT algorithm for discrete sample sequence. For example if the data sample consists of an N-point sequence, the DFT-estimate for periodogram is, [Proakis 1992]:

$$P_{xx}\left(\frac{k}{N}\right) = \frac{1}{N}\left|\sum_{n=0}^{N-1} x(n) e^{-j2\pi nk/N}\right|^2 , \; k = 0, 1, \ldots, N-1 . \tag{3.27}$$

This means, that the periodogram has discrete frequency samples at frequencies $f_k = k/N$. This discrete time sampled signal and discrete time Fourier transform contains N samples from the total sample sequence M of the signal. The spectral resolution Δf_D for the DFT is, [Proakis 1989]

$$\Delta f_D = \frac{2\pi}{N} = \frac{f_{SA}}{N} . \tag{3.28}$$

The sample length and DFT/FFT-length has thus an immediate effect on the frequency resolution of the discrete spectrum estimate. Common property for all classical spectrum estimation methods is that the frequency axis is evenly distributed over the whole frequency range. The spectral resolution of the estimate is constant and can be calculated from the estimation parameters. In the case of DFT, the resulted spectrum estimate is a two-sided, periodic function with a period of sampling frequency f_{SA}. The spectrum is defined in frequency range $-1/2\, f_{SA} < f < 1/2\, f_{SA}$. The limited observation period of the sampled signal places a limit on the spectral resolution. This means that two different frequencies cannot be detected if the separation of these frequencies is less than the frequency resolution of the estimate.

The variance of the periodogram estimate is proportional to the square of the power spectral density and does not approach zero as the number of samples/points N in FFT algorithm increases. The periodogram estimates at different frequencies are uncorrelated random variables, [Leon-Garcia 1994]. This variance causes fluctuation in the periodogram estimate. High spikes at some frequencies generated by this random fluctuation may be misunderstood as periodic signals if the basic Fourier theory is misconstrued in random signal analysis. The sharpness of the spikes of a spectral estimate is not related to the resolution of the spectral estimator, [Kay 1987]. This means that the periodogram power spectrum estimate is not a consistent spectrum estimate of the true power density spectrum D_{xx} of the signal, [Proakis 1992].

In many cases of practical interest, the data contains both sinusoidal or narrowband signals in white noise. If the direct Fourier calculations are made to the signal parts of the signal may be lost under the sidelobes of the higher-level signal if the signals are closely spaced. To alleviate this sidelobe or smearing effect caused by truncation of the signal sample, a data window is commonly utilized. Windowing smoothes the ends of the truncated data segment thus making the signal periodic with period of data segment length N without discontinuity being caused by violent truncation. Data windowing reduces the magnitude of the periodogram at frequencies not near the signal frequency, [Kay 1988]. This kind of smoothing of the periodogram reduces the variance of the periodogram at the expense of reducing the spectral resolution, [Proakis 1992]. As an example, Hamming window is defined as [Kay 1987],

$$w(k) = \begin{cases} 0.54 + 0.46\cos\dfrac{\pi k}{M} & |k| \le N \\ 0 & |k| > N \end{cases} \tag{3.29}$$

Hamming window is also used in a later part of this work.

To clarify the effect of spectral resolution, variance and windowing in DFT, four different examples were calculated, Figure 3.3. It is clearly visible, that the number of points in DFT has an effect on the spectral resolution according to Equation (3.29). It can also be seen, that the signal power originally concentrated at a single frequency will smear over the frequency range and this leakage will generate sidelobes to the spectrum. These sidelobes and thus variance in the spectrum do not decrease if the number of points N in the DFT is increased. To reduce the leakage effect data has been windowed with the Hamming window in Figure 3.3 c) and d). It is evident, that the variance of the spectrum decreases. However, windowing decreases the spectral resolution and has a smoothing effect on the spectrum. It can be seen that the windowing has an effect on the magnitude and on the amplitude accuracy of the estimate.

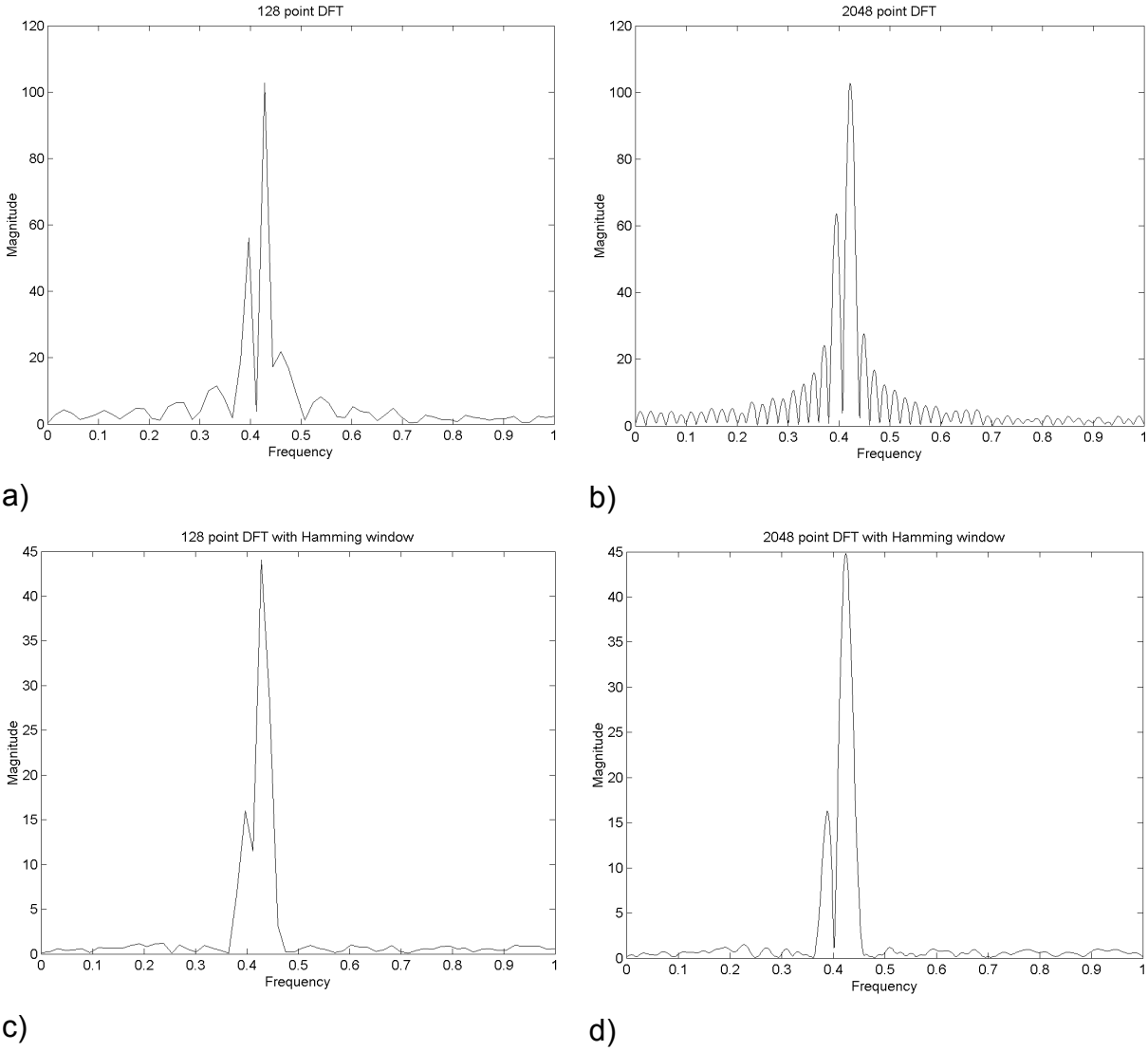

Figure 3.3. An example of spectral resolution, leakage and windowing in DFT. Original signal consists of two sinusoidal signals at frequencies 0.4 Hz and 0.41 Hz. The amplitude of lower frequency signal is half of the other signal. a) 128 point DFT without window, b) 2048 point DFT without window, c) 128 point DFT with Hamming window, d) 2048 point DFT with Hamming window.

The windowing function has an effect on the spectral resolution of the estimate. For the Hamming window, efficient spectral resolution $\Delta f_{\mathrm{D,H}}$ can be approximated from the calculation parameters, [Aumala 1998]:

$$\Delta f_{\mathrm{D,H}} \approx 1.30 \cdot \frac{f_{\mathrm{SA}}}{N} . \tag{3.30}$$

3.3.1 Welch Power Spectrum Estimate

In this thesis, the Welch power spectrum estimation method was chosen to be the one used in spectrum estimation in simulations. The Welch method uses a long sample set, calculating multiple spectrum estimates with a possible window function. After calculation of the multiple estimates, the average of these results is calculated to get the final result. This is an especially useful property when dealing with an SSM-signal, where the instantaneous spectrum estimate is changing continuously. This method was also proposed in the literature in spread spectrum analysis, [Mihalic 1999-1] and [Mihalic 1999-2] for example. The main idea of the Welch-method is presented in Figure 3.4.

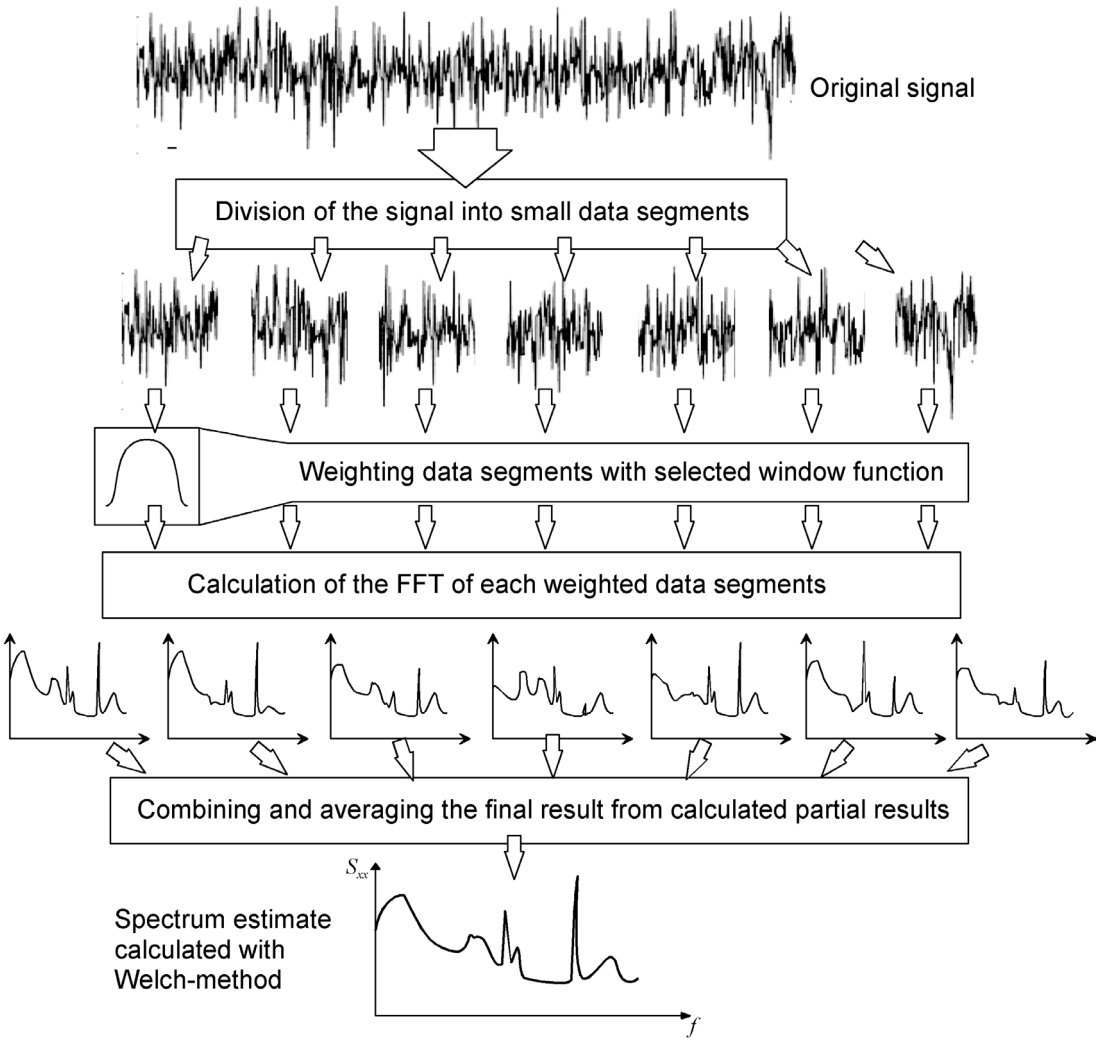

Figure 3.4. The main principle of Welch spectrum estimate. The original signal is divided into *L* data segments, weighted with a window function and a spectrum estimate of each data segment is calculated. Separate estimates are then combined and averaged to obtain a Welch spectrum estimate.

The Welch-method divides the signal sample in *L* data segments with an individual segment length of *N*. The segments used to calculate the individual Fourier transforms may overlap to artificially produce new points in the estimation. Figure 3.5 presents overlapping (a) and windowing (b) principle in the time domain.

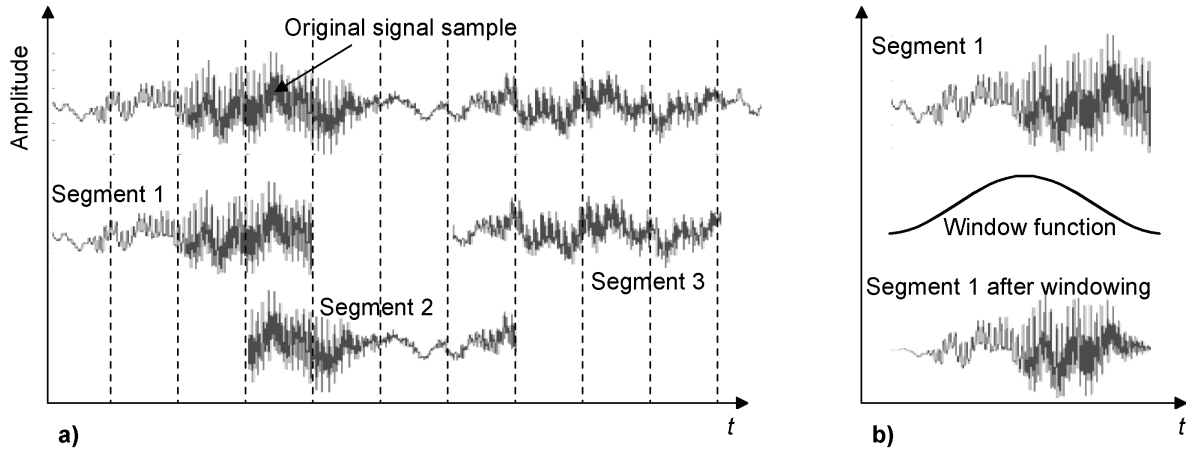

Figure 3.5. Overlapping and the windowing principle in Welch spectrum estimation. a) Original signal is divided here into three overlapping segments. Here the overlapping is 25 %. b) Each segment is windowed to get rid of discontinuities in the beginning and the end of the segment.

The so called modified periodogram used in the Welch method is defined as, [Proakis 1992]:

$$P_{xx}^{(i)}(f) = \frac{1}{NU}\left|\sum_{n=0}^{N-1} x_i(n)w(n)e^{-j2\pi fn}\right|^2 , \quad i = 0, 1,\ldots, L-1 , \tag{3.31}$$

where U is the normalization factor of the window function,

$$U = \frac{1}{N}\sum_{n=0}^{N-1} w^2(n) . \tag{3.32}$$

The Welch power spectrum estimate is the average of these modified periodograms, [Proakis 1992],

$$P_{xx}^{W}(f) = \frac{1}{L}\sum_{i=0}^{L-1} P_{xx}^{(i)}(f) \tag{3.33}$$

To clarify differences in spectral estimation, an example of two different spectrum estimates are presented in Figure 3.6. The frequency-hopping signal presented Appendix A is the same in both cases, only the time interval from where the spectrum estimate is calculated is changed. In Figure 3.6 a) and c), the signal used to calculate the estimate is from the beginning of the sampled segment and in b) and d) the sample sequence is from the end of the segment, for details see Appendix A.

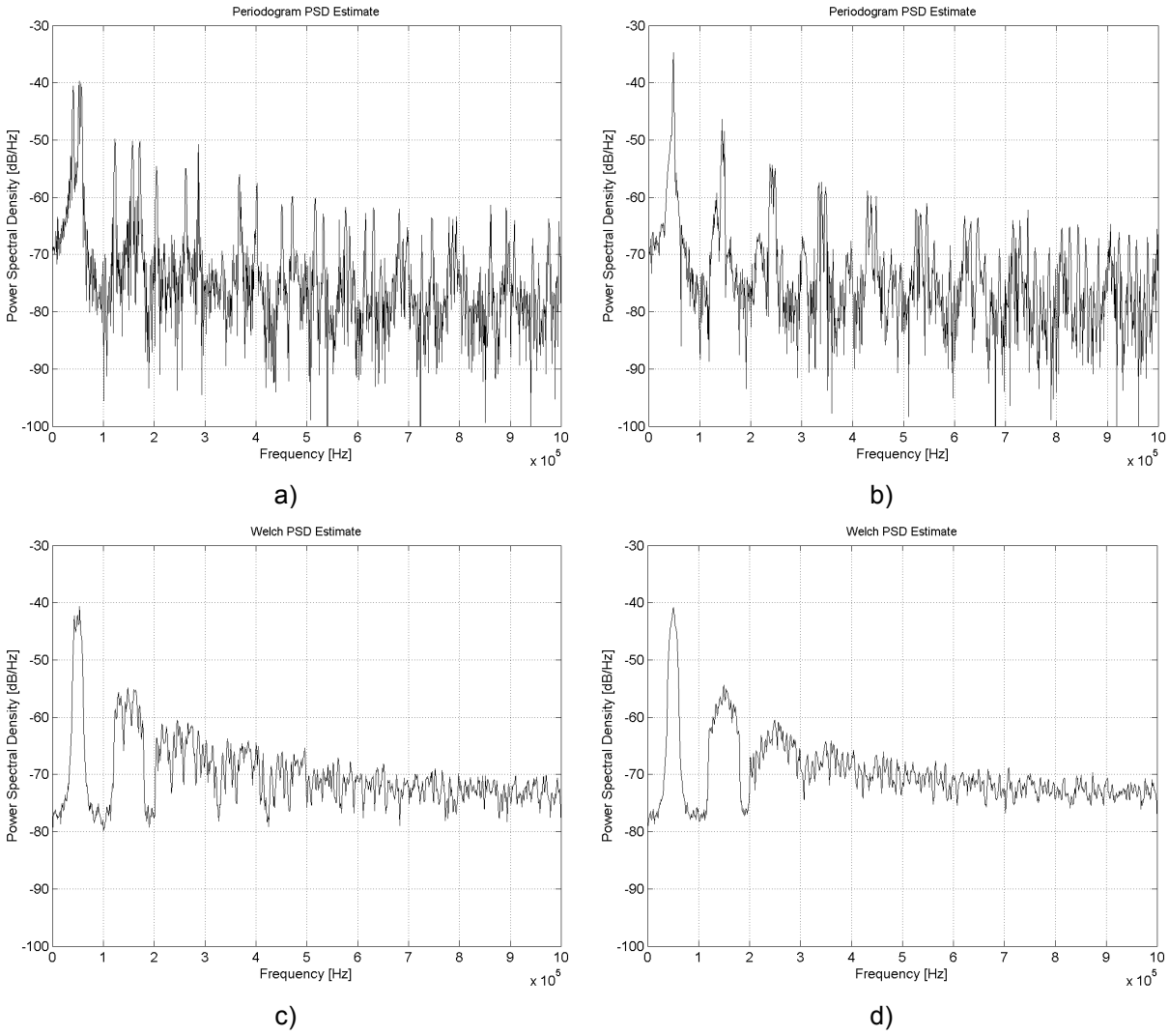

Figure 3.6. Calculated periodogram (a & b) and Welch (c & d) spectrum estimates of an example signal. The signal is from a simulated frequency-hopping converter. The sample data segment for the spectral estimation was picked up from an arbitrarily chosen time interval. Both estimates used a 2048-point discrete Fourier-transform, but the Welch-estimate was averaged over a longer period with several segments thus giving a smoother and repeatable spectrum estimate.

When using a periodogram estimate, Equation (3.27), the spectrum estimate looks quite different in Figure 3.6 a) and b), although this is presenting the spectrum estimate of the same signal. The Welch method (c & d) gives a power spectral estimate with less variance. Although the shape of the estimate is a little different in c) and d), the difference is not so dramatic that it is in the case of periodogram estimate.

It is obvious from the example, that averaging the spectrum estimate over a longer period reduces the variance in the magnitude of the spectrum estimate. This is very important when analyzing variable-frequency techniques. As a drawback, averaging loses part of the spectral information.

3.4 Spectrogram in EMI-Analysis

A given signal can be presented in numerous different ways, although the most important and fundamental representations are made in time-domain and in frequency domain. The link between time and frequency is the Fourier transform. Spectral information in the frequency domain is essential in customary EMI-analysis. However, there are several problems when analyzing continuously changing signals with traditional analysis tools such as Fourier-based methods or with ordinary EMI measuring devices: the fundamental theory behind these methods assumes the signal frequency content to be constant over infinite time.

One very useful time-frequency analysis tool is the *spectrogram,* especially when dealing with constantly varying signals. The spectrogram is a time-dependent short-time Fourier transform (STFT) for a sequence computed using a sliding window. STFT can be used to localize both time and frequency. The theory behind the STFT was originally introduced by Daniel Gabor, [Gabor 1946] and the STFT spectrogram was documented in [Koenig 1946]. Spectrograms are used in applications where the spectral content of the signal changes continuously, such as speech recognizing, analysis of biomedical signals, radar, communication and condition monitoring, [Qian 1999], [Dripps 1997], [Kim 2000], [Au 1998], [Lindh 2003]. There are also other time-frequency analysis tools, such as wavelets, [Daubechies 1990] and Wigner-Wille distribution, [Qian 1999]. Hung and Chi, [Hung 2001] proposes even the use of wavelet transform for the analysis of electromagnetic power system transient.

It is impossible to figure out the essence of the non-stationary signal from a single sample with a normal, time-independent spectrum estimation method. The resulting estimate of the signal is dependent on the instantaneous time when the sample is acquired. With the aid of the STFT spectrogram, the spectrum estimate can be analyzed over a long period and changes of the spectral content of the signal in time can be detected. The spectrogram can be formalized as a graph, which presents multiple spectral estimations against time, calculated from small sample sequences. A conventional time-window spectrogram of the signal $x(t)$ is, [Altes 1984],

$$STFT(t_i, f) = \left| \int_{-\infty}^{\infty} x(t) w(t - t_i) e^{-j2\pi ft} dt \right|^2 , \tag{3.34}$$

where $w(t)$ is the window function for local spectral analysis in the neighborhood of the time instant t_i. Instead of processing the entire signal at once, the STFT calculates the Fourier transform on a block-by-block basis. The resulting Fourier transform contains both the frequency and time behavior of the signal. Individual blocks used in the calculation can overlap and some weighted windowing function can be used like presented in Figure 3.5.

The window function balances the time and frequency resolution of the spectrogram. If DFT is used in spectrum estimation, the spectrogram has a spectral resolution according to Equation (3.28), where N is now the window length. Since the spectrogram is plotted against time, the window length N affects also on the time resolution. The time resolution in a conventional spectrogram is

$$\Delta t = \frac{N}{f_{sa}}. \tag{3.35}$$

This means that a short window leads to a good time resolution and poor frequency resolution and vice versa, [Qian 1999].

In a graphical form, a spectrogram is a plot of sequential spectrum estimates. These short-term spectrum estimates are calculated with selected frequency resolution and the process is repeated many times over a long sample sequence in chronological order. One axis represents the signal spectral estimate magnitude, another axis presents the frequency and the third axis presents time, Figure 3.7. A three-dimensional graph is quite impractical; usually colors are used to express the signal level and to put the spectrogram in 2-D format.

In this thesis, the spectrogram has been used as one measure of noise level. Therefore, the main features of the spectrogram are presented next. In the example analyzed next, there is a frequency-modulated signal, where the carrier signal is a 50 kHz square-wave and the modulating wave is a triangular wave. The frequency of the modulating triangular wave is 33 Hz thus giving a period of approximately 30 ms. The frequency-modulator has been set so, that the instantaneous frequency of the modulated signal changes between 35 kHz and 65 kHz. The signal and both the spectrum and the spectrogram presented next are calculated with Matlab™.

First, the spectrogram calculated in Figure 3.7 is presented as a three-dimensional graph to introduce the idea of a spectrogram. A change in instantaneous frequency is visible and the triangular waveform of the modulating wave is clear. Also the period of the modulating wave can be tracked from the graph.

A two-dimensional spectrogram is presented in Figure 3.8. This form of spectrogram is used later in this study. The amplitude reading accuracy is poor in 2-D format, but the time-dependent nature of the signal is clearer. The frequency of the modulating wave (33 Hz) and the frequency deviation (15 kHz in fundamental) can be defined from the graph.

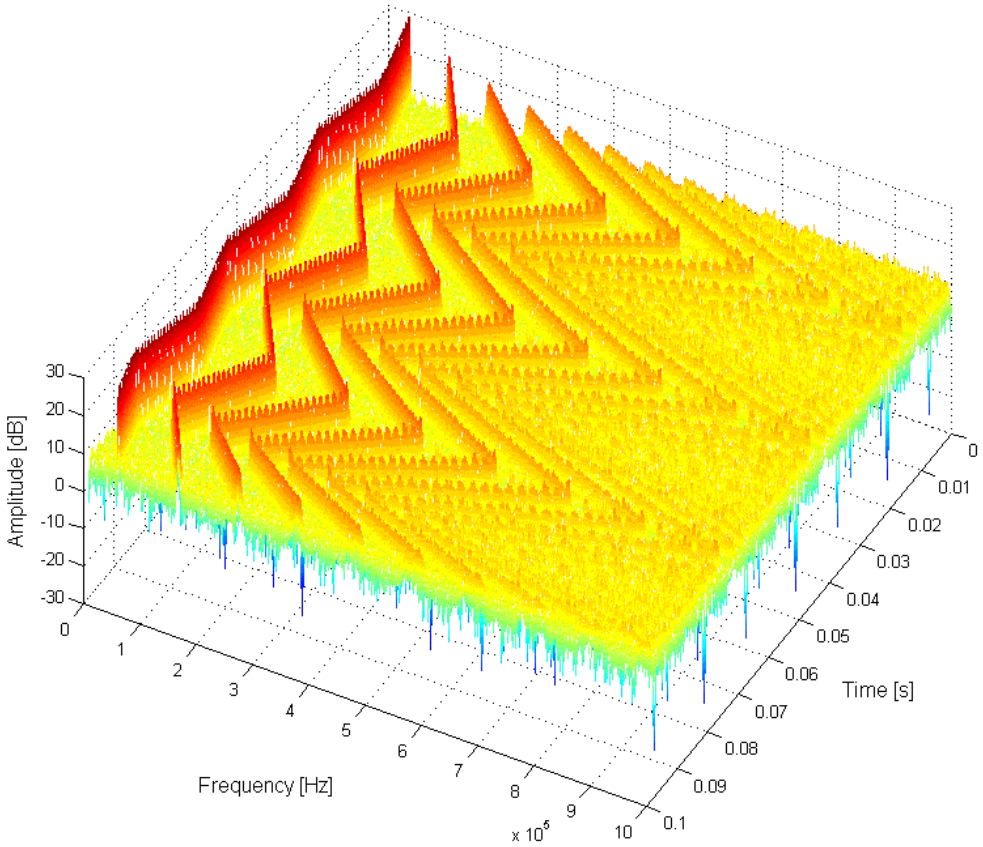

Figure 3.7. The spectrogram as a three-dimensional plot. Frequency and time are presented in the horizontal axes, signal power spectral density is presented in the vertical axis.

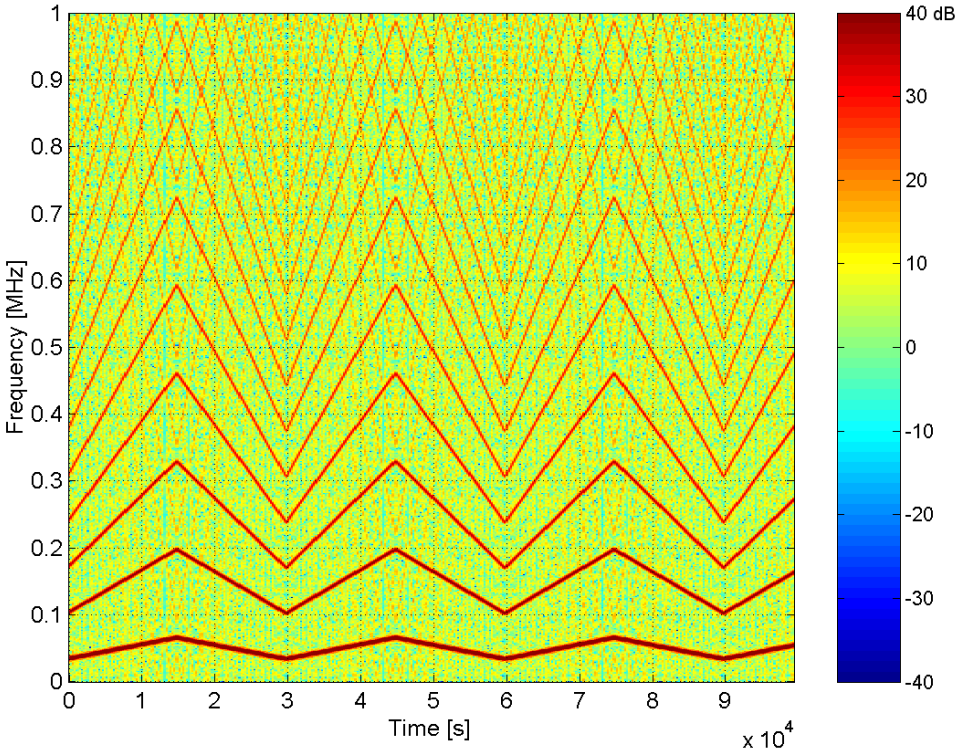

Figure 3.8. The spectrogram in 2-D format. Time is presented in the horizontal axis and frequency in the vertical axis. “Hot” colors in the graph represent high spectral magnitudes and “cold” colors represent low spectral levels, see the color bar on the right. This form of spectrogram is used later in this study.

For a comparison, the Welch power spectrum estimates with two different FFT-lengths were calculated from the same example signal, Figure 3.9. Frequency resolution Δf of these estimates is 200 Hz and 9 kHz. A skilled person with experience in frequency modulation could estimate some properties of the signal, but the modulating wave, very clearly detectable in Figure 3.8, cannot be accurately read from the PSD estimate.

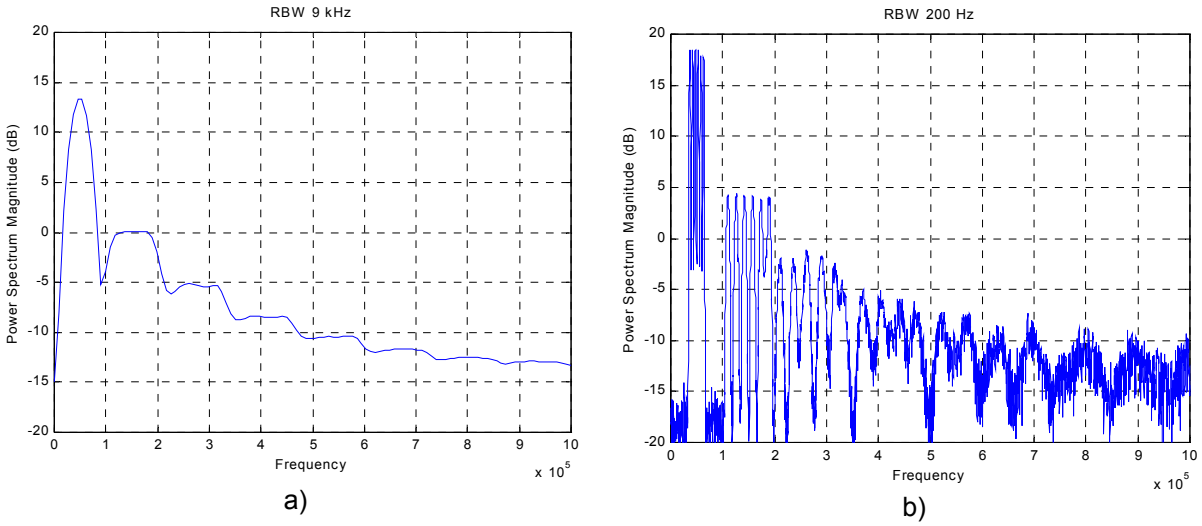

Figure 3.9. The PSD calculated in Matlab from the frequency-modulated signal, (a) FFT length 222, overlapping 111, Δf 9 kHz (b) FFT-length 10000, overlapping 5000, Δf 200 Hz. Signal properties are much harder to detect, especially the frequency of the modulating wave is impossible to define from these graphs.

A spectrogram is not only a numerical analysis tool for simulations. There are several test instruments capable of spectrogram mode display. For example, Tektronix WCA 380 wireless communication analyzer has a bandwidth over DC to a 8 GHz range, [Tektronix 2003]. It can simultaneously acquire a 30 MHz bandwidth, and plot a real time spectrogram over this frequency range. A screenshot from Tektronix WCA 330 is presented in Figure 3.10. The algorithm for the frequency hopping signal used in this example is presented in Appendix A. Unfortunately, the instrument could not be used in practical measurements of this work because the instrument was not available during these measurements.

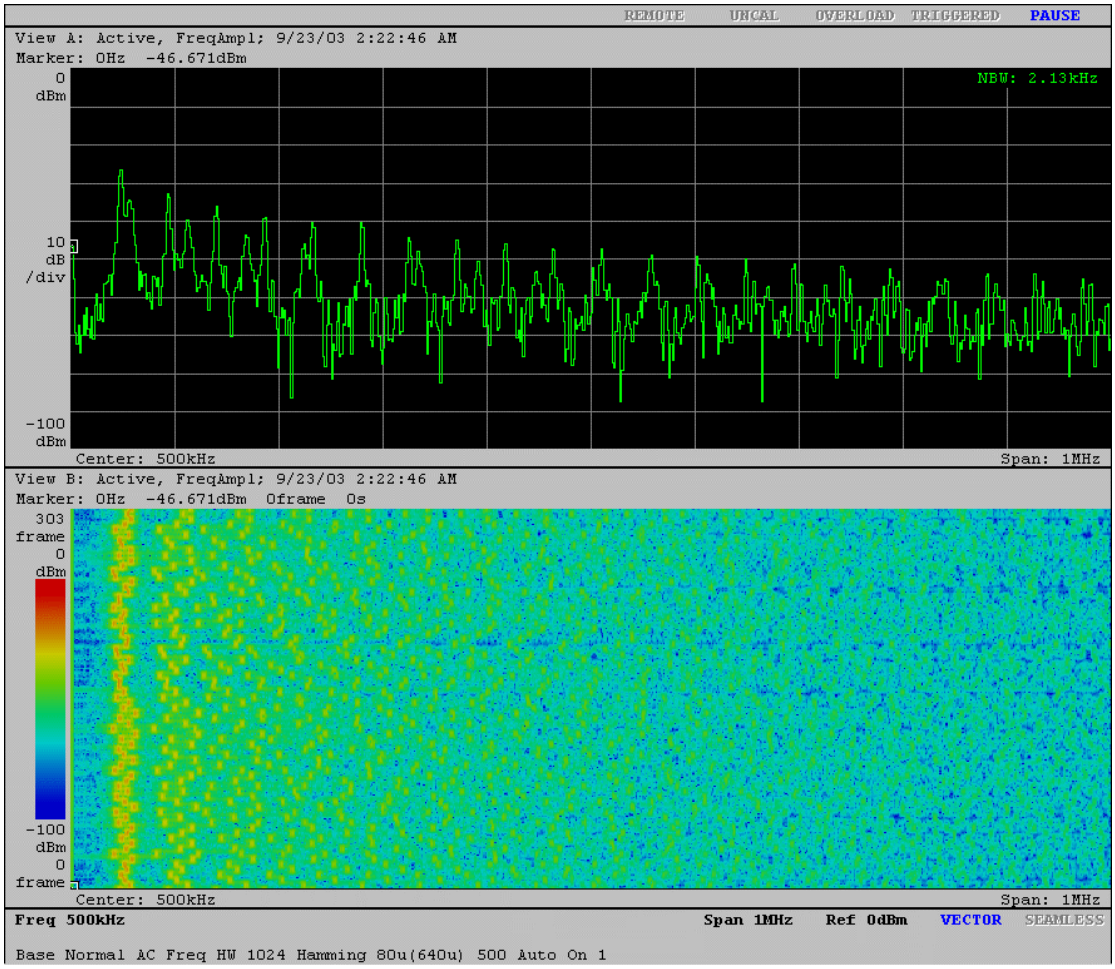

Figure 3.10. Measured spectrum and spectrogram of the frequency hopping signal. The upper graph is the single spectrum calculated at some specific time instant. The lower part is the spectrogram of the signal, time in the vertical axis. The horizontal axis is frequency from 0 Hz to 1 MHz. The amplitude unit is dBm, decibels compared to one milliwatt.

There are also several drawbacks in the spectrogram. First, the graph itself is hard to read accurately, and therefore visual reading accuracy is poor in 2D-format. However, this is not a problem if the data is analyzed numerically. Secondly, if a graphical presentation is needed, color pictures are preferred. Of course, the 2-D spectrogram can be scaled on grayscale, but parts of the information may be lost. Finally, a person with color-blindness may find it difficult to read these kinds of figures.

The spectrogram cannot be used as an accurate tool when analyzing the EMI performance of the system according to the common EMC–standards. There is no mention about the use of a spectrogram in compliance testing, and there will not be for awhile. The reason behind this is that there are several problems in reading the spectrogram: the main problem is that the graph changes continuously with time. Absolute values are also hard to read from the graph. Therefore, the usefulness of the spectrogram is strongly dependent on the skills and experience in reading the spectrogram. Still, it can be a very valuable aid in design and testing when anticipating EMI–properties of the system. Of course, the information in the spectrogram can be analyzed numerically and there is no reason why the spectrogram cannot be used in compliance engineering if common limits and methods are agreed.

3.5 Few Aspects in EMC Measurements

First EMI test receivers were manually tuned radio receivers with analog meters for indication. The receiver was tuned to measure some specific frequency band and the indicated voltage or power level was recorded. To measure the whole frequency range of interest, several sequential measurements have to be carried out. The measurements in different sequential frequency bands are made in steps, thus giving the name of stepping receiver. Currently available EMI test receivers use digitally controlled measuring options, and the measurement can be automatized. However, the general operation principle of the receiver itself has remained the same over the last decades. The EMI test receiver is one of the most important instruments for measuring interference emissions and in many cases the only possible one.

A scanning spectrum analyzer (SA) is another test instrument suitable for frequency domain analysis. The low price and wider applicability of a general-purpose spectrum analyzer makes the idea of using an SA in EMI measurements tempting. In addition, the operating principle of a scanning SA and a stepping receiver is very similar. When the analyzer is swept or tuned (stepped) over the frequency range of interest, graphical presentation of the measured spectrum can be obtained. Both an SA and EMI receiver are superheterodyne receivers and measure the signal voltage level frequency selectively. Both types are also used to make radiated and conducted EMI measurements, [Schaefer 1998].

Operation of a typical receiver is based on stepping or sweeping the resolution bandwidth (RBW) or intermediate frequency bandwidth (IFBW) over the frequency range of interest. The IFBW should be narrow to have good spectral resolution. On the other hand, a narrow IFBW directly effects on the spectrum measuring time and quickly changing pulses and aperiodic signals may be lost in the final test results. A test receiver also has several components such as a preselection filter, an IF-filter, average and quasi-peak detectors and a detector diode that have finite settling times. Therefore, the measuring has to be done with a long enough measuring period. A simplified block diagram of a test receiver is presented in Figure 3.11.

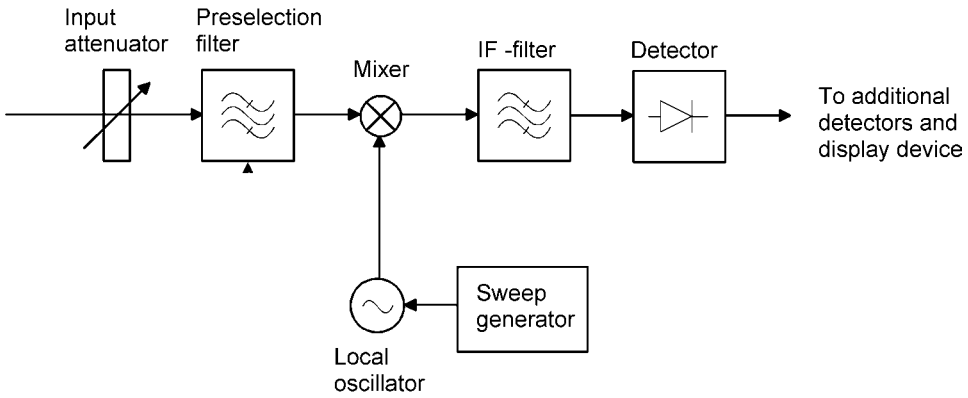

Figure 3.11. The simplified operating principle of a typical EMI test receiver. A tunable preselection filter limits the input signal bandwidth to prevent mixer overload. A suitable IF-filter with a proper IFBW (RBW) is placed after the mixer and the desired detector is connected to the output.

The operating principle of a typical EMI-test receiver is quite similar to a normal sweeping spectrum analyzer. The main difference is the lack of the preselection filter

and different kinds of special detectors in a spectrum analyzer, [Maroney 1999]. Absence of the preselection filter may cause overload and nonlinear operation in the mixer of the SA, thus generating distortion and erroneous results when a broadband signal is measured. Another drawback in a common SA without the preselection filter is that calibration test pulses specified in standard CISPR 16-1 requires an insertion of a RF attenuation to prevent mixer overload and to satisfy the linearity requirements. This additional attenuator decreases the sensitivity of the SA, [CISPR 16-2 1999]. There are also concerns within the EMC community about the measurement capability of the sweeping spectrum analyzer, [Maroney 1999], [Schaefer 1998].

Evolution in digital techniques has raised the interest in fully digital implementation of the EMI spectrum analyzer. So far, digital EMC compliance test instruments are not commercially available for RF-emission measurements. Only frequency range of line harmonics [EN61000-3-2 2001] can be covered on these FFT-based spectrum analyzers. The main problem in broadband digital spectrum analyzers is the poor resolution of the high-speed analog to digital converters (ADC). A requirement on the dynamic range in a practical measurement is over 100 dB, which is still too much for ADCs in the gigahertz-range.

One low cost approach in digital sampling of an EMI signal is the use of a digital oscilloscope with sufficient sample memory capacity. For example, Parvis et al. [Parvis 2003] propose a precompliance EMC test setup based on a sampling oscilloscope and computer calculating the spectrum by filtering the sample data. The setup follows the CISPR-16 recommendations with peak detection capability. Proposed setup uses 8-bit ADC thus giving poor amplitude dynamics. The signal to quantization noise ratio (SQNR) can be used to estimate the dynamic range of the ADC, [Proakis 1992]:

$$\mathrm{SQNR} \approx 6.02b + 1.25 \quad [\mathrm{dB}] , \tag{3.36}$$

where b is the number of bits in ADC. The theoretical dynamic range for a 8-bit instrument is approximately 50 dB and in practice even lower. This is almost one third of the dynamic range of a high-end analog receiver.

Another limiting factor in a sampling oscilloscope is the length of the sample memory. For example, in the test setup proposed in [Parvis 2003], the maximum frequency was limited to 10 MHz because of the sample memory length, which was 8000 points. However, the maximum frequency is dependent on the measuring apparatus and can be much higher in top-class oscilloscopes.

CISPR 16-1 [CISPR 16-1 1999] defines requirements and specifications of a EMI test receiver. A receiver's intermediate frequency (IF) bandwidth, IF filter shapes, detectors, amplitude accuracy and other electrical characteristics are specified. In the frequency band from 9 kHz to 1 MHz, a specific EMI receiver is preferred in a standard CISPR 16-1.

3.5.1 Detectors in EMI-Measurements

The detector of a measuring instrument plays an important role in EMI-measurements. For example, CISPR 16-1 specifies the characteristics of detectors that are required to perform EMC-measurements. Several of the specific product categories require the use of both quasi-peak (QP) and average detectors for disturbance measurements. Many spectrum analyzers do not have these detectors. A basic form of detector that is used in both EMI receivers and spectrum analyzers is the peak detector (envelope detector). A simple envelope detector consists of a diode followed by an *RC* circuit, Figure 3.12. The *RC* time constant is selected so that the output can follow the peak value of the input coming from the IF section.

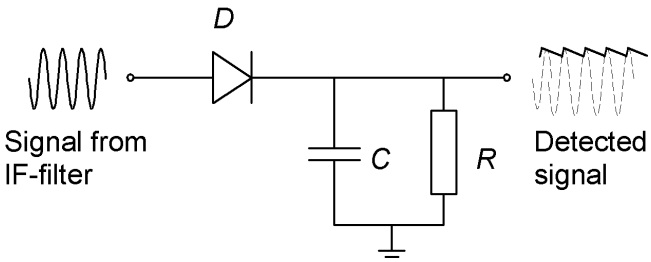

Figure 3.12. A simple peak detector with a sinusoidal input signal.

The peak detector is the most practical detector mode for preliminary testing. QP and average detectors are used when compliance testing is performed. The time constants of both QP and average detectors are very long, and the measurement is very time consuming. Therefore, a peak detector is often used for product testing. If the results with a peak detector measurements fall inside the limits of the standard limits, it will also fulfill the requirements with QP or average detectors, because the reading will be less with these detectors compared to a peak detector, see Figure 3.13. Examples of time constants in the QP-detector are presented in Table 3-2.

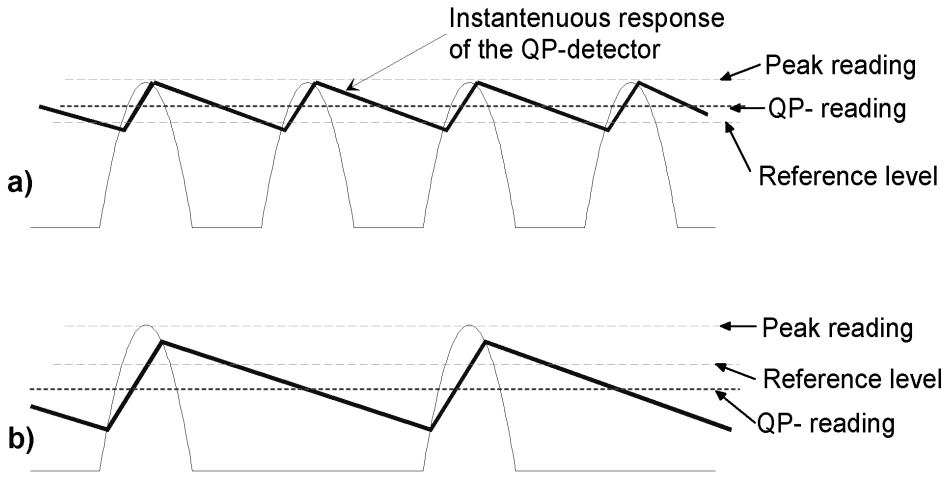

Figure 3.13. Operation of the quasi-peak detector with different input signals. The QP-reading will be less than the peak reading of the detector. The difference will be even much larger when the signal has a low repetition rate.

Figure 3.13 also illustrates the benefit of the SS-signal when measured with an QP-detector: A constantly changing repetition rate will give a lower QP-reading than a constant signal. An QP detector weighs signals according to their repetition rate, which is a way of measuring annoyance factor of the signal. Originally the QP-detector was designed to obtain a reading proportional to the annoyance effect of interference on broadband radio listeners, [Schaefer 1998]. A detailed analytical approach of the modulation effect on QP-detectors is presented in the paper from Ristau and Hansen [Ristau 1997]. Some practical aspects about detectors are also presented by [Schaefer 1998].

Table 3-2. Parameter values for a quasi-peak detector according to CISPR 16.

	Frequency range	
	0.15 - 30 MHz	30 - 1000 MHz
Bandwidth, kHz	9	120
Charging time constant, ms	1	1
Discharging time constant, ms	160	550

An average detection is similar in many respects to peak detection. First, the signal is fed from the IF-section to the envelope detector. After the envelope detector, the peak detected signal is fed through a filter whose bandwidth is much less than the IF bandwidth. The filter averages the higher frequency components at the output of the envelope detector.

The most important detector modes in EMI measurements are summarized next:

- *The peak detector*, produces an output proportional to the maximum peak value of the signal emerging from the IF-filter without any relation to the shape of the signal envelope
- *The quasi-peak detector*, produces an output that is a weighted, complicated product of the envelope of the signal emerging form the IF-filter.
- *The average detector*, detects the long time average of the amplitude of the envelope of the signal emerging from the IF-filter.

An example of the results with different detector modes is presented in Figure 3.14. The test signal is a frequency-hopping signal measured directly from the arbitrary signal generator. The algorithm generating the signal is presented in Appendix A.

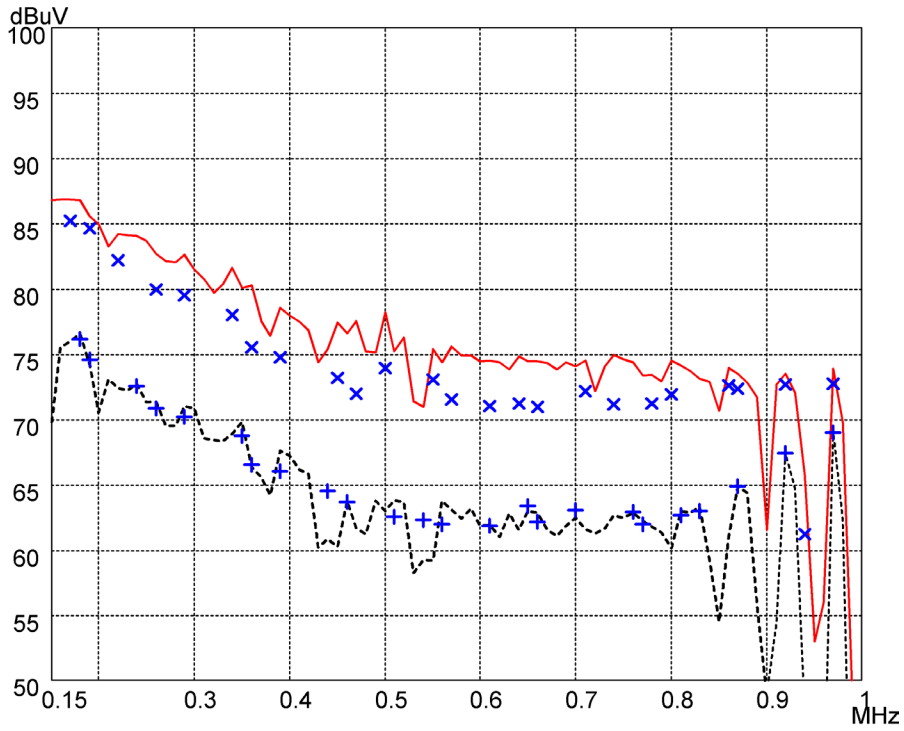

Figure 3.14. An example of different readings with different detector and measurement time setups from the same test signal. The solid line represents the peak reading and the dotted line the average reading with a 100 ms measuring time/IFBW. The x-marked points are QP-readings and the +-marked points are the average readings with a 1 s measuring time/IFBW. The IFBW in all measurements is 10 kHz.

Figure 3.14 shows that reading with a peak detector gives maximum values compared to other detector modes. The measuring time for both peak and average detector pre-scans were 100 ms for 10 kHz IFBW and the stepping was 10 kHz. After this pre-scan, quasi-peak and average measurements were made at 25 sub-ranges around a local maximum of pre-scan data. These sub-range measurements were made with a one second measuring time to better expose the possible maximums of the varying signal. An envelope of the QP-detector quite closely follows the peak reading, despite the different measuring time and detector operating principles.

Measurements in this work have been made with the peak detector. This gives a uniform platform for the comparative study made in this thesis. This is also common practice in practical compliance engineering where the initial EMI measurements are made using a peak detector. This mode is much faster than quasi-peak or average modes of detection. It would make a good subject for another study to examine the effect of detector modes and test receiver properties in different spread spectrum signals. A peak detector will also give the maximum reading of the signal under test.

3.5.2 Sweep of the Test Instrument

The stepping and sweeping operating principle of the current EMC-test equipments causes also a small error on the spectrum estimate and sets limits on the signal detection, [Southwick 1989]. The operating principle of a typical stepping test receiver and sweeping spectrum analyzer frequency scan is presented in Figure 3.15, [Schaefer 1998].

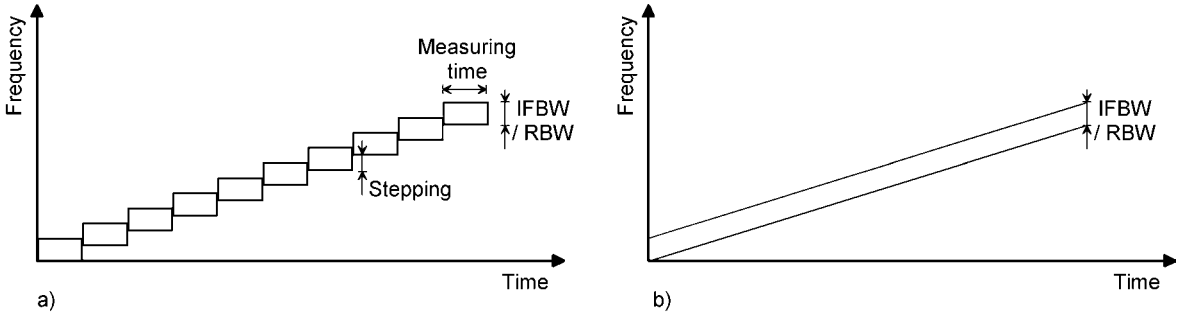

Figure 3.15. Operating principle of a) a stepping EMI test receiver and b) a sweeping spectrum analyzer. Within the measuring time, the level of the signal in the small bandwidth (IFBW/RBW) is detected and the measurement bandwidth is stepped to the next center frequency, a). A sweeping SA makes the single or multiple frequency sweeps over the frequency range with some specific sweep rate, b).

Both instrument types measure only a small part of the frequency range in some instantaneous time of the frequency scan. The bandwidth under detection equals the selected IFBW/RBW. Measurements in the stepping receiver are made sequentially with specific measurement time. After this measuring time, the receiver is tuned to the next center frequency with some specific frequency step. This frequency step equals typically the bandwidth of the IF-filter or half of the IFBW. The sweeping analyzer continuously tunes the mixer of the analyzer with some specific sweep rate. The sweep rate is expressed generally in units of Hz/s.

Instantaneous noise power in several frequency bands can be high without detection owing to the measuring principle: frequency range is stepped or scanned sequentially, detecting the signal with only a small bandwidth with time. An example of this kind of signal detection is presented in Figure 3.16, where the receiver is scanning a spread spectrum signal.

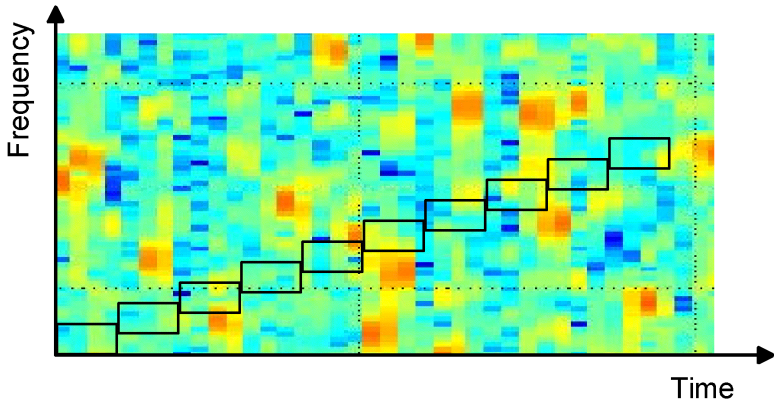

Figure 3.16. The measurement result may contain a large error and uncertainty while measuring the spread spectrum signal. The figure presents a stepping receiver scan over a spread spectrum signal, which is presented here as the form of a spectrogram. The rectangles in the picture represent the frequency scan of the stepping receiver.

It is obvious, that the signal in Figure 3.16 is not properly detected, and the resulting measurement result is a random variable. This has to be taken into consideration when making EMC-measurements with SS–signals, [Southwick 1989].

SA has one strength over the stepping receiver: Multiple past scans be performed to detect the broadband signals. After detection, a slow scan be used to measure these

signals. A typical stepping receiver does not have this quick-scan ability for signal recognizing and therefore the measurement with a stepping test receiver can be very time consuming.

The IFBW of the test receiver plays an important role in measuring the aperiodic and modulated signals. In theory, with spread spectrum techniques, it is possible to spread the energy from one harmonic to an infinite number of closely spaced frequencies [Stone 1995]. If all these frequencies fall within the IFBW of the test receiver, they will appear at same frequency. If the deviation of the switching frequency modulation is more than the IFBW of the test receiver, these frequencies cannot be measured accurately.

The resolution bandwidth has also a significant meaning in tracking fast changing signals. As a rough estimate, the settling time T_{set} of the filter is approximately the inverse of the filter bandwidth, [Sander 2003]:

$$T_{set} \approx \frac{1}{\mathrm{RBW}} \tag{3.37}$$

For measurement of the peak power, the analyzer RBW has to be set wide enough to settle within the pulse duration. The settling times for filters used in this work according to Equation (3.37) are 100 μs for 10 kHz IFBW and 5 ms for 200 Hz IFBW.

The article from Deb [Deb 1999] concerning the EMI measurement problems in frequency hopping communication sets, emphasizes on the correct sweep rate of the receiver. The dwell time T_D of the receiver is defined as, [Deb 1999]:

$$T_D = \frac{\text{Receiver IFBW } [\text{Hz}]}{\text{Sweep rate } [\text{Hz/s}]} \tag{3.38}$$

Deb concludes that the dwell time of the receiver has to be longer than the length of the hopping sequence to increase the probability of signal detection. Impulse bandwidth considerations of the test receiver were also reported by [Schaefer 1999].

In general, the measured signal should be stable long enough to get a reliable measurement result. If the EMI spectrum is time variant, the result of the measurement will be inaccurate. Effects of the limited response time of a test receiver system were analyzed in [Silventoinen 2001] and [P1]. Based on this test, the measurement time of the test receiver with 10 kHz IFBW should be at least 750 μs, which means that the signal should be stable at least that time to achieve stable result in signal detection.

The effect of the measurement time is compared in Figure 3.17. The same frequency-hopping test signal described in Appendix A was used in this measurement made with Rohde & Schwarz ESHS-30.

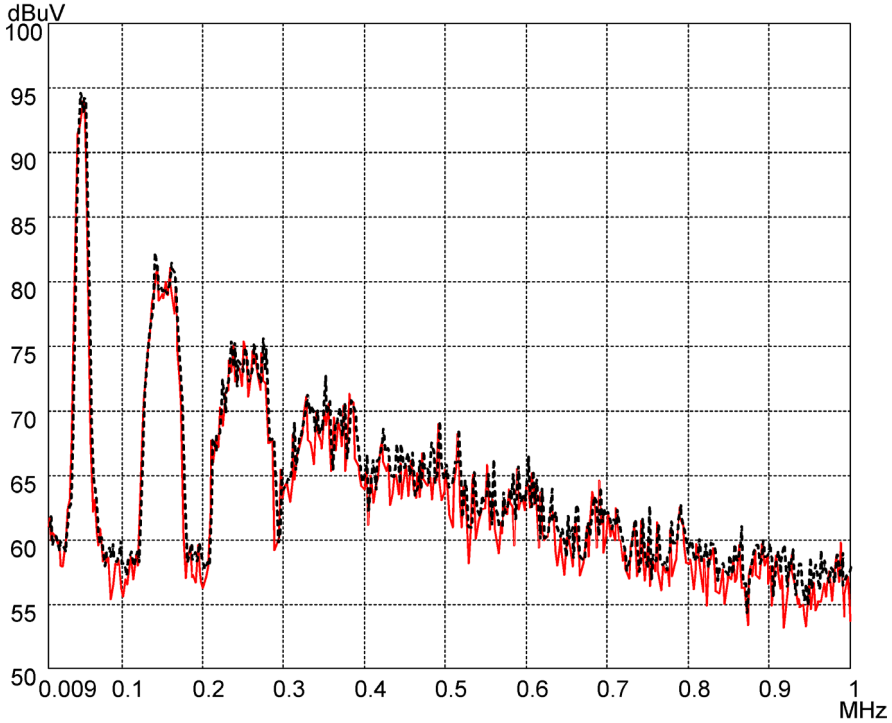

Figure 3.17. Measurement of the frequency-hopping test signal with different measuring times. The solid line represents the result obtained with a 20 ms measuring time/IFBW and the dotted line represents the measurement with a 100ms/IFBW. Both measurements are made with a peak detector and 200 Hz IFBW.

It can be seen that the difference is small, approximately less than 1 dB for the whole frequency range. The difference can be explained by the quasi-random nature of the signal. This test was repeated several times and the results were parallel with this example presented in Figure 3.17. Therefore 20 ms measuring time was selected in this study to reduce the measuring time in EMI-tests.

A comparison was made also between a spectrum analyzer (Agilent E7402A) and an EMI receiver (Rohde & Schwarz ESHS-30) to find out the possible differences in the results, Figure 3.18. The signal used in the test was the same signal as in a previous example.

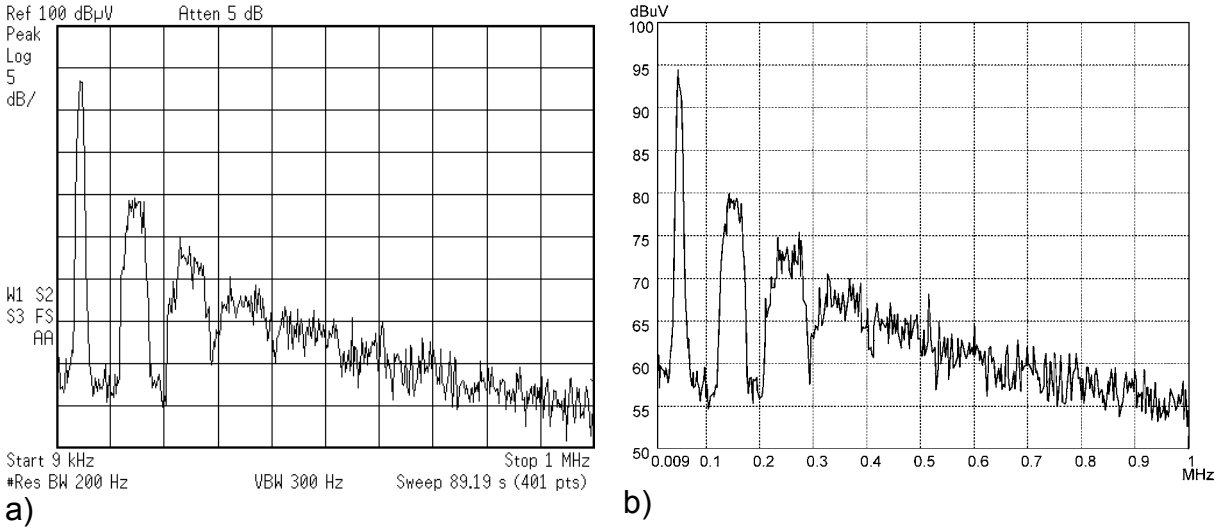

Figure 3.18. A test signal measured with a) a spectrum analyzer and b) an EMI test receiver.

According to this test, which was performed several times, only a negligible difference could be found. Differences can be again explained with the quasi-random nature of the test signal: No two identical measurements can be made with an QR-signal. Resolution bandwidth (IFBW) in both measurements were 200 Hz. The sweep time for the SA measurement was 89.19 s, which gives a dwell time of 18 ms for the spectrum analyzer settings according to Equation (3.38). The measuring time of the EMI receiver was 20 ms/IFBW with 200 Hz stepping.

3.5.3 Stabilizing Network

The impedance levels of actual networks such as the power mains and telephone networks are location dependent and time varying. Therefore, conduction emission setup requires a stabilized impedance simulation network referred to as an artificial network (AN) or a line impedance stabilization network (LISN), [CISPR 16-2 1999]. Actually, there are several reasons why AN or LISN is required in several compliance measurements. These are:

- To present constant impedance to the power inlet over the frequency range.
- Make different measurements comparable between different measurement sites.
- Attenuate emissions originating from the feeding power supply.
- Match the impedance of the measurement port to 50 Ω.

There are also circumstances where AN is not needed or the use of AN is even impossible. For example, CISPR 16 [CISPR 16-2 1999] lists some applications, where AN is not applicable. These include:

- An installed system.
- EUT with very high currents.
- Measuring the lower end of the frequency range.
- Power electronic devices which are fed from their own separate power supplies or battery devices to which separately installed lines are connected which are not to be loaded.

In this work, no artificial network was used. There are several reasons for this. Firstly, the aim of this work is not to compare emissions to some standardized levels. Secondly, a standardized stabilization network increases the uncertainty of the test setup. The impedance vs. frequency curve of the network defined in [CISPR 16-1 1999] is also non-linear in the frequency range of interest. The current clamp used in this work has practically no effect on the impedance of the supply leads. Finally, the test converter is supplied from a lead-acid battery thus no extra conducted noise originating from other devices is present.

3.6 The Relation between Calculated and Measured Spectrum

In general, spectral estimation is generally considered as a preliminary data analysis tool. Kay puts it in this way in his book: “ A spectral estimate should not be used to answer specific questions about the data, such as whether a resonance is present, but only to suggest possible hypotheses.”, [Kay 1987]. This statement is a good starting point when analyzing the spectrum of some selected system. It has to be

kept in mind that the estimated spectrum of a signal is just an *estimate* of the real spectrum of the signal.

One problem arises when we are comparing the simulation results to the test results or to the standard EMC-limits. The natural quantity to be studied in a random modulation setup is the *power spectrum* of the signal, not the *harmonic spectrum* of the signal, [Stankovic 1995], [Mihalic 1999-1]. Current EMC-regulations are, however, given in terms of the harmonic spectrum, [CISPR 22 2003], for example.

Calculated spectrum estimates present the power density spectrum, not an amplitude spectrum. This is a correct way to analyze WSS random signals. The units of the spectrum estimate are therefore power density or energy, watts per unit of frequency, e.g. V^2/Hz or W/Hz. Conversion between the power quantity and amplitude quantity has to be made if we want to change the power spectrum estimate to represent the amplitude spectrum of the signal. However, this conversion is not mathematically correct, because the harmonic parts of the signal spectrum are in units of power (V^2 or A^2) and the spectrum is defined at discrete frequencies. The random part of the signal causes continuous density spectrum and therefore it is not directly comparable to harmonic spectrum.

Comparison between the calculated and measured spectrum is problematic because of the operating principle of a selected detector mode in a test instrument. An example of a peak detector is presented in Figure 3.19, where the signal coming from the IF-section of the instrument has high short-term spikes. It is obvious from this example, that because the peak detection is a non-linear operation, the reading of the detector has nothing to do with the real power density spectrum reading of the signal at the selected frequency band. The calculated FFT transform or PSD estimate produces a result with a mean amplitude or power spectral density at a specific frequency.

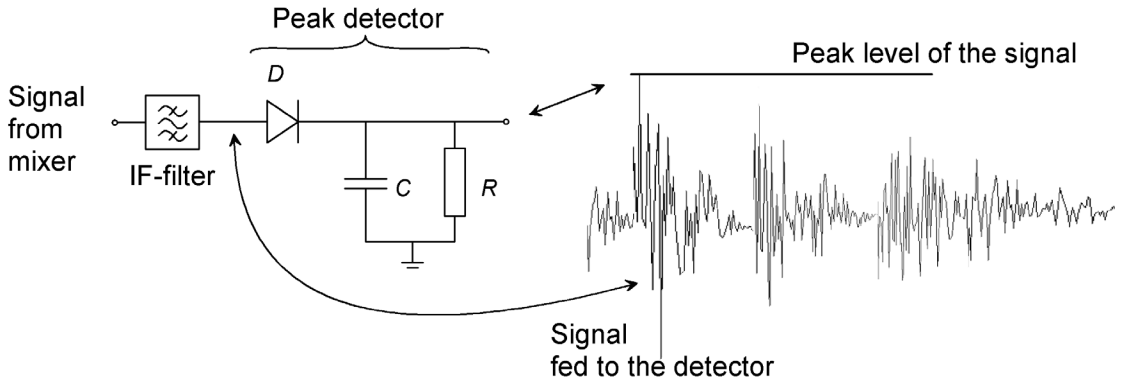

Figure 3.19. A dramatized example of a peak detector reading of a variable signal in an EMI-receiver. This peak reading has nothing to do with the signal power spectral density at the selected IF-bandwidth.

One attempt to simulate the emissions of a power converter is presented in the paper by Rahkala et al. [Rahkala 2002]. This paper presents a method to convert FFT data to correspond with the defined measurement bandwidths defined in EMI standards with QP and average detectors. In addition, a simulation model of an EMI receiver is presented with simplified homodyne approximation. This kind of model can be used when predicting EMI-performance of a system with simulations.

In the Welch PSD estimate used in this work, some part of the information is lost due to the averaging process. The resulting estimate is in units of power density, although there exists harmonic parts in the original signal. The operating principle of the measuring instrument also makes the analysis of the signal in a very different way if it is compared to the basic Fourier theory. It is obvious that the signal obtained from a measurement instrument is not particularly a good estimate of the real spectrum of the signal.

3.7 Summary

Important aspects on spectrum estimation and on EMI measurements were discussed in this chapter. Firstly, analytical equations for Fourier spectrum analysis for both a periodic and aperiodic signal were presented. For numerical spectrum estimation, the Welch-algorithm was selected for the power spectral density (PSD) estimation. The spectrogram was introduced and proposed for EMI-analysis in SS-modulated power converters. The most important facts in the EMI-test receiver were discussed concerning detection of the SS-signals. In the end of this chapter the dilemma in spectral units was discussed.

4 Selected Spread Spectrum Modulation Methods with Simulations

In general, the word *modulation* means the *interaction* of two or several signals. The modulating base-band signal, which is usually at lower frequency, modulates with some other signal at a different frequency range if we approach the modulation theory by means of basic communication theory. Usually, this other signal, often called the carrier signal or carrier wave, operates at a much higher constant frequency than the modulating base-band signal. The *frequency transformation* is the main property of the modulation: with the frequency transform, the information of the base-band signal can be translated to a new frequency range. In the pulse width modulation, for example, the modulating low frequency signal comes often from the control loop, and represents the instantaneous or average value of some specific voltage or current in the converter. The modulating feedback signal modulates then the switching function $q(t)$ and the duty cycle $d(t)$ with the system clock (switching frequency, carrier wave). Thus, the low frequency feedback information transforms to the higher frequency by means of the duty cycle of the switching function $q(t)$.

An example of the use of spread spectrum modulation in a PWM-scheme is depicted in Figure 4.1. This method modulates the constant frequency system clock of the PWM-circuit thus generating a variable-frequency (VF) switching signal to the power circuitry. Frequency modulation (FM) is one of the most suitable methods for this scheme. FM has been in use for many decades and therefore the spectral effects of the frequency-modulated signal are well known, [Haykin 1989], [Schweber 1999], [Miller 2002]. This method has been employed also in some configurations in this thesis.

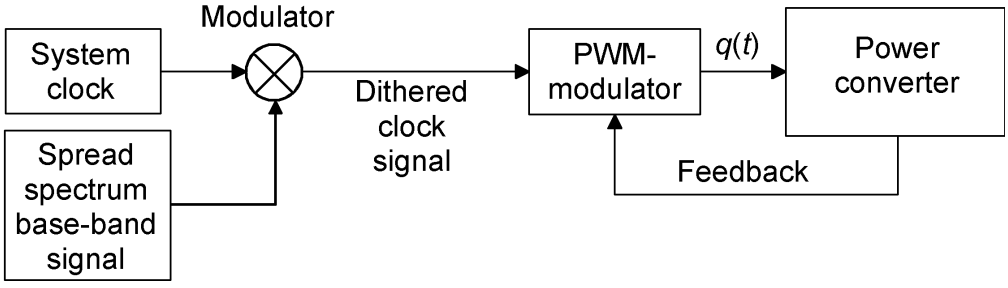

Figure 4.1. An example of a dual modulator in a spread spectrum modulation power supply. This principle uses the clock signal dithering to generate a varying clock signal to a normal PWM-modulator, [P4].

The example above is a straightforward utilization of spread spectrum methods in conventional power supply configuration. The VF modulation can be used in many other ways in power supply applications without the PWM-circuit and frequency modulator. An example of other kind of modulation method is the sigma-delta –modulation.

A basic PWM with a variable-frequency saw-tooth wave comparator is shown in Figure 4.2. This example clarifies the implementation of VF techniques with a basic PWM-circuit.

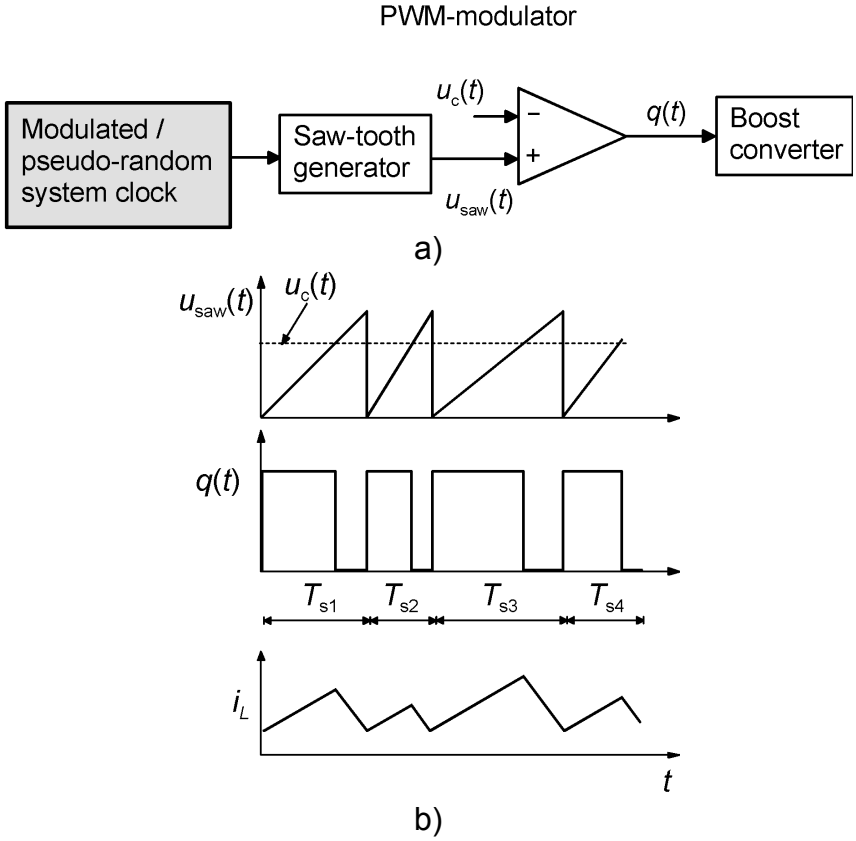

Figure 4.2. a) The use of a basic form PWM-comparator in variable-frequency power controller control. The instantaneous frequency of the saw-tooth wave is varied with the SS modulated or pseudo-random system clock. b) is an example of modulator waveforms $u_{saw}(t)$, $u_c(t)$, $q(t)$ and an inductor waveform $i_L(t)$ in a boost converter.

In Figure 4.2. b), the randomized system clock changes continuously the instantaneous frequency of saw-tooth wave. The nominal period T_s of the saw-tooth wave is changing from T_{s1} to T_{s4} in this example. The frequency of the switching function $q(t)$ also changes continuously within the limits set by the random generator. The scheme illustrated in Figure 4.2 has been used in some configurations in this work. In those cases, the control signal $u_c(t)$ was kept constant and no voltage feedback was used in the converter control.

As mentioned in Chapter 1 there are several different possibilities in spread spectrum generation. To have an overall picture of the applicability of different methods in power converter EMI-mitigation, the main types of different SS-techniques were selected for further studies. According to the literature survey and preliminary simulations, the following techniques were selected for prototyping:

- CASE 1 – Frequency modulation – modulating wave sine
- CASE 2 – FM – modulating wave sine + noise
- CASE 3 – FM – modulating wave triangular wave + noise
- CASE 4 – Frequency hopping
- CASE 5 – Chaotic peak current control
- CASE 6 – Chaotic Sigma-Delta control

Frequency modulation was selected because the technique is customary in communication and therefore the general properties of the frequency-modulated signal are well known. The efficiency of frequency modulation was studied with three basic modulating waveforms. Frequency hopping is another technique based on communication theory. It will be briefly discussed why other spread spectrum techniques in modern communication are not well suited for power supply applications and were therefore omitted from this study. From the controller based variable techniques two techniques were selected for further studies. Chaos is a well-known phenomenon in a peak current controlled boost controller, but it has been usually neglected as a possible EMI-reduction technique. A sigma-delta controller is another nonlinear control technique capable of a chaotic, variable frequency operation.

This study mainly focuses on general comparison of different techniques and therefore optimization of the synthesis is beyond the scope of this work. Anyhow, some general guidelines are discussed also in this Chapter. One starting point for selecting the length of the sequence is the measurement time used in the EMI-test system: The period of the modulation sequence should be at least the time used by the measurement device in one specific measurement bandwidth. In this case, the reading of the EMI-analyzer is slightly lower because there is no period in the modulation sequence during the measurement time. This may sound like manipulation of the measurement result according to EMI-regulations, but a long quasi-random sequence and the EMI excitation caused by the converter is less effective onto the possible victim circuit than in the case of a short modulation sequence, [P4], [Beck 2000-2].

The performance of different techniques was compared onto the performance of the constant frequency boost converter. This reference converter was operating at a nominal operating point of 50 kHz switching frequency, with parameters listed in Table 2-1. The main purpose of this comparison is to find out if SS-techniques can reduce discrete spikes in EMI spectrum. In addition, comparison of the steady-state operation will be presented in Chapter 5 to see the effect of variable-frequency operation on the normal operation of the boost converter.

Different kinds of simulations were run for EMI-performance analysis with different spread spectrum models in Matlab/Simulink™. The main types of simulations made in this work are listed in Table 4-1. The simulations were forced to operate at a maximum time step of 500 ns, and the simulation results were stored with sampling frequency f_{sa} of 2 MHz.

Table 4-1. The main simulations conducted for the evaluation of the performance of selected spread spectrum modulation methods.

Simulation type	Method used
Power spectral density PSD of the switching function $q(t)$ (Chapter 4)	MATLAB *pwelch*-function, FFT length N = 13000, overlapping 6500, Hamming window
Spectrogram of the switching function $q(t)$ (Chapter 4)	MATLAB *specgram*-function, FFT length N = 2048, overlapping 1024
Unbiased autocorrelation of the switching function $q(t)$ (Chapter 4)	MATLAB *xcorr*-function, unbiased
Power spectral density PSD of the input current I_L (Chapter 5)	MATLAB *pwelch*-function, FFT length N = 13000, overlapping 6500, Hamming window
Spectrogram of the input current I_L (Chapter 5)	MATLAB *specgram*-function, FFT length N = 2048, overlapping 1024
Output voltage U_O (Chapter 5)	Plot of time-series calculated with Simulink™, time step 500 ns
Input current I_L (Chapter 5)	Plot of time-series calculated with Simulink™, time step 500 ns

According to Equation (3.28), the spectral resolution in a Welch PSD estimate with 13000 point FFT is 200 Hz. This frequency was selected because it is also the IFBW in the EMI test receiver. The spectral resolution in the spectrogram estimate is approximately 980 Hz, Equation (3.29). The reason for a different resolution in the spectrogram is the time resolution, which decreases if the FFT length N increases. According to Equation (3.35), the time resolution in the calculated spectrograms is 1.024 ms.

In a power converter, the signal is rarely sinusoidal. More often, the signal (current or voltage) is more like a square wave or triangular wave. The square wave was therefore chosen to be the reference signal in the comparison of different modulation methods in this preliminary simulation part of the work. The square wave signal that naturally appears in all switching power converters is the switching function $q(t)$. Therefore all **calculated spectrum estimates presented in Chapter 4 are calculated from the switching function $q(t)$.** Use of a switching function is also reasoned for general applicability of simulation results shown in this chapter. The switching function is not dependent for example on the power ranking of the switching converter and inherent spectral properties of different VF methods can be emphasized. It also will be shown, that there is a correlation between the spectrum estimation of the simulated switching function and the measured EMI-spectrum of the boost converter. The simulated $q(t)$ was normalized to ± 1 before numerical estimation of the spectrum and autocorrelation to get rid of the DC-bias of the switching function. Simulation models and MATLAB –scripts are collected in Appendix A.

Next, simulations made for EMI-performance analysis are presented. Selected spread spectrum modulation schemes are introduced and spectrum estimates of different cases from the switching function $q(t)$ are obtained. Finally, spectral results of different cases are summarized.

4.1 Simulations with the Constant-Frequency Reference Converter

First, the calculated Welch spectrum estimate and the spectrogram of the constant frequency reference converter are shown in Figure 4.3.

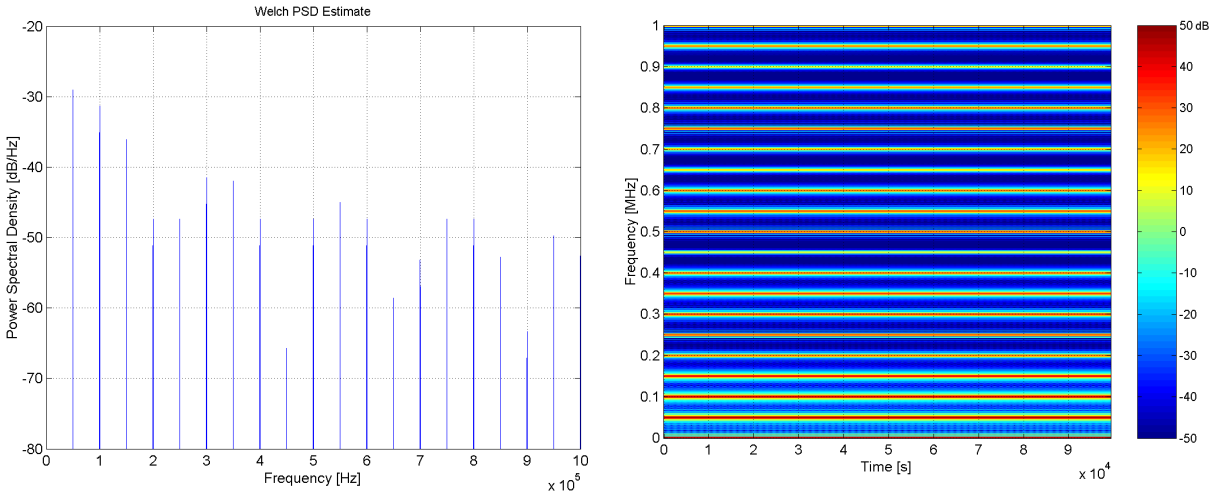

Figure 4.3. a) A Welch power spectrum estimate of the switching function of the constant frequency reference converter operating at 50 kHz. b) Spectrogram of the switching function of the reference converter.

A periodic switching function $q(t)$ in the reference converter causes a typical spectrum estimate of a periodic signal with fundamental frequency and harmonics. The spectrogram also shows the constant nature of the reference converter: vertical lines with high harmonically related peak values. There is no change in the spectral content along the horizontal time axis because the converter switching function is operating at a constant frequency. Another visual test is the autocorrelation of the switching function, Equation (3.21). Figure 4.4. represents the calculated autocorrelation sequence of the reference converter.

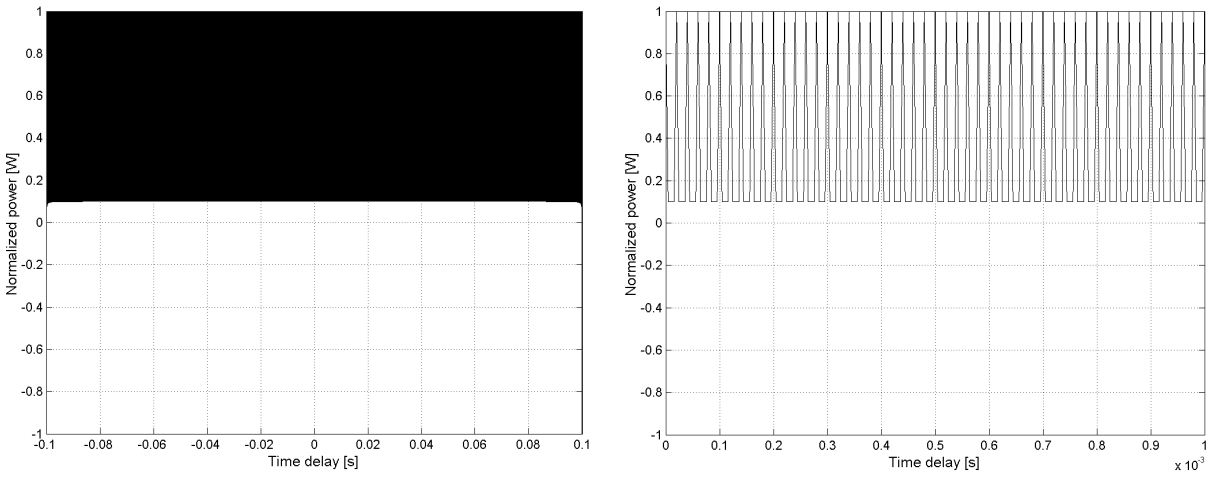

a) b)

Figure 4.4. Calculated autocorrelation sequence of the reference converter. High level and periodic maximums of the autocorrelation is predictable in the case of a constant periodic signal. A nominal switching period is clearly visible in the close-up, (b). Horizontal axis scaling from –100 ms to 100 ms in a) and from 0 to 1 ms in b).

An autocorrelation sequence of an ideal spread spectrum signal is a line at zero level and it has one spike at time $\tau = 0$, when the spike represents the signal power according to Equation (3.24). If there exist periodic parts in the signal, the autocorrelation will have local maximums at these time delay values. Possible periods and thus frequencies can be tracked from these maximums. The autocorrelation sequence shown in Figure 4.4 shows the periodic nature of the reference converter. The period of the signal is clearly visible in Figure 4.4 b).

4.2 Angle Modulation

The term *angle modulation* includes both the *frequency modulation* (FM) and the *phase modulation* (PM). In these modulation methods, the phase angle of the carrier wave is modulated with some other base-band signal. The resultant modulated wave consists of a nonlinear product of the original signals.

One great advantage of this nonlinear nature of the modulation process is that the power spectrum of the modulated wave is spread over a wide frequency range. This property can be exploited by spreading the power spectrum of power supply switching. Although angle modulation is not a true spread spectrum technique according to modern communication theory, the spectrum of an angle-modulated wave is spread over the frequency range. The amount of the spread, or the effective spectral bandwidth, depends on the parameters and complexity of the modulator.

The use of angle modulation in power supplies is limited on the modulation of the system clock, as shown in Figure 4.1. In this case, there is no constant system clock or switching frequency, and the power switch is driven with the drive circuit clocked at the modulated clock signal. In practical power supply applications, the modulated clock signal is fed to the clock input of a PWM-modulator circuit. The PWM-circuit and the control of the power supply operate normally but the *instantaneous switching frequency changes* continuously. The EMI-noise can be spread from a single switching frequency and harmonics to a wide frequency range depending on the modulation level. Of course, the frequency limits set by the power switches, magnetic components and other limitations in the power converter must be taken in to consideration.

4.2.1 Theoretical Background of Angle Modulation

The angle modulated signal $s(t)$ can be expressed mathematically, [Oppenheim 1997],

$$s(t) = A_c \cos[\omega_c t + \phi(t)] = A_c \cos\theta(t), \tag{4.1}$$

where A_c and ω_c are constants depending on the carrier wave, $\phi(t)$ is the function of a modulating signal $m(t)$ and the angle argument is,

$$\theta(t) = \omega_c t + \phi(t). \tag{4.2}$$

The instantaneous angular frequency ω_i is, [Oppenheim 1997],

$$\omega_i = \frac{d\theta(t)}{dt} = \omega_c + \frac{d\phi(t)}{dt}. \tag{4.3}$$

From Equation (4.3), it can be seen that the instantaneous frequency stays constant if the derivative of the phase angle remains constant, [Haykin 1989]. Function $d\phi(t)/dt$ represents the instantaneous *frequency deviation* of the modulated wave. Function $\theta(t)/dt$ represents the instantaneous phase deviation of the modulated wave. One important property of the angle-modulated wave is the maximum angular frequency deviation, which can be formulated as

$$\Delta\omega = \left|\omega_i - \omega_c\right|_{max}. \tag{4.4}$$

The maximum frequency deviation represents the maximum instantaneous frequency deviation from the carrier wave frequency. In FM, the $\Delta\omega$ (or Δf) is proportional to the *amplitude* of the modulating wave $m(t)$. The deviation is independent of the frequency range of the modulating signal.

Next, we concentrate on properties and parameters of frequency modulation, because FM is a useful and easily utilized angle modulation method in power supply design. In frequency modulation, the instantaneous frequency deviation is proportional to the modulating signal $m(t)$. This relation can be expressed as, [Oppenheim 1997],

$$\frac{d\phi(t)}{dt} = k_f m(t), \tag{4.5}$$

where k_f is the frequency deviation constant (frequency sensitivity, deviation sensitivity), expressed in [rad/s/V] or [Hz/V]. Solving for function $\phi(t)$, we get

$$\phi(t) = k_f \int_0^t m(t)dt + \phi(t_0). \tag{4.6}$$

Finally, by assuming the phase shift $\phi(t_0) = 0$, the mathematical expression for the frequency modulated signal $s(t)$ can be simplified as, [Haykin 1989],

$$s(t) = A_c \cos\left\{\omega_c t + k_f \int_0^t m(t)dt\right\}. \tag{4.7}$$

The modulating signal $m(t)$ changes the instantaneous frequency of the modulated wave and the amplitude A_c remains constant in the frequency modulation. The instantaneous frequency is

$$\omega_i(t) = \omega_c + k_f m(t). \tag{4.8}$$

In a single tone modulation with a sinusoidal modulating wave, the modulating wave can be written as

$$m(t) = A_{\mathrm{m}} \cos(\omega_{\mathrm{m}} t). \tag{4.9}$$

An example of a sinusoidally modulated FM wave is shown in Figure 4.5.

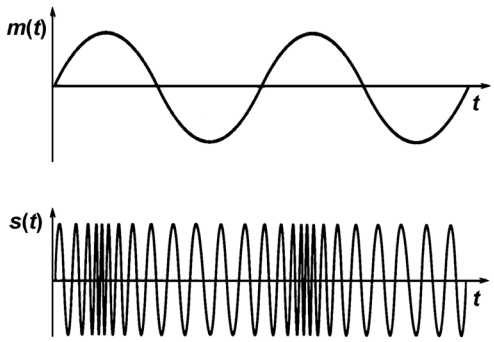

Figure 4.5. An example of the waveforms in single tone FM. The upper waveform represents the modulating sine-wave $m(t)$ and the lower waveform is the frequency modulated waveform $s(t)$.

In the case of a sinusoidal modulating wave $m(t)$, the relation between the frequency deviation $\Delta\omega$ of the modulated wave and the frequency ω_{m} of the modulating wave (in FM) is called the *modulation index* β, [Haykin 1989], [Hsu 1993]*:*

$$\beta = \frac{\Delta\omega}{\omega_{\mathrm{m}}} = \frac{k_f A_{\mathrm{m}}}{\omega_{\mathrm{m}}}. \tag{4.10}$$

The effect of the modulation index β (modulation depth) on the output of the frequency modulator spectrum can be seen from the example illustrated next. Figure 4.6. shows the scattering effect of the modulation depth to the amplitude spectrum of the frequency modulated signal.

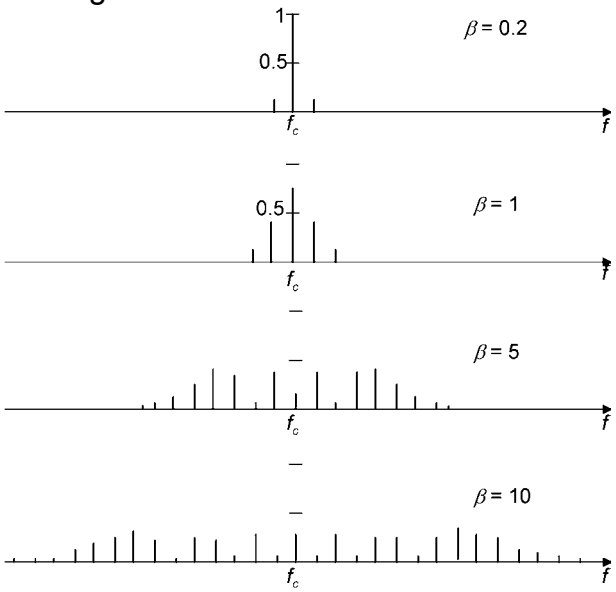

Figure 4.6. The amplitude spectra of a frequency modulated wave with different values of modulation index β. The modulating sine wave frequency is fixed. The *x*-axis is the frequency and the *y*-axis is normalized power density, [Hsu 1993].

4.2.2 The Spectrum of the Angle Modulated Signal

In sinusoidal modulation, according to Equations (4.7), (4.9) and (4.10), the modulated signal $s(t)$ is

$$s(t) = A_c \cos(\omega_c t + \beta \sin(\omega_m t)). \tag{4.11}$$

The frequency-modulated wave in Equation (4.11) can be converted to an exponential form with Eulers' relation:

$$s(t) = \mathrm{Re}(A_c e^{j(\omega_c t + \phi(t))}) = \mathrm{Re}(A_c e^{j\omega_c t} e^{j\phi(t)}) \tag{4.12}$$

With the use of the series expansion, the modulated wave can now be expressed as

$$\begin{aligned} s(t) &= \mathrm{Re}\left[A_c e^{j\omega_c t} \left(1 + j\phi(t) - \frac{\phi^2(t)}{2!} - \cdots + j^n \frac{\phi^n(t)}{n!} + \cdots \right) \right] \\ &= A_c \left(\cos\omega_c t - \phi(t) \sin\omega_c t - \frac{\phi^2(t)}{2!} \cos\omega_c t + \frac{\phi^3(t)}{3!} \sin\omega_c t + \cdots \right) \end{aligned} \tag{4.13}$$

It can be clearly seen that the spectral content of the frequency-modulated wave is complex, even in the case of a simple sinusoidal excitation signal. The spectrum of the sinusoidal modulated FM-wave consists of the carrier wave frequency and numerous nonlinear amplitude modulated terms. In theory, the spectrum consists of an infinite number of side-frequencies and is then unsolvable. However, the spectrum can be estimated with practical approximations with reasonable accuracy.

The spectrum of the sinusoidal modulated FM-wave can be solved analytically with Bessel functions. The derivation and the result of the frequency content is presented in basic textbooks of communication theory, for example [Hsu 1993], [Haykin 1989], [Miller 2002], [Schweber 1999], therefore only selected results are given next.

As allready stated, the frequency modulator spreads the spectrum of the modulated wave to a wide frequency range. The resultant spectrum consists of an infinite number of sidebands in theory. The spectral content of the sinusoidaly modulated wave can be estimated quite easily with the *Carson rule,* [Haykin 1989]. The Carson rule states that the bandwitdh (*BW*) of the sinusoidally modulated wave is approximately

$$BW \approx 2(\beta + 1)\omega_m. \tag{4.14}$$

According to the Carson rule, 98 % of the total signal power lies within this bandwidth, [Haykin 1989].

A drawback of the Carson rule is, that it is limited only to sinusoidally modulated waves. However, when dealing with non-sinusoidal modulating waves, the spectral bandwidth can be estimated with the Carson rule, after the deviation ratio *D* has been calculated. The deviation ratio is defined as, [Haykin 1989],

$$D = \frac{\text{maximum deviation}}{\text{bandwidth of } m(t)} = \frac{\Delta\omega}{\omega_{\text{m}}}. \tag{4.15}$$

The deviation ratio D can be considered as an approximation of the modulation index β for non-sinusoidal modulating signals. The bandwidth of the modulated wave $s(t)$ can be estimated with the Carson rule as follows, [Hsu 1993]:

$$BW \approx 2(D+1)\omega_{\text{m}} \ . \tag{4.16}$$

The pulse-shaped waveform itself contains harmonics. Usually, the switching power supply waveforms are triangle or pulse-shaped, so the harmonic content of current and voltage waveforms are high. Frequency modulation of the pulse-waveform distributes each of the harmonic components into side-band harmonics. The frequency difference between each adjacent side-band harmonic is ω_{m}. However, the modulation index β_n of each harmonic is different. The modulation index can be calculated simply by multiplying the fundamental modulation index β with the harmonic number n, $\beta_n = n\beta$, [Lin 1994]. For example, if the fundamental modulation index is 10, then the modulation index for the fifth harmonic is $\beta_5 = 50$.

Since the modulation index changes with each switching harmonic, the scattering effect of each switching harmonic is different. The Carson rule applies to each harmonic. The higher the harmonic number, the more even is the spread-out power, [Lin 1994]. The scattering effect of each harmonic frequency of a modulated square wave is visually shown in Figure 4.7.

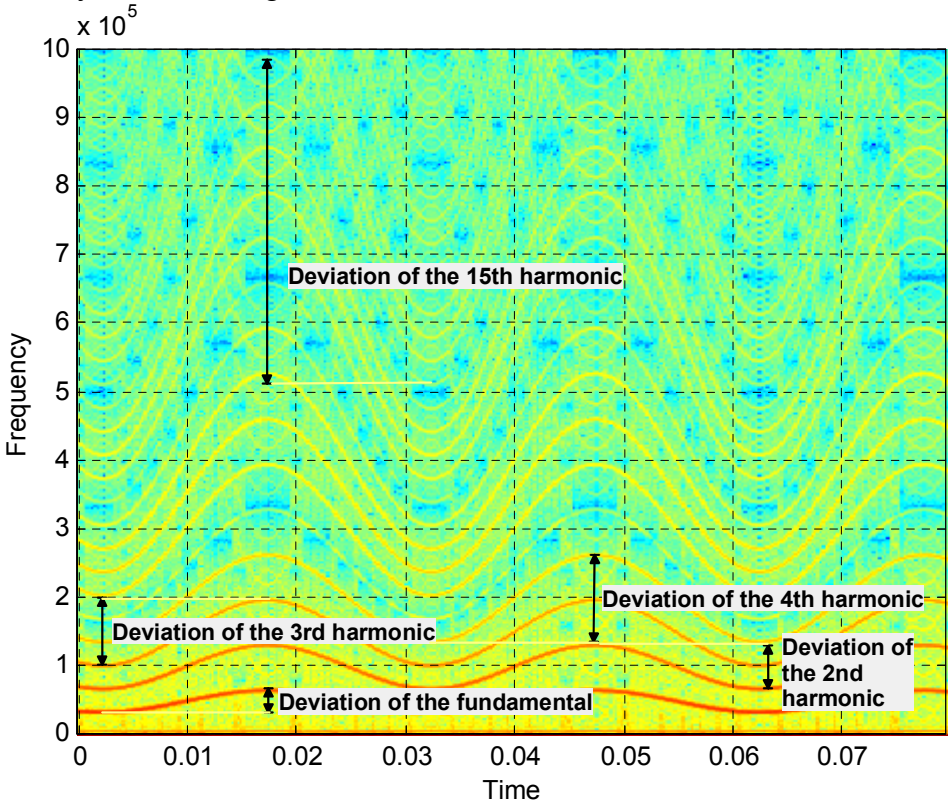

Figure 4.7. A spectrogram of a modulated square-wave. The modulating wave is sine, 33 Hz. The difference between each harmonic is the same at each selected time instant. However, the modulation index, and thus the frequency deviation of each harmonic is different.

4.2.3 Simulation with Selected FM-Signals

The basic theory of FM in power supply applications is reported for example in [Lin 1994], [Stone 1995] and [Tse 2002]. Basic guidelines for design can be found for example in the paper [Vilathgamuwa 1999]. Santolaria et al. [Santolaria 2002] has made a study on spectral effects of different modulating wave shapes. According to these results, a triangular and exponential wave outperforms sinusoidal modulation.

According to preliminary simulation work and findings reported in publications, three different basic signals were selected for FM implementation. Firstly, modulation with a sinusoidal single tone signal was conducted. A sinusoid is a very common modulation signal and therefore needs to be compared to other SS–modulation methods. Results from a combination of sinusoidal and triangular wave with a pseudo random noise will also be presented. Generation of the frequency modulated clock signal for the converter was made with the simulation model shown in Figure 4.8. The implementation of the model shown in Figure 4.8 is based directly on Equation (4.7).

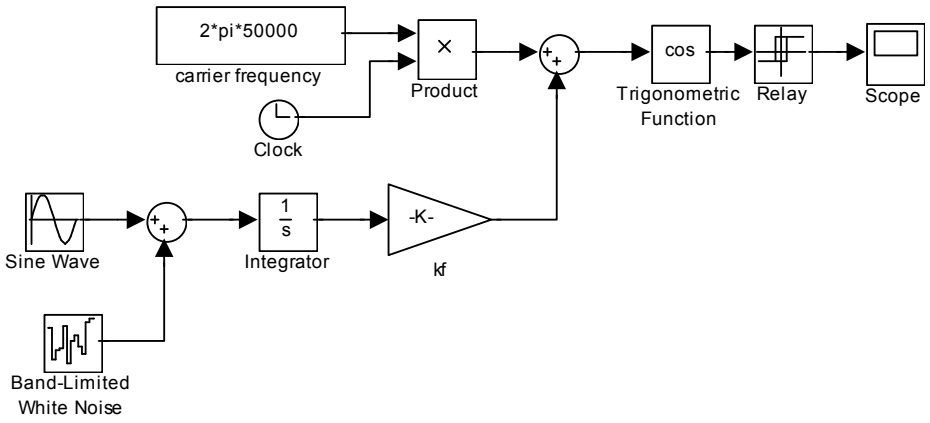

Figure 4.8. Simulink™ simulation model used in FM-simulations. The signal generator signal is either sinusoidal or triangular, amplitude 1, frequency 33 Hz. The random noise generator was used in two simulation configurations. The carrier frequency is 50 kHz. A relay is used in the model to generate a square-wave switching function $q(t)$.

The frequency of the modulating wave is 33 Hz so the period of the signal is approximately 30 ms. These values were selected according to the specifications mentioned in Chapter 3.5: Spectral efficiency can be increased by choosing the frequency variation to be more than the IFBW or RBW of the measuring instrument and selecting the possible repetition frequency to be more than the measuring time at a single frequency band.

4.2.4 CASE 1: Single-Tone Frequency Modulation

In Case 1, the frequency deviation constant k_f was selected so, that the fundamental frequency changed from 35 kHz to 65 kHz, thus Δf was15 kHz. Simulated estimates for the power spectrum density and spectrogram are shown in Figure 4.9.

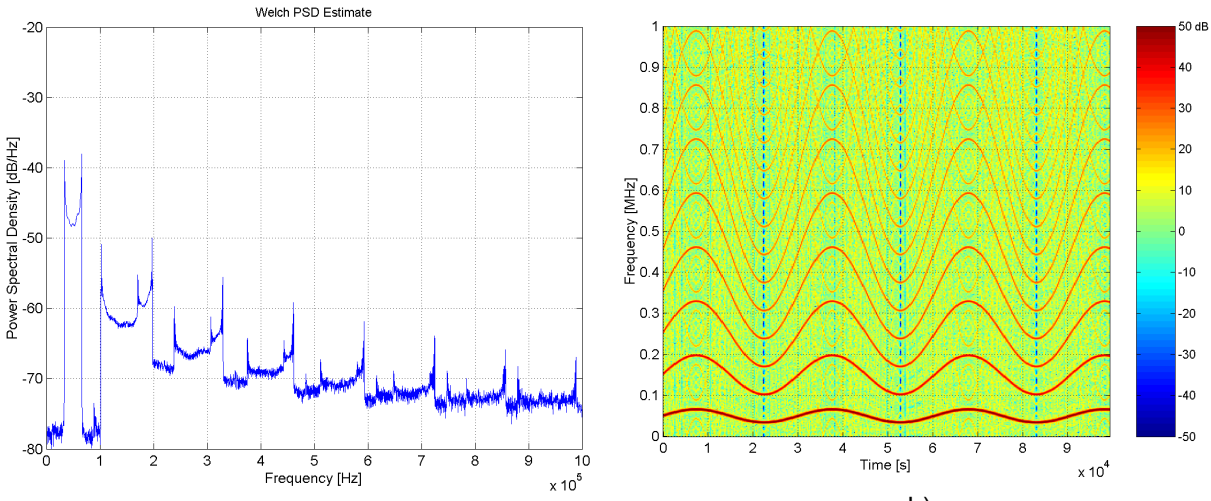

a) b)

Figure 4.9. FM-signal with single tone (sine) modulation. (a) the PSD, (b) the spectrogram of the switching function $q(t)$. These results can be compared to the reference, Figure 4.3.

The spectrum estimate of the signal is a typical textbook example of single tone modulated FM-spectrum with harmonics. High spikes are visible on both sides of the carrier (50 kHz) wave. The deviation Δf can be seen on both the PSD and the spectrogram. The shape of the spectrogram was already introduced in Figure 4.7. The sinusoidal modulating wave is clearly visible, and the period, 30 ms, of the modulating wave can be read from the graph.

The period of the modulating wave is also visible in the autocorrelation sequence of the switching function, Figure 4.10 a). High spikes also in the autocorrelation sequence predict poor spectral performance. The modulation sequence length and thus the period 30 ms of the modulating wave can be seen in the autocorrelation sequence.

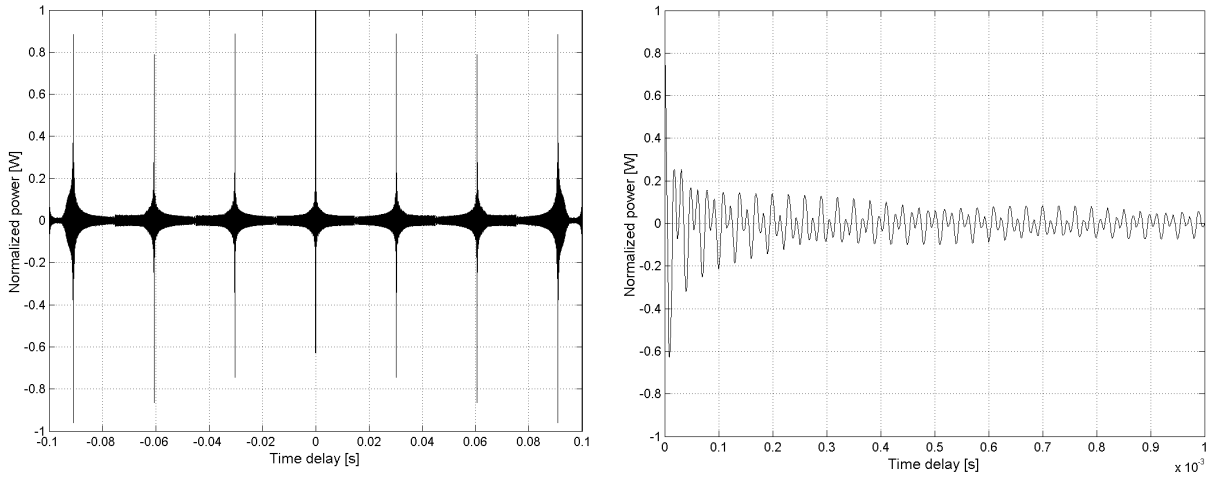

a) b)

Figure 4.10. The autocorrelation of the sine-modulated FM signal. The modulation sequence length 30 ms causes evident maximums to the autocorrelation sequence in a). In the close-up (b), the nominal switching period is visible although it is continuously changing, see also Figure 4.4. The horizontal axis scaling is a) from –100 ms to 100 ms and b) from 0 to 1 ms.

4.2.5 CASE 2: Modulation with Sinusoidal Wave + Added Random Noise

The second case uses the sinusoidal wave introduced in Case 1 with pseudo-random noise added to this modulating signal. The purpose of this additional noise component is to increase randomness and thus reduce the relational level of periodic part of the modulating signal. Pseudo-random noise was generated with MATLAB^{TM} without any optimization of the random sequence. The simulation setup was shown in Figure 4.8. The simulated spectrum estimate and spectrogram is shown in Figure 4.11.

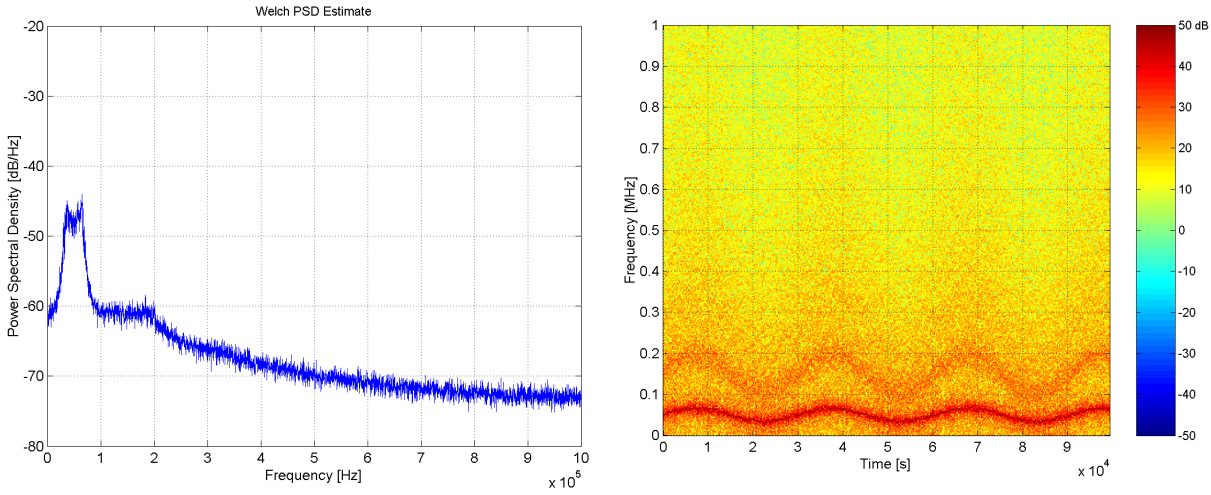

Figure 4.11. FM-signal with a sinusoidal wave + added noise as a modulating wave. (a) the PSD, (b) the spectrogram of the switching function $q(t)$. These results can be compared to the reference, Figure 4.3.

If the PSD is compared to the PSD of the pure sine wave modulation, it can be seen that the spikes have reduced. Reduction is noticeable especially at higher frequencies, where the spectrum estimate looks almost like the noise spectrum without any harmonic spikes. The same effect is noticeable in the spectrogram, where only a fundamental and third harmonic is clearly visible. The period of the fundamental modulating wave is still clear.

The period of the modulating wave sequence can be seen in the plotted autocorrelation sequence, Figure 4.12 a). The spikes are not so high as in the cases of sinusoidal modulating wave and some reduction is clearly noticeable.

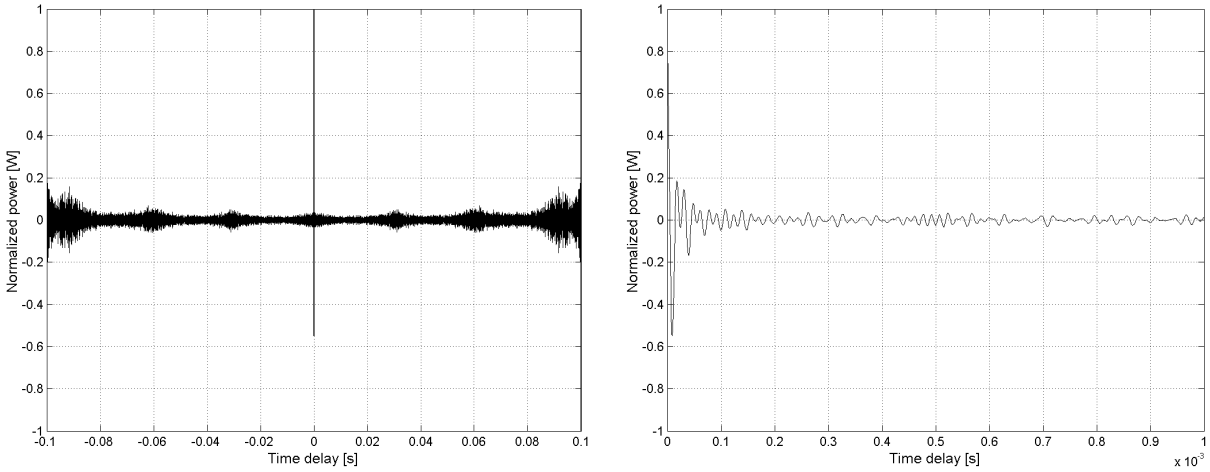

a) b)

Figure 4.12. The autocorrelation of the sine + noise FM signal. The maximums are not so evident as in the previous case, but the modulation sequence length 30 ms is still present in (a). The horizontal axis scaling is a) from –100 ms to 100 ms and b) from 0 to 1 ms.

4.2.6 CASE 3: Modulation with Triangular Wave + Added Random Noise

The third case uses a triangular wave as suggested in [Santolaria 2002]. The frequency of this modulating wave is again 33 Hz. Pseudo random noise was also added to the triangular wave because of the promising results obtained from Case 2. The estimated power spectral density function and spectrogram are shown in Figure 4.13.

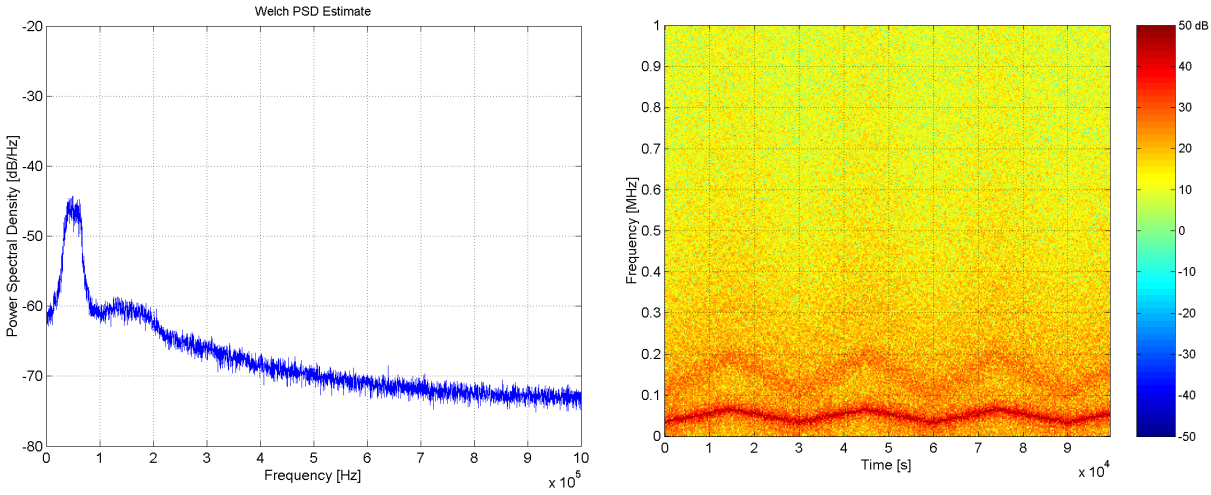

a) b)

Figure 4.13. The FM-signal with a triangular wave + added noise as a modulating wave. (a) the PSD, (b) the spectrogram of the switching function $q(t)$. These results can be compared to the reference, Figure 4.3.

The shape of the PSD looks even better than in Figure 4.11. The third harmonic is almost buried in the background noise and there are no harmonic spikes at high frequencies or around the nominal switching frequency. The spectrogram exposes the modulating signal and the fundamental frequency of the triangular wave. In addition, the form of the triangular wave can be observed from the spectrogram.

The plotted autocorrelation sequence is almost the same as the sinusoidal wave with noise, Case 2. The period of the signal is clearly 30 ms, although the signal is slightly smoother, especially in Figure 4.14 b).

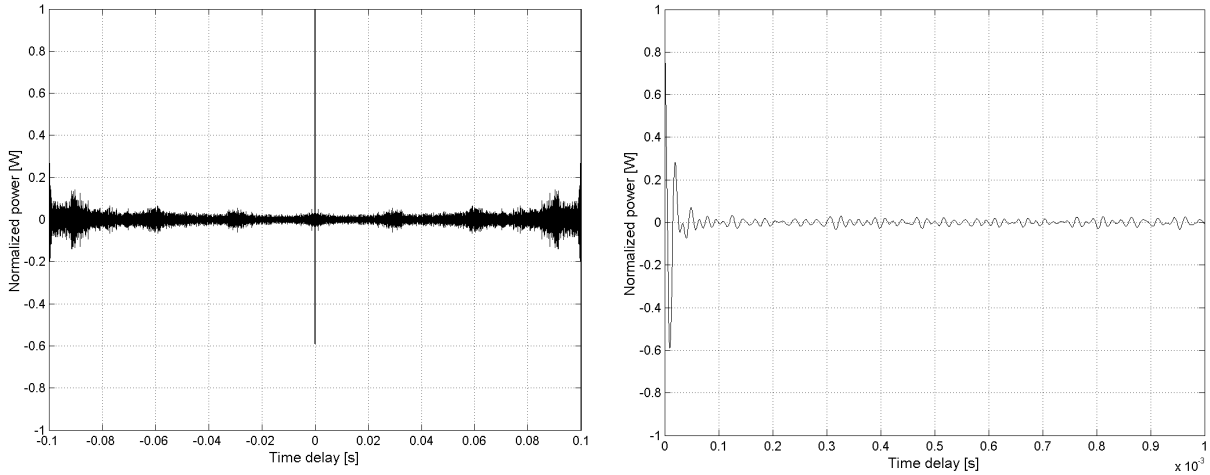

a) b)

Figure 4.14. The autocorrelation of the triangle + noise FM signal. 30 ms period of the modulation sequence is still visible in (a), but the nominal switching period is very low in (b) compared to Case 1 and especially to the reference, Figure 4.4. The horizontal axis scaling is a) from –100 ms to 100 ms and b) from 0 to 1 ms.

4.3 Frequency-Hopping

Spread spectrum techniques were first mainly used in military applications. In these military applications, the main objective is to prevent the unintentional (enemy) listener from catching the message. Spread spectrum uses wide band, noise-like signals. Since SS signals are noise-like, they are hard to detect or intercept. SS signals are also harder to *jam* than narrowband signals. The low probability of the intercept (LPI) and anti-jam (AJ) features are why the military has used spread spectrum for so many years, [Kosola 2000].

The signal is not transmitted in the traditional way with a single carrier wave in spread spectrum communication. There are many possibilities generating the spread spectrum signal, but all these techniques share the common idea: The frequency band used in signal transmission is divided into sub-frequency bands, which are all used simultaneously in signal transmission. Spread spectrum signal transmission is distinguished by the characteristic that the bandwidth used for signal transmission is much higher than the original signal bandwidth. Another important property of the SS-signal is the pseudo-randomness, [Proakis 1989].

There are two basic methods in SS generation in modern communications:

- Frequency-hopping (FH)
- Direct sequence (DS)

DSSS -modulation produces a signal spectrum centered at the carrier frequency and the envelope of a frequency spectrum has a shape of function $(\sin x/x)^2$, [Proakis 1989]. In frequency hopping, the generated spectrum envelope is not like that in the DS-case. The spectrum is flat consisting of discrete peaks, which are in an ideal

case placed evenly in the desired frequency band according to the code sequence. The bandwidth of a frequency-hopping signal is simply *w* times the number of frequency slots available, where *w* is the bandwidth of each hop channel. This is shown in Figure 4.15, where DSSS and FHSS signals are illustrated in the frequency domain.

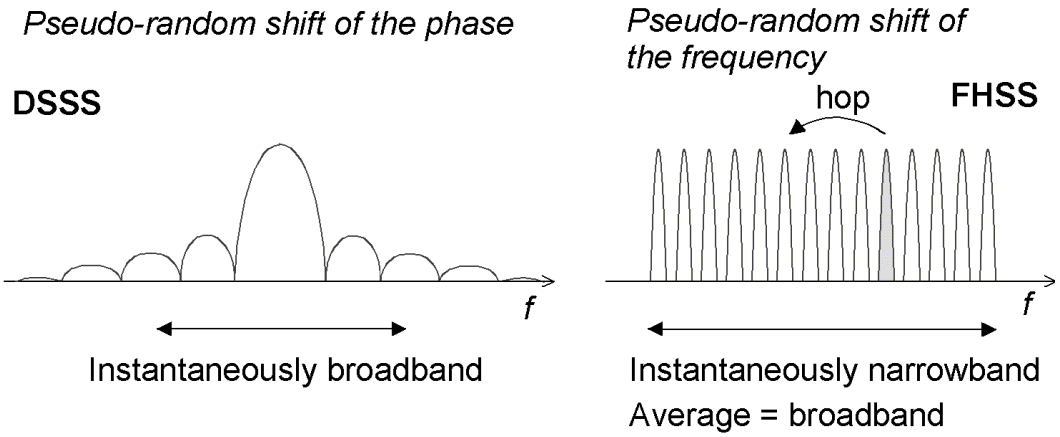

Figure 4.15. The main differences between DSSS and FHSS signal spectrum.

The DSSS signal has a pseudo random shift of phase, while the FHSS signal has a pseudo random shift of frequency. The DSSS signal is instantly broadband and the FHSS signal is instantly narrowband, as shown in Figure 4.15. However, the FHSS signal is a broadband signal when the average of the frequencies is considered over a longer period.

The direct-sequence has more or less developed for the needs of telecommunications, and therefore it is not suitable for spread spectrum modulated power supplies. In fact, DS uses much more bandwidth than is needed for the signal transmission in order to achieve low average power transmission compared to the common noise floor in the propagation channel. This approach is not suitable for power supplies because the average transferable power is the main signal in the power supply, and thus cannot be reduced.

Spreading codes in digital communication are called *pseudo-random* (PR) or *pseudo-noise* (PN) codes. They are called pseudo, because they are not Gaussian noise. A typical PN-code is a digitally generated sequence, which appears to have random behavior. Autocorrelation properties of the PN codes are the most important design objectives: an ideal PN-sequence has autocorrelation properties similar to those of white noise.

A maximum length sequence (*m-sequence*) is commonly used in traditional SS-applications. A maximum length sequence is a binary sequence generated by the shift register with feedback and modulo-two (xor) adder/adders, [Haykin 1989], [Proakis 1989]. One application of the m-sequence in power converter is reported in paper from Tanaka et al. [Tanaka 1997]. Another paper concerning FH in power applications is by Stone et al. [Stone 1996]. One simple circuitry for m-sequence generation is depicted in Figure 4.16. The application note from Maxim [Maxim 2002] proposes the use of a pseudo-noise generator accompanying their basic DC-DC converter circuit MAX 1703. This application note uses a typical textbook pseudo-

noise generator circuitry to generate a random-like clock signal to the DC-DC converter.

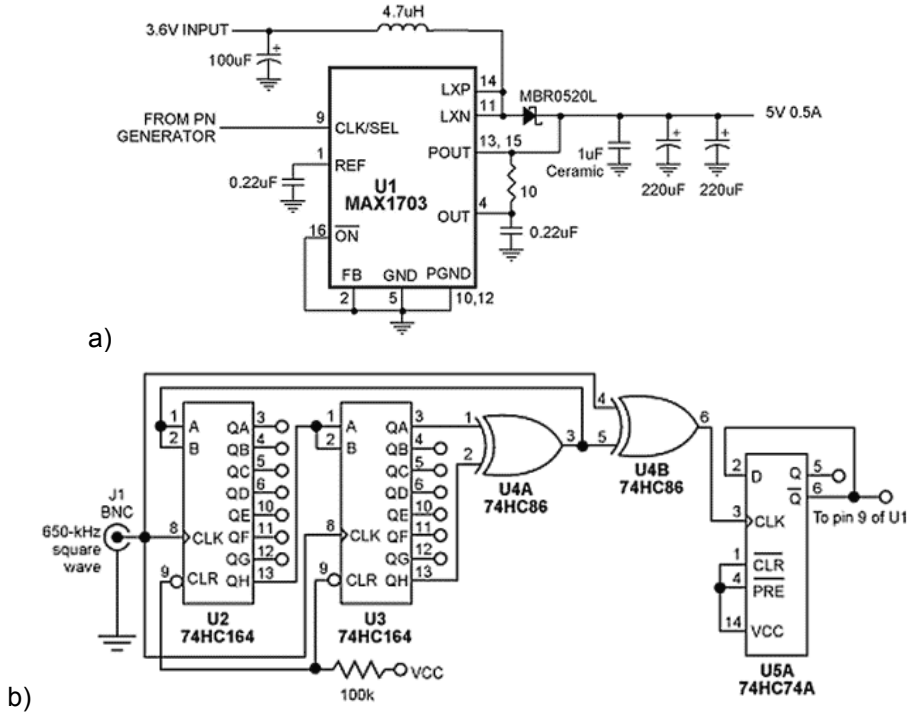

Figure 4.16. An example of generating the pseudo-random clock sequence for the DC/DC converter, [Maxim 2002]. (a), the power converter circuit and (b), the digital pseudo-noise generator.

Several other different pseudo random generation methods are in wide use among communication engineers. Usually these algorithms try to improve cross-correlation properties of the signal or signal detection in the receiver, trying to avoid problems in multi-user applications. In power converter applications, this is rarely a problem. Therefore, more advanced pseudo-random generation algorithms, such as Gold code, [Budisin 1992], chaotic PN, [Leon 2000], Reed-Solomon, [Proakis 1989] and Hadamard, are omitted in this study. Autocorrelation and spectral properties cannot be better than in the m-sequence. Mutagi, [Mutagi 1996], gives a good overview on the topic of generating pseudo-random sequences.

Not many of the PN-algorithms presented in communication applications are directly applicable to switching frequency modulation in power controller because of the limitations of the converter operation. The magnetics, ripple requirements and power losses set some limits on the frequencies that are suitable for a practical power supply. Therefore, after many test runs with various m-sequences, a simple algorithm was developed for power supply frequency hopping. Design parameters were manually selected so that the frequency shift was at least 12 kHz in every hop and at least 6 kHz from the previous hop. The upper limit of the frequency range was 75 kHz and the lower limit 35 kHz. The duration of one frequency component was selected to be approximately 333 μs (100ms/300). This is less than the settling time 5 ms of the test instrument calculated from Equation (3.37) with a 200 Hz IF-filter. The algorithm used in the frequency-hopping signal generation is shown in flowchart, Figure 4.17.

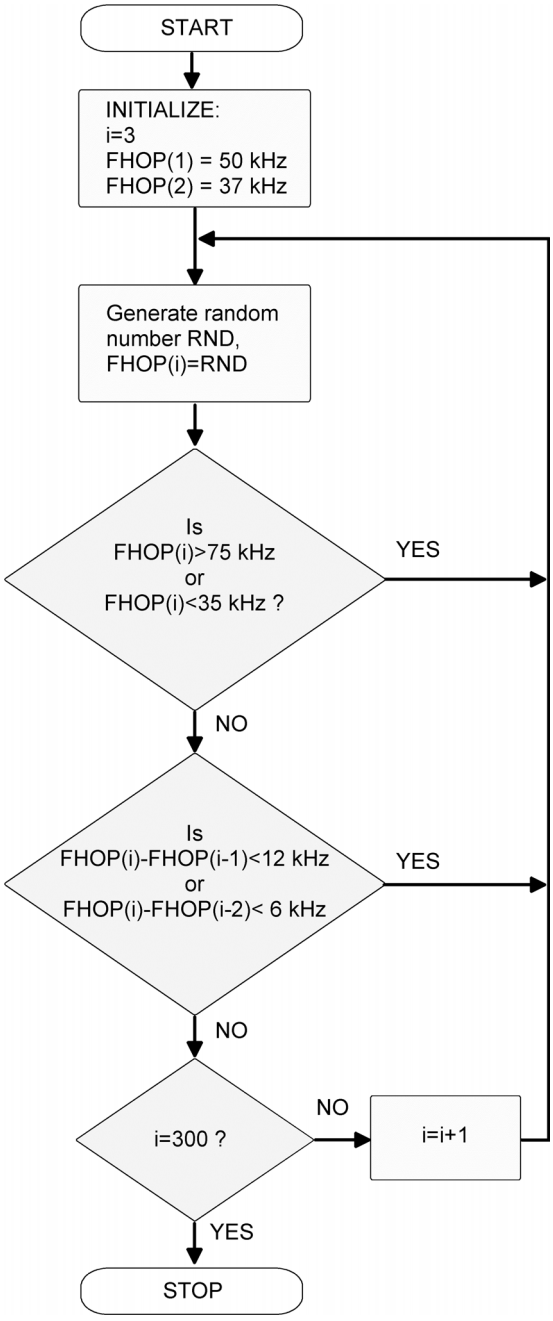

Figure 4.17. Flowchart of the frequency-hopping signal (FHOP) generation. The algorithm gives the nominal switching frequency in the range of 35 kHz to 75 kHz. The sequence length is 300 points, 100 ms.

4.3.1 CASE 4: Simulations with a Frequency-Hopping Switching Function

Calculated spectral results of a frequency-hopping signal are shown in Figure 4.18.

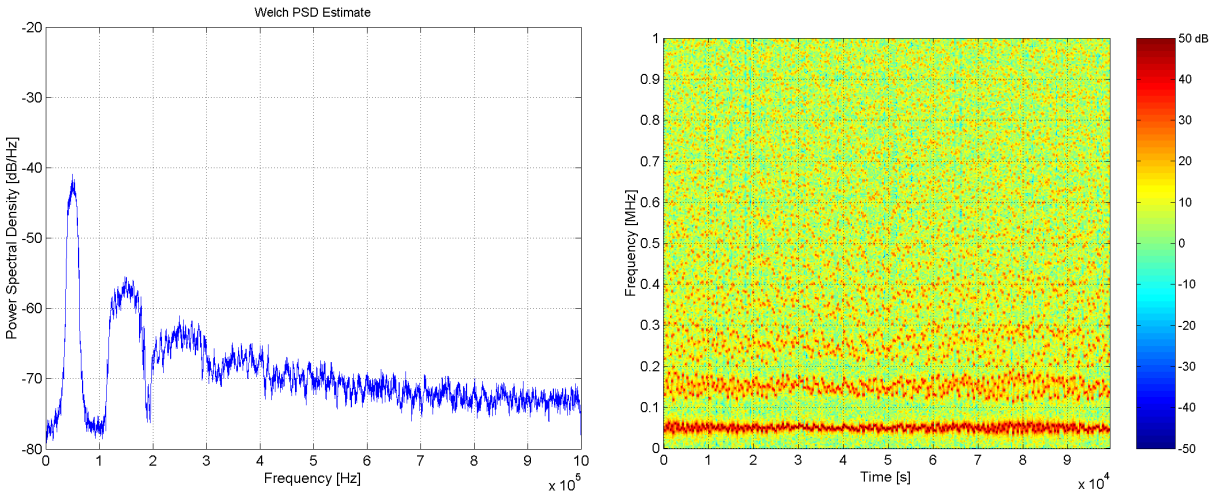

a) b)

Figure 4.18. Modulation with a frequency-hopping signal. a) the PSD and b) the spectrogram of the switching function $q(t)$. These results can be compared to the reference, Figure 4.3.

The nature of the frequency hopping spread spectrum signal can be seen in the spectrogram. Both the spectrogram and PSD shows that the frequency variation could have been larger for more effective low frequency spreading of the signal. The variation in the instantaneous frequency was larger in selected frequency modulation cases, and it is clearly visible if the spectrograms in Cases 1-3 are compared to Figure 4.18. b). However, the optimization of the hopping sequence is out of the scope of this study.

Autocorrelation of the frequency hopping $q(t)$ is plotted in Figure 4.19. There are no clear periodic parts in the autocorrelation sequence.

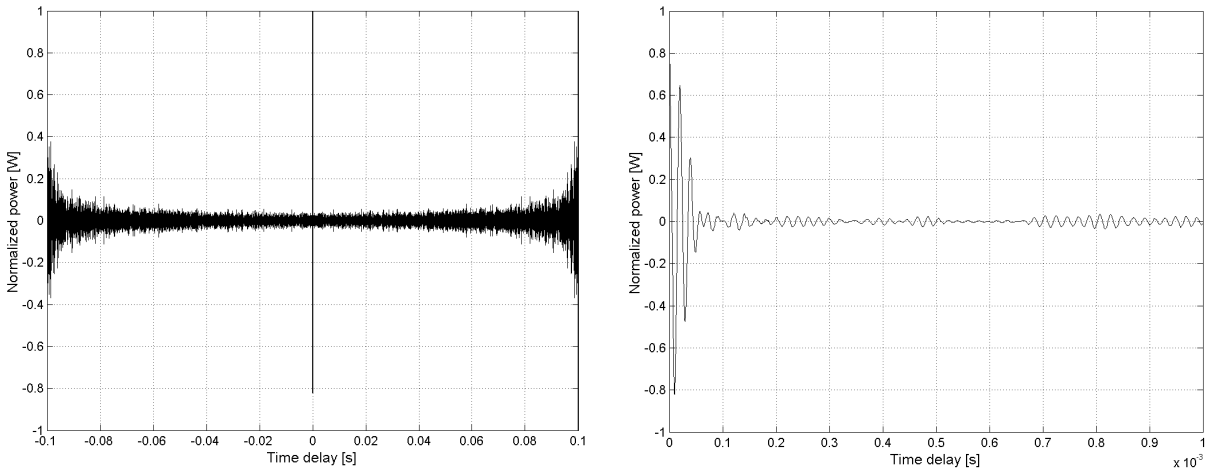

a) b)

Figure 4.19. The autocorrelation of the frequency hopping signal. The hopping sequence length is 100 ms, which causes maximums in the ends of the autocorrelation sequence in (a). There are no other visible periodic parts in the sequence. (b) The short-term periodic parts of the hopping signal are revealed in the close-up. The horizontal axis scaling is a) from –100 ms to 100 ms and b) from 0 to 1 ms.

4.4 Chaotic Peak Current Mode Controlled Boost-Converter

Chaos can be loosely defined as apparently random behavior in a nonlinear system. Since all switch mode power electronic circuits are nonlinear, chaotic behavior can be expected in the power electronic circuits with some specific component and parameter values. Usually this chaotic behavior is undesirable, but if the chaotic behavior can be controlled (or actually understood) it is very simple and an effective way to reduce the measurable EMI-content of the SMPS [Deane 1996], [Hamill 1997], [Deane 1999], [Mazzini 2001], [Banerjee 2002], [Callegari 2002].

The nonlinear nature of a switch mode power supply presents a potential for the chaotic operation of the converter. Especially when converter has a current-mode controller, chaotic behavior can easily occur with some system parameters. The chaotic operation of power converters has been investigated widely in the literature, and the phenomenon has been proven true both theoretically and experimentally. The longest tradition in chaotic system research is in the field of meteorology. Edward Lorenz, a meteorologist at the Massachusetts Institute of Technology, was one of the first who did fundamental research work in this area in the 1960's, [Lorenz 1963].

Predicting the weather is a demanding task, and even nowadays impossible because of the chaotic properties of the climate system. Still, many improvements have been made in weather forecasting since chaotic theory research begun in the middle of the 20^{th} century. Regardless of the computer calculation capacity, we cannot make a precise weather forecast - not until we know the exact values of all the initial system parameters and their changes. The *butterfly effect* is one classical example of a chaotic weather system: The flight of a butterfly in China can cause next month a typhoon in Florida. The climatic conditions on Earth (chaotic weather system) are an example of a chaotic behavior. Although not the exact temperature values can be predicted, it can still be predicted that it is hot in the summer and cold in the winter. A chaotic system also has limits, so it is not likely that the temperature will go down to absolute zero or up to 5000 °C. This also applies to a power converter. If the operation of the converter is chaotic, it still has limits (bounded) and the output voltage, for example, can remain at the desired value.

Chaotic operation is deterministic but not predictable. This often misleads someone to think that a chaotic system is a random process. Chaos is not a random process, but it usually looks like random. If *exact* values of *all* system parameters are not known, the exact operation of the chaotic system cannot be predicted. Sometimes a chaotic system (i.e. power converter) is not recognized as chaotic, and a weird looking operation has been explained by sub-harmonic oscillations and instability of the converter.

The unique characteristics of the chaotic system may be seen by imaging the system to be started twice. If we do not have exactly the same initial conditions (for example from measurement error or from thermal noise), we cannot exactly predict the system behavior in the future. For a *non-chaotic* system this uncertainty leads only to an error in prediction that grows *linearly* with time. For a *chaotic* system the error grows *exponentially* with time, so the state of the system is essentially unknown after

a short time. This phenomenon is known as *sensitivity to initial conditions*, [Baker 1990].

The general form of the equation presenting the *n*:th-order autonomous[3] dynamical system can be written as:

$$\frac{dx}{dt} = f(x) \qquad x(t_0) = x_0 \ , \tag{4.17}$$

where $x(t) \in \Re^n$ is the state at time t and $f:\Re^n \to \Re^n$ is called the vector field, [Parker 1987]. The solution to the above equation with initial conditions x_0 at time t_0 is called a *trajectory*, $\phi_t(x_0)$. The system described can be linear or nonlinear and depends on $f(x)$. In the case of a boost converter, $f(x)$ is described by Equations (2.11) - (2.13) presented earlier in Chapter 2.4.

There are four steady state behavior (solutions) associated with a nonlinear system, [Chiang 1993]:

- equilibrium points
- periodic solutions
- quasi-periodic solutions
- chaos.

Most solutions in power electronic circuits operate at a stable equilibrium point or they may have a periodic solution. All these four solutions are briefly described next. The definitions are based on [Slotine 1991], [Parker 1987] and [Chiang 1993].

1. The state of the system is called an *equilibrium point* x_{eq} if once $x(t)$ is equal to x_{eq} and it remains x_{eq} for all future time, so $\phi_t(x_{eq}) = x_{eq}$ for all *t.*
2. $\phi_t(x^*)$ is a *periodic solution*, if $\phi_t(x^*) = \phi_{t+T}(x^*)$ for all t and some minimal period $T_P > 0$. Periodic solutions have a Fourier transform consisting of a fundamental at $f = 1/T_P$ and evenly spaced harmonics at k/T_P, $k = 2, 3, \ldots$, some of these components may be zero.
3. *Quasi-periodic* solutions are ones that can be written as the sum of the periodic functions

$$x(t) = \sum_i h_i(t), \tag{4.18}$$

   where function h_i has a minimal period T_i and frequency f_i. Base frequencies of each function h_i are (or some of them are) incommensurate, i.e. the ratio of frequencies is irrational. One example of a quasi-periodic signal is an amplitude-modulated signal, where the modulating signal is a periodic. Nonlinear interaction in the modulator between the message signal and the carrier frequency can easily generate a quasi-periodic signal.
4. *Chaos* has no generally accepted definition. Usually it can be defined as *bounded* steady state behavior, which does not fall into categories described in 1, 2 and 3. One characteristic property of a chaotic system is the *sensitivity to initial conditions*, [Baker 1990].

[3] In autonomous system the vector field is time-independent, and the initial time can be set to 0.

There are two requirements for the system before chaos can exist, [Baker 1990]:

- System must have at least three independent dynamical variables
- System must have some nonlinear term

4.4.1 Chaos in a Power Converter

Large signal characteristics of the nonlinear system (i.e. converter) have to be analyzed when studying chaotic operation, [Deane 1990]. Sometimes the converter circuit and controller are linearized in the power supply design for convenient analysis and simple controller tuning of the circuit. The designer may even make a linear small signal model for the converter. This kind of *linear model can in no way explain the real dynamics or chaos of the real converter*. Still the linear model can give acceptable results when the steady state operation of the real converter is traditionally stable. Often in practice chaotic behavior is not even recognized, and the outcome is understood as a result of loose contacts or from a burnt circuit.

Even basic textbooks on nonlinear systems and control do not consider stability in a simple way, [Slotine 1991], for example, reported: "… since nonlinear systems may have much more complex and exotic behavior than linear system, the mere notion of stability is not enough to describe the essential features of their motion. A number of more refined stability concepts, such as asymptotic stability, exponential stability and global asymptotic stability are needed."

For example Zafrany et al. [Zafrany 1995] and Poddar et al. [Poddar 1995] use terms stability and instability quite carelessly when describing the operation of the peak current controlled boost converter, even though these papers consider the chaotic operation. This slightly deceptive practice can also commonly be found in papers dealing with a current compensation ramp, [Zafrany 1995] for example. A stabilizing ramp is normally introduced in order to prevent periodic solutions and chaotic operation and extend the range for stable periodic operation beyond $D > 0.5$. If the converter operates in chaotic mode, it does not necessarily mean that the converter is unstable or uncontrollable. The paper from Marrero et al. [Marrero 1996] is so far the only one that focuses on this important aspect of the chaotic operation of the converter. This paper proposes the averaging method to compute various averages of interest for the chaotic regime of the boost, buck-boost and buck converters.

General analysis of the chaotic operation is presented for example in papers by [Chiang 1993], [Deane 1990], [Jefferies 1989] and [Chan 1996]. Chaotic control for power supply EMI-reduction is proposed by [Hamill 1997] and [Deane 1996]. Mathematical analysis of the DC-DC converters in chaos can be found in papers by [Chan 1996] and [Deane 1999]. [Marrero 1996] gives very useful techniques when designing a converter and control operating in the chaotic regime. The author has also published two papers concerning chaos-based EMI reduction techniques in SMPS applications. [P1] proposes a peak current controlled boost controller and [P3] utilizes sliding mode control in the chaotic regime of a buck converter.

In current-mode control, a DC-DC converter controller has a peak inductor current limit. This limit controls the power switch and sets the constantly changing duty

cycle. In constant frequency operation, the switch is turned on at a constant time interval. The switch is turned off when the current reaches the limit set by the controller. With some parameters, the system will operate at a varying frequency, and the operation looks like random or unstable. This kind of operation was shown in Figure 2.8, where the operation of the peak current control was introduced.

The sensibility of the system to parameter variations and the tendency for chaotic operation can be studied with the bifurcation diagram. In the bifurcation diagram, one system parameter is varied and the other system state is sampled. The bifurcation diagram illustrates the creation of sub-harmonic oscillations and chaos as a function of the selected system parameter. The varied system parameters in the test converter were the peak current reference level, Figure 4.20, inductance value, capacitance value and the input voltage, Figure 3.26.

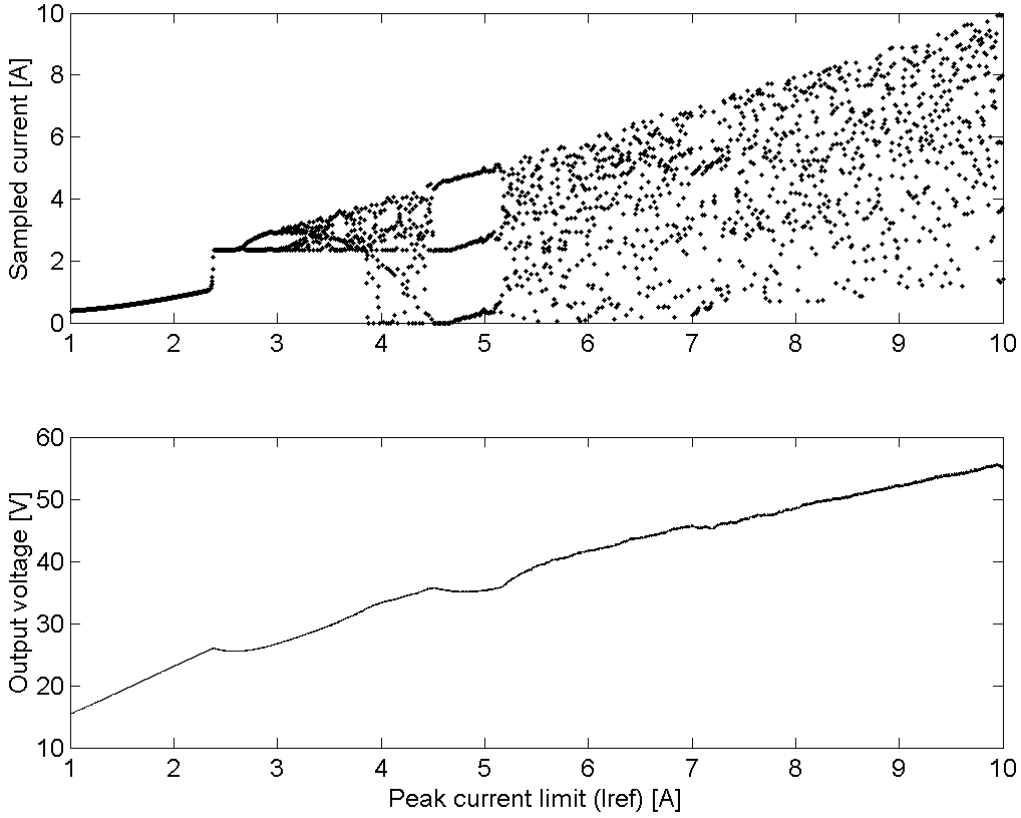

Figure 4.20. The bifurcation diagram (upper) generated by sweeping the current peak limit (I_{ref}) of the controller. By increasing the peak reference level the converter operation will bifurcate. The lower part of the figure represents the output voltage at different peak current limit values.

In the first bifurcation diagram, the input current was sampled with a system clock frequency of 50 kHz and the instantaneous value was plotted in the graph. Figure 4.20 shows how the peak current reference (I_{ref}) affects on the sampled current and on the output voltage. Below 2.3 A, the converter is in normal periodic operation mode. After approximately 2.3 A, the first periodic doubling occurs and the converter changes continuously the operation point between two periodic solutions. After 2.6 A, another periodic doubling occurs, and the operation is four-periodic. Between 3.7 A and 4.5 A there is no clear periodic operation at all, and the system behaves chaotically. Again, after 4.5 A, the system returns to periodic operation until it goes to

chaos after several bifurcations at 5.3 A. Figure 4.21 and Figure 4.22 present bifurcation diagrams of other selected converter parameters.

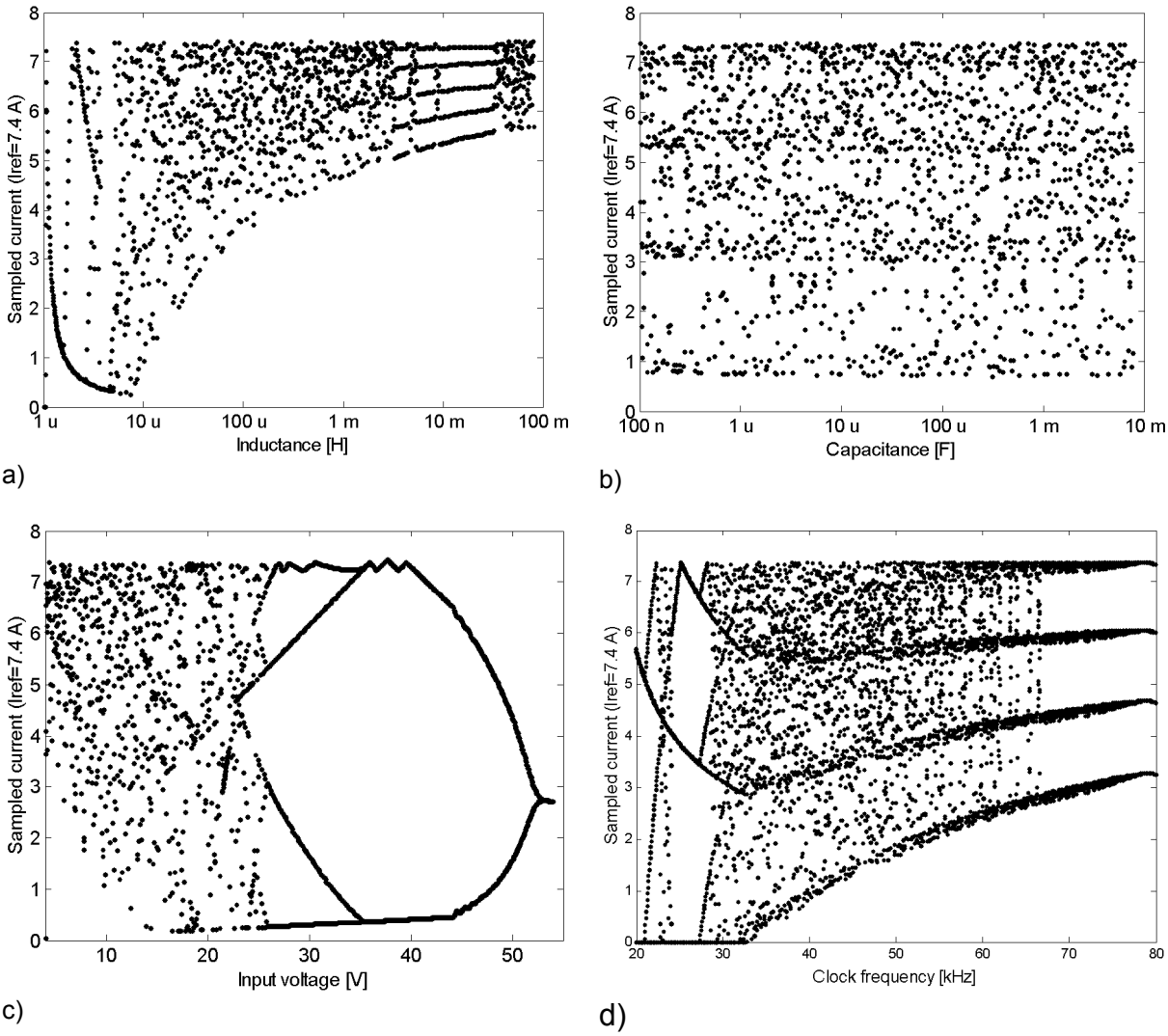

Figure 4.21. Bifurcation diagrams of the converter operation. Varied parameters are (a) inductor, (b) capacitance, (c) clock frequency and (d) input voltage. Other parameters are at nominal values in each case.

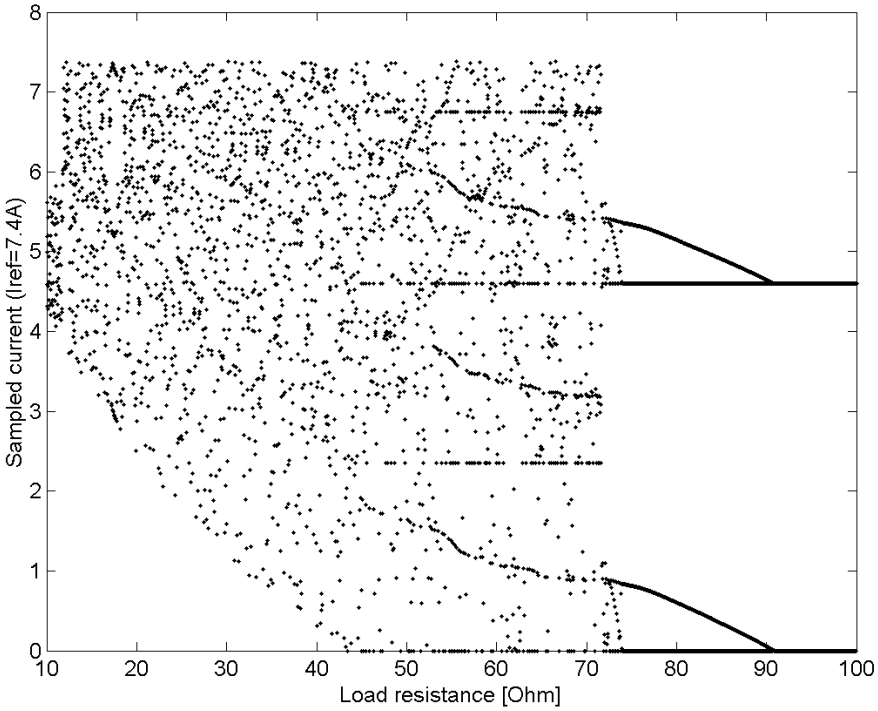

Figure 4.22. The bifurcation diagram generated by sweeping the load resistor from 10 Ω to 100 Ω. The operation will go to (single) periodic mode when the resistance is over 90 Ω. Multi-periodic operation is visible in the range between 45 Ω to 90 Ω.

Figure 4.21 shows the effect of the selected system parameter on the operation of the converter. The inductor value (a) does not have much of an effect on the operation mode, which seems to be chaotic at all inductor values shown in the graph. The only effect is on the current ripple, which naturally decreases when the inductor value increases. The same kinds of results can be obtained from the variation of the capacitor value (b), which seems to have no effect on the operation mode of the converter. Clock frequency (c) and input voltage (d) have a clear effect on the operation mode and there are several areas where the converter operation is chaotic. Figure 4.22 shows the effect of the load on the converter operation.

4.4.2 Case 5: Chaotic Peak Current Control

The simulation procedure for the chaotic converter differs from cases presented earlier, because the chaotic operation in the peak controlled boost converter is an inherent property of the converter/controller combination. Therefore, the boost converter model with controller had to be used in the simulation to obtain the switching function. For details of the model, see Appendix A. The PSD and the spectrogram of the switching function of the chaotic converter are shown in Figure 4.23.

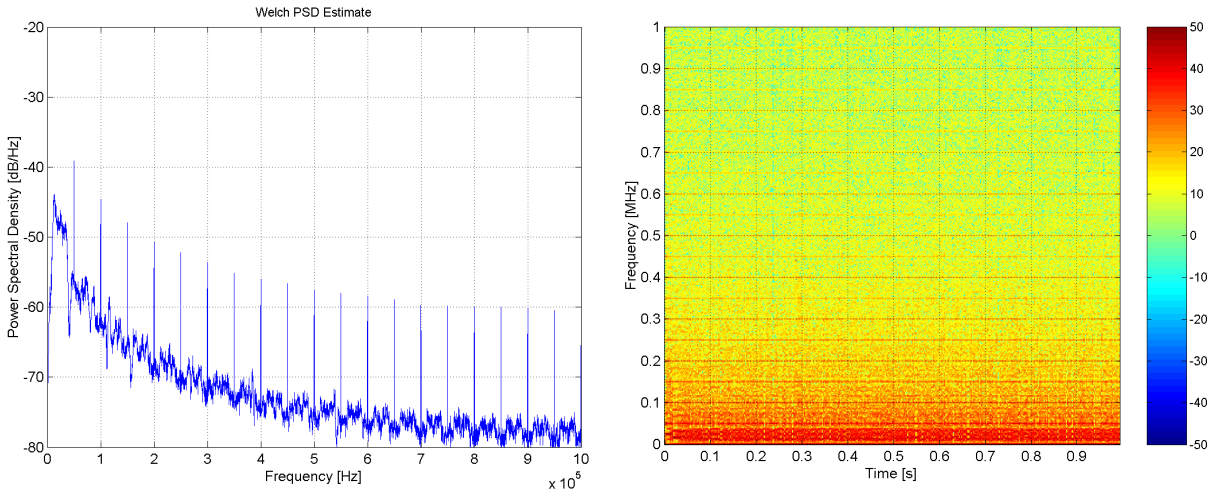

a) b)

Figure 4.23. Spectrum estimates of the chaotic peak current control mode. a) The PSD, b) the spectrogram of the switching function $q(t)$. These results can be compared to the reference, Figure 4.3.

The estimated PSD shows, that a 50 kHz system clock is present in the spectrum. This is also detectable in the spectrogram. A non-periodic operation causes a noise-like rise in the PSD background noise level, which can be seen in the spectrogram as blurry hot areas all around the graph. One characteristic spectral property of the chaotic mode is high power concentration in the low frequency range.

The autocorrelation sequence of this case is not promising, Figure 4.24. The dc-level of the plotted autocorrelation exposes the periodic nature of the signal. However, there are no long-term periodic parts in the sequence like in Cases 1-3.

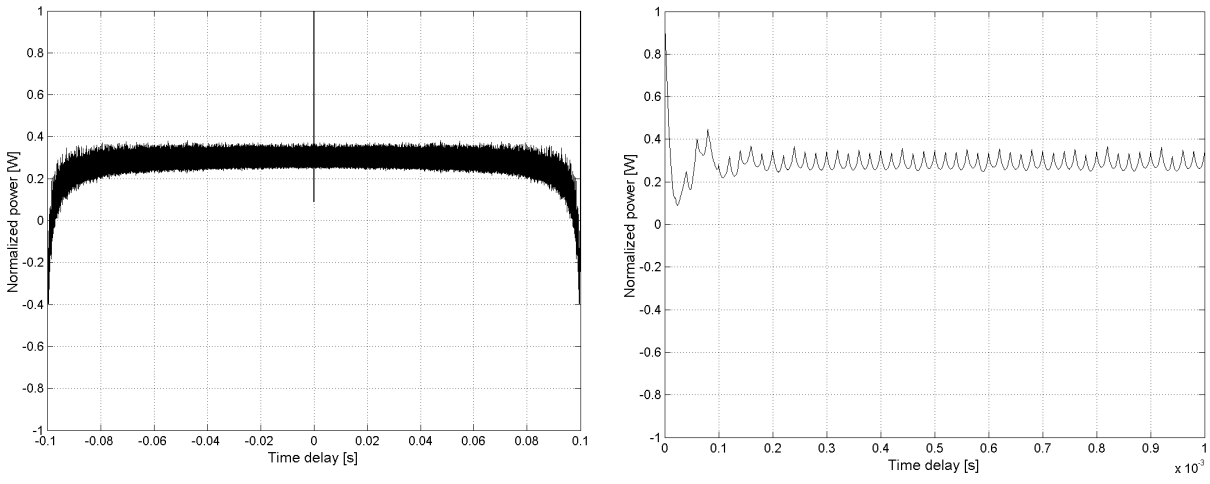

a) b)

Figure 4.24. The autocorrelation sequence of the switching function in peak current controlled chaotic operation. The dc-level of the sequence has climbed compared to previous cases. Close-up from the sequence shows periodic parts of the signal, (b). The horizontal axis scaling is a) from –100 ms to 100 ms and b) from 0 to 1 ms.

The high dc-level of the autocorrelation sequence correlates to the spectrum estimate in this case, Figure 4.23 a). Like in the constant frequency reference converter, there are several harmonic spikes in the Welch spectrum estimate.

4.5 Sigma-Delta Modulation

Sigma-delta modulator ($\Sigma\Delta$) has been traditionally used in analog to digital and digital to analog converters (ADC, DAC) and in communication systems. The technique and concept of a $\Sigma\Delta$-converter has existed since the middle of the 20th century. However, only in the last three decades the $\Sigma\Delta$-technique has been widely used. One reason behind this is, that the integration level has increased in semiconductor manufacturing, which makes the use of $\Sigma\Delta$ ADC and DAC cost effective. In some references and application fields, sigma-delta devices are still called delta-sigma converters. This term may be more correct in that, in its basic form, the converter consists of a delta modulator. A delta modulator has been utilized for many years in telecommunications. Unfortunately, nowadays the words delta and sigma seem to have been interchanged arbitrarily.

The main advantages in ADC and DAC applications are the simplicity of the one bit analog to digital converter, high number of effective bits and the character of the quantization noise: The quantization noise is spread over a wide frequency range. The quantization noise can, in some circumstances, be treaded as white noise, [Aziz 1996]. Although the noise is not actually white, this white noise-like property of quantization noise is very useful, for example, in ADC and DAC applications.

One power electronic related application is *class D audio power amplifiers* [Tousi 2002], [Magrath 1997], [Kok 1999]. The main idea using a $\Sigma\Delta$-power stage in audio power amplifiers is the efficiency and power consumption. In a $\Sigma\Delta$-based class D audio amplifier the efficiency can be over 90%. This means a much lower power consumption than at traditional class A or B audio power stages, where the efficiency is lower than 50 %.

A $\Sigma\Delta$-modulator has been proposed to be used in the field of power supply applications to reduce electromagnetic noise [Chang 2002], [Paramesh 2001]. This method is similar to the randomized PWM and FM schemes so that it attempts to disperse the noise spectrum over a continuous range of frequencies. $\Sigma\Delta$-modulation has also been used in resonant power converters, [Finney 1993]. The idea of using $\Sigma\Delta$ modulation in a resonant converter is, that the modulator and switching instances can be synchronized with the resonant frequency of the *LC* tank circuit. Another example of $\Sigma\Delta$-application in power electronics is reduction of the torque ripple and acoustic noise in motor drives.

In power supply applications, the $\Sigma\Delta$-modulator acts as a controller on the power converter. Since the $\Sigma\Delta$-modulator is, in basic form, a 1-bit digital device, the power switch state can present the logical state of the $\Sigma\Delta$-modulator output. Many of papers considering $\Sigma\Delta$-modulator concentrate on theoretical aspects such as stability, limit cycles and quantization noise. The main area of interest is also concentrated on VLSI-implementation of a $\Sigma\Delta$ ADC or DAC. A quite extensive overview of the $\Sigma\Delta$-technique is presented in [Aziz 1996], which also includes a long list of useful references.

4.5.1 Basic Operation of the ΣΔ-Converter

The ΣΔ-modulator operates using synchronized switching (sampling) instants, that can also be seen from the EMI-spectrum of the ΣΔ-operating power converter. The ΣΔ-modulator has a system clock that operates at a constant frequency. However, it also has been proposed to use a dithered ΣΔ system clock to even more effectively spread the noise spectrum, [Chang 2002], but this scheme has not been used in this work.

The basic principle of operation of the first order ΣΔ-converter is shown in Figure 4.25. The input signal is fed through an integrator and is then quantized to one bit resolution. The one-bit quantizer (comparator) output is then sampled with a high frequency system clock.

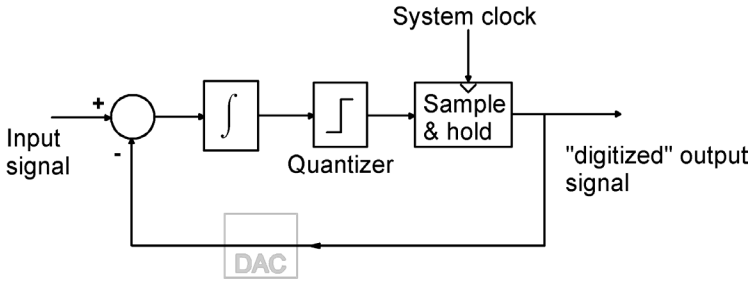

Figure 4.25. Operation of first order Sigma-Delta modulator. DAC in the figure presents a possible digital-to-analog converter in the modulator.

The output signal of the quantizer/sample&hold–circuit is fed back to the summing input and subtracted from the input. Note that the feedback signal is delayed by one sample cycle before being subtracted from the input. The negative feedback loop from the comparator output through the 1-bit DAC back to the summing point forces the average feedback DC voltage before the summing point to be equal to the input signal. Thus, the average of the digital output equals the input signal. The digitized output of the input signal is a pulse train and the output is often called *a pulse code modulated* (PCM) output.

The system clock frequency has to be much higher than the maximum frequency of the input signal. Frequency has to be even higher than the Nyquist rate, which is at least twice the highest frequency component (Nyquist frequency) of the input signal. The Nyquist rate conversion can be used in traditional AD-converters, where the quantizer uses more than one quantization level. In these traditional converters, the input is sampled at a Nyquist rate, and the resolution is dependent on the number of quantization levels. In a one-bit converter, like the ΣΔ-converter, the resolution is dependent on the *oversampling rate* of the converter. In practice, this means that a higher sampling rate gives a more accurate digital replica of the analog input signal.

Digitizing generates a quantization noise when continuous amplitude has been quantized in amplitude. Note that, quantization is a non-invertible, nonlinear operation. To analyze the ΣΔ-converter quantization noise, the quantization process is usually linearized, and the quantization noise is modeled as a noise source $e(n)$. Then, the quantized output signal $y(n)$ can be expressed as, [Aziz 1996]:

$$y(n) = x(n) + e(n), \tag{4.19}$$

where $x(n)$ presents the discrete input signal, which is not yet quantized.

The following assumptions [Aziz 1996] are usually made, when analyzing the performance and signal properties in a ΣΔ-converter:

- The quantization noise sequence $e(n)$ is a sample sequence of a stationary random process.
- The quantization noise $e[n]$ is uncorrelated with the converted signal $x(n)$.
- The probability density function of the error process is uniform over the range of quantization error.
- The random variables of the error process are uncorrelated, i.e., the error is a white noise process.

Of course, these conditions are not exactly satisfied: for example, the quantizer has only two output levels and the quantization noise can be correlated to the input.

However, when mathematically analyzing a one bit quantizer, the noise power spreads to a frequency range from zero to half of the sampling frequency, Figure 4.26.

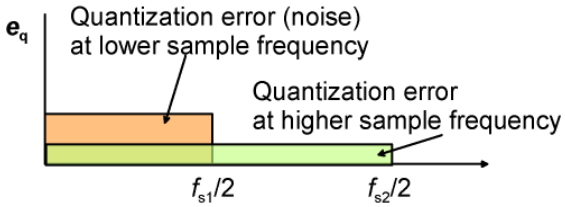

Figure 4.26. The quantization error/noise as a function of the frequency at two different sampling frequencies. Raising the sampling frequency spreads the spectrum of the quantization error to a wider frequency range.

A first order sigma-delta modulator has harmonic spikes in the case of DC-input and in the case of AC-input with a low modulation index, [Chang 2002]. In order to eliminate these spikes, a higher order modulator or random dithering can be utilized. Random dithering means, that either the clock of a sample-and-hold-circuit has been dithered or a random noise sequence is added to the input of the sigma-delta converter. One possible implementation of a dithered sigma-delta modulator is presented in [Chang 2002].

One problem with the basic first-order system, resulting directly from its nonlinear nature and feedback, is the presence of limit cycle oscillations. This will produce periodic components in the output in response to DC inputs and low frequency. Even when using a higher order modulator, limit cycle oscillations can occur. Actually, this means that a Sigma-Delta operation can go to chaos via bifurcations. The phenomenon, limit cycle oscillations, can be seen in Figure 4.27. The input signal was set at a DC value of 0.1. Sampling instants, when the output can change state from –1 to 1, are illustrated with blue dots.

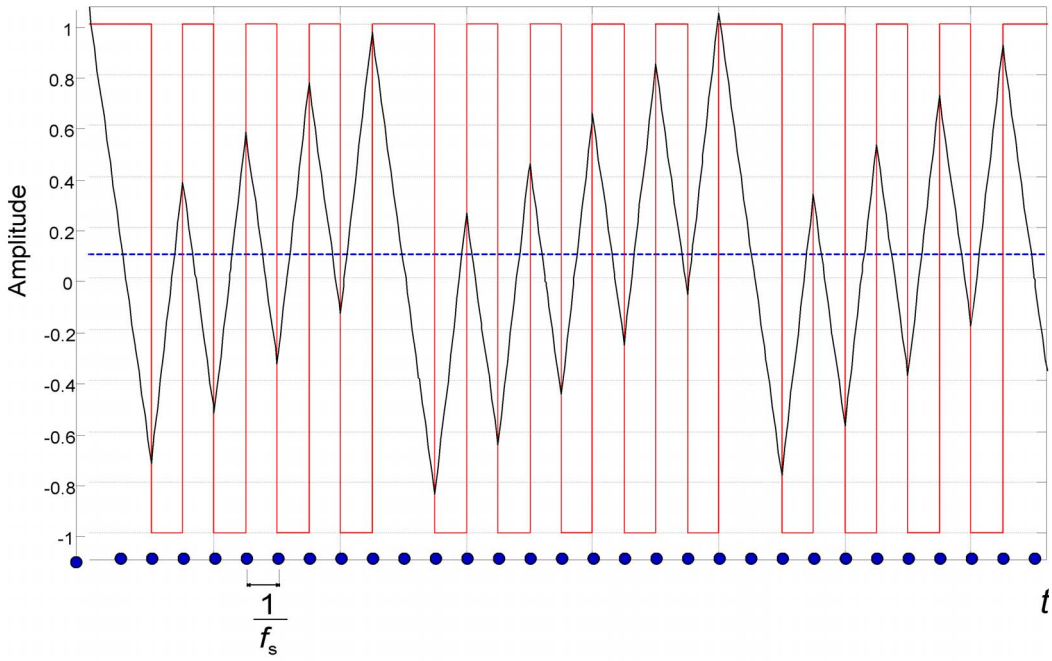

Figure 4.27. An example of limit cycle oscillations in a Sigma-Delta converter at constant DC-input (amplitude 0.1, dotted line). Owing to the fixed, constant period switching time instants with the frequency f_s, the output of the ΣΔ-converter oscillates around the desired output. Note that here the feedback signal (black) is an integral of the output (red).

To reduce the quantization noise and improve the spectral performance (i.e. reduce spikes), a second or higher order ΣΔ-modulator can be used. The structure of the second order ΣΔ-modulator is quite straightforward: another integrator and feedback loop is added to the circuit. The main idea is shown in Figure 4.28.

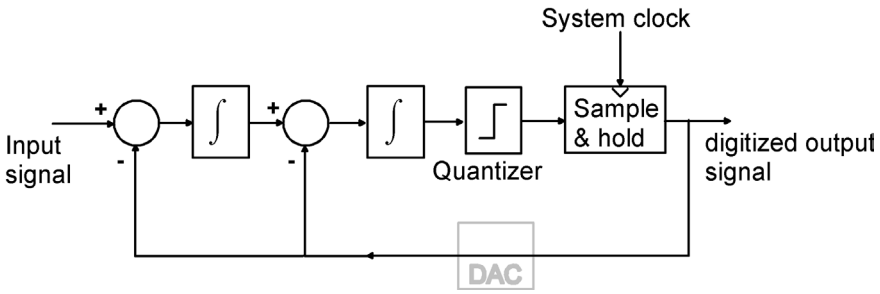

Figure 4.28. A block diagram of a second order Sigma-Delta modulator.

Figure 4.29 clarifies the effect of the modulator order to the resulted spectral content. In Figure 4.29 a), a first order ΣΔ-modulator is used. The operation is clearly periodic with harmonic spikes in the spectrum. In the case of the second order modulator the resulting spectrum is continuous and no harmonic spikes are present in Figure 4.29, b).

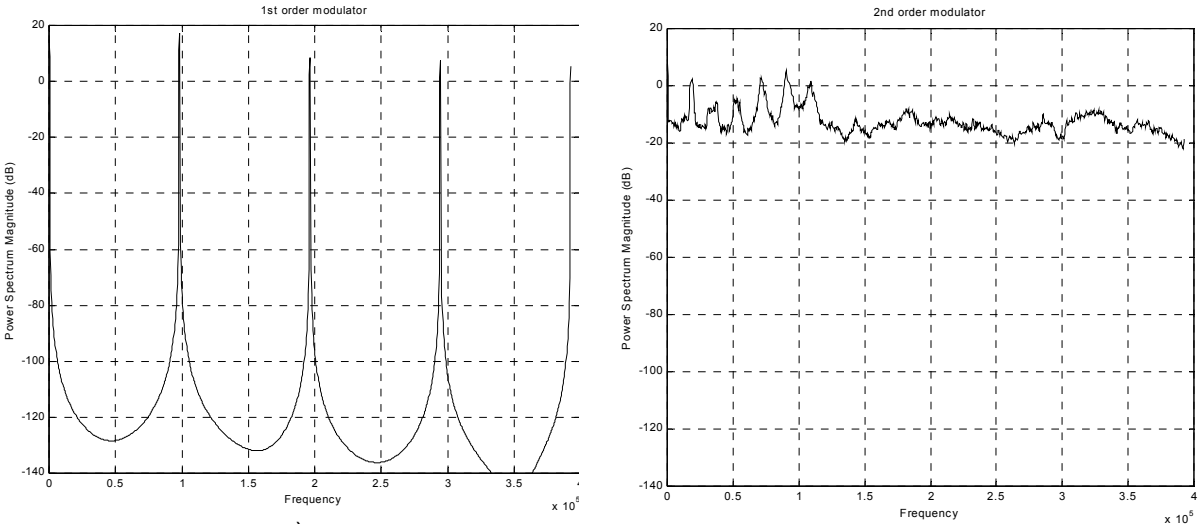

Figure 4.29. An example of the spectral content of a ΣΔ -modulator output in the case of a first (a) and second order (b) modulator.

With a higher order modulator, spectral spikes have been decreased, but again, the overall noise floor has increased. The reduction of the spikes in this example is approximately 10 dB. The simulation model of the example in Figure 4.29 is shown in Appendix A.

4.5.2 A Sigma-Delta Modulator in a Power Converter

Since the ΣΔ-controlled switch mode power supply does not operate at a constant switching frequency, the designer has to select a proper clock frequency and over-sampling rate. These frequencies are dependent on the system parameters of the converter (i.e. inductor and capacitor values, load). Improperly selected design parameters may even result in a periodic operation at a sub-harmonic frequency of the ΣΔ-converter clock. Simulation tools are necessary, when selecting the right component values, over-sampling frequency and ΣΔ -parameters to ensure aperiodic operation at different load conditions.

Switching losses and limitations from the magnetic components set the limit for the maximum operation frequency of the switching converter. Switching losses may also increase if varying switching frequency and constantly changing duty cycle is used. However, Dallago et al., [Dallago 2001], have reported in their study on a sigma-delta modulator controlled boost converter, that a varying switching frequency has no significant effect on the power switch or diode losses.

A second order ΣΔ-topology was selected in the power converter test set-up. An *RC*-low pass filter forms an approximate integrator in an inner integrator loop. The power switch and the main inductor form the other integrator loop. The power switch is controlled via a modulator output. A simplified block diagram of the converter control is shown in Figure 4.30.

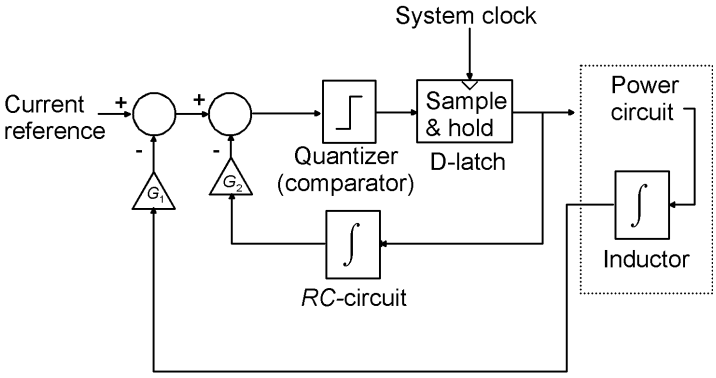

Figure 4.30. Simplified block diagram of the experimental ΣΔ-controlled boost converter.

G_1 and G_2 represent the gain of different feedback loops. The system clock frequency was selected to be 200 kHz. This is four times over-sampled system clock to the power converter system, which was designed earlier to operate at a nominal switching frequency of 50 kHz. The over-sampling rate could be much higher, but a lower over-sampling rate will force the system to operate at different sub-harmonic frequencies of the system clock: if the system clock rate is set to be infinite, the converter will operate at a constant frequency and no frequency variation occurs. Selection of other controller parameters was based on simulations made with the Matlab™ model, Appendix A.

4.5.3 Case 6: Chaotic Sigma-Delta Controller

The whole converter and control had to be used in a Sigma-Delta controlled converter simulations to achieve the switching function. Again, same normalization was made before calculating the spectral performance. Calculated estimations are shown in Figure 4.31.

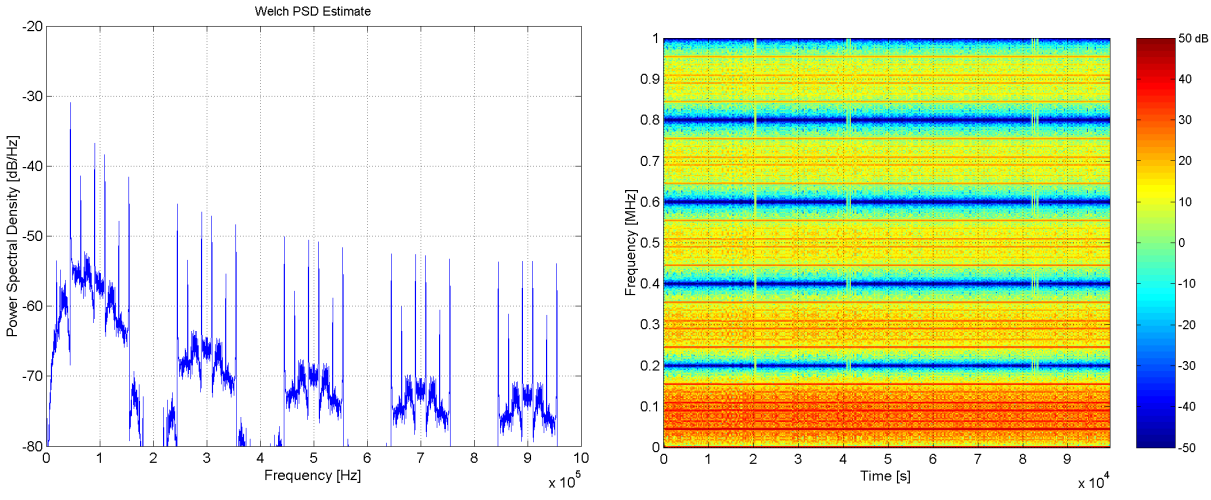

a) b)

Figure 4.31. Spectral effects of the Sigma-Delta controlled controller. a) The PSD, b) the spectrogram of the switching function q(t). These results can be compared to those in Figure 4.3.

The oversampling frequency of the Sigma-Delta converter is present in both the PSD and spectrogram. The shape is nevertheless totally opposite when compared for example to the peak controlled chaotic converter: there are minimums at the clock frequency and even harmonics. Periodic operation causes also some noticeable

spikes in the PSD. Constantly (chaotically) changing frequency causes again blurry hot areas in the spectrogram. High low-frequency content is also characteristic of a Sigma-Delta converter.

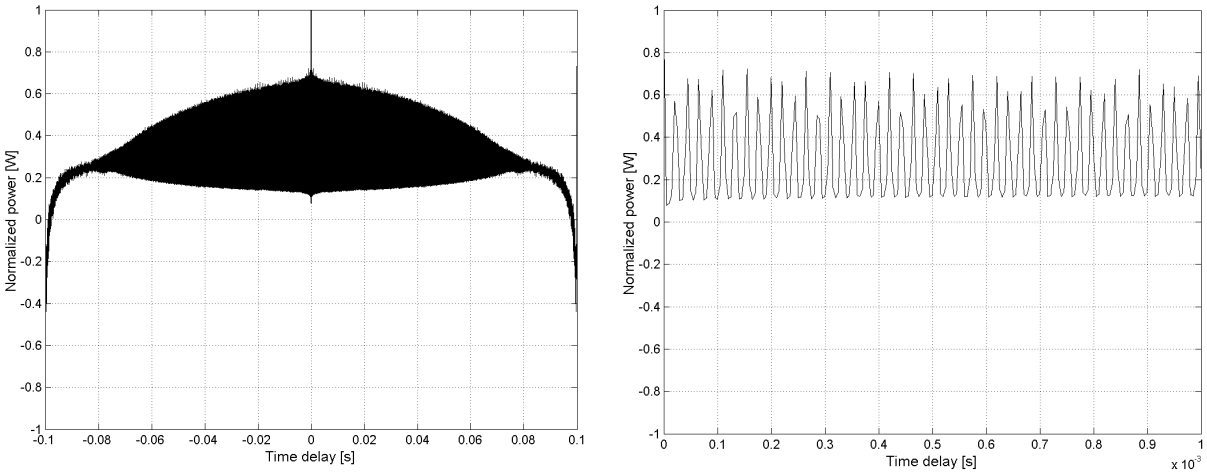

a) b)

Figure 4.32. An autocorrelation sequence of the switching function in Sigma-Delta controlled chaotic operation. A high dc-level predicts poor frequency-domain performance. There are also clear periodic spikes in the sequence (b). The horizontal axis scaling is a) from –100 ms to 100 ms and b) from 0 to 1 ms.

The plotted autocorrelation sequence shows again a high dc-level predicting periodic operation. This can be seen also in the spectrum estimate of the $\Sigma\Delta$-converter shown in Figure 4.31, where high harmonic spikes can be seen.

4.6 Summary of Spectral Results

To have numeric values from the frequency analysis of the switching function, the frequency range from 0 Hz to 1 MHz was divided into ten equal parts and the maximum values of each frequency range were recorded. These calculated peak values are collected in Table 4-2. In addition, the reduction compared to the reference is calculated respectively. The average of this reduction is finally calculated for each case. This numerical value cannot be considered as an accurate result but it gives a trend of spectral performance for different modulation techniques.

Table 4-2. (**SEE ERRATA**) Calculated peak values of the Welch estimate of the switching function at different frequency ranges. The first row represents the peak values of the constant frequency reference converter. Different cases are listed in different rows where peak values, attenuation to the reference converter and average attenuation (mean) are listed.

CASE ↓	Frequency band, [Hz] →	10kHz - 100kHz	101kHz - 200kHz	201kHz - 300kHz	301kHz - 400kHz	401kHz - 500kHz	501kHz - 600kHz	601kHz - 700kHz	701kHz - 800kHz	801kHz - 900kHz	901kHz - 1MHz
PWM-reference	Peak [dB]	-29.5	-29.0	-31.4	-36.1	-47.4	-44.3	-47.4	-41.5	-42.0	-47.4
Case 1: FM-sine	Peak [dB]	-39.0	-38.0	-50.9	-61.2	-50.0	-59.8	-65.5	-60.2	-55.5	-64.3
	Reduction [dB]	**9.5**	**9.0**	**19.5**	**25.1**	**2.6**	**15.5**	**18.1**	**18.7**	**13.5**	**16.9**
	Mean reduction	**14.9 dB**									
Case 2: FM-sine+noise	Peak [dB]	-44.9	-44.1	-58.1	-59.1	-58.4	-61.3	-63.8	-64.5	-64.8	-65.9
	Reduction [dB]	**15.4**	**15.1**	**26.7**	**23.0**	**11.0**	**17.0**	**16.4**	**23.0**	**22.8**	**18.5**
	Mean reduction	**18.9 dB**									
Case 3: FM-triangle +noise	Peak [dB]	-45.1	-44.3	-58.6	-58.7	-59.5	-60.4	-63.4	-64.3	-65.3	-66.4
	Reduction [dB]	**15.1**	**15.3**	**27.2**	**22.6**	**12.1**	**16.1**	**16.0**	**22.8**	**23.3**	**19.0**
	Mean reduction	**19.0 dB**									
Case 4: Frequency hopping	Peak [dB]	-46.1	-40.9	-59.1	-55.5	-56.3	-62.6	-61.1	-63.0	-64.9	-65.0
	Reduction [dB]	**16.6**	**11.9**	**27.7**	**19.4**	**8.9**	**18.3**	**13.7**	**21.5**	**22.9**	**17.6**
	Mean reduction	**17.9 dB**									
Case 5: Chaotic peak current	Peak [dB]	-29.8	-39.1	-44.6	-48.0	-50.7	-65.2	-52.2	-53.6	-55.1	-56.0
	Reduction [dB]	**0.3**	**10.1**	**13.2**	**11.9**	**3.3**	**20.9**	**4.8**	**12.1**	**13.1**	**8.6**
	Mean reduction	**9.8 dB**									
Case 6: Chaotic $\Sigma\Delta$-modulation	Peak [dB]	-29.7	-30.9	-36.7	-41.5	-70.2	-45.4	-53.5	-46.6	-48.4	-77.4
	Reduction [dB]	**0.2**	**1.9**	**5.4**	**5.4**	**22.8**	**1.1**	**6.1**	**5.1**	**6.4**	**30.0**
	Mean reduction	**8.5 dB**									

Table 4-2 shows, that significant reduction can be achieved with spread spectrum modulation. According to these results, the most promising techniques are FM with triangular modulating wave+noise, FM with added random noise in a modulating sinusoidal wave and the frequency-hopping signal.

4.7 Summary

Four different spread-spectrum techniques in six different configurations were presented and theories behind these techniques were introduced. The Welch spectrum estimates of the switching functions of different SS-techniques were calculated for harmonic spectrum analysis. In addition to the Welch PSD, the periodic nature of the signal was analyzed with time-frequency analysis, a spectrogram and by a calculated autocorrelation sequence of the switching function.

5 The Test Setup and Test Results

The EMI-effectiveness of different modulation methods was studied with several simulations and measurements made with the boost converter. The quantity for the conducted EMI analysis was the differential input current of the converter. In addition, the steady-state performance of the converter was examined with simulations and measurements made from the converter input current and output voltage. The main purpose of steady-state analysis is to find out effects of the variable frequency operation to the normal operation on the power converter.

The conducted emissions test setup of the prototype converter was made according to standard [CISPR 16-2 1999]. Settings for the test receiver were taken from CISPR 16-2 and [CISPR 22 2003]. Measurements were made in a non-standardized frequency range from 9 kHz – 1 MHz with a 200 Hz IF filter. The purpose of this non-standardized setup was the aim of this study to make a uniform test environment to clarify the effect of the selected modulation method. By using this method and settings, differences in modulation methods could be easily compared. The main idea in this study was to compare spectral characteristics of different modulation methods, not to compare them to international standard levels. Therefore, absolute values of the emissions were irrelevant in this comparative study. In addition, the measurement setup used is a direct realization of the simulated system, and therefore the results can be easily compared to the simulation results.

This chapter focuses on the steady-state current and voltage measurements and EMI-spectrum measurements made from the input current of the converter. Measurements were confirmed with simulations. Firstly, results from the input current and the output voltage ripple are shown. These waveforms were recorded with an oscilloscope and compared to the simulations. Secondly, simulated and measured conducted noise spectra were depicted. The test setup for all measurements is also described in the next pages.

5.1 The Test Setup

The heart of the test setup was the boost converter prototype designed and constructed by the author. The prototype was designed so, that all different modulation methods could be tested with the same main power circuit. Only minor configuration changes had to be done to the control circuitry when changing to a different modulation method. The modulation sequence was calculated and stored in Matlab™. During the test, saved waveforms were programmed in a Sony-Tektronix AWG 2021 arbitrary waveform generator, [Sony-Tektronix 2001], to modulate the power circuit in FM and the frequency-hopping converters. A constant clock frequency was used in $\Sigma\Delta$ and the peak current controlled converters. The converter prototype was assembled to a two-sided printed circuit board containing both the boost power circuitry and the configurable control circuitry. A resistive load was used in tests. A general test assembly is shown in Figure 5.1, and the physical layout of

the test setup is shown in Figure 5.2.

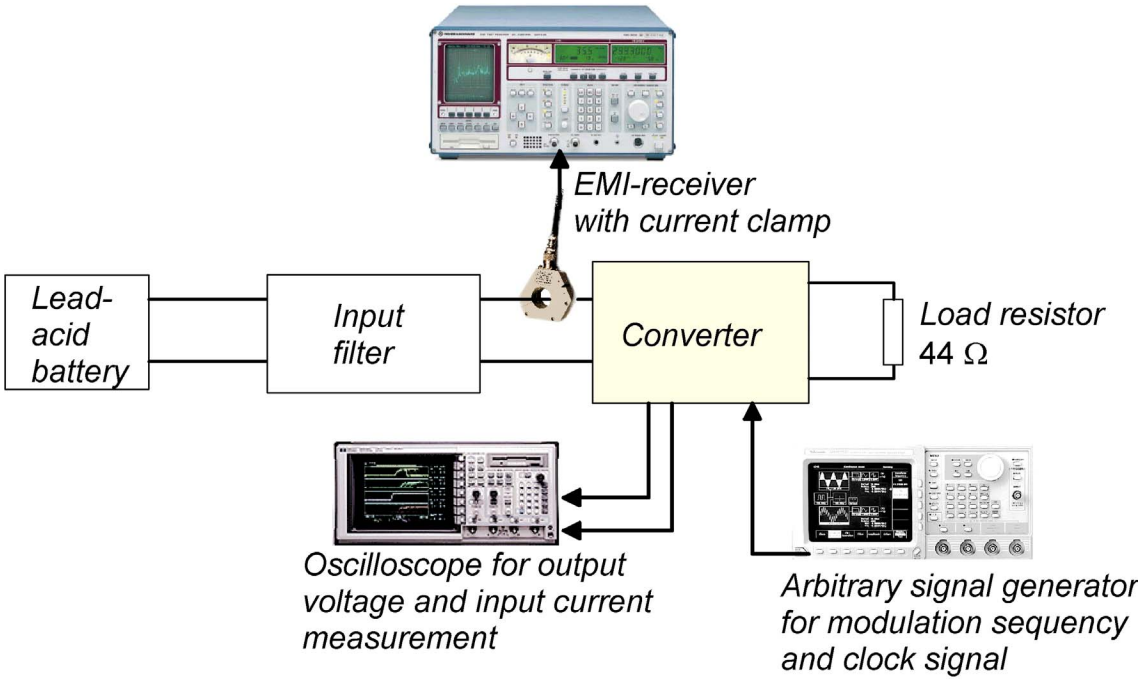

Figure 5.1. Connections and the general layout of the test setup. The EMI-current spectrum was recorded with an EMI test receiver with a current clamp. The input current and output voltage waveforms were recorded with an oscilloscope. A programmable signal generator was used for the modulation sequence or the clock signal generation. Lead-acid battery was used as a noiseless voltage source for the setup.

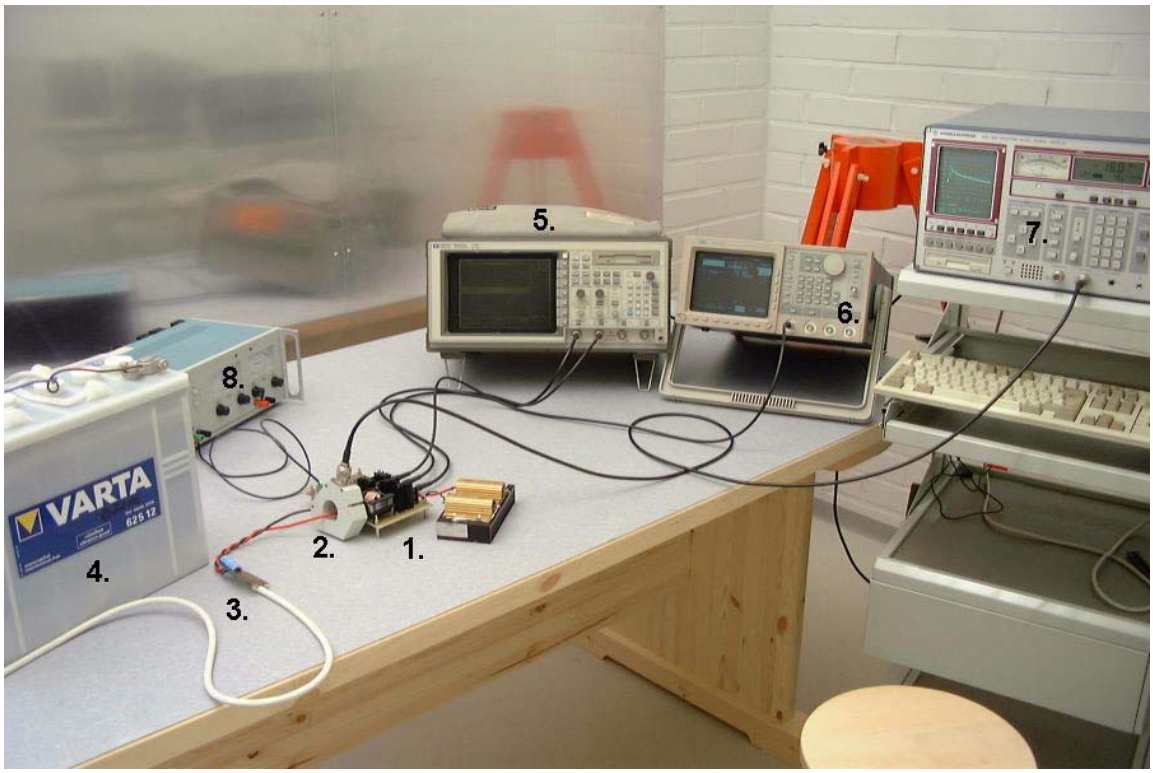

Figure 5.2. The physical layout of the test setup. 1: The prototype converter with the load. 2: The current clamp measurement from the input current. 3: The input filter. 4: The lead acid battery, 5: The oscilloscope. 6: The arbitrary signal generator. 7: The EMI test receiver. 8: The power supply for the control electronics of the prototype.

The picture of the circuit layout of the converter and load is in Figure 5.3. A more detailed close-up of the printed circuit layout of the converter is shown in Figure 5.4.

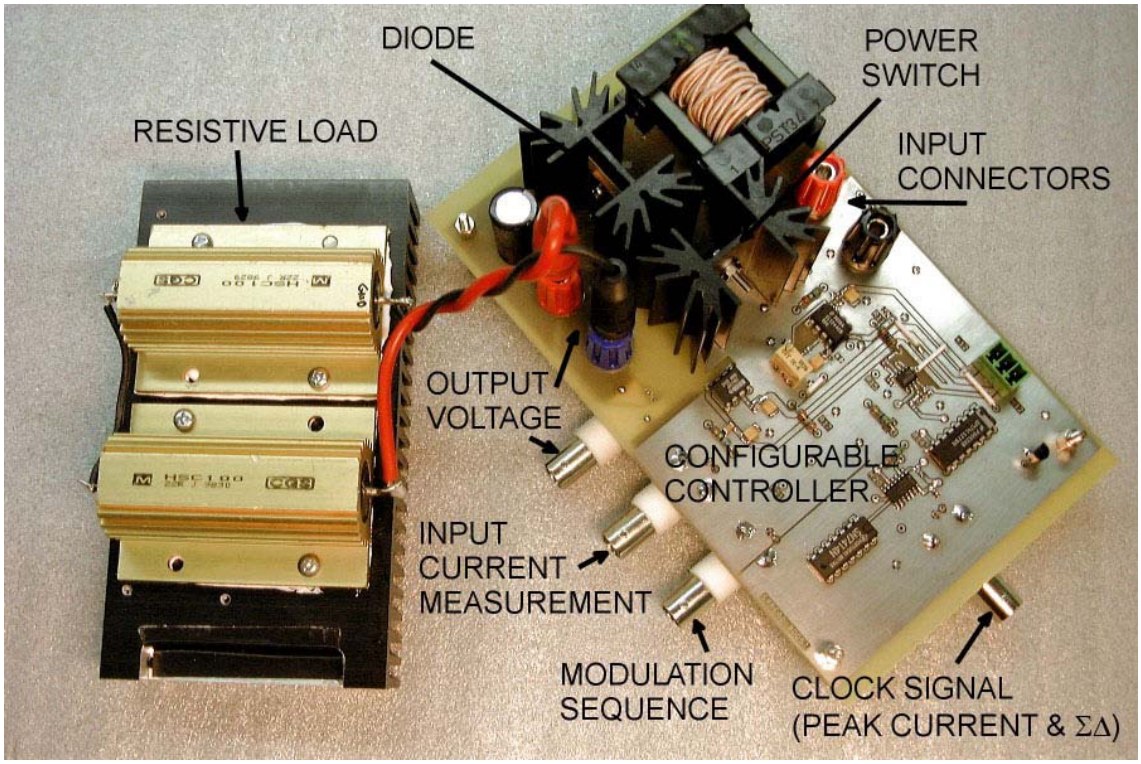

Figure 5.3. A general view of the prototype converter and the load. With minor jumper settings and connection changes, the converter can be configured to operate in different SSM-modes.

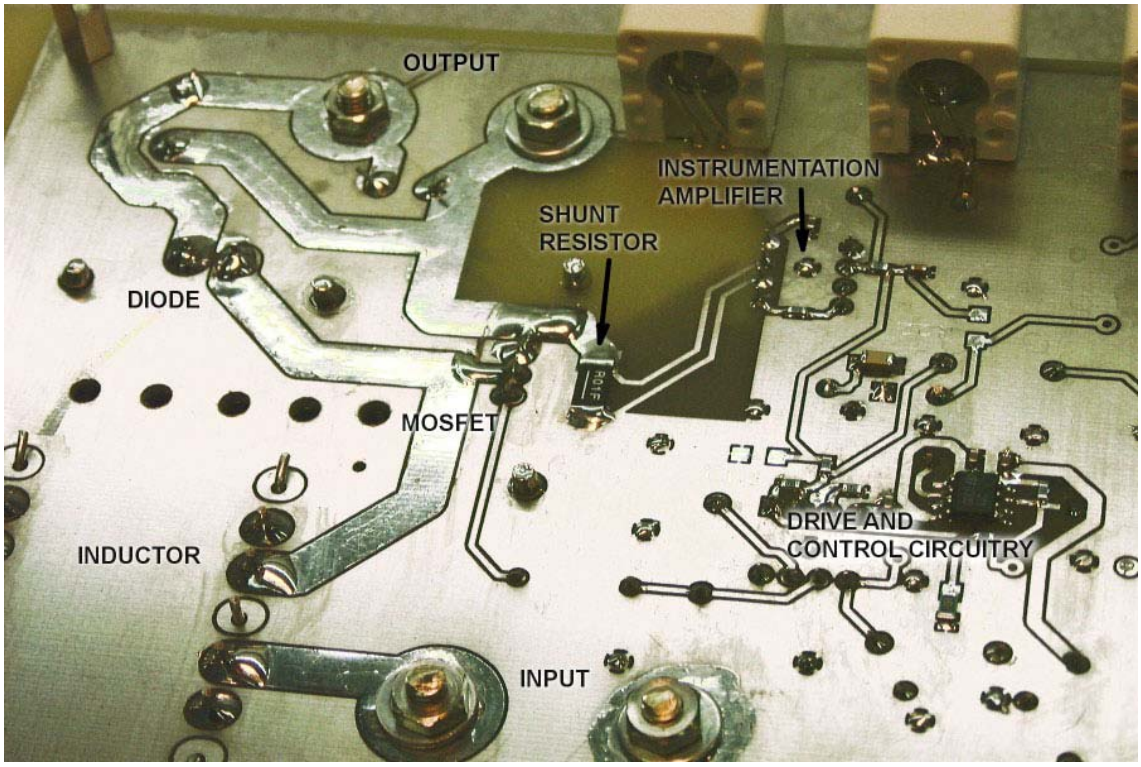

Figure 5.4. A close-up from the bottom side of the printed circuit board. Short PCB-tracks, minimal loops and a two-sided ground plane fill were used to achieve minimum inductance and proper EMC-properties of the layout.

The basic operating principle of this test setup was published in [P4]. Implementation of different variable-frequency techniques are shown in the simplified schematic diagram of the boost converter controller, Figure 5.5 b – d. The first four cases (i.e. FM and FH) utilize the basic PWM approach in the converter control introduced in Chapter 2.3. The only difference to the traditional implementation is that the saw-tooth wave was a preprogrammed variable frequency signal rather than a constant frequency signal, which is used normally in PWM power supplies. The programmable signal generator AWG 2021 used in the prototype measurements had a 12-bit DAC-resolution, a 250 megasample/s clock rate and a 256 kB memory, [Sony-Tektronix 2001]. The programming was made with Matlab™ waveforms illustrated in Chapter 4.

The controller of the chaotic peak current control is shown in Figure 5.5 c). In this control mode, the constant frequency clock signal sets the SR-latch output and thus the $q(t)$ to high-state. The current feedback signal that comes from the converter input current resets the latch and turns off the power transistor when the current reaches the selected peak current level. A more detailed description of the controller was given in Chapters 2.3 and 4.4.

Figure 5.5 d) shows the operating principle of the double-loop sigma-delta controller in the prototype. The inner loop consists of an approximate integrator implemented with an *RC*-circuit. The time constant 10 μs of the *RC*-circuit is much lower than the operation of the controller and therefore the circuit behaves as an integrator. The outer feedback signal comes from the inductor current. The inductor current of a boost converter can be evaluated from Equation (2.3), and it can be shown that the current is proportional to the integral of the inductor voltage and thus the switching function $q(t)$. A comparator is used as a one-bit quantizer and a D-latch in the circuit diagram acts as a sample and hold circuit. General operation of the ΣΔ-converter was described in Chapter 4.5.

There was no voltage feedback in the controller and the converter was operating in open voltage loop mode. It was illustrated in Chapter 4 that the controller itself has effect on the instantaneous switching frequency of the converter. The converter transfer function and dynamic properties directly effect on the spectral performance. Therefore, these additional design variables coming from the voltage loop were left out of this study to highlight inherent spectral properties of the selected variable-frequency techniques. The output voltage U_{out}, Figure 5.5 a), was adjusted to a nominal 48 V each time the modulation method was changed. The output voltage was also monitored during the measurements, and adjustments were made, if necessary, to keep the output DC voltage as a nominal ± 1 V. The reference voltage of the inner modulator (i.e. PWM, ΣΔ or peak current) can be adjusted with a potentiometer to achieve the desired output voltage, in this case 48 V.

A detailed circuit diagram, component list and layout of the prototype test converter can be found in Appendix C.

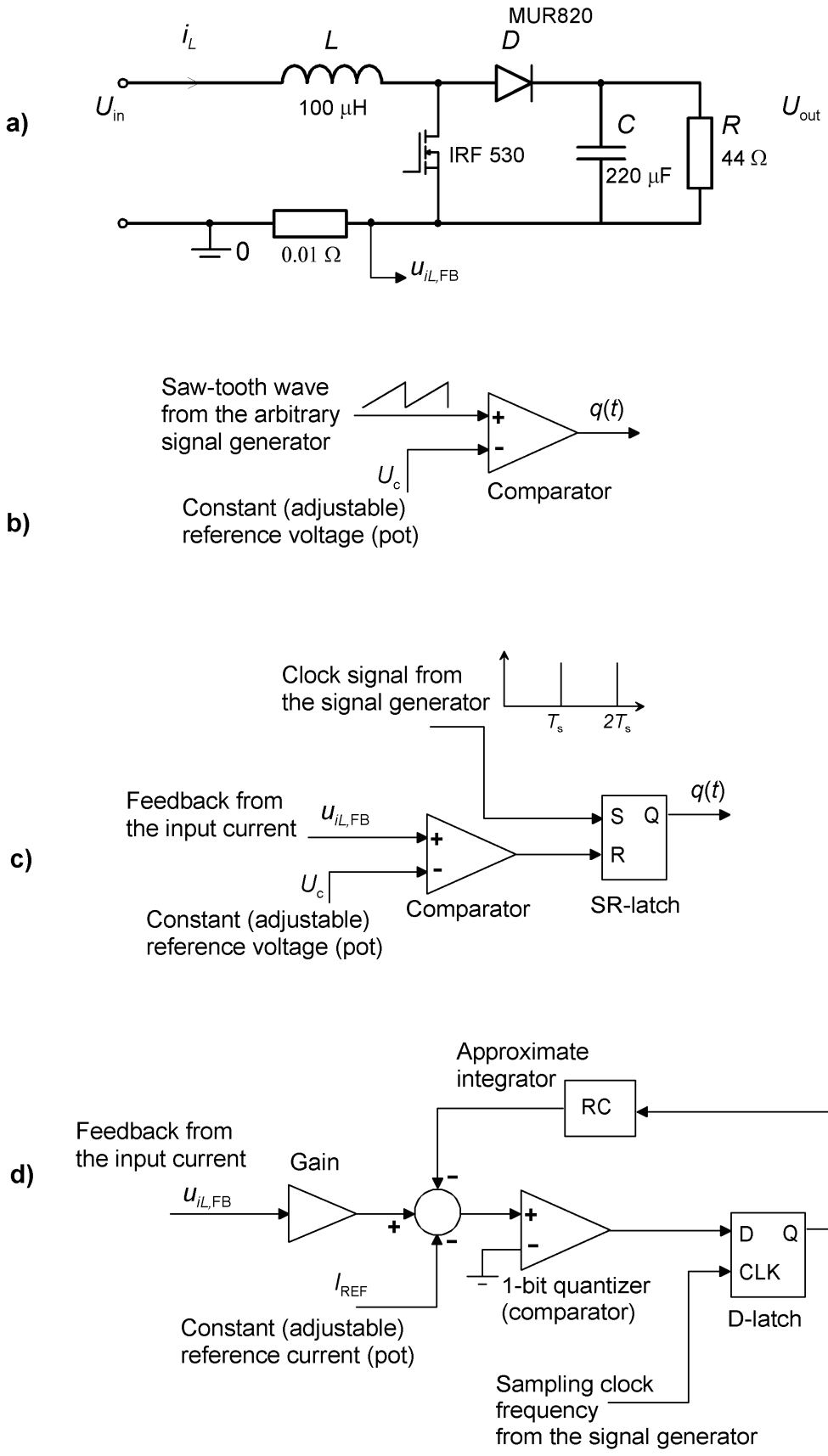

Figure 5.5. a) A simplified schematic diagram of the boost main circuit. b) Configuration of the controller in PWM-operation. c) The controller in chaotic peak-current control mode. d) A block diagram of the chaotic ΣΔ-controller.

Frequency modulation was used in the selected three basic forms described earlier in Chapter 4.2. Different modulation signals were treated as different Cases 1 - 3. Case 4, frequency-hopping, was introduced in Chapter 4.3. The same algorithm and modulation sequence used in Chapter 4.3 was used in the prototype measurements.

Some modifications had to be done to the control circuit of the prototype to get the converter to operate in peak current controlled chaotic mode, Case 5. Previous Cases 1 – 4 used a pre-programmed saw-tooth wave in a simple PWM comparator to generate the switching signal $q(t)$. The peak current controlled converter utilize the current-loop controller shown in Figure 5.5 c). However, the main circuit remained the same and these adjustments could be done with a few jumper changes in the prototype and with an external system clock, see Appendix C.

Case 6, Sigma-Delta operation of the converter control utilized the digital part of the converter control, Figure 5.5 d). The main power circuit was again the same, only minor jumper modifications and an external clock was needed. The system clock was running at 200 kHz in the selected case. This mean four times over-sampling compared to the nominal switching frequency. The sigma-delta controller was operating in chaotic mode, although the operation principle and route to chaos differed from Case 5.

The 12 V nominal input was fed from a lead acid battery to minimize the effect of the power supply noise. The power lead was a 1.5 m long, 2 x 2.5 mm^2 multi-core installation cable. To minimize the effect of the cable inductance and resistance, a filter was connected before the converter. The filter section also included a fuse to prevent converter damage in the case of controller failure or an accidental short circuit. The schematic diagram of the filter is shown in Figure 5.6 and measured parameters of the filter are given in Appendix B. 20 cm long test leads were used to connect the input filter to the converter. The EMI spectrum of the converter was measured from this connection with a current clamp, see Figure 5.2.

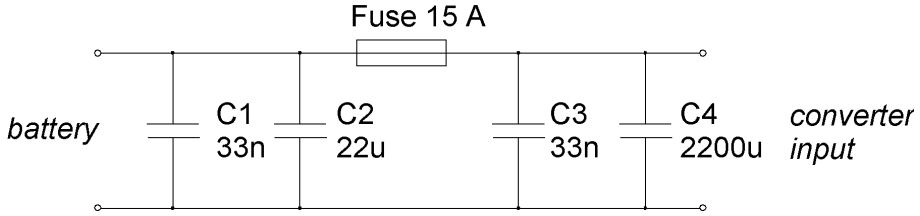

Figure 5.6. Input filter for minimization of the effect of the cable inductance and resistance and for circuit protection. The EMI current spectrum was measured with a current clamp from the positive output lead of the filter.

Aluminum clad wire-wound power resistors (2 * Tyco/Electronics-CGS HSC 100, 22 Ω/100W) were used as a load resistor for the converter test circuit. Resistors were mounted on a heat sink. Although the resistors were wire-wound design, measurements showed that the impedance was well controlled and even over the measurement frequency range of up to 1 MHz, see Appendix B.

5.2 Analysis of the Converter Steady-state Performance

Numerous papers have been written and different VF-techniques have been proposed in the literature to improve the EMI-performance of the switching power supply. Low frequency output voltage ripple has been considered as a major problem in variable-frequency DC/DC converters, [Shrivastava 1997], [Hui 1998], [Tse 1999-2]. However, not many papers concerning this important aspect have been published.

The effect of the VF-operation on the output voltage ripple is analyzed in this study with simulations and measurements. The amount of ripple and overall output voltage variation is a typical design parameter of a switching converter. If the ripple is large, it may also cause problems when the voltage feedback controller is added to the circuit, because there can be problems like oscillations in the feedback system with some selected parameters. The output voltage measurement was made with an oscilloscope from the BNC-connector after the output capacitor.

Input current waveform of the converter is also analyzed. Among the output voltage ripple, the current ripple is another converter design parameter and one of the main design factors in inductor design. Both simulated and measured results are shown. The input current was measured from a current shunt resistor placed in the power circuit. This resistor is part of the current feedback controller. Measured gain from the input current to the output of the instrumentation amplifier is approximately 0.1 V/A. A measured current waveform is shown here as a visual aid to evaluate the effect of the modulation, not as an absolute accurate measurement result.

Test results are collected together in the following pages. Firstly, simulated voltage and current waveforms of the constant frequency reference converter are shown. After this, simulated and measured voltage waveforms of different VF-techniques are illustrated with measured ripple values. Finally, the effect of the modulation method on the current ripple is analyzed with simulations and measurements. The oscilloscope used in these measurements was HP 54542 C, [Agilent 2003], which had a two gigasample/s sampling capacity, 500 MHz continuous bandwidth and 32 kB sample memory.

5.2.1 Constant-frequency Reference Converter

Figure 5.7 shows the simulated and measured output voltage and input current waveforms of the constant-frequency PWM-reference. This reference converter emulates the operation of a customary switching converter. The VF-operation of the converter can be compared to the following results.

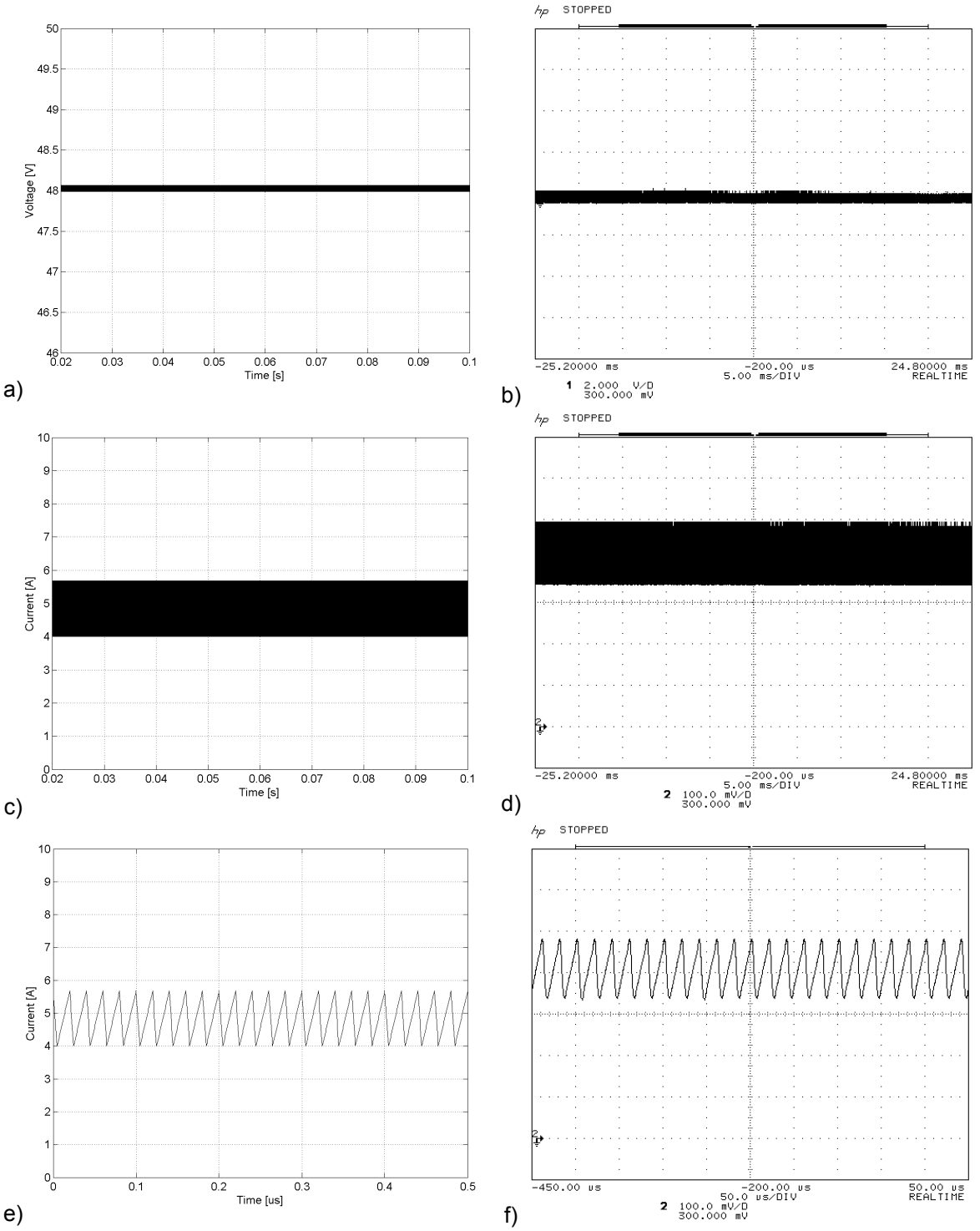

Figure 5.7. The simulated output voltage (a) and input current (c) and (d) of the reference PWM converter. The measured voltage (b) and current (d & f) waveforms of the reference converter. The switching frequency of 50 kHz and the duty cycle was kept constant. Scaling for measured voltage is 2 V/div vertical and 5 ms/div horizontal. Scaling for measured current is 1 A/div vertical and the horizontal is 5 ms/div in (d) and 50 µs/div in (f).

A 0.2 V voltage and 1.6 A current ripple were measured from the simulations. The measured current ripple of the reference prototype converter is 1.3 A. Also the measured voltage ripple of 0.6 V is slightly higher than in the simulations.

5.2.2 Voltage Ripple in Different VF-techniques

Figures 5.8 and 5.9 show the effect of the variable frequency operation on the output voltage of the converter. Simulated output waveforms of different variable frequency converters are depicted in Figure 5.8.

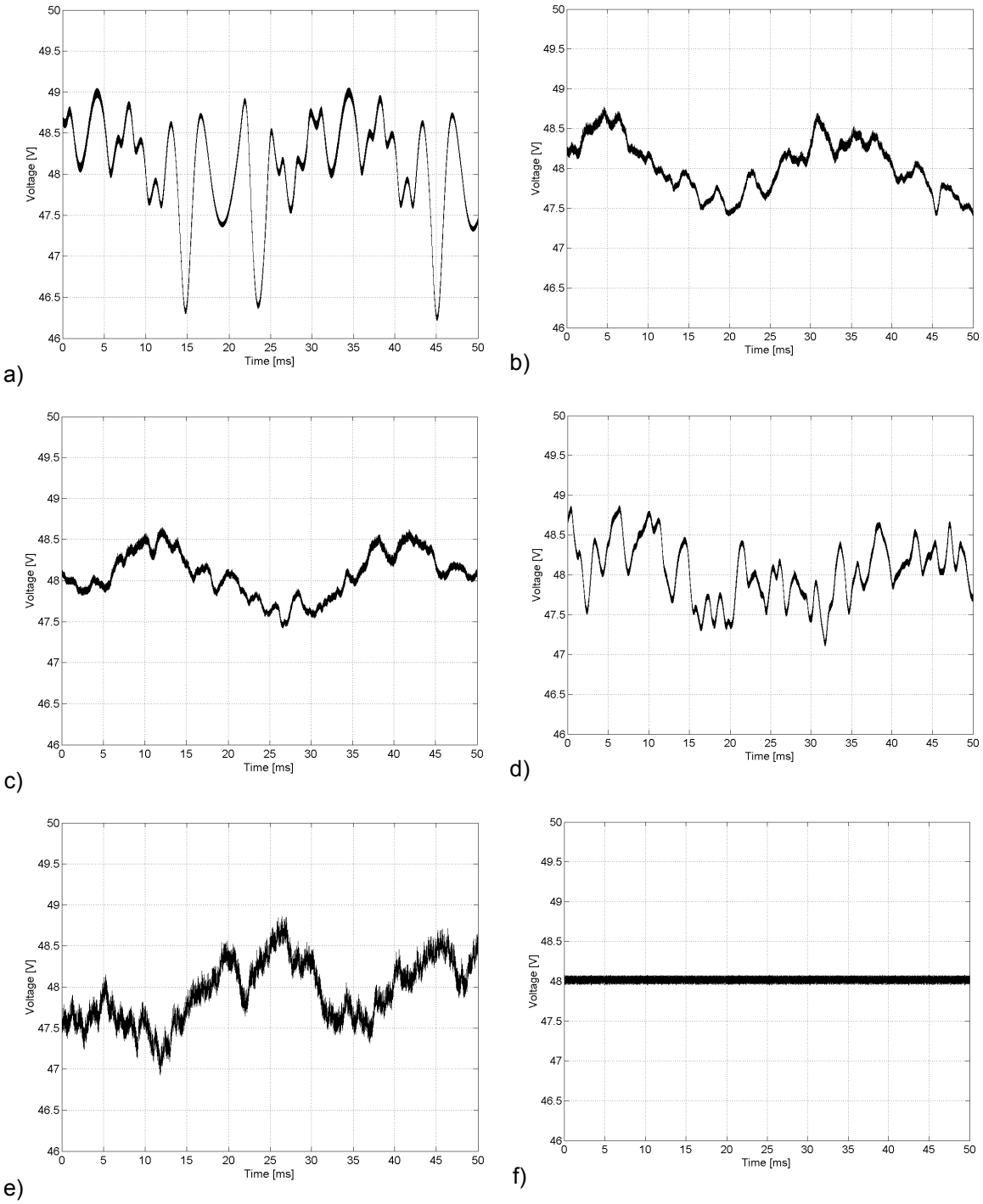

Figure 5.8. Simulated output voltage waveforms of the boost converter in different cases. a) FM-sine, b) FM-sine + noise, c) FM-triangle + noise, d) frequency-hopping, e) chaotic peak-current control and f) chaotic $\Sigma\Delta$ control. These waveforms can be compared to the simulated reference converter waveform shown in Figure 5.7 a).

Voltage measurements made with the prototype converter are shown in Figure 5.9.

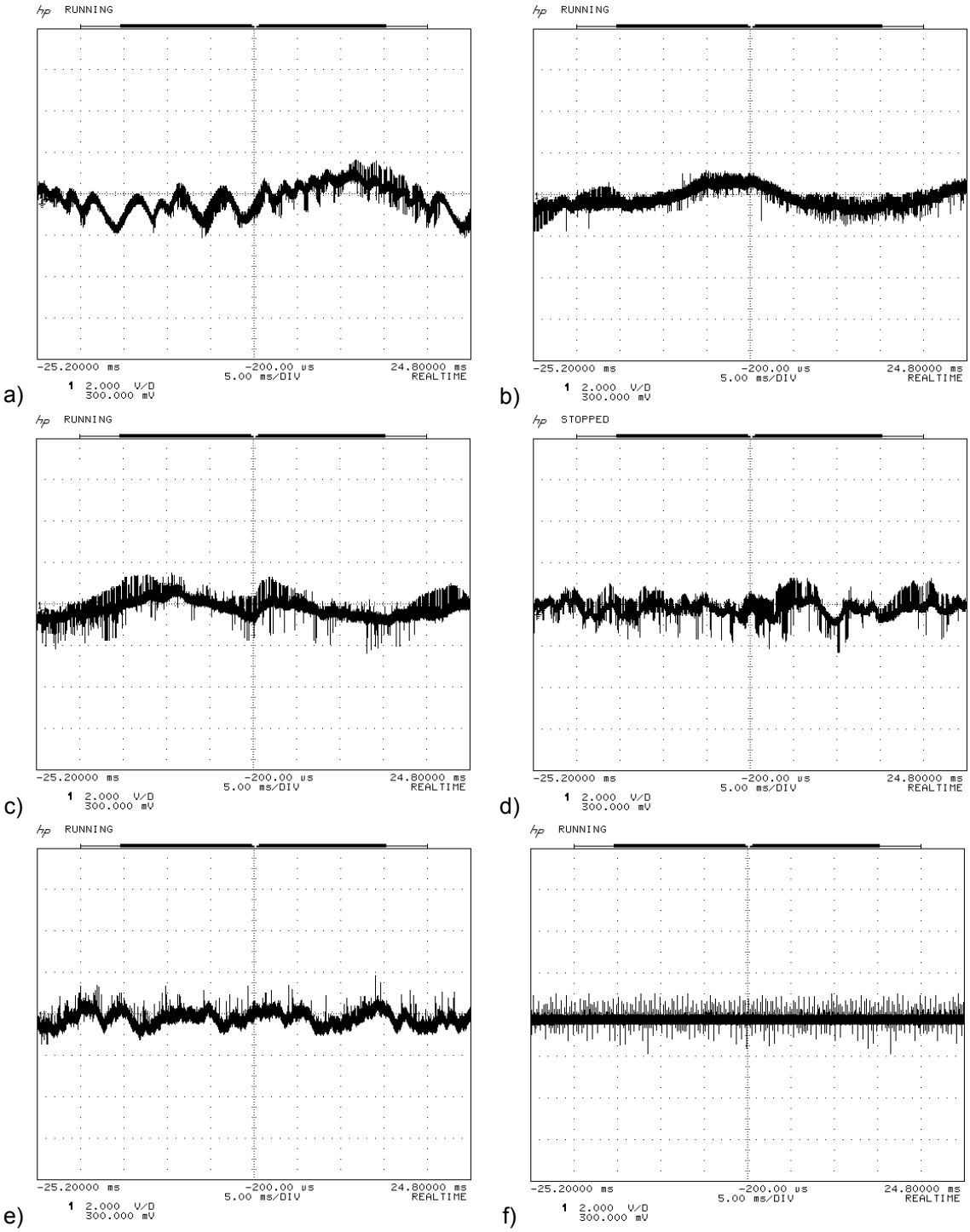

Figure 5.9. Measured voltage waveforms of the boost converter in different cases. a) FM-sine, b) FM-sine + noise, c) FM-triangle + noise, d) frequency-hopping, e) chaotic peak-current control and f) chaotic $\Sigma\Delta$. Oscilloscope is AC-coupled, the horizontal axis is 5 ms/division and the vertical axis 2 V/division. These waveforms can be compared to the measured reference converter waveform shown in Figure 5.7 b).

In Case 1, the modulation sequence length is clearly visible as a periodic ripple component in the simulated voltage waveform of the converter. The calculated ripple is 2.7 V. The same 30 ms period of the modulating wave is present in the measured voltage waveform, where the ripple is 3.5 V.

In Case 2, an added pseudo-random noise component in the modulating wave reduces the variance in the voltage waveform, and the ripple is lower than in Case 1. The simulated output voltage ripple is 1.5 V. The ripple in the output voltage is almost double when comparing simulated results to the measured 2.8 V. Simulated waveforms look almost the same in Cases 2 and 3. The first impression when looking at Figure 5.8 is that the waveform shape is identical to Case 2. However, the output voltage ripple in Case 3 has been reduced 0.2 V. The result is opposite in the measurements, where the ripple has increased from 2.8 V to 3.8 V when comparing Cases 2 and 3.

In the FH-converter Case 4, the simulated voltage ripple is 1.8 V. The measurements show that the ripple is approximately 3.5 V. There is no clear period in the simulated or in the measured waveform. The level of the ripple is at an equal level compared to previous cases.

A simulation from the chaotic peak current controlled converter shows a voltage ripple of 1.9 V. The measured voltage ripple in Case 5 is 3.0 V. The envelope of the voltage waveform looks random without any detectable period.

The simulated voltage ripple in the Sigma-Delta controlled converter is 0.1 V, which is the same as the ripple in the constant frequency reference converter. Oversampling of the Sigma-Delta converter affects clearly on the output voltage ripple of the converter. Measurements show that the output voltage ripple is higher also in this case when comparing measurements to the simulations. However, it is evident that the higher peak-to-peak readings in measurements originate from high frequency switching noise caused by the nonideal behavior of converter components, [Paul 1992], [Tihanyi 1995]. This can be seen in Figure 5.9 f), where the envelope of the waveform is almost identical to the simulated waveform in Figure 5.8 f). The main difference between these waveforms is the short duration spikes present in the measurement. The same phenomenon is also present in other measurements shown in Figure 5.9.

5.2.3 Current Waveforms in VF-converter

Simulated and measured input current waveforms are shown next. First, simulations and measurements are shown in Figure 5.10 and in Figure 5.11 in time scale of 50 ms to see the envelope and the long-time behavior of the signal. Figure 5.12 and Figure 5.13 show detailed close-ups from the signal to see the short-term behavior of the current at an arbitrarily chosen time instant with a time scale of 500 μs.

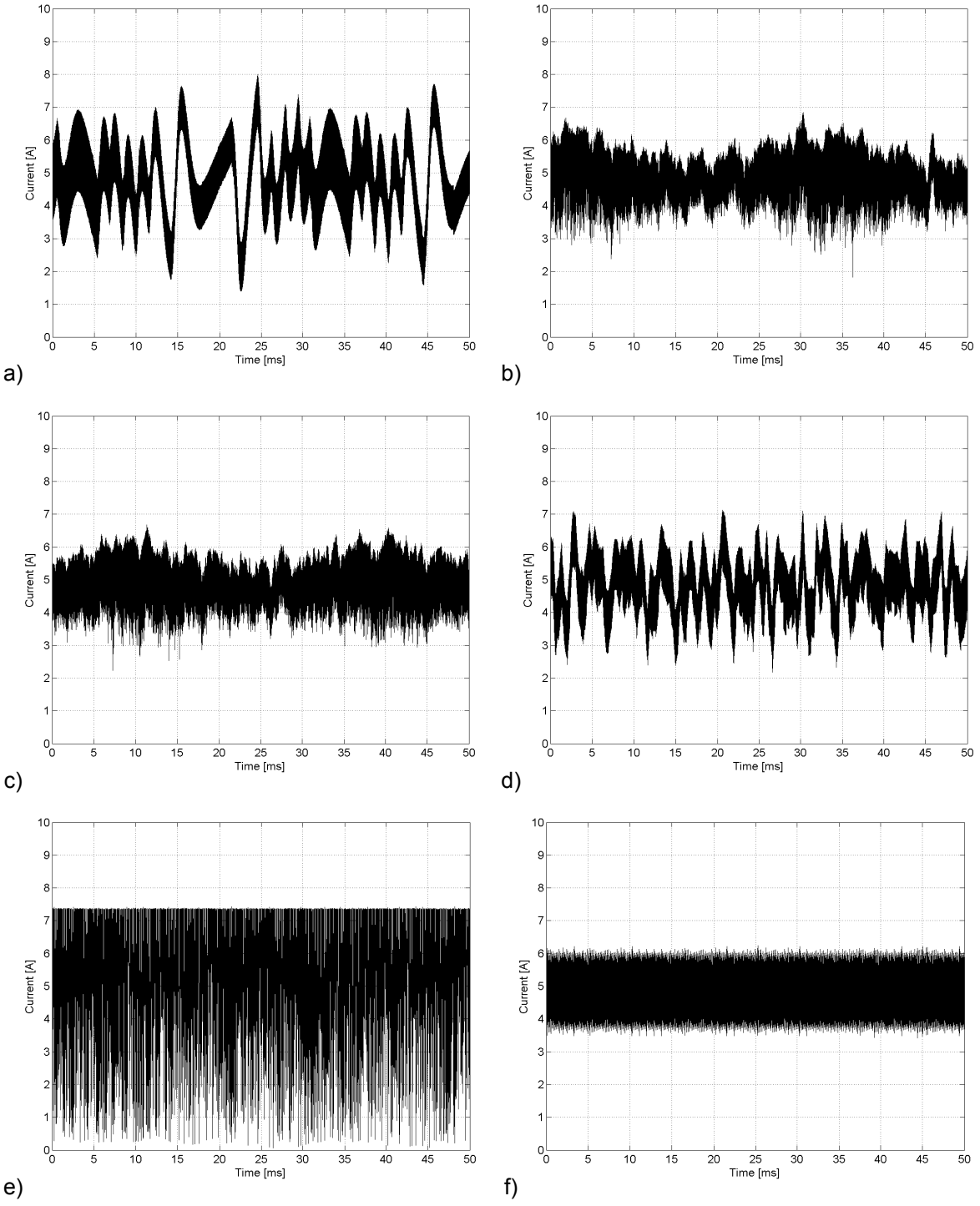

Figure 5.10. Simulated envelopes of the input current waveforms in different cases. a) FM-sine, b) FM-sine + noise, c) FM-triangle + noise, d) Frequency-hopping, e) chaotic peak-current control and f) chaotic $\Sigma\Delta$. Horizontal axis 5 ms/division, vertical axis 1 A/division. These waveforms can be compared to the simulated reference converter waveform shown in Figure 5.7 c).

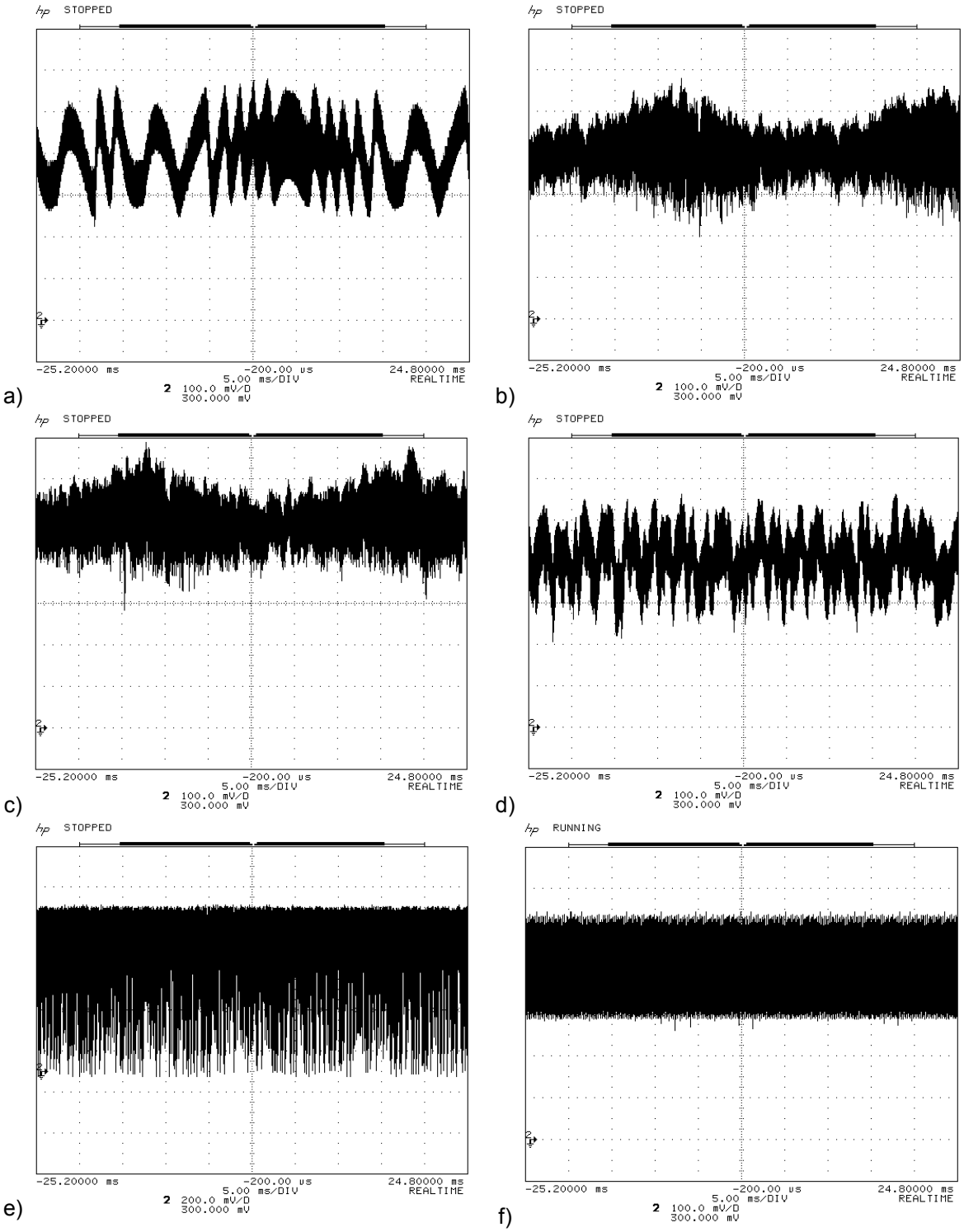

Figure 5.11. Measured envelopes of the input current waveforms in different cases. a) FM-sine, b) FM-sine + noise, c) FM-triangle + noise, d) Frequency-hopping, e) chaotic peak-current control and f) chaotic ΣΔ. Oscilloscope is DC-coupled, zero level at "2"-marker, horizontal axis 5 ms/division, vertical axis 1 A/division except in e), where the vertical setting is 2 A/division. These waveforms can be compared to the measured reference converter waveform shown in Figure 5.7 d).

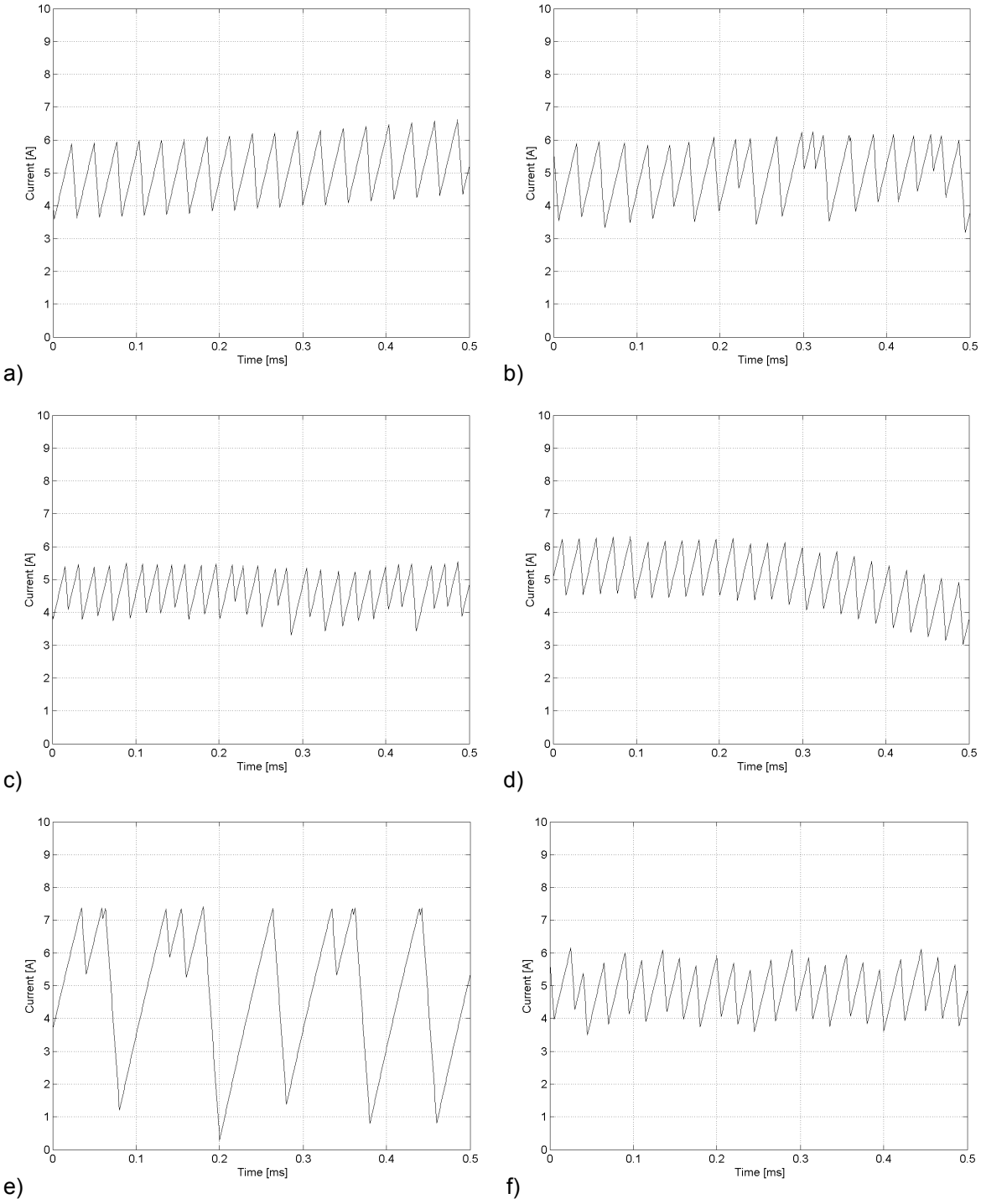

Figure 5.12. Simulated input current waveforms of the test converter at arbitrarily chosen time instant. a) FM-sine, b) FM-sine + noise, c) FM-triangle + noise, d) Frequency-hopping, e) chaotic peak-current control and f) chaotic ΣΔ. Horizontal axis 100 μs/division, vertical axis 1 A/division. These waveforms can be compared to the simulated reference converter waveform shown in Figure 5.7 e).

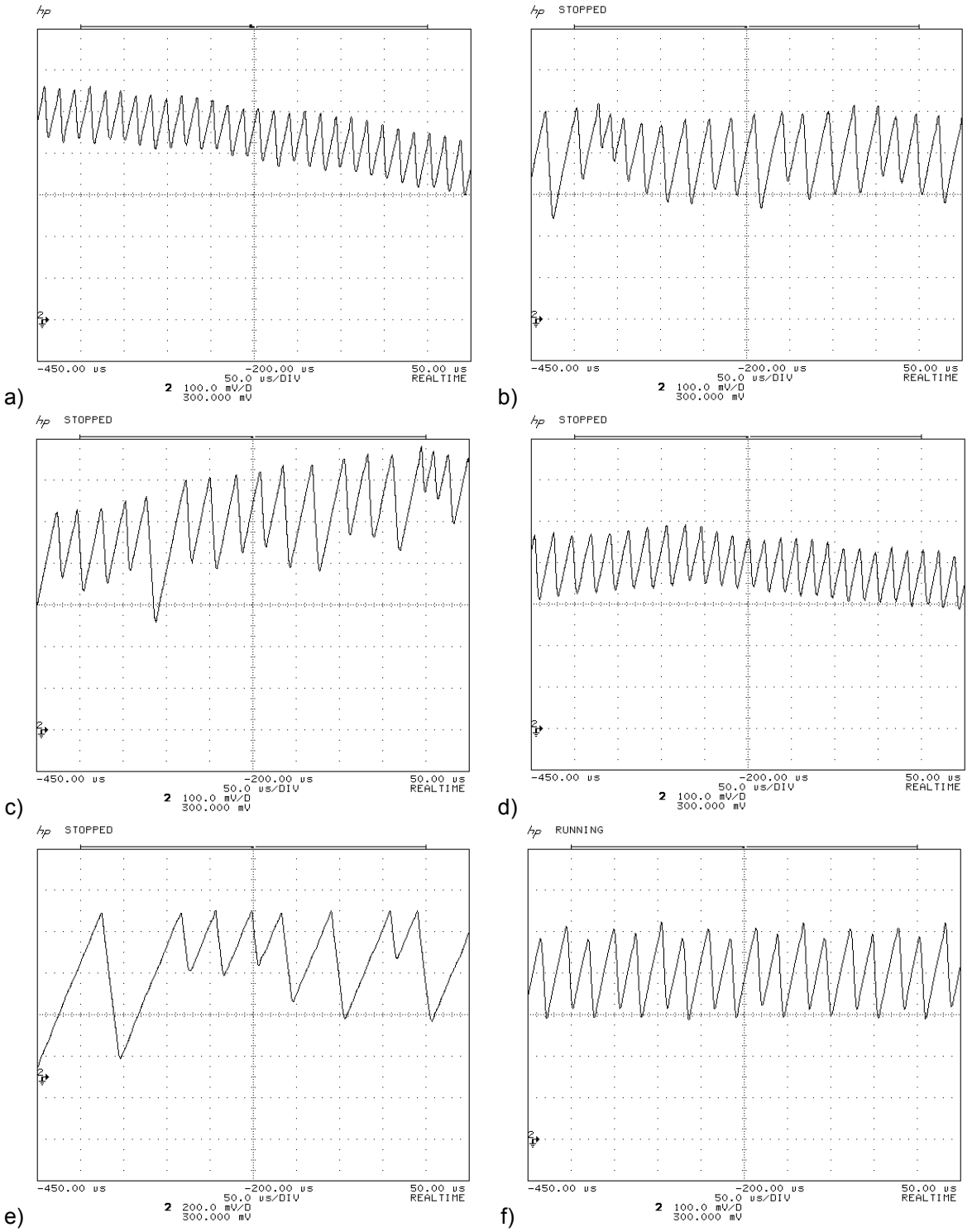

Figure 5.13. Measured input current waveforms of the test converter at an arbitrarily chosen time instant. a) FM-sine, b) FM-sine + noise, c) FM-triangle + noise, d) Frequency-hopping, e) chaotic peak-current control and f) chaotic $\Sigma\Delta$. Oscilloscope DC-coupled, zero level at "2"-marker, horizontal axis 50 μs/division, vertical axis 1 A/division except in e), where the vertical setting is 2 A/division. These waveforms can be compared to the measured reference converter waveform shown in Figure 5.7 f).

In Case 1 simulations show that the current ripple can be as high as 6.6 A. The ripple is at maximum when the instantaneous frequency of modulating signal is at a minimum. This cannot be clearly seen in the figures because the rate of change in the instantaneous frequency is low. However, this can be explained with Equation (2.6). The measured input current ripple is approximately 3.5 A peak-to-peak. Both the simulated and measured waveforms have the same shape envelope and the period of 30 ms for the modulating signal is clearly present in Figure 5.10 a) and Figure 5.11 a).

In Case 2 the simulated input current ripple is 4.2 A. The same level of current ripple and the same shape of the waveform can be seen from measurements where the current ripple is approximately 3.7 A peak-to-peak. An added noise component in Case 2 reduces the ripple level compared to Case 1. The period of the modulating signal is present in the current for both of the Cases 2 and 3 in Figure 5.10 b) & c) and in Figure 5.11 b) & c). The simulated input current ripple is 3.8 A and the measured current is 3.9 A in Case 3.

The current ripple in Case 4 is 5.3 A in simulations and 3.6 A in measurements. There exists no visible period in the envelope of the current in the frequency-hopping converter, Figure 5.10 d) and Figure 5.11 d). This was expected because the hopping sequence is a pseudo-random sequence without any periodic modulating wave.

The current of the peak current chaotically operating controller is predictable, and it was already shown in Chapter 2.3. The peak current level of the controller sets the upper level of the input current and the lower level is zero in the case when the converter is operating occasionally in DCM, which can be seen on Figure 5.12 e) and Figure 5.13 e). The current limit was set at 7.5 A in simulations which is also the peak-to-peak current in this case, and is visible in Figure 5.10. The shapes of simulated and measured waveforms are similar, as can be seen from Figure 5.10 to Figure 5.13. The current ripple is 7.8 A in the prototype converter. The difference here is due to the required adjustments that had to be made in the real (lossy) converter to achieve the desired output voltage. In addition, the input voltage of the battery is not exactly the same voltage that was used in the simulations.

In Case 6, it seems that the controller is operating at a constant switching frequency when analyzing Figure 5.10 f) and Figure 5.11 f). However, the current is fluctuating as predicted in Chapter 4.5, which can be seen in Figure 5.12 f) and in Figure 5.13 f). The current waveform has similar elements compared to Case 5, although the peak-to-peak current is approximately three times higher in Case 5. The simulated peak-to-peak current in Case 6 is 2.4 A and the measured current is 2.3 A.

5.2.4 Summary of Voltage and Current waveforms

Numerical values of the steady-state voltage and current waveforms are collected in Table 5-1 for comparative analysis. Both the simulated and measured peak-to-peak values are listed.

Table 5-1. Peak-to-peak voltage and current ripple in simulation and prototype models.

	Voltage, peak-to-peak simulated/measured		Current, peak-to-peak simulated/measured
Reference	0.1 V/ 0.6 V	0.2% / 1.3%	1.6 A / 1.4 A
Case 1: FM-sine	2.7 V / 3.5 V	5.6% / 7.3%	6.6 A / 3.5 A
Case 2: FM-sine + noise	1.5 V / 2.8 V	3.1% / 5.8%	4.2 A / 3.7 A
Case 3: FM-triangle + noise	1.3 V / 3.8 V	2.7% / 7.9%	3.8 A / 3.9 A
Case 4: Frequency hopping	1.8 V / 3.5 V	4.4% / 7.3%	5.3 A / 3.6 A
Case 5: Chaotic peak current	1.9 V / 3.0 V	4.0% / 6.3%	7.5 A / 7.8 A
Case 6: Chaotic Sigma-Delta	0.1 V / 2.9 V	0.2% / 6.0%	2.4 A / 2.3 A

The differences in voltage ripple between simulated and measured voltages are mainly affected by the switching noise in the prototype converter. As mentioned, the switching noise originates from the parasitic components of the circuit and from the non-ideal switching properties of semiconductor devices. These high frequency switching spikes cause higher peak-to-peak readings when acquired from the oscilloscope. Simulation results give therefore a better picture in the fluctuation of the output voltage caused by the modulation method.

Fluctuation and ripple of the input current is more dependable on the control methodology and magnetic circuit design of the converter than in the case of voltage fluctuation. Especially in Case 5, the converter is operating partly in discontinuous conduction mode (DCM) and the current ripple is therefore greater than in other cases. The differences between simulated and calculated current values are mainly affected by the input voltage of the converter: The input voltage of the converter was set to be 12 V in simulations whereas it was approximately two volts higher and dependent on the charge of the battery in the prototype converter.

5.3 EMC Simulations and Measurements

EMI test results shown in the next pages can be divided into the following parts:

- Results from the constant-frequency reference converter.
- Simulated spectrogram of the input current of the boost converter.
- Simulated EMI power spectrum estimate of the input current of the boost converter, frequency range 0 Hz – 1 MHz, Welch PSD, frequency resolution 200 Hz.
- Measured EMI-spectrum of the input current in frequency range of 9kHz - 1MHz, IFBW 200 Hz.
- Comparison of the measured spectrum to the reference converter EMI spectrum in the same picture.

The EMI-performance of the test converter was measured from the differential input current of the converter with a Rohde & Schwarz ESHS-30 EMI test receiver, Figure 5.14. The measurement was taken from the input test lead, with an R&S EZ17 model 02 current probe, see Figure 5.2. The current probe was selected here to perform the emission measurement because other coupling networks, such as line-

impedance stabilization networks, are not particularly suitable in this kind of test setup.

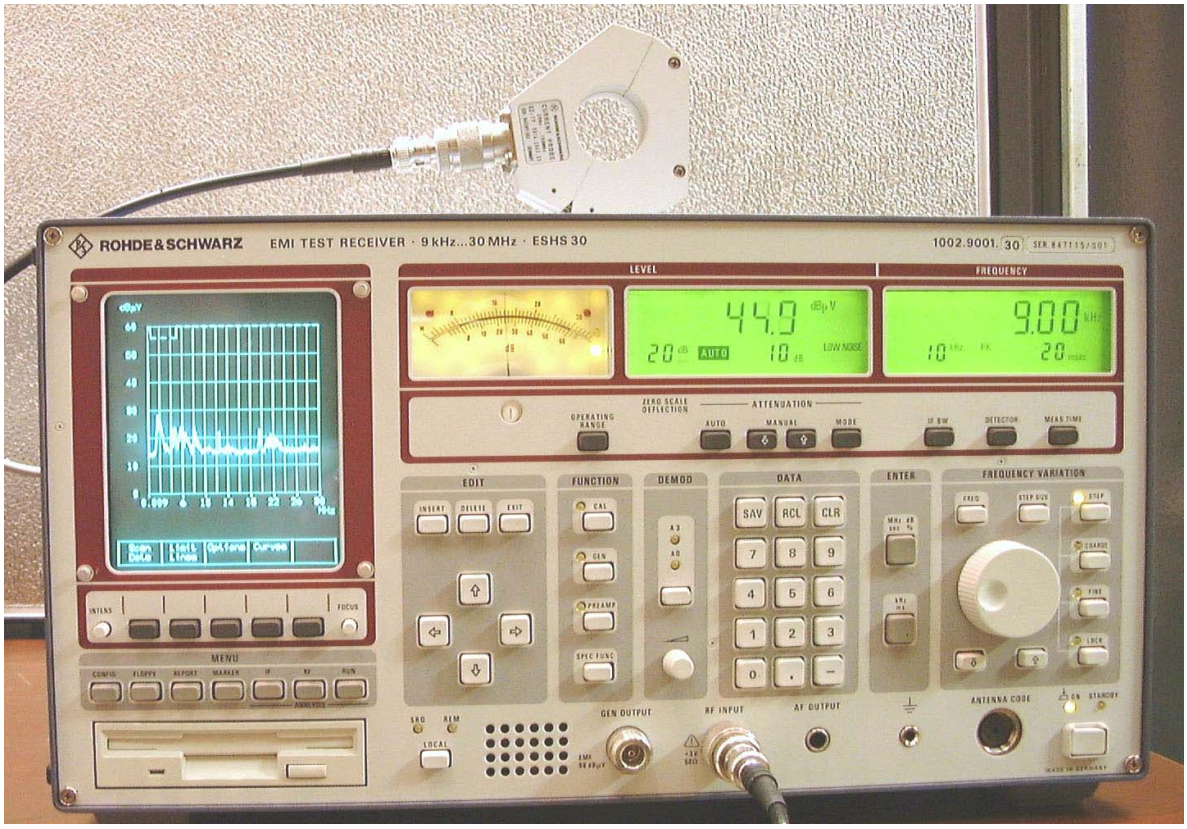

Figure 5.14. A Rohde & Schwarz ESHS-30 EMI test receiver with an R&S EZ-17 current probe used in the test setup.

Settings for the test receiver were: Scan frequency range: 9 kHz – 1 MHz, IFBW (RBW): 200 Hz, measuring time 20ms/IFBW, stepping 200 Hz (scan rate 100 ms/kHz), peak detector. Also the antenna factor correction for the EZ-17 current probe were used. These settings and equipment fulfill the requirements set in standards [CISPR 16-1 1999] and [CISPR 16-2 1999]. Limits mentioned in standard [CISPR 22 2003] are not taken into consideration, because the main objective is to compare different modulation methods, not to make any compliance tests. Additional measurements were also made at the conducted RF–frequency band of 9 kHz to 30 MHz. The IF bandwidth was 200 Hz for Band A (9 kHz-150 kHz) and 10 kHz for Band B (150 kHz – 30 MHz). The scan rate for Band A was 100 ms/kHz and for Band B 100ms/MHz. These results are depicted in Appendix E.

The measured spectrum is an amplitude spectrum measured with a peak detector. The results are in dB-scale, compared to one microampere. The simulated spectrum is a Welch power spectrum estimate calculated from the input current of the simulation model. These two spectrum estimates cannot be directly compared because one represents the peak amplitude spectrum and the other one represents the power spectrum[4]. The reference level is also different. This causes no problem because the absolute values are not important: Only the spectral shape and relative changes are important when comparing different modulation schemes.

[4] See Chapter 3.6 Relation between Calculated and Measured Spectrum

5.3.1 Constant-frequency Reference Converter

First, the EMI performance of the constant-frequency reference converter is shown in Figure 5.15.

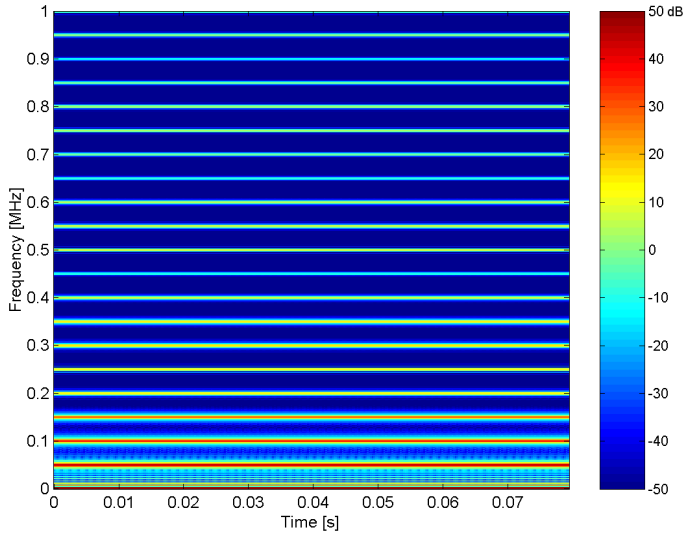

a)

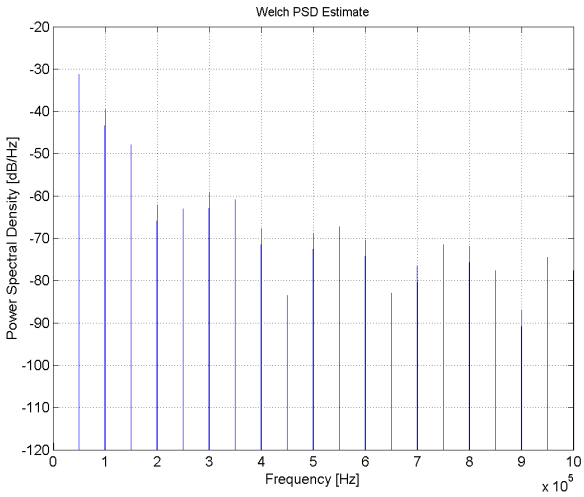

b)

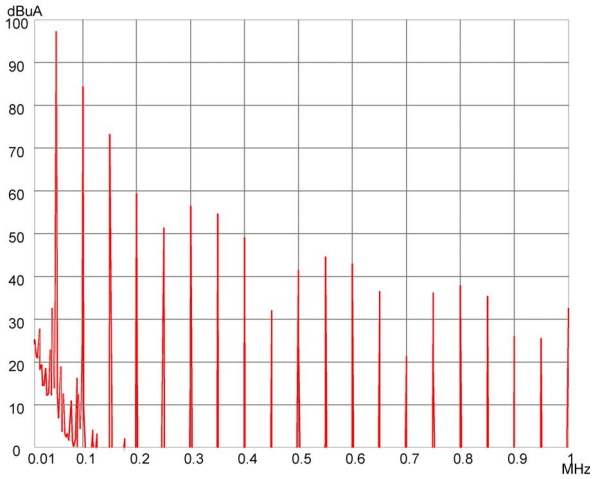

c)

Figure 5.15. EMI properties of the constant-frequency PWM converter. a) A simulated input current spectrogram. b) The estimated Welch-PSD of the input current, RBW 200 Hz. c) The measured input current spectrum of the prototype converter, 200 Hz IFBW, peak detector.

The spectrogram and PSD-estimate of the constant-frequency reference converter has the same appearance as the spectrogram and PSD of the switching function presented in Chapter 4.1. The spectrogram clearly shows that the frequency content of the input current is not time-dependent. Both the PSD-estimate and the measurement result show typical line spectrum of the periodic signal as presented in Chapter 3.1. The fundamental signal frequency of 50 kHz with odd and even harmonic components is evident. Low-frequency continuous spectrum noise in Figure 5.15 c) originates from the inherent noise properties of the test receiver and from the background noise of the setup, not from the signal, see Appendix D.

5.3.2 Simulated Input Current Spectrograms

Simulated input current spectrograms of the converter in different spread-spectrum modes are shown in Figure 5.16.

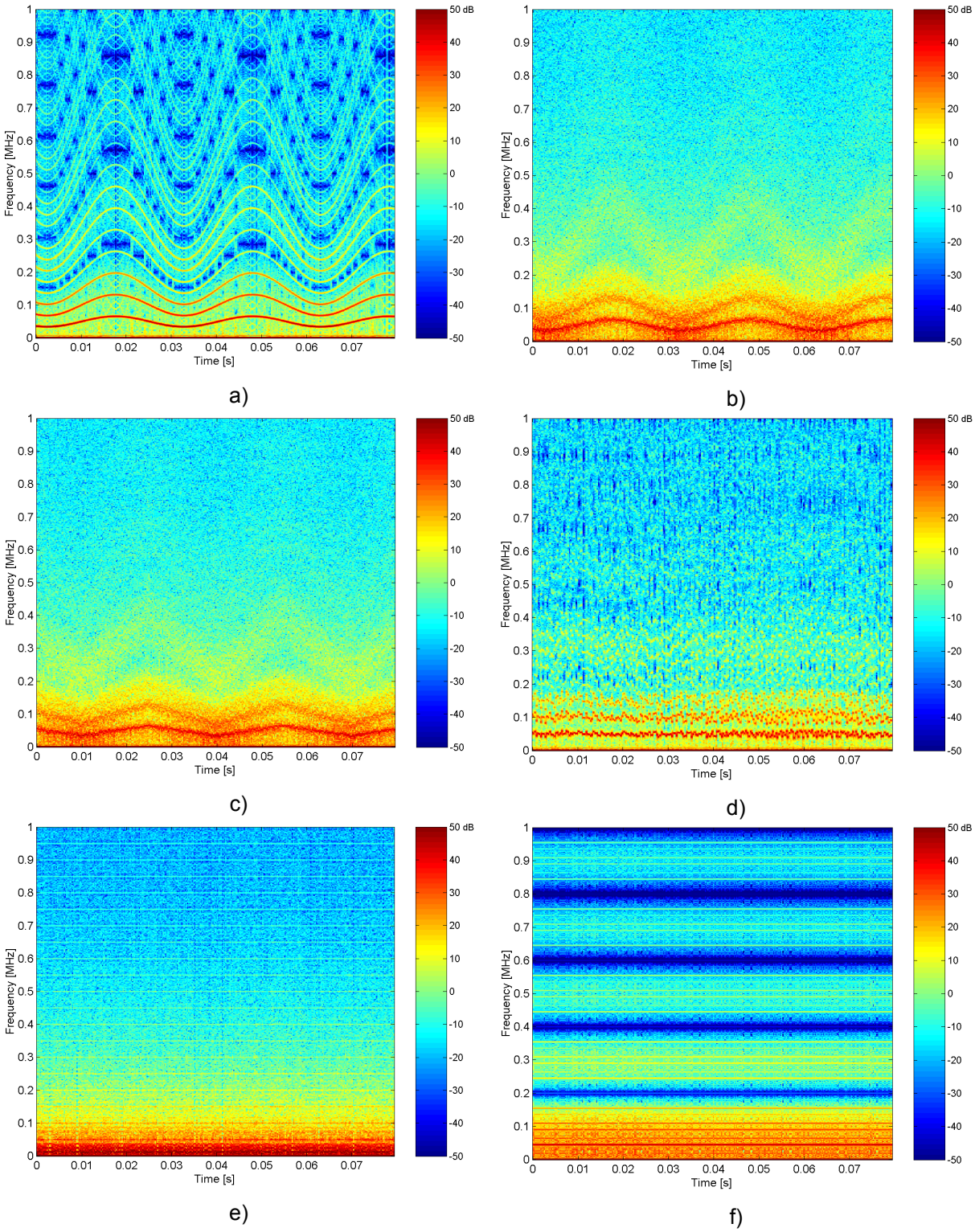

Figure 5.16. Simulated spectrograms of the boost converter input current. a) Case 1, b) Case 2, c) Case 3, d) Case 4, e) Case 5 and f) Case 6. These spectrograms can be compared to the spectrogram of the reference converter shown in Figure 5.15 a) and spectrograms of the switching function shown in Chapter 4.

In frequency-modulated Cases 1 to 3, the modulation sequence length 30 ms is clearly present in the simulated input current spectrograms, Figure 5.16 a) – c). This same period is also present in voltage and current waveforms depicted in Figure 5.8 to Figure 5.11 and in autocorrelation sequences of the switching function shown in Chapter 4. Spectrogram again shows, that the modulation index[5] β_N of higher harmonics is N-times (N is the harmonic number) the modulation index β_1 of the fundamental frequency. However, harmonics are not so clearly visible when the random signal is added to the modulating wave in Cases 2 and 3 as in the case of pure sine modulation. The simulated spectrogram of the third case is similar to the second case. The modulating waveform is still recognizable in the graph, Figure 5.16 b) and c), but higher harmonics are not so evident.

The spectrogram of the FH-converter is different from those shown earlier because of the lack of the periodic modulation signal. Actually, the length of the hopping sequence is 100 ms as described in Chapter 4.3, but there exists no other periodic component like sine in the modulation sequence. Non-periodic operation is clear in the spectrogram, where the instantaneous switching frequency is changing continuously. There are noticeable maximums around 50 kHz, 100 kHz, 150 kHz and 300 kHz.

The low frequency power is clearly visible in the spectrogram of chaotic peak current controlled converter, Figure 5.16 e). The nominal switching frequency generates one visible line on the spectrogram, but the harmonics are not clearly detectable. However there exists fine horizontal lines with 50 kHz spacing in the spectrogram exposing the periodic clock frequency of the controller. There is not any period on the vertical (time) axis. Fluctuation of the instantaneous switching frequency causes the smooth appearance of the spectrogram.

The simulated spectrogram in the Sigma-Delta operating converter shows, that there is no periodic modulation signal in the time domain, Figure 5.16 f). The nominal switching frequency is visible and fluctuation of the instantaneous switching frequency causes the spectrogram to look smooth like in the case of the chaotic peak current controlled converter. Minimums are at the system clock frequency and its harmonics. The power density is high at low frequencies. Although the spectrogram shows periodic parts in the signal, the signal power is not concentrated on single frequencies like in the reference converter shown in Figure 5.15 c).

5.3.3 Simulated and Measured Input Current Spectra

Simulated and measured input current spectral results are given next. The spectral units in the simulated and measured results differ from each other and simulated results cannot be therefore directly compared to the measured ones. The main purpose of Figure 5.17 and Figure 5.18 is to validate the accuracy of the simulation model and the spectral estimation theory with selected parameters introduced in Chapter 3.

[5] Modulation index was defined in Chapter 4.2.

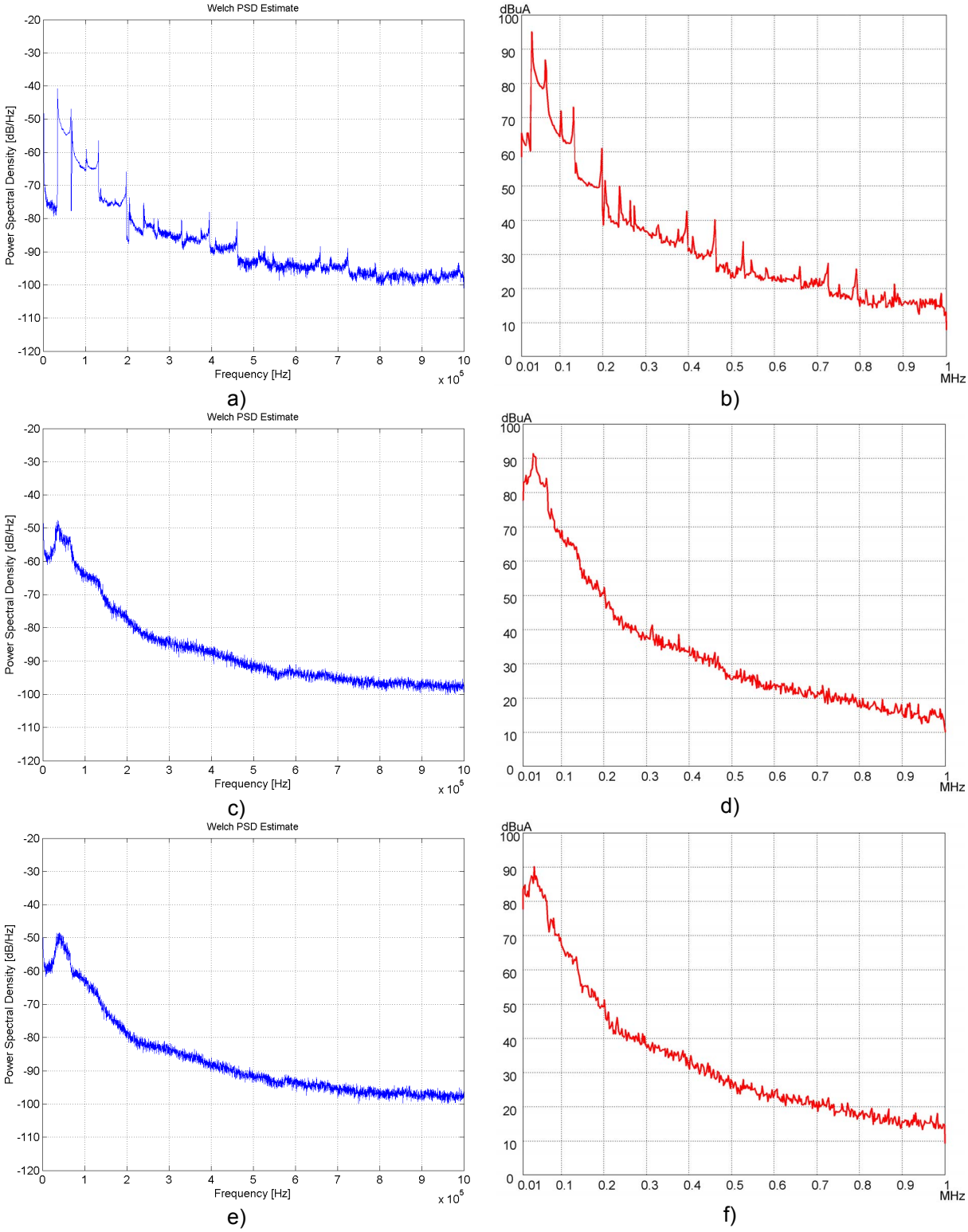

Figure 5.17. The Welch power spectral density estimates (left column) and measured spectra (right column) of the input current. a) and b) Case 1. c) and d), Case 2. e) and f) Case 3. The results shown here can be compared to Figure 5.15 b) and c).

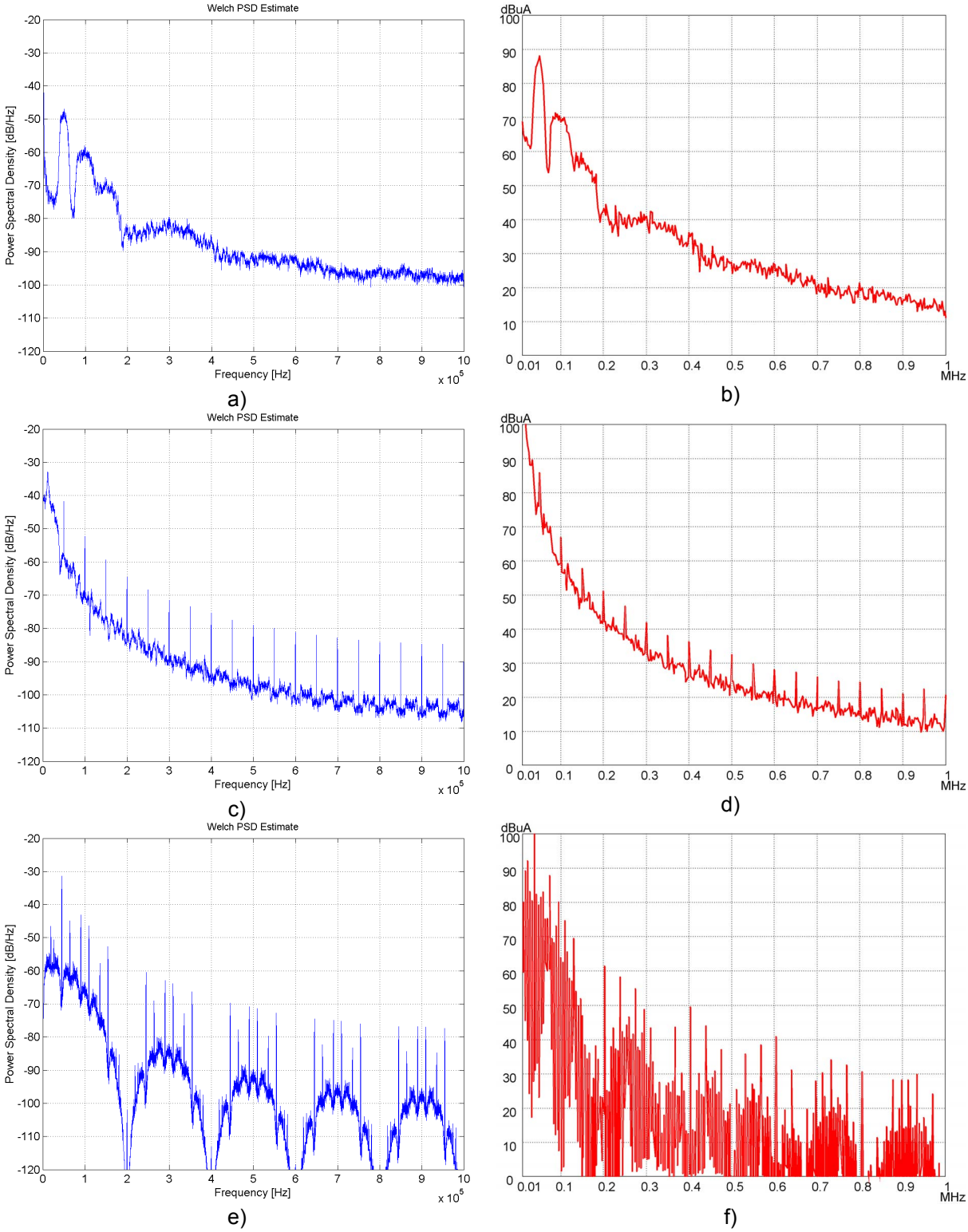

Figure 5.18 The Welch power spectral density estimates (left column) and measured spectra (right column) of the input current, continued from Figure 5.17. a) and b) Case 4. c) and d), Case 5. e) and f) Case 6. The results shown here can be compared to Figure 5.15 b) and c).

The main difference between the spectrum of the constant-frequency reference converter, Figure 5.15, and the SS spectra, Figure 5.17 and Figure 5.18, is the continuous part of the signal spectrum in the SS-converter. The overall noise floor has been raised whereas discrete spikes have been reduced in the spectra of the SS-techniques. The results shown in Figure 5.18 and in Figure 5.19 show that the

shape of the simulated spectrum is close to the measured one. If these results are compared to the spectral shapes of the switching function shown in Chapter 4, the same trend can also be seen. When comparing the time-domain and spectral results, it is hard to see any correlation between the current waveform and the measured spectrum. In Case 1, the sine-modulated converter clock can be seen on the EMI test results, Figure 5.17 a) and b). The nominal 50 kHz system clock and its harmonics are clearly present on the current spectrum. Two spectral spikes can be recognized around the nominal switching frequency and harmonics as expected from the simulations and from basic FM-theory introduced in Chapter 4.2. The spectrum of the sine-modulated switching frequency generates spectrum with reduced peaks and a raised overall noise floor.

The noise signal added to the sine wave in Case 2 causes discrete peaks in the spectrum to decrease if compared to the first case. Discrete spectral spikes have almost vanished and there is only one major jump in the spectral curve around the nominal switching frequency. Spectral performance of Case 3 seems to be like in Case 2 and there are no noticeable spikes in the spectrum. Again, like in Case 2, the spectrum is smoother than in the first case.

There are no sharp spikes in the input current spectrum of the frequency-hopping converter, Case 4, although the nominal switching frequency and harmonics can be seen. It is expectable that this kind of pre-programmed modulation method gives a smooth spectral curve, because this is the main goal in the sequence synthesis. The spectral curve has several jumps around the nominal switching frequency and its harmonics. The spectrum at higher frequencies is noise-like.

The shape of the spectrum of the chaotic peak current controlled converter, Case 5, is different compared to Cases 1-4. The rise in overall noise floor clearly indicates the spread spectrum mode of the converter operation. The nominal switching frequency and harmonics are visible. The main difference is that the low frequency power has increased. This reduces the high frequency amplitude level of the measured spectrum compared to the reference, Figure 5.15. Chaotic mode seems to concentrate the signal power to a low frequency range. Harmonic frequencies are hard to find from spectrogram, Figure 5.16 e), although they can be recognized in a normal spectrum, Figure 5.18 c) and d).

The system clock frequency of 200 kHz and harmonics of the $\Sigma\Delta$-controlled converter can be seen in Figure 5.18 e) and f). Theoretically, there are minimums at a system clock frequency and harmonics like in Figure 5.18, e). Practically, some power can be measured in these frequencies, Figure 5.18 f), although the general shape of the spectrum is like in simulation. There is much more variance in the measured spectrum which originates from the chaotic nature of the controller – parameters were not exactly the same in the simulations and in the prototype.

5.3.4 Measured Spectra Compared to the Reference

Next, the measured test results in different cases are collected in the same picture with the measured spectrum of the constant frequency reference converter. Figure 5.19, Figure 5.20 and Figure 5.21 show the effect of different SS techniques on the spectral shape and spectral levels compared to the constant frequency converter.

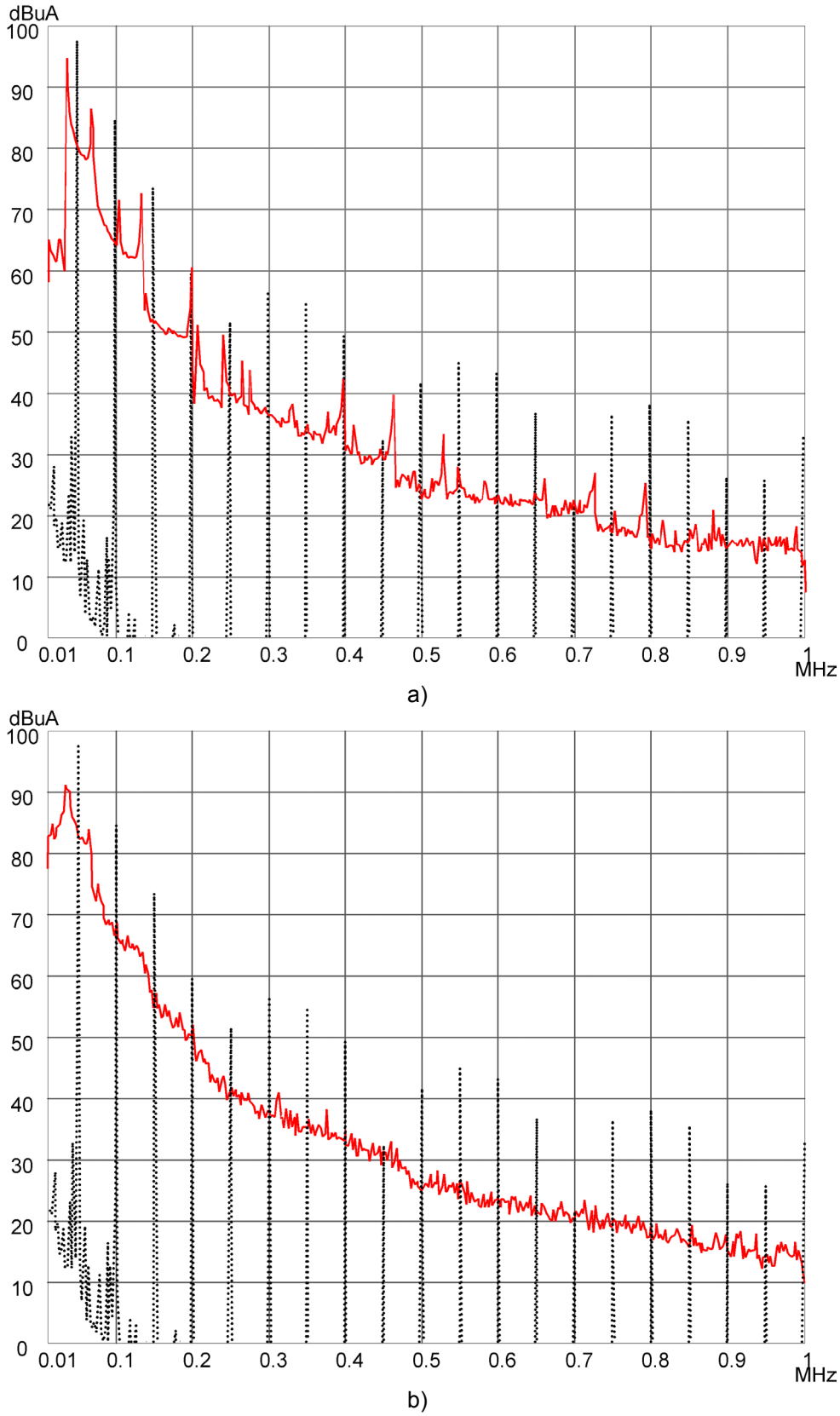

Figure 5.19. Measured input current spectra in the frequency range 10 kHz – 1MHz compared to the constant frequency PWM converter, dotted line. a) FM with sine, Case 1, solid line. b) FM with sine + random noise, Case 2, solid line.

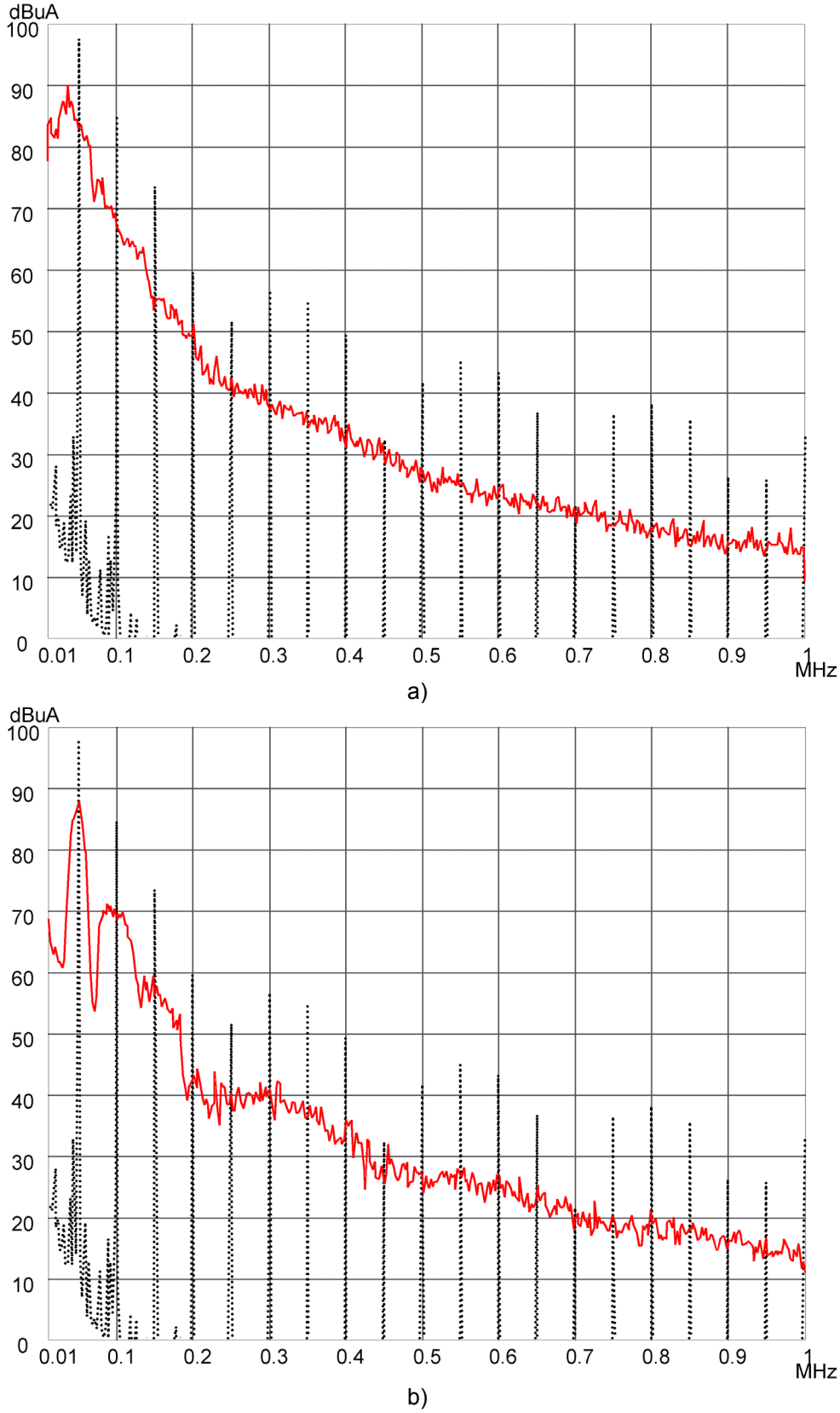

Figure 5.20. Measured input current spectra in the frequency range 10 kHz – 1MHz compared to the constant frequency PWM converter, dotted line. a) FM with triangle wave + random noise, Case 3, solid line. b) Frequency-hopping converter, Case 4, solid line.

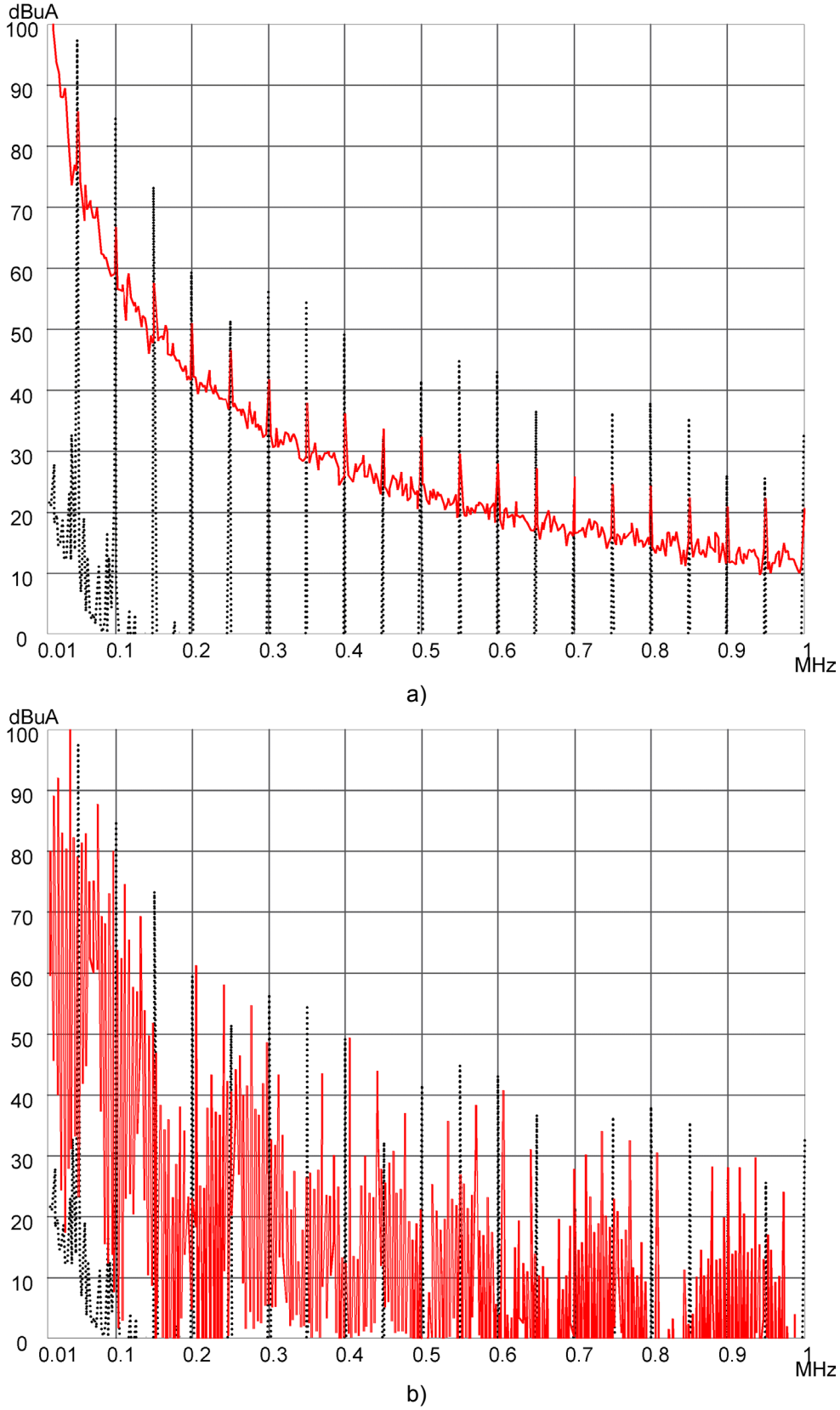

Figure 5.21. Measured input current spectra in the frequency range 10 kHz – 1MHz compared to the constant frequency PWM converter, dotted line. a) Chaotic peak current controlled converter, Case 5, solid line. b) Chaotic Sigma-Delta controlled converter, Case 6, solid line.

Although there are still visible spikes in test results in Case 1, the magnitude of the spikes have been reduced compared to the reference converter operating at

constant system clock, Figure 5.19 a). This shows that a noticeable reduction can be achieved with simple single tone modulation. The spectrum of the single tone modulated converter represents the spectrum of an SSM converter with a high noise floor and reduced spectral spikes. The difference is evident especially at higher frequencies.

In Cases 2 and 3, reduction is clearly visible and much easier to detect than in Case 1. There are almost no spikes in the SSM spectrum. Figure 5.19 b) and Figure 5.20 a) show that spectral spikes have been reduced almost at all frequencies compared to the PWM reference. The EMI-spectrum of Case 2 is smoother than in the first case. There is not much difference between Cases 2 and 3, and the reduction is identical within the measurement uncertainty[6].

When comparing measured EMI-spectrum of the FH converter to the reference, reduction is easy to notice. Although there are jumps on the spectral curve, no harmonic spikes exist and the spectrum is a typical continuous spectrum of an aperiodic signal. The magnitude of the spectrum is reduced by approximately 10 dB over the whole frequency range.

Noticeable reduction in spectral spikes can be seen when comparing the spectrum of the chaotically operating peak controlled converter to the reference converter, Figure 5.21 a). However, there still exist spikes in the spectrum. A characteristic property of chaotic modulation is the power concentration at low frequency range below the system clock frequency of 50 kHz. Odd and even harmonics with approximately 10 dB over the continuous spectrum noise floor are clearly present.

Hardly any reduction can be reached when comparing measurements of selected chaotic sigma-delta controlled controller to the reference converter. Of course, this can be due to the selected parameters used in the sigma-delta converter. Other chaotic controller in Case 5 gave results that are more promising. Although there are some frequency ranges where reduction is remarkable, overall performance is poor and high spikes at system clock harmonic and sub-harmonic frequencies spoil the EMI-performance of this control strategy.

5.3.5 Summarized EMI Test Results

In general, the simulation model is accurate enough to model the operation of the prototype converter, although there are differences in simulated and measured waveforms. The shape of the spectrum is almost the same when comparing PSD calculated from the switching function $q(t)$, PSD from the simulated input current or measured EMI-spectrum. The main differences are in spectral units and in the operating principle of the EMI-receiver compared to numerical spectrum estimation methods.

Measured EMI-spectrum data was analyzed like in Chapter 4.6 to get numerical results based on the measurements. Although the spectrum itself is a useful graph

[6] See Appendix F for estimated measurement uncertainty of the EMI-measurement test setup

representing the EMI-content and giving a good general overview of the converter operation, it is quite hard to compare the graphical information in general. Therefore, measured graphical spectral data is analyzed and tabulated in next three tables. It must be pointed out, that results given next are manually sorted and should be used more like additional information than accurate test results, giving only a trend of capabilities of the selected techniques. Firstly, calculated values from the simulations are listed in Table 5-2. Results are divided into ten frequency bands and the maximum values of each band are recorded.

Table 5-2. (**SEE ERRATA**) Calculated maximum values of the simulated input current Welch PSD at selected frequency bands. The highest value (in dB/Hz) of the PWM-reference converter in each frequency band is shown in the first row. The peak value and reduction compared to the reference at the same frequency band is listed in the following rows

CASE ↓	Frequency band, [Hz] →	10kHz - 100kHz	101kHz - 200kHz	201kHz - 300kHz	301kHz - 400kHz	401kHz - 500kHz	501kHz - 600kHz	601kHz - 700kHz	701kHz - 800kHz	801kHz - 900kHz	901kHz - 1MHz
PWM-reference	Peak [dB]	-10.7	-31.2	-39.6	-48.0	-62.1	-62.1	-63.0	-59.0	-60.9	-67.8
Case 1: FM-sine	Peak [dB]	-10.7	-46.9	-59.0	-56.5	-66.0	-75.2	-80.0	-83.3	-80.3	-78.1
	Reduction [dB]	0	15.7	19.4	8.5	3.9	13.1	17.0	24.3	19.4	10.3
Case 2: FM-sine+noise	Peak [dB]	-10.7	-49.9	-60.6	-64.2	-71.8	-77.3	-80.2	-82.2	-83.1	-84.8
	Reduction [dB]	0	18.7	21.0	16.2	9.7	15.2	17.2	23.2	22.2	17.0
Case 3: FM-triangle +noise	Peak [dB]	-10.7	-48.6	-59.3	-64.6	-72.6	-78.1	-80.3	-81.1	-83.4	-84.7
	Reduction [dB]	0	17.4	19.7	16.6	10.5	16.0	17.3	22.1	22.5	16.9
Case 4: Frequency hopping	Peak [dB]	-10.7	-46.9	-58.0	-67.1	-69.5	-81.7	-80.2	-79.5	-80.1	-84.1
	Reduction [dB]	0	15.7	18.4	19.1	7.4	19.6	17.2	20.5	19.2	16.3
Case 5: Chaotic modulation	Peak [dB]	-10.7	-41.8	-52.3	-59.3	-64.5	-79.8	-68.3	-71.5	-73.4	-75.3
	Reduction [dB]	0	10.6	12.7	11.3	2.4	17.7	5.3	12.5	12.5	7.5
Case 6: Chaotic ΣΔ-modulation	Peak [dB]	-10.6	-31.4	-43.1	-52.7	-82.9	-60.4	-69.0	-62.9	-66.3	-96.0
	Reduction [dB]	-0.1	0.2	3.5	4.7	20.8	-1.7	6.0	3.9	5.4	28.2

Table 5-3 shows measured maximum peak values of each converter divided into 10 frequency bands. Test results are analyzed manually and maximum peak values of each frequency band are tabulated. Reduction compared to the reference converter are also calculated and listed in the second row of each case.

Table 5-3. Measured peak values of the converter EMI spectrum at selected frequency bands. The highest peak value (in dBμA) of the PWM-reference converter in each frequency band is listed in the first row. The peak value and reduction compared to the reference at the same frequency band is listed in the following rows.

CASE ↓	Frequency band, [Hz] →	10kHz - 100kHz	101kHz - 200kHz	201kHz - 300kHz	301kHz - 400kHz	401kHz - 500kHz	501kHz - 600kHz	601kHz - 700kHz	701kHz - 800kHz	801kHz - 900kHz	901kHz - 1MHz
PWM-reference	Peak [dB]	98	73	57	55	42	45	37	38	35	33
Case 1: FM-sine	Peak [dB]	95	73	52	43	40	34	27	28	22	19
	Reduction [dB]	3	0	5	12	2	11	10	10	13	14
Case 2: FM-sine+noise	Peak [dB]	91	68	53	41	35	29	24	24	20	19
	Reduction [dB]	7	5	4	14	7	16	13	14	15	14
Case 3: FM-triangle +noise	Peak [dB]	90	68	51	39	35	28	25	23	20	19
	Reduction [dB]	8	5	6	16	7	17	12	15	15	14
Case 4: Frequency hopping	Peak [dB]	88	70	44	43	36	28	27	23	20	18
	Reduction [dB]	10	3	13	12	6	17	10	15	15	15
Case 5: Chaotic modulation	Peak [dB]	>100	67	48	40	35	30	28	25	23	23
	Reduction [dB]	> -2	6	9	15	7	15	9	13	12	10
Case 6: ΣΔ-modulation	Peak [dB]	>100	74	61	44	50	38	41	34	30	30
	Reduction [dB]	> -2	- 1	- 4	11	- 8	7	- 4	4	5	3

Table 5-4 summarizes the information shown in Table 4.2, Table 5-2 and Table 5-3 in a single number. Average attenuation mentioned in the table is the average calculated from the reduction of the peak values. The standard deviation of the average is also calculated respectively. Table 5-4 indicates that cases 2, 3 and 4 have an attenuation of more than 10 dB's. Measurements from Case 6, ΣΔ-modulation, show that there is almost no effect on the noise reduction compared to the reference converter.

Table 5-4. (**SEE ERRATA**) The average attenuation and standard deviation for each case calculated from the simulations and measurements analyzed in Table 5-3.

	Simulated $q(t)$		Simulated current		Measured current	
	Average Attenuation [db/Hz]	Standard deviation [dB unit]	Average Attenuation [db/Hz]	Standard deviation [dB unit]	Average Attenuation [dbμA]	Standard deviation [dB unit]
Case 1: FM-sin	14.9 dB	6.4	13.2 dB	7.5	8.0 dB	5.0
Case 2: FM-sin+noise	18.9 dB	4.8	16.1 dB	6.8	10.9 dB	4.6
Case 3: FM-triangle +noise	19.0 dB	4.8	15.9 dB	6.5	11.5 dB	4.6
Case 4: Frequency hopping	17.9 dB	5.5	15.3 dB	6.5	11.6 dB	4.4
Case 5: Chaotic modulation	9.8 dB	5.9	9.2 dB	5.3	9.4 dB	5.1
Case 6: ΣΔ-modulation	8.5 dB	9.8	7.1 dB	9.7	1.1 dB	5.9

The standard deviation calculated in Table 5-4 shows if there is a large difference in attenuation at the different frequency bands used in the calculation. The largest standard deviation is in Case 6. This can be seen also in Table 5-3 and in Table 5-4, where there is attenuation that is more than 10 dB at some frequency ranges, but at other frequency ranges, the noise level is more than in the case for constant frequency operation. The other technique, which has also a slightly higher standard deviation, is Case 1 - sinusoidal FM. This is mainly because of the harmonic spikes present in the spectrum of the converter.

According to results shown in Table 5-4, the most effective methods for EMI-reduction is FM with triangular wave + noise, FM with sinusoidal wave + noise and frequency-hopping. The chaotic peak-current controlled converter (in this particular case) outperformed simple sinusoidal FM in measurements, although the difference is within the measurement uncertainty. The chaotically operating Sigma-Delta-controlled converter didn't show promising results with practical measurements – this affirms the problematic design and susceptibility to parameter variations of controller based spread spectrum techniques.

5.4 Discussion

5.4.1 Output Voltage and Input Current Ripple

Low frequency output voltage ripple has been considered as a major problem in variable-frequency DC/DC converters. Random switching schemes have an inherent noise induced low-frequency voltage ripple problem when compared with the deterministic PWM method, [Shrivastava 1997], [Hui 1998]. Hui et al. also conclude, that the randomized modulation schemes are suitable for motor drive systems and not a particularly good solution in DC/DC converters because of the fluctuation in the output voltage. This is only partially true, because the voltage fluctuation can be

controlled with a proper component, modulation sequence and controller selection. Results in this chapter a show, that spread spectrum modulation methods have an effect on the output voltage ripple. However, the output voltage ripple is satisfactory low, even without any voltage feedback control.

A five-percent ripple of the output voltage may be too much for some applications, but for other applications, even more than 10 % is enough. This is especially true for applications where two-stage distributed power supply architecture is used. These kinds of distributed architectures are becoming very popular and have been in use for a long time for example in the fields of telecommunication and other multiboard applications. The idea in distributed power supply divides the power conversion scheme from the input source to the load in two stages, like that presented in Chapter 2.2. The first stage generates from the AC mains or from another power source (e.g. battery) an intermediate DC bus voltage. This DC bus supplies power to the load through different DC/DC converters, located on the same board where the supplied circuits are connected. The final application has its own regulated power supply stabilizing the output voltage to the desired level regardless of the voltage variations in the DC bus. For example an ETSI standard [ETSI 2003] for a DC power supply interface of a telecommunications equipment specifies the normal service voltage to be in the range -40.5 to -57,0 V_{dc} for a nominal –48,0V power supply.

When the output voltage feedback is added to the converter control circuit, the ripple can be reduced. Of course, one very important issue is proper capacitor selection of the converter main circuit, which cannot be neglected. The capacitor value directly affects on the output voltage ripple, Equation 2.10.

To show the effect of the voltage feedback on the output ripple, a simulation with a voltage feedback loop was made. The SS-modulation method was like in Case 1, where sinusoidal modulation was used. The only difference was the voltage feedback, which was added to the circuit like in Figure 1.3. The gain of the compensator was in this case:

$$G_c(s) = \frac{1}{2(0.0003183s + 1)} \ , \qquad (5.1)$$

thus giving approximately a 500 Hz corner frequency to the approximate integrator. Simulated Welch-PSD, output voltage and input current ripple are shown in Figure 5.22.

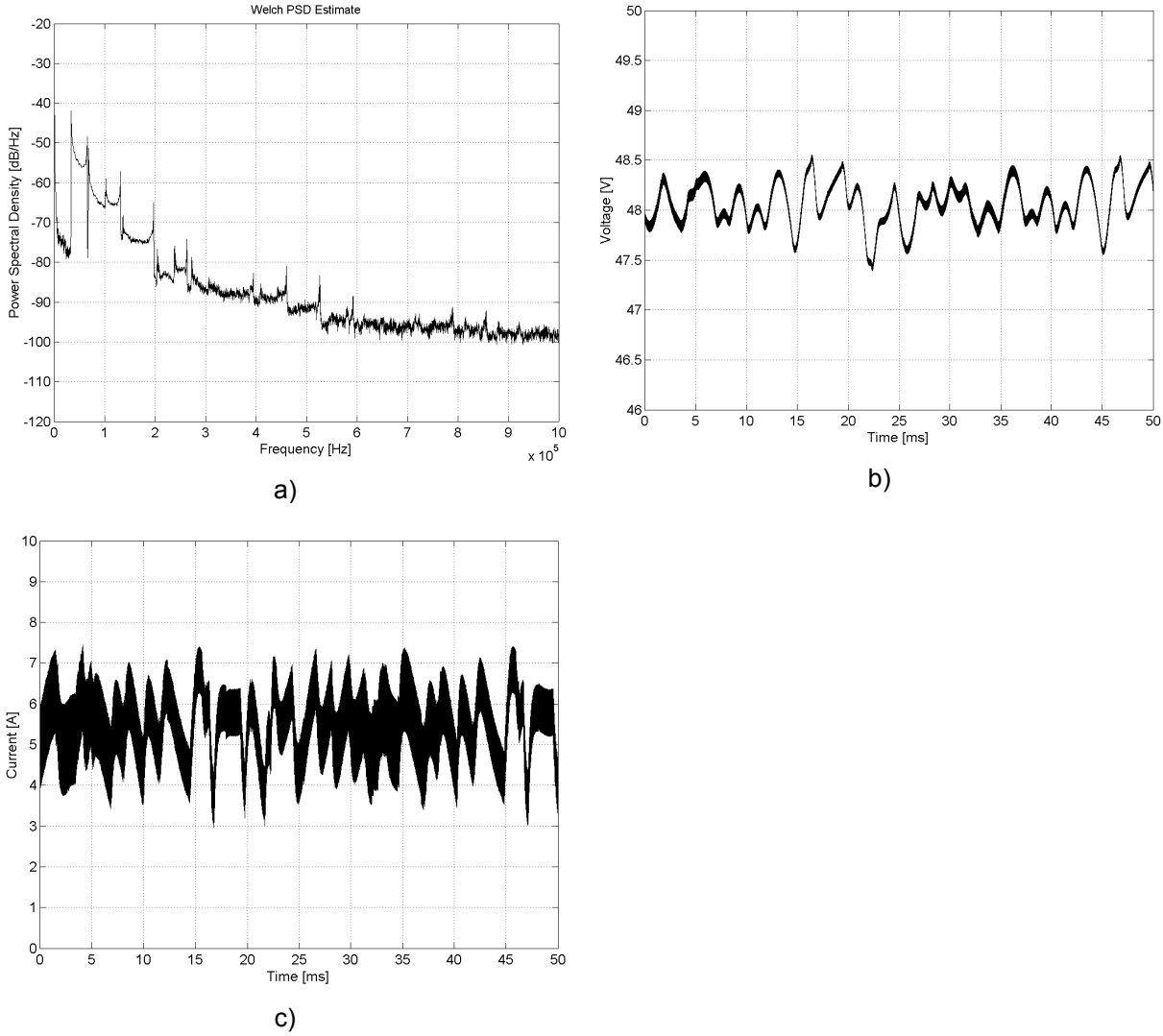

Figure 5.22. Simulated input current Welch-PSD (a), output voltage ripple (b) and input current waveform of a sinusoidal modulated VF-converter with a voltage feedback controller. The output ripple is reduced to 2.5 % without noticeable change in the spectral performance, compare to Figure 5.8 a), Figure 5.10 a) and Figure 5.17 a).

Simulated peak-to-peak output voltage ripple is 1.2 V / 2.5 %, which is less than half of the simulated ripple in Case 1, where there is no feedback from the output voltage. Current ripple is approximately 4.5 A peak-to-peak, which is also less than 6.6 A obtained from Case 1. However, there is no noticeable difference in spectral performance when comparing the spectrum estimates in Figure 5.17 and Figure 5.22.

Voltage feedback has only little or no effect on the spectral performance of the converter in Cases 1-4, because the controller itself is not generating the spread-spectrum signal. In Cases 5 and 6, the voltage feedback has an effect on the EMI spectrum of the converter because of the chaotic nature and inherent spread-spectrum operation of these controllers. Therefore controller-based SS-methods are more complicated to use in SS-applications.

The current ripple also must be considered during the converter overall design. The peak-to-peak value of the input current is almost linearly dependant on the power switch on-time. The instantaneous on-time of the switch changes continuously in an

SS-converter and therefore affecting on the peak-to-peak current (Δi_{in}) of the converter. This has to be taken into consideration when designing magnetic parts or rating component values in the converter design.

5.4.2 EMI-Measurements in CISPR Conducted RF-Emission Band 150 kHz to 30 MHz

The EMI spectrum was also measured in normal [CISPR 22 2003] conducted RF-emission band from 150 kHz to 30 MHz with 10 kHz IFBW, see Appendix E. These measurements show that no difference can be seen with the peak detector mode and values are the same within the measurement uncertainty. However, this is partly unexpectable because it can be seen for example in the spectrogram of the FM-sine modulated converter, Figure 5.16 a), that the frequency deviation at higher frequencies is more than the used 10 kHz IFBW of the test receiver.

Poor performance can be explained with the modulation sequence type and length used in the prototype, because the dwell time (settling time) is less for the 10 kHz IF filter. Equation 3.38 gives a 100 μs dwell time for a 10 kHz filter and 5 ms for a 200 Hz IF filter. Therefore, the modulation sequence should be optimized for a 10 kHz filter bandwidth for a 150 kHz – 30 MHz measuring band. This means that the rate of change of the instantaneous frequency is too low. For example in Case 1, the 20 ms measuring time is almost as long as the fundamental period of the modulating wave. Therefore, the maximum of all signal components at some specific measurement bandwidth is recorded with the peak detector over this 20 ms measurement time. Instantaneous frequencies of these signal components are constantly changing and the recorded result is even worse than in the case of constant frequency operation. This is illustrated in Figure 5.23.

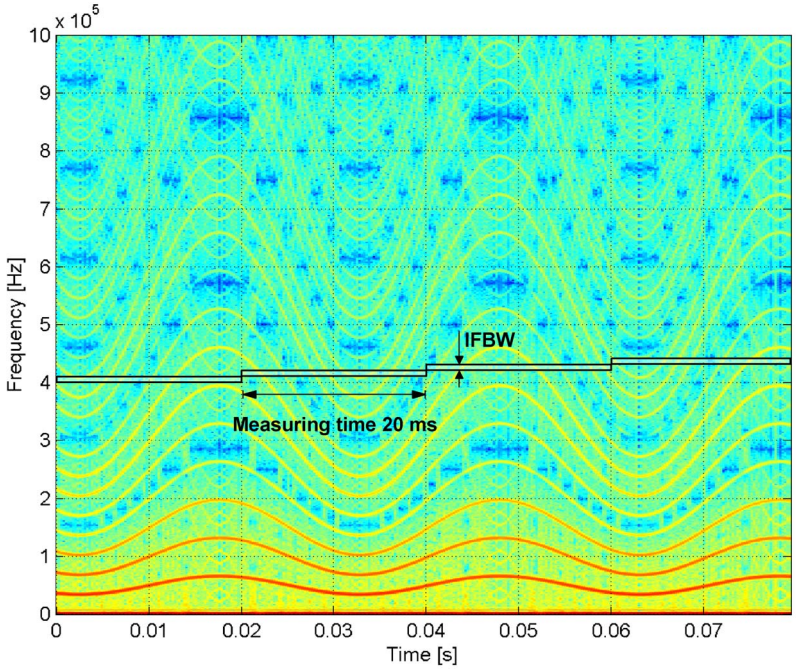

Figure 5.23. An example of 10 kHz IFBW sweep of the test receiver with 10 kHz stepping and a 20 ms measuring time. It is obvious that the rate of change of the modulating signal is too low and the maximums at different harmonics are detected with a dwell time of 100 μs. This explains the poor performance in all measurements made at 30 MHz band.

Requirements for compliance measurements must be taken into consideration and the SS modulating sequence must be optimized according to these requirements when designing SS-techniques for commercial applications. The results and methods shown in the 1 MHz band are scalable for example to the 30 MHz band, because the operating principle of the measuring device is identical in both cases. The main difference in measurements shown in Chapter 5.3.4 and in Appendix E is the different IFBW used in these measurements.

5.4.3 Implementation Complexity in Different Cases

Implementing complexity of different techniques can be quite different when concerning issues in practical power supply design. Use of readily available power control IC with a separate SS-clock circuit gives the easiest but not the most cost effective approach in SS-converter design. However, many of these controller circuits are suitable for spread spectrum operation without any additional design work needed if the converter is allowed to operate in a chaotic mode.

In addition to the converter control circuit, a traditionally implemented frequency modulator needs two signal generators and a frequency modulator for the clock signal generation. Of course, the modulation sequence can be pre-programmed in some memory devices, especially when design of an integrated circuit can be considered. In some cases a 50Hz/60Hz line frequency can be exploited as a modulating wave.

A frequency-hopping converter needs a preprogrammed memory device or PN-generation circuit with the power controller circuit. This is usually too expensive or too complicated for a small production series. The frequency-hopping (and similar) approach is very suitable in mass production, because the spectral performance can be tuned, and complex circuitry can be integrated in ASIC.
Controller-based spread spectrum approaches are easy to implement, because there is no need for an additional circuit. There are several controller circuits on the market, which can be directly utilized in spread spectrum generation with proper design. Therefore this kind of approach is very cost effective – the only drawback is the spectral performance, which cannot be tailored like in freely programmable frequency hopping. The spectral performance is dependent on the operation mode of the converter (i.e. load) and controller parameters, which cannot be arbitrarily selected.

The spread spectrum modulation has been constructed in this work with a simple PWM controller in Cases 1-4. The SS-triangular wave calculated in Matlab™ is fed to the circuit from an arbitrary waveform generator. This waveform generator can be replaced with some memory device with the proper modulating sequence if a more practical converter construction is needed.

In Cases 5 and 6, two different controllers were built. These controllers need a constant clock frequency, which was 50 kHz for the chaotic controller and 200 kHz for the Sigma-Delta-converter. These two examples proved, that spread spectrum generation might be done with very simple circuitry: only a couple of operational amplifiers, comparators and a digital flip-flop and D-latch were needed for the

converter control circuit.A summary of the main properties of different spread spectrum generation techniques are listed in Table 5-5.

Table 5-5. Summary of the main properties of different SS-generation techniques, [P3].

	Design complexity - hardware	Design complexity – control	Spectral efficiency	Cost
Frequency modulation	Moderate	Low - Traditional methods (ie. PI) can be applied	Moderate-high, not affected by converter variables	Moderate-high
Frequency hopping	Moderate - high	Low - Traditional methods (ie. PI) can be applied	High, easily tailored, not affected by converter variables	Moderate-high
Chaos	Low-moderate Traditional control circuitry can be utilized	Moderate - Both spectral and dynamic performance are affected by control design	Low-moderate, depends on converter variables (i.e. load)	Low No extra component cost compared to “normal” converter
Sigma-delta	Low-moderate Simple control circuitry	Moderate - Both spectral and dynamic performance are affected by control design	Low-moderate, depends on converter variables (i.e. load)	Low

A combination of different schemes is one interesting possibility in an SS power converter. This is especially applicable with controller-based SS generation where the spread spectrum operation can be ensured with quasi-random or a frequency-modulated system clock. For example Chang et al. [Chang 2002], proposed the use of a sigma-delta converter with a random clock signal.

Although the scope of this work is on conducted emissions, the spectral reduction is analogous to radiated emissions. The effect of a spread spectrum clock signal on radiated emissions is reported for example in papers [Hardin 1994], [Stone 1995-2] and [Yoonjae 2002]. These papers consider mainly the radiation of a clock signal, but the theory can be applied also in power converter applications.

5.4.4 How Disturbing is the Spread Spectrum Noise, [P4]

Very often, the wide band disturbance is more acceptable in practical situations, because there is no periodic excitation to a possible victim system. On the other hand, wide spectrum noise may be viewed more acceptable than narrow band noise because of the current EMC regulations. The regulations describe the measurement instruments to be used in EMC-tests. These devices, such as swept spectrum analyzers and test receivers are optimized to measure continuous periodic signals. If the switching frequency were to be changed at a wider frequency band than that of the resolution bandwidth or the actual IF filter bandwidth of the measuring device, the measured level would be lower than the fleeting true value.

Analog Victim Circuits

Analog systems are often quite sensitive to non-periodic disturbances. If an occasional noise is coupled to the analogue circuit, it is difficult to filter it out of the signal by any means. Increased background noise may be very disturbing for example in the analogue parts of several measurement instruments such as preamplifiers and filters. Also the performance of many analog audio applications may decline because of the rise in the noise floor. In some cases, noise in a fixed frequency can be removed from the information signal by just filtering it out. A wide band noise will most probably appear also at the information signal frequency. On the other hand, peak power at some fixed frequencies is lowered thus decreasing the probability of the disturbance.

Digital Victim Circuits

Digital circuits usually have correction algorithms that may even correct a highly corrupted signal. These algorithms are widely used in almost all digital systems to increase the reliability of the system. However, if an occasional electromagnetic disturbance is coupled to the digital logic circuit, it may lead the system to some unpredictable state. When the electromagnetic disturbance is only occasional, the reason for the malfunctioning may be difficult to trace. Sometimes the logic circuit hast to be observed for several hours with a logic analyzer to find the origin of the odd behavior in the circuit.

RF-communication

In RF-communication, a fixed frequency disturbance usually decreases significantly the usability of that specific spot frequency. To what extent the specific frequency range is spoilt is dependent on the power emitted from the noise source and naturally on the frequency of the disturbance. Very often the harmonic frequencies of the main emission also contain fixed frequency noise and thus disturb the possible radio communication. Therefore, in radio communication the spread spectrum noise is more acceptable than the fixed frequency noise.

5.5 Summary

Voltage and current ripple have been considered as a major problem with spread spectrum modulated power supplies. Results from steady-state voltage measurements show, that the variable-frequency operation of the SMPS has an effect on the voltage ripple, but the ripple measured from the prototype is still acceptable in some applications. This voltage fluctuation caused by the modulation can be reduced with a normal voltage feedback control. Fluctuation and ripple of the input current is more dependent on the control methodology and magnetic circuit design of the converter than the voltage ripple. Both current and voltage ripple can be controlled with proper main circuit design.

Measurements confirmed the efficiency of the spread spectrum modulation on the EMI-spectrum of the switch mode power converter. Results obtained in this chapter differed a little from those calculated from the simulated switching function although the trend was similar with different types of modulation techniques. The largest

difference was in the case of the Sigma-Delta converter, which demonstrated poor performance in prototyping. The main reason behind this was the susceptibility to small variations in system variables, which is typical for chaotic operation – With slightly different component values the performance could have been totally different. Results shown here are only from a limited set of selected modulation methods. There are also a huge amount of parameters to be selected, even in this limited set of modulation methods. However, this gives an overview of the possibilities and problems of different types of common spread spectrum techniques in power supply applications.

The spectrogram was used in the time-frequency analysis of the converter performance. A spectrogram can be used in evaluating both spectral properties and time-domain performance of a converter. It was shown that there was a correlation between the spectrogram and time-domain performance (i.e. current and voltage waveforms, autocorrelation sequence) of the converter. Therefore, the spectrogram is proposed as a general analysis tool for SS-converter design and analysis.

Evident correlation between the calculated spectrum of switching function and measured input current EMI spectrum of the boost converter can be seen. This encouraging result implies that basic modulation methods used in a boost converter can be utilized also in other switching converter topologies when SS modulation methods are considered.

6 Conclusions and Future Work

The major contributions and the main results of this thesis are summarized in this chapter. The main objective of this study was to compare the EMI and steady-state performance of a switch mode power supply with different spread spectrum methods. Another goal was to find out suitable tools for variable frequency EMI analysis.

Chapter 3 covered analysis methods used in this thesis. The Welch-algorithm was selected for numerical spectrum estimation and results were congruent with measurements made with the EMI test receiver. The spectrogram was proposed for time-frequency analysis when analyzing the EMI performance of a spread spectrum power supply system. Different kinds of spread spectrum techniques were introduced in Chapter 4 and selected cases were tested with the prototype. According to the results shown in Chapter 5 and partly in Chapter 4, electromagnetic interference of switch mode power converters can be reduced with spread spectrum techniques. This was proven by numerous simulations and measurements made with the prototype DC/DC boost power converter. In addition to the EMI-tests, analysis of the steady-state performance of different spread spectrum techniques was made in Chapter 5.

The main contributions of this thesis can be summarized as follows:

- **Comparison of EMI-performance of different types of spread spectrum techniques:** Four different techniques in six different configurations were analyzed and the EMI performance was compared to the constant frequency operation. The analysis was done with simulations and measurements made with the prototype.
- **Comparison of the steady-state performance of different types of spread spectrum techniques:** Output voltage and input current waveforms were analyzed in the time domain to see the effect of the spread spectrum operation on these quantities. Results from the steady-state voltage measurements showed, that the variable-frequency operation of the SMPS had an effect on the voltage ripple, but the ripple measured from the prototype was still acceptable in some applications. Both the current and voltage ripple can be controlled with proper main circuit and controller design.
- **Use of a spectrogram in the EMI analysis:** A spectrogram was proposed and used in the time-frequency EMI analysis of the power converter. A spectrogram is very useful in tracking variable frequency signals present in spread spectrum power supplies although not reported previously in this kind of application.
- **Evaluation of different signal analysis tools in spread spectrum applications:** The theory of signal analysis and measurement in variable frequency applications was studied. Combination of the autocorrelation function, Welch spectrum estimate and the spectrogram was used as a substitute for ordinary Fourier methods. It was also shown that the switching

function could be used in preliminary EMC analysis of a SMPS and the spectrum and autocorrelation sequence of the switching function correlated with the final EMI spectrum.

- **Design and construction of uniform prototyping platform for EMI-measurements:** The prototype of a boost converter with a configurable control circuit was designed and constructed. The prototype design made it possible to compare different techniques with the same main power circuit thus improving repeatability and reliability of the analysis. The prototype design also showed that spread spectrum techniques could be implemented with simple analog and digital electronics.

Preprogrammed spread spectrum techniques, such as frequency modulation and frequency hopping, gave reliable and predictable results in EMI-reduction. These techniques allowed freedom of tailoring the spectral performance of the converter. The drawbacks of the preprogrammed techniques were the need for more complex circuitry and the design effort in modulation technique selection. EMI-tests from these techniques showed promising and guaranteed results.

The controller-based chaotic SS-techniques, such as Sigma-Delta and peak current control, are the fastest and the simplest way to utilize spread spectrum methods in power supplies, especially if these control techniques are previously employed in SMPS-design. In these techniques, the spread spectrum modulation is inherent part of the normal control loop. There is no need for extra components or circuitry for the spread spectrum operation thus making the solution very cost effective. These methods only require different design parameters compared to the conventional design methodology. However, the chaotic operation point of the converter is usually considered as a non-stable operation of the converter, so the designer needs to study and accept the chaotic operation of the power converter. This simplicity is also a disadvantage of these modulators, because the effective spread spectrum modulation can be optimized only at some specific operating point at a given load. In addition, the component value tolerances affect on the operation, which can arise as a problem especially in mass production.

6.1. Usability of the Results

The results obtained in this work are generally easily usable due to the practical nature of the work. The modulation based EMI-reduction techniques are of great importance in mass production, where the component count needs to be minimized for cost effectiveness. In mass production, more complex spread spectrum modulation methods can also be implemented in a single ASIC.

Methods and techniques presented are independent of the end application. Guidelines and spectral effects are the same when dealing with DC/DC, AC/DC, AC/AC or DC/AC switch mode converters, active power factor controllers or motor drives. Of course, the nature and demands of the end application set different requirements and restrictions on the spread spectrum modulation of the converter.

Analysis tools covered in this work are generally suitable for EMI analysis of non-stationary signals. Especially the spectrogram can be used both in power converter analysis and in compliance engineering to speed-up the test procedure.

6.2. Suggestions for Future Research

Modulation sequence optimization: A survey for optimization of an algorithm for effective spread spectrum modulation pattern needs to be done. For practical power supply design, such an algorithm is essential. Some guidelines can be found in communication theory, but the limitations of power supply components and the power quality need to be fully taken into consideration.

Controller design and analysis: A proper study of the effect of the voltage control loop and different control strategies needs to be done. Although two nonlinear control techniques were proposed in this work and one in [P2], the analysis was simplistic. Effect of the voltage feedback on both output voltage ripple and EMI spectral performance needs to be analyzed.

Operation on a wider frequency band: The analysis bandwidth of this work was limited mainly to the frequency range of up to 1 MHz, although selected results in 150 kHz to 30 MHz band were discussed. Optimization of the modulation method and survey on higher frequency operation range should be done.

Efficiency in variable frequency operation: A detailed study on the efficiency at different variable frequency applications should be done. This is especially important if the frequency deviation is much larger than in this study.

Time-frequency analysis / Spectrogram: The use of time-frequency analysis methods in EMC is one interesting topic and the usability and applications should be studied.

Spread spectrum and EMI test instruments: Detection of SS-signaling with an EMI measurement instrument need to be considered. For example a quasi-peak detector in an EMI-test receiver will favor non-periodic spread spectrum signals. Many of the compliance tests require the use of different frequency ranges and different detectors, so this kind of study is vital in commercial applications.

References

Agilent Technologies. 2003. *54542C Oscilloscope, Data Sheet*. Agilent Technologies Inc. www.agilent.com, 20.09.2003. 5 pages.

Ahmed, M., Kuisma, M., Tolsa, K., Silventoinen, P. 2003. *Implementing sliding mode control for buck converter*. IEEE 34th Annual Conference on Power Electronics Specialist, PESC '03. Vol. 2. Acapulco, Mexico. 15-19 June 2003. pp. 634-637.

Altes, R. 1984. *Spectrograms and generalized spectrograms for classification of random processes.* IEEE International Conference on Acoustics, Speech, and Signal Processing, ICASSP '84. 26-29 March. San Diego, California, USA. pp. 282- 285, Vol. 9.

Au, O.C., Lam, K.H. 1998. *A novel output-based objective speech quality measure for wireless communication*. 1998 Fourth International Conference on Signal Processing, ICSP '98. 12-16 October 1998. Beijing, China. pp. 666-669, Vol. 1.

Aumala, O., Ihalainen, H., Jokinen, H., Kortelainen, J. 1998. *Mittaussignaalien käsittely*, 3. painos. Pressus Oy. ISBN 952-9835-32-9, in Finnish. 323 pages.

Aziz, P.M., Sorensen, H.V., van der Spiegel, J. 1996. *An overview of sigma-delta converters.* IEEE Signal Processing Magazine. Vol. 13, No. 1. pp. 61-84.

Baker, G., Gollub, J. 1990. *Chaotic Dynamics, An Introduction*. Cambridge University Press. ISBN 0-521-38258-0. 272 pages.

Banerjee, S., Verghese, G., editors. 2001. *Nonlinear phenomena in power electronics – Attractors, bifurcations, chaos, and nonlinear control*. IEEE press, 2001. ISBN 0-7803-5383-8. 441 pages.

Banerjee, S., Kasths, D., SenGupta, S. 2002. *Minimising EMI problems with chaos*. Proceedings of the International Conference on Electromagnetic Interference and Compatibility, 21-23 February 2002. Bangalore, India. pp. 162-167.

Bech, M., Blaabjerg, F., Pedersen, J. 2000-1. *Random modulation techniques with fixed switching frequency for three-phase power converters*. IEEE Transactions on Power Electronics, Vol. 15, No. 4. pp. 753-761.

Bech, M. 2000-2. *Analysis of random pulse-width modulation techniques for power electronic converters*. Dissertation. Aalborg University, Denmark. ISBN 87-89179-32-3. 313 pages.

Benitez, H. 1997. *European Union EMC Directive: the new world of product family standards*. IEEE 1997 International Symposium on Electromagnetic Compatibility. Austin, TX, USA. 18-22. August,1997. Pages 1-7.

Björklöf, D. 1999. *EMC Standards and Their Application*. Compliance Engineering magazine Online. Annual reference guide 1999. http://www.ce-mag.com/99ARG/toc.html, 20.8.2003.

Boashash, B. 1992-1. *Estimating and interpreting the instantaneous frequency of a signal. I. Fundamentals.* Proceedings of the IEEE, Vol. 80, No. 4. pp. 520-538.

Boashash, B. 1992-2. *Estimating and interpreting the instantaneous frequency of a signal. II. Algorithms and applications.* Proceedings of the IEEE, Vol. 80, No 4. pp. 540 –568.

Bolden, C., Ferdowsi, M., Patel, N., Cochrane, D., Fatehi, F., Lee, F., Homaifar, A. 2001. *Survey of EMI Reduction Techniques in Switched-mode Power Supplies*. Proceedings of CPES-Seminar 2001, Virginia Tech., USA. pp. 525-532.

Boys, J.T., Handley, P.G. 1992. *Spread spectrum switching: low noise modulation technique for PWM inverter drives*. IEE Proceedings of Electric Power Applications B, Vol. 139, No. 3. pp. 252-260.

Boys, J.T., Andrews, M. 1993. *Random PWM inverter drive systems: theory and practice.* Industrial Electronics, International Conference on Control, and Instrumentation, IECON'93. 15-19 November 1993. Maui, HI, USA. pp. 695-700, Vol. 2.

Bronaugh, E.L., Osburn, J.D.M. 1996. *A process for the analysis of the physics of measurement and determination of measurement uncertainty in EMC test procedures*. IEEE 1996 International Symposium on Electromagnetic Compatibility. 19-23 August 1996. Santa Clara, CA, USA. pp. 245-249.

Budisin, S. 1992. *Golay complementary sequences are superior to PN sequences*. IEEE International Conference on Systems Engineering.17-19 September 1992. Kobe, Japan. pp. 101-104.

Callegari, S., Rovatti, R., Setti, G. 2002. *Chaotic modulations can outperform random ones in electromagnetic interference reduction tasks*. Electronics Letters, Vol. 38, No. 12. pp. 543-544.

Caponet, M.C., Profumo, F., Tenconi, A. 2002. *EMI filters design for power electronics*. IEEE 33rd Annual Power Electronics Specialists Conference, PESC 02. 23-27 June 2002. Cairns, Australia. pp. 2027-2032, Vol. 4.

Chang Han Bae, Joon Hyoung Ryu, Kwang Won Lee. 2002. *Suppression of harmonic spikes in switching converter output using dithered Sigma–Delta modulation*. IEEE Transactions on Industry Applications, Vol. 38, No. 1. pp. 159-166.

Chan, W.C.Y., Tse, C.K. 1996. *Studies of routes to chaos for current-programmed DC/DC converters*. 27th Annual IEEE Power Electronics Specialists Conference, PESC '96. 23-27 June 1996. Baveno, Italy. pp. 789-795, Vol. 1.

Chiang, H., Liu, C., Varaiya, P., Wu, F., Lauby, M. 1993. *Chaos in Simple Power System*. IEEE Transactions on power systems, Vol. 8, No. 4. pp. 1407-1417.

CISPR 16-1. 1999. *Specifications for radio disturbance and immunity measuring apparatus and methods – Part 1: Radio disturbance and immunity measuring apparatus*. 2nd edition. IEC, Geneva, Switzerland. 407 pages.

CISPR 16-2. 1999. *Specifications for radio disturbance and immunity measuring apparatus and methods – Part 2: Methods of measurement of disturbances and immunity*, edition 1.1. IEC, Geneva, Switzerland. 169 pages.

CISPR 22. 2003. *Information technology equipment – Radio disturbance characteristics – Limits and methods of measurement,* 4th edition. IEC, Geneva, Switzerland. 133 pages.

Clarke, P.W., Bell Telephone Laboratories. 1969. *Switching Regulator with Random Noise Generator*. US Patent No 3,579,091. 7 pages.

Cooley, J., Tukey, J. 1965. *An Algorithm for the Machine Computation of the Complex Fourier Series*. Mathematics of Computation, Vol. 19, April 1965. pp. 297-301.

Dallago, E., Passoni, M., Venchi, G. 2001. *Boost-type power factor correction system with three-level sigma-delta modulation*. The 8th IEEE International Conference on Electronics, Circuits and Systems, ICECS 2001. 2-5 September 2001. Malta. pp. 137-140, Vol. 1.

Daubechies, I. 1990. *The wavelet transform, time-frequency localization and signal analysis.* IEEE Transactions on Information Theory, Vol. 36, No. 5. pp. 961-1005.

Deb, G.K. 1999. *EMI problems for frequency hopping communication sets*. 1999 International Symposium on Electromagnetic Compatibility. 17-21 May 1999. Tokyo, Japan. pp. 754 –757.

Deane, J., Hamill, D. 1990. *Instability, Subharmonics, and Chaos in Power Electronic Systems*. IEEE Transactions on power electronics, Vol. 5, No. 3. pp. 260-268.

Deane, J., Hamill, D. 1996. *Improvement of Power Supply EMC by Chaos*. Electronics Letters, Vol. 32 No. 12. 1996. Page 1045.

Deane, J., Ashwin, P., Hamill, D., Jefferies, D. 1999. *Calculation of the periodic spectral components in a chaotic DC-DC converter*. IEEE Transactions on Circuits and Systems I: Fundamental Theory and Applications, Vol. 46, No. 11. pp. 1313 – 1319.

Dorf, R., Bishop, R. 1995. *Modern Control Systems*, 7th edition. Addison-Wesley Publishing Company. ISBN 0-201-84559-8. 807 pages.

Dripps, J.H. 1997. *An introduction to time-frequency methods applied to biomedical signals*. IEE Colloquium on Time-Frequency Analysis of Biomedical Signals (Digest No. 1997/006). 29 January 1997. London, UK. pp. 1/1-1/4.

EN 61000-3-2. 2001. *Electromagnetic compatibility (EMC) - Part 3-2: Limits - Limits for harmonic current emissions (equipment input current up to and including 16 A per phase).* IEC 2001. 55 pages.

Erickson, R. 1997. *Fundamentals of Power Electronics.* Kluwer Academic Publishers. ISBN 0-412-08541-0. 773 pages.

ETSI EN 300 132-2 v2.1.2. 2003. *Environmental Engineering (EE); Power supply interface at the input to telecommunication equipment; Part 2: Operated by direct current*. European Telecommunications Standards Institute. 23 pages.

FCC CFR 47-15. 2002. *Title 47, part 15 of the Code of Federal Regulations*. Federal communications commission, Washington DC. Pages 675-763.

Ferroxcube. 2002. *Soft Ferrites and Accessories. Ferroxcube Data Handbook 2002*. 975 pages. http://www.ferroxcube.com/appl/info/HB2002.pdf, 8.8.2003.

Finney, S.J., Green, T.C., Williams, B.W. 1993. *Spectral characteristics of resonant-link inverters*. IEEE Transactions on Power Electronics, Vol. 8, No. 4. pp. 562-570.

Gabor, D. 1946. *Theory of communication*. The Journal of the IEE, Vol. 93, part III, No. 26. pp. 429-457.

Habetler, T.G., Divan, D.M. 1991. *Acoustic noise reduction in sinusoidal PWM drives using a randomly modulated carrier*. IEEE Transactions on Power Electronics, Vol. 6, No. 3. pp. 356-363.

Hamill, D., Deane, J., Aston, P. 1997. *Some Applications of Chaos in Power Converters*. IEE Colloquium on Update on New Power Electronic Techniques (Digest No: 1997/091), 1997. pp. 5/1-5/5.

Hardin, K.B. Fessler, J.T. Bush, D.R. 1994. *Spread spectrum clock generation for the reduction of radiated emissions.* IEEE International Symposium on Electromagnetic Compatibility. 22-26 August 1994. Chicago, IL, USA. pp. 227-231.

Haykin, S. 1989. *An introduction to analog and digital communications*. Wiley. ISBN 0-471-85978-8. 652 pages.

Hsu, H., P. 1993. *Analog and Digital Communication*. McGraw-Hill. ISBN 0-07-030636. 328 pages.

Hua, G., Tabisz, W., Leu, C., Dai, N., Watson, R., Lee, F. 1994. *Development of a DC distributed power system*. Proceedings of Ninth Annual Applied Power Electronics Conference and Exposition, APEC '94. 13-17 February 1994. Orlando, FL, USA. pp. 763-769, Vol. 2.

Hung H.-L., Chi C-T. 2001. *Electromagnetic interference detection using wavelet transform*. IEEE/PES Transmission and Distribution Conference and Exposition 2001. 28 October – 2 November 2001. Atlanta, GA, USA. pp. 385-390, Vol.1.

Hui, S.Y., Shrivastava, Y., Sathiakumar, S., Tse, K.K., Henry Shu-Hung Chun. 1998. *A comparison of nondeterministic and deterministic switching methods for DC-DC power converters*. IEEE Transactions on Power Electronics, Vol. 13, No 6. pp. 1046-1055.

Jefferies, D., Deane, J., Johnstone, G. 1989. *An Introduction to Chaos*. Electronics & Communication Engineering Journal, Vol. 1, No 3. pp. 115-123.

Kay, S., M. 1988. *Modern Spectral Estimation*. Prentice Hall, Inc. ISBN 0-13-598582-X. 543 pages.

Kim, K.-T., Choi, I.-S., Kim, H.-T. 2000. *Efficient radar target classification using adaptive joint time-frequency processing*. IEEE Transactions on Antennas and Propagation, Vol. 48, No. 12. pp. 1789-1801.

Koenig, R., Dunn, H., Lacy, L. 1946. *The Sound Spectrograph*. Journal of the Acoustical Society of America, Vol. 18. pp. 19-49.

Kok, R., Weber, D.M. 1999. *On designing sigma-delta converter systems for class-D power amplifiers.* IEEE AFRICON, 1999. 28 September – 1 October 1999. Cape Town, South Africa. pp. 715-718, Vol. 2.

Kosola, J., Solane, T. 2000. *Digitaalinen taistelukenttä - informaatioajan sotakoneen tekniikka*. MpKK TeknL, Helsinki. 402 pages. In Finnish.

Krattenmacher, H., Schwab, A. 1999. *Measurement of conducted emissions. Possible sources for measurement uncertainties*. IEEE International Symposium on Electromagnetic Compatibility. 2-6 August 1999. Seattle, WA, USA. pp. 370-375, Vol. 1.

Kuisma, M., Järveläinen, T., Silventoinen, P, Vesterinen, T. 2000. *Effects of Nonperiodic and Chaotic Switching on the Conducted EMI Emissions of Switch Mode Power Supplies.* Proceedings of the 2000 IEEE Nordic Workshop on Power and Industrial Electronics. Aalborg, Denmark. 13-16 August 2000. pp. 185-190.

Kuisma, M., Ahmed, M., Silventoinen, P. 2003. *Comparison of Conducted RF-Emissions between PID and Sliding Mode Controlled DC-DC Converter*. 10th European Conference on Power Electronics and Applications, EPE 2003. September 2 - 4 2003. Toulouse, France. CD-ROM.

Kuisma, M. 2003-2. *Variable Frequency Switching in Power Supply EMI-control: An Overview*. IEEE Aerospace and Electronic Systems Magazine. Vol. 18, No 12. pp. 18 – 22.

Leon, D., Balkir, S., Hoffman, M., Perez, L.C. 2000. *Fully programmable, scalable chaos-based PN sequence generation [CDMA]*. Electronics Letters, Vol. 36, No. 16. pp. 1371-1372.

Leon-Garcia, A. 1994. *Probability and Random Processes for Electrical Engineering,* 2nd edition. Addison-Wesley Publishing Company. ISBN 0-201-50037-X. 596 pages.

Lev-Ari, H., Stankovic, A.M. 2002. *Statistical analysis of power spectra of signals governed by Markov chains*. IEEE International Symposium on Circuits and Systems, ISCAS 2002. pp. 560-563, Vol. 4.

Lin, F., Chen, D. 1994. *Reduction of power supply EMI emission by switching frequency modulation*. IEEE Transactions on Power Electronics, Vol. 9, No. 1. pp. 132 –137.

Lindh, T. 2003. *On the condition monitoring of induction machines.* Dissertation. Lappeenranta University of Technology. ISBN 951-764-841-3 146 pages.

Lorenz, E. 1963. *Deterministic nonperiod flow*. Journal of Atmospheric Sciences, Vol. 20, No. 2. pp.130-141.

Magrath, A.J., Clark, I.G., Sandler, M.B. 1997. *Design and implementation of a FPGA sigma-delta power DAC*. 1997 IEEE Workshop on Signal Processing Systems, SIPS 97 - Design and Implementation. 3-5 November 1997. Leicester, UK. pp. 511-521.

Maroney, J. 1999. *The use of scanning receivers in EMI compliance measurements*. International Symposium on Electromagnetic Compatibility. 17 – 21 May 1999. Tokyo, Japan. Page 791.

Marrero, J.L.R., Font, J.M., Verghese, G.C. 1996*. Analysis of the chaotic regime for DC-DC converters under current-mode control*. 27th Annual IEEE Power Electronics Specialists Conference, PESC '96. 23-27 June. Baveno, Italy. pp. 1477-1483, Vol. 2.

Mathworks, Inc. 2002. *Signal processing toolbox, Users guide. Version 6.* The MathWorks, Inc. 1035 pages.

Maxim application note DI428. 2002. *DC-to-DC Converter Combats EMI*. Maxim Integrated Products, Inc.

Mazzini, G. Rovatti, R. Setti, G. 2001*. Statistical approach and application to EMI reduction - Statistical approach to discrete-time chotic systems: some tools for studying chaos with densities and application to EMI reduction*. The IEEE International Symposium on Circuits and Systems, 2001. Tutorial Guide: ISCAS 2001. 6-9 May 2001. pp. 8.1_1-8.1_14.

MCWP 3-40.5. 2001. *Electronic warfare*, Coordinating Draft. U.S. Marine Corps, Department of the Navy. Washington, DC, USA. 56 pages.

Mihalic, F., Milanovic, M. 1998. *Power spectrum estimation of the input current in random modulated boost rectifier*. Proceedings of the 24th Annual Conference of the IEEE Industrial Electronics Society. IECON '98. 31 August - 4 September 1998. Aachen, Germany. pp. 1382-1387, Vol. 3.

Mihalic, F., Milanovic, M. 1999-1. *Power density spectrum estimation of the random controlled PWM single-phase boost rectifier*. 1999 IEEE International Symposium on Electromagnetic Compatibility. 2-6 August 1999. Seattle, WA, USA. pp. 803-805.

Mihalic, F., Milanovic, M. 1999-2. *EMI reduction in randomized boost rectifier*. Proceedings of the IEEE International Symposium on Industrial Electronics, ISIE '99. Bled, Slovenia. 12-16 July 1999. pp. 457-462.

Miller, G., Beasley, J. 2002. *Modern electronic communication*, 7th edition. Prentice-Hall, Inc. ISBN 0-13-016762-2. 883 pages.

Mohan, N., Undeland, T., Robbins, W. 1989. *Power electronics: Converters, applications, and design.* Wiley. ISBN 0-471-50537-4. 667 pages.

Mutagi, R.N. 1996. *Pseudo noise sequences for engineers*. Electronics & Communication Engineering Journal, Vol. 8 No. 2. pp. 79-87.

Nagel, A., De Doncker R. W. 1997. *Analytical Approximation of Interference Spectra Generated by Power Converters.* Annual Meeting of IEEE Industrial Applications Society. 5-9 October 1997. New Orleans, LA, USA. pp. 1564-1570, Vol. 2.

Oppenheim, A., Willsky, A., Nawab, H. 1997. *Signals and Systems,* second edition. Prentice Hall. ISBN 0-13-651175-9. 957 pages.

Ott, H.W. 1988. *Noise reduction techniques in electronic systems,* second edition. Wiley. ISBN 0-471-85068-3. 426 pages.

Paramesh, J. von Jouanne, A. 2001. *Use of sigma-delta modulation to control EMI from switch-mode power supplies*. IEEE Transactions on Industrial Electronics, Vol. 48, No. 1. pp. 111-117.

Parker, T., Chua, L.1987. *Chaos: A Tutorial for Engineers*. Proceedings of the IEEE, vol. 75, No. 8. August, 1987.

Parvis, M., Perrone, G., Vallan, A. 2003. *A precompliance EMC test-set based on a sampling oscilloscope*. IEEE Transactions on Instrumentation and Measurement, Vol. 52, No. 4. pp. 1220-1223.

Paul, C. 1992. *Introduction to Electromagnetic Compatibility*. Wiley. ISBN 0-471-54927-4. 765 pages.

Perez, R., editor. 1995. *Handbook of electromagnetic compatibility*. Academic press. ISBN 0-12-550710-0. 1098 pages.

Poddar, G., Chakrabarty, K., Banerjee, S. 1995. *Control of chaos in the boost converter.* Electronics Letters, Vol. 31. No. 11. pp. 841-842.

Proakis, J. 1989. *Digital Communications,* 2nd edition. McGraw-Hill. ISBN 0-07-100269-3. 905 pages.

Proakis, J., Manolakis, D. 1992. *Digital signal processing: principles, algorithms and applications*, 2nd edition. Macmillan. ISBN 0-02-396815-X. 969 pages.

Qian, S., Dapang, C. 1999. *Joint time-frequency analysis*. IEEE Signal Processing Magazine, Vol. 16, No 2. pp. 52-67.

Rahkala, M., Suntio, T., Kalliomaki, K. 2002. *Effects of switching frequency modulation on EMI performance of a converter using spread spectrum approach*. Seventeenth Annual IEEE Applied Power Electronics Conference and Exposition, APEC 2002. 10-14 March 2002. Dallas, TX, USA. pp. 93-99, Vol. 1.

Redl, R. 1996. *Power electronics and electromagnetic compatibility*. 27th Annual IEEE Power Electronics Specialists Conference, PESC '96. June 23-27, 1996. Baveno, Italy. pp. 15-21, Vol.1.

Redl, R., Tenti, P., Daan van Wyk, J. 1997. *Power electronics' polluting effects*. IEEE Spectrum, Vol. 34, No 5. pp. 32-39.

Ristau, D., Hansen, D. 1997. *Modulation impact on quasi-peak detector response.* IEEE 1997 International Symposium on Electromagnetic Compatibility. August 18-22, 1997. Austin, TX , USA. pp. 90-95.

Rohde & Schwarz. 1989. *EMI test receiver ESHS 20/30 – Operating manual*.

Sander, K. 2003. *Power Measurement on Pulsed Signals with Spectrum Analyzers*. Rohde & Schwarz Application note 1EF48. http://www.rohde-schwarz.com, 7.8.2003.

Santolaria, A., Balcells, J., Gonzalez, D. 2002. *Theoretical and experimental results of power converter frequency modulation.* IEEE 2002 28th Annual Conference of the Industrial Electronics Society, IECON 02. 5-8 November 2002. Barcelona, Spain. pp. 193-197, Vol. 1.

Schaefer, W. 1998. *Signal detection with EMI receivers.* 1998 IEEE International Symposium on Electromagnetic Compatibility. 24-28August, 1998. Denver, CO, USA. pp. 761-765, Vol. 2.

Schaefer, W. 1999 *Understanding impulse bandwidth specifications of EMI receivers*. IEEE International Symposium on Electromagnetic Compatibility. 2-6 August 1999. Seattle, WA, USA. pp. 958-961.

Schweber, W. 1999. *Electronic communication systems: a complete course,* 3rd edition. Prentice-Hall Inc. ISBN 0-13-780016-9. 788 pages.

Shrivastava, Y., Hui, S.Y.R., Sathiakumar, S., Chung, H., Tse, K.K. 1997. *Effects of continuous noise in randomised switching DC-DC converters.* Electronics Letters, Vol. 33, No. 11. pp. 919-921.

Shrivastava, Y. Hui, S.Y. Sathiakumar, S. Shu-Hung Chung, H. Tse, K.K. 2000. *Harmonic analysis of nondeterministic switching methods for DC-DC power converters*. IEEE Transactions on Circuits and Systems I: Fundamental Theory and Applications. Vol. 47, No 6. pp. 868-884.

Silventoinen, P. 2001. *Electromagnetic compatibility and EMC-measurements in DC-voltage link converters*. Dissertation. Lappeenranta University of Technology. ISBN 951-764-588-0. 115 pages.

Silventoinen, P., Kuisma, M., Pyrhönen, J., Huppunen, J. 2002. *Effects of the Modulation Technique on the Conducted RF-Emissions of an Adjustable Speed Motor Drive*. 15th International Conference on Electrical Machines, ICEM2002. 25-28 August 2002. Bruges, Belgium.

Slotine, J., Li, W. 1991. *Applied Nonlinear Control*. Prentice-Hall, Inc. Englewood Cliffs. ISBN 0-13-040049-1. 461 pages.

Sony-Tektronix. 2001. *AWG 2021 Arbitrary Waveform Generator, User Manual*. Tektronix, Inc. 580 Pages.

Southwick, R., Runger, G. 1989*. A theory to optimize the detection and measurement of EMI signals*. IEEE Transactions on Electromagnetic Compatibility, Vol. 31, No. 4. Pages 409-413.

Stankovic, A.M., Verghese, G.C., Hinds, R.O. 1992. *Monte-Carlo verification of power spectrum formulas for random modulation schemes*. IEEE Workshop on Computers in Power Electronics. 9-11 August 1992. Berkeley, CA, USA. pp. 187-194.

Stankovic, A.M., Verghese, G.C., Perreault, D.J. 1993. *Analysis and synthesis of random modulation schemes for power converters*. 24th Annual IEEE Power Electronics Specialists Conference, PESC '93. 20-24 June 1993. Seattle, WA, USA. pp. 1068-1074.

Stankovic, A.M. 1993. *Random pulse modulation with applications to power electronic converters.* Dissertation. Massachusetts Institute of Technology. 205 pages.

Stankovic, A.M., Verghese, G.C., Perreault, D.J. 1995. *Randomized modulation schemes for power converters governed by Markov chains.* Proceedings of the 4th IEEE Conference on Control Applications. 28-29 September 1995. Albany, NY, USA. pp. 372-377.

Stecher, M. 1997. *Measurement uncertainty in EMI emission measurements*. 1997 International Symposium on Electromagnetic Compatibility. 21-23 May 1997. Beijing, China. pp. 270-273.

Stecher, M. 2001. *A detailed analysis of EMI test receiver measurement uncertainty*. IEEE International Symposium on Electromagnetic Compatibility, EMC 2001. 13-17 August 2001. Montreal, Canada. pp. 464-468, Vol.1.

Stone, D.A., Chambers, B., Howe, D. 1995-1. *Random carrier frequency modulation of PWM waveforms to ease EMC problems in switched mode power supplies*. Proceedings of 1995 International Conference on Power Electronics and Drive Systems. 21-24 February 1995. Singapore. pp. 16-21, Vol.1.

Stone, D., Chambers, B.1995-2. *Easing radiated EMC problems with spread-spectrum modulation of computer clock signals*. Electronics Letters, Vol. 31, No. 24. pp. 2072-2074.

Stone, D.A., Chambers, B., Howe, D. 1996*. Easing EMC problems in switched mode power converters by random modulation of the PWM carrier frequency*. Eleventh Annual Applied Power Electronics Conference and Exposition, APEC '96. 3-7 March 1996. San Jose, CA, USA. pp. 327-332, Vol.1.

Tabisz, W, Jovanovic, M., Lee, F. 1992. *Present and future of distributed power systems.* Proceedings of Seventh Annual Applied Power Electronics Conference and Exposition, APEC '92. 23-27 February 1992. Boston, MA, USA. pp. 11-18.

Takahashi, I., Noguchi, T. 1985. *New Quick-Response and High-Efficiency Control Strategy of an Induction Motor.* Conference proceedings of IEEE IAS annual meeting 1995. pp. 496-502.

Tanaka, T. Ninomiya, T. Harada, K. 1989. *Random-switching control in DC-to-DC converters*. 20th Annual IEEE Power Electronics Specialists Conference, PESC '89. 26-29 June 1989. Milwaukee, WI, USA. pp. 500-507, Vol.1.

Tanaka, T., Kameda, H., Ninomiya, T. 1991*. Noise analysis of DC-to-DC converter with random-switching control*. 13th International Telecommunications Energy Conference, INTELEC '91. 5-8 November 1991. Kyoto, Japan. pp. 283-290.

Tanaka, T., Hamasaki, H., Yoshida, H. 1997. *Random-switching control in DC-to-DC converters: an implementation using M-sequence.* 19th International Telecommunications Energy Conference, INTELEC 97. 19-23 October 1997. Melbourne, Australia. pp. 431-437.

Taylor, B., Kuyatt, C. 1994. *NIST Technical Note 1297; Guidelines for Evaluating and Expressing the Uncertainty of NIST Measurement Results*, 1994 Edition. United States Department of Commerce, Technology Administration. National Institute of Standards and Technology. Washington, DC. 25 pages.

Tekes 2002. *ETX – Electronics for the Information Society 1997–2001, Final Report.* Technology Programme Report 3/2002. Tekes, The National Technology Agency of Finland, Helsinki, 2002. 387 pages.

Tektronix. 2003. *Wireless Communication Analyzer WCA330 - WCA380. Datasheet*. http://www.tek.com/. 10.9.2003.

Tihanyi, L. 1995. *Electromagnetic Compatibility in Power Electronics.* IEEE Press. ISBN 0-7803-0416-0. 403 pages.

Tousi, V.M., Sahandi, F., Atarodi, M., Shojaei, M. 2002. *A 3.3V/1W class D audio power amplifier with 103dB DR and 90% efficiency*. 23rd International Conference on Microelectronics, MIEL 2002. 12-15 May 2002. Nis, Yugoslavia. pp. 581-584, Vol. 2.

Tse, K.K., Chung, H.S.H., Hui, S.Y.R., So, H.C. 1999-1. *Spectral characteristics of random carrier frequency switching in off-line switched mode power supply.* Fourteenth Annual Applied Power Electronics Conference and Exposition, APEC '99. 14-18 March 1999. Dallas, TX, USA. pp. 139-145, Vol. 1.

Tse, K.K., Chung, H.S.H., Hui, S.Y., So, H.C. 1999-2*. A comparative study of using random switching schemes for DC/DC converters.* Fourteenth Annual Applied Power Electronics Conference and Exposition, APEC '99. Vol.1. 14-18 March 1999. Dallas, TX, USA. pp. 160-166.

Tse, K.K., Chung, H.S.H., Hui, S.Y., So, H.C. 2000. *Analysis and spectral characteristics of a spread-spectrum technique for conducted EMI suppression.* IEEE Transactions on Power Electronics, Vol. 15, No. 2. pp. 399-410.

Tse, K.K., Chung, H.S.H, Hui, S.Y., So, H.C. 2002. *A comparative study of carrier-frequency modulation techniques for conducted EMI suppression in PWM converters.* IEEE Transactions on Industrial Electronics, Vol. 49, No. 3. pp. 618-627.

Vilathgamuwa, M., Deng, J. Tseng, K.J. 1999. *EMI suppression with switching frequency modulated DC-DC converters.* IEEE Industry Applications Magazine, Vol. 5, No 6. pp. 27-33.

Wang, A., Sanders, S.R. 1990. *Random and programmed pulse-width modulation techniques for DC-DC converters.* IEEE International Conference on Systems Engineering. 9-11 August 1990. Pittsburgh, PA, USA. pp. 589-592.

Watson, R. 1998. *New Techniques in the Design of Distributed Power Systems*. Dissertation. Blacksburg, Virginia, USA. 258 pages.

Welch, P. 1967. *The Use of Fast Fourier Transform for the Estimation of Power Spectra: A Method Based on Time Averaging Over Short, Modified Periodograms.* IEEE Transaction on Audio Electroacoustics, Vol. AU-15. pp. 70-73.

Williams, D.A. 1996. *A tutorial on EMI characterization of switching regulators.* Applied Power Electronics Conference and Exposition, APEC '96. 3-7 March 1996. San Jose, California, USA. pp. 257-262, Vol. 1.

Wong, H., Chan, Y., Ma, S.W. 2002. *Electromagnetic interference of switching mode power regulator with chaotic frequency modulation*. 23rd International Conference on Microelectronics, MIEL 2002. 12-15 May 2002. Nis, Yugoslavia. pp. 577-580, Vol. 2.

Yoonjae, L., Mittra, R. 2002. *Electromagnetic interference mitigation by using a spread-spectrum approach.* IEEE Transactions on Electromagnetic Compatibility, Vol. 44, No. 2. pp. 380-385.

Zafrany, I., Ben-Yaakov, S. 1995. *A chaos model of subharmonic oscillations in current mode PWM boost converters*. 26th Annual IEEE Power Electronics Specialists Conference, PESC '95. 18-22 June 1995. Atlanta, GA, USA. pp. 1111-1117, Vol. 2.

Zigliotto, M., Trzynadlowski, A.M. 1998. *Effective random space vector modulation for EMI reduction in low-cost PWM inverters.* Seventh International Conference on Power Electronics and Variable Speed Drives, 1998. (IEE Conf. Publ. No. 456). 21-23 September, 1998. London, UK. pp. 163-168.

APPENDIX A

Simulation models and Matlab scripts

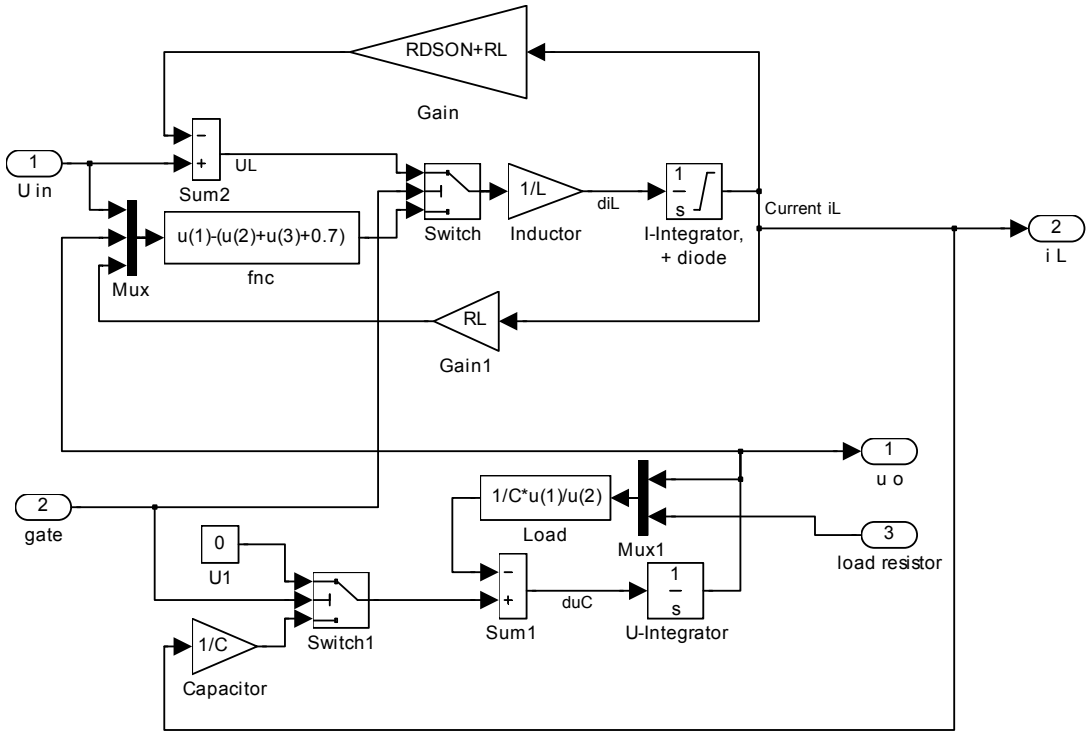

Figure A.1.Simulink^{TM} model for the Boost converter

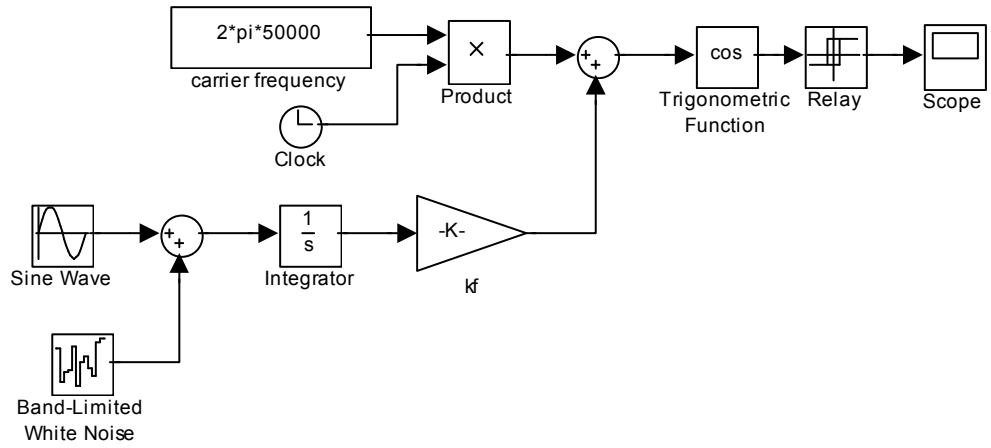

Figure A.2. Simulink^{TM} model for generating frequency modulated system clock.

APPENDIX A

MATLAB -scripts for generating frequency hopping quasi-random sequence:

```
FHOP=[50000 37000];
for n=3:300;
  apua=1;
  eiok=1;
  while eiok==1
    apua=apua+1;
    FHOP(n)=rand*100000;
    if (FHOP(n)<25000)
      eiok=1;
    elseif (FHOP(n)>75000)
      eiok=1;
    elseif abs(diff([FHOP(n) FHOP(n-1)]))<12000
      eiok=1;
    elseif abs(diff([FHOP(n) FHOP(n-2)]))<6000
      eiok=1;
    elseif apua>1000
        break
    else eiok=0;
    end
  end
end
TT=linspace(0,.1,300);

%removing DC-bias
FHOP=FHOP-mean(FHOP);
%Rescaling to +1/-1
FHOP=FHOP./max(FHOP);
```

MATLAB-script for analysis of switching function *q*(*t*):

(Here *q(t)* is ScopeData)

```
figure;
%Plotting the spectrogram
specgram(ScopeData(:,2),2048,2,1026)
set(gca,'FontSize',12)
xlabel('Time [s]','FontSize',12)
ylabel('Frequency [MHz]','FontSize',12)
set(gca,'YTickLabel',{'0','0.1','0.2','0.3','0.4','0.5','0.6','0.7','0.8','0.9','1'})
caxis([-30 30])
grid

figure;
%Plotting the power spectral density estimation
%Freq. resolution 2e6/NFFT*1.3 with Hamming window = 200 Hz
pwelch(ScopeData(:,2),13000,6500,13000,2e6);
axis([0 1e6  -80 -20])
set(gca,'FontSize',12)
xlabel('Frequency [Hz]','FontSize',12)
ylabel('Power Spectral Density [dB/Hz]','FontSize',12)

figure;
%Calculating and plotting the autocorrelation function
t=linspace(-.1,.1,2*length(ScopeData)-1);
corrr=xcorr(ScopeData(:,2),'unbiased');
plot(t,corrr)
grid;
axis([-.1 .1 -1 1])
xlabel('Time delay [s]','FontSize',12)
ylabel('Normalized power [W]','FontSize',12)

%Calculating maximum values of spectrum estimate, 10 frequency ranges
pxx=pwelch(ScopeData(:,2),13000,6500,13000,2e6);

N=205;v=1;
dbmax(v)=max(10*log10(pxx(1:N)));
v=v+1;
dbmax(v)=max(10*log10(pxx(N+1:N+205)))
N=N+205;v=v+1;
dbmax(v)=max(10*log10(pxx(N+1:N+205)))
```

APPENDIX A

```
N=N+205;v=v+1;
dbmax(v)=max(10*log10(pxx(N+1:N+205)))
N=N+205;v=v+1;
dbmax(v)=max(10*log10(pxx(N+1:N+205)))
N=N+205;v=v+1;
dbmax(v)=max(10*log10(pxx(N+1:N+205)))
N=N+205;v=v+1;
dbmax(v)=max(10*log10(pxx(N+1:N+205)))
N=N+205;v=v+1;
dbmax(v)=max(10*log10(pxx(N+1:N+205)))
N=N+205;v=v+1;
dbmax(v)=max(10*log10(pxx(N+1:N+205)))
N=N+205;v=v+1;
dbmax(v)=max(10*log10(pxx(N+1:N+204)))
N=N+205;v=v+1;
```

MATLAB -script for generating variable frequency triangle wave for PWM modulator:

```
n=length(find(diff(ScopeData)>1))-1
D=diff(find(diff(ScopeData)>1));
Q=[]
for i=1:n
   Q=[Q linspace(0,1,D(i))];
end
T=linspace(0,.1,length(Q));
```

Simulation models of a boost converter with controller:

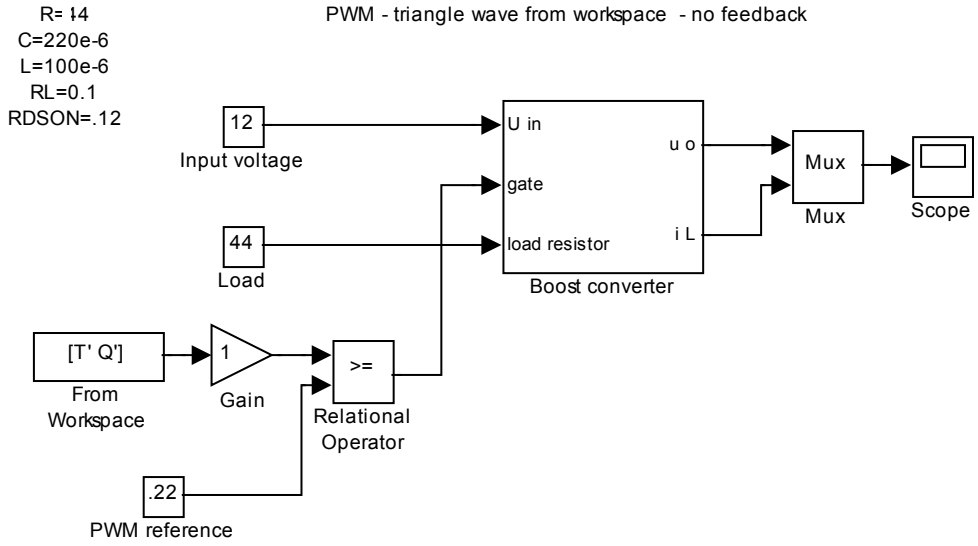

Figure A.3. Simulation model for PWM Boost converter simulation, cases 1 – 4.

APPENDIX A

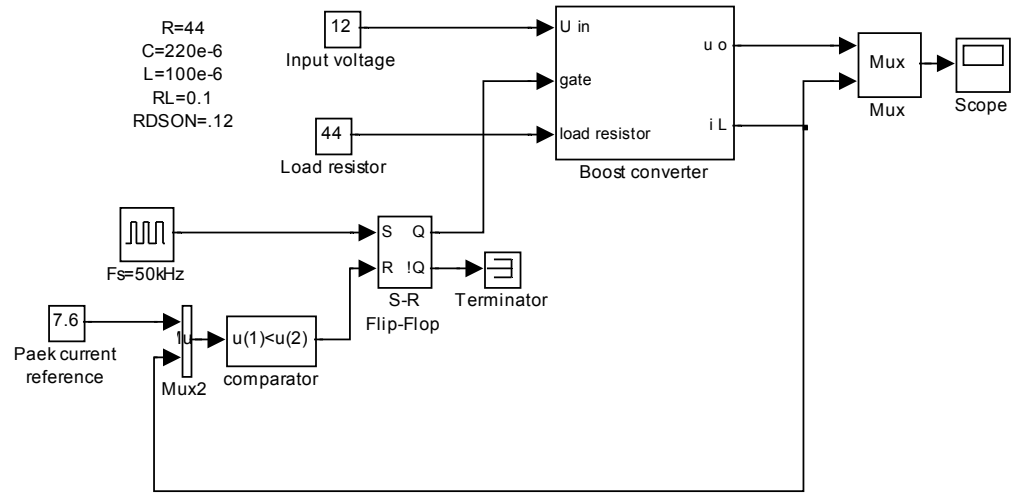

Figure A.4. Simulation model for the Boost converter simulation, case 5 – Chaotic peak current control.

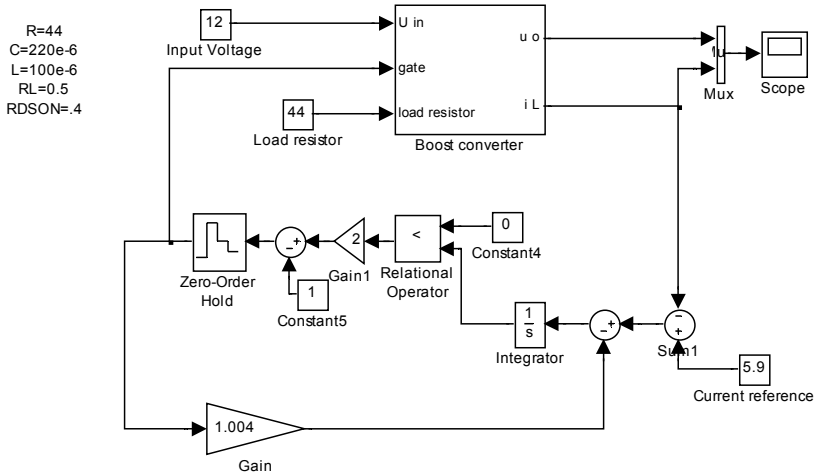

Figure A.5.Simulation model for Boost converter simulation, case 6 – Sigma-Delta

MATLAB-script for analysis of simulated input current and output voltage:

(Here UI is matrix containing simulated output voltage and input current)

```
I1=(UI((length(UI)-160000):length(UI),3));
pwelch(ScopeData(:,2),13000,6500,13000,2e6); %200Hz RBW
axis([0 1e6  -120 -20])
set(gca,'FontSize',12)
xlabel('Frequency [Hz]','FontSize',12)
ylabel('Power Spectral Density [dB/Hz]','FontSize',12)

figure;
specgram(I1,2048,2e6,1024)
set(gca,'FontSize',12)
xlabel('Time [s]','FontSize',12)
Grid;
set(gca,'FontSize',12)
ylabel('Frequency [MHz]','FontSize',12)
set(gca,'YTickLabel',{'0','0.1','0.2','0.3','0.4','0.5','0.6','0.7','0.8','0.9','1'})
caxis([-50 50])
```

APPENDIX A

```
grid

figure
plot((linspace(0,.1,length(UI))),UI(:,2))
axis([0.05 .1 46 50])
Grid;
set(gca,'XTickLabel',{'0','5','10','15','20','25','30','35','40','45','50'})
xlabel('Time [ms]','FontSize',12)
ylabel('Voltage [V]','FontSize',12)
set(gca,'FontSize',12)

figure
plot((linspace(0,.1,length(UI))),UI(:,3))
axis([0.05 .1 0 10])
set(gca,'XTickLabel',{'0','5','10','15','20','25','30','35','40','45','50'})
xlabel('Time [ms]','FontSize',12)
ylabel('Current [A]','FontSize',12)
Grid;
set(gca,'FontSize',12)
figure
plot((linspace(0,.1,length(UI))),UI(:,3))
axis([.05 .0505 0 10])
set(gca,'XTickLabel',{'0','0.1','0.2','0.3','0.4','0.5'})
xlabel('Time [ms]','FontSize',12)
ylabel('Current [A]','FontSize',12)
set(gca,'FontSize',12)
Grid;
```

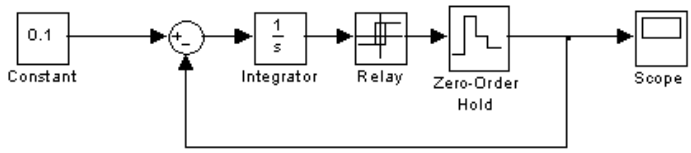

Figure A.6.Simulink™ model for first-order Sigma-Delta modulator presented in Chapter 4.

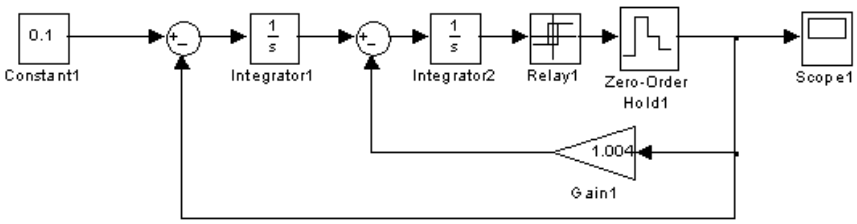

Figure A.7.Simulink™ model for second-order Sigma-Delta modulator presented in Chapter 4.

APPENDIX A

Matlab™ code for example in Chapter 3.

```
pwelch(ScopeData(10000:80000,2),2048,1048,2048,2e6);
axis([0 1e6  -100 -30])
set(gca,'FontSize',12)
xlabel('Frequency [Hz]','FontSize',12)
ylabel('Power Spectral Density [dB/Hz]','FontSize',12)

figure
periodogram(ScopeData(10000:12048,2),[],2048,2e6)
axis([0 1e6  -100 -30])
set(gca,'FontSize',12)
xlabel('Frequency [Hz]','FontSize',12)
ylabel('Power Spectral Density [dB/Hz]','FontSize',12)


figure
pwelch(ScopeData(100000:130000,2),2048,1048,2048,2e6);
axis([0 1e6  -100 -30])
set(gca,'FontSize',12)
xlabel('Frequency [Hz]','FontSize',12)
ylabel('Power Spectral Density [dB/Hz]','FontSize',12)


figure
periodogram(ScopeData(100000:102048,2),[],2048,2e6)
axis([0 1e6  -100 -30])
set(gca,'FontSize',12)
xlabel('Frequency [Hz]','FontSize',12)
ylabel('Power Spectral Density [dB/Hz]','FontSize',12)
```

APPENDIX B

Measurements from the input filter and load resistor

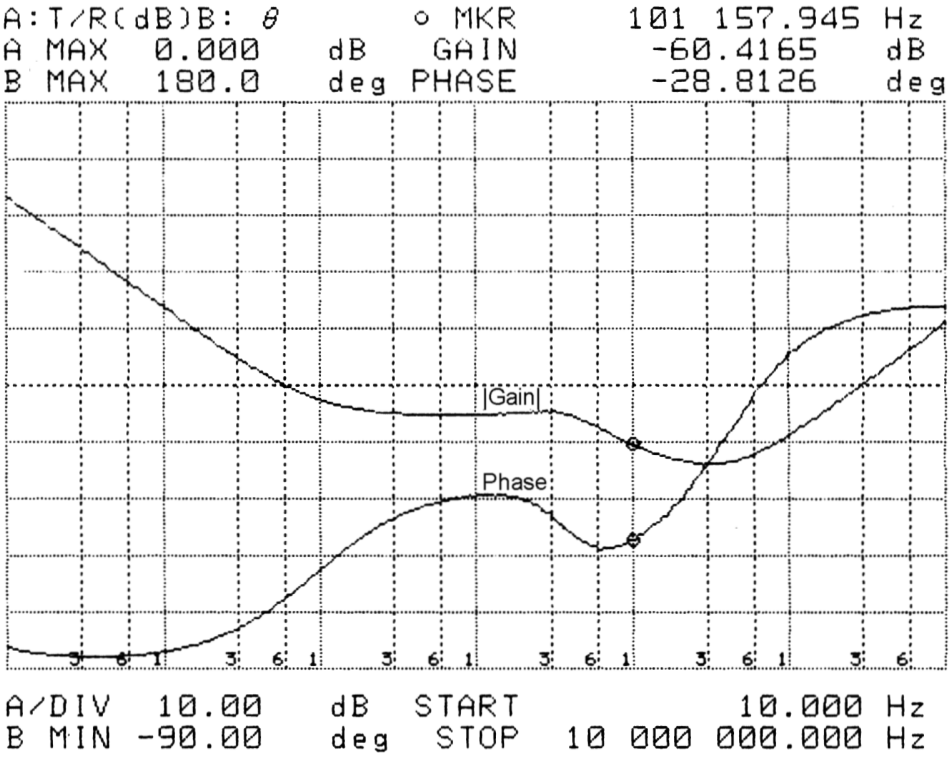

Figure B. 1 Measured Bode-diagram of the input filter. Attenuation is over 50 dB in EMI measurement range from 9 kHz to 1 MHz.

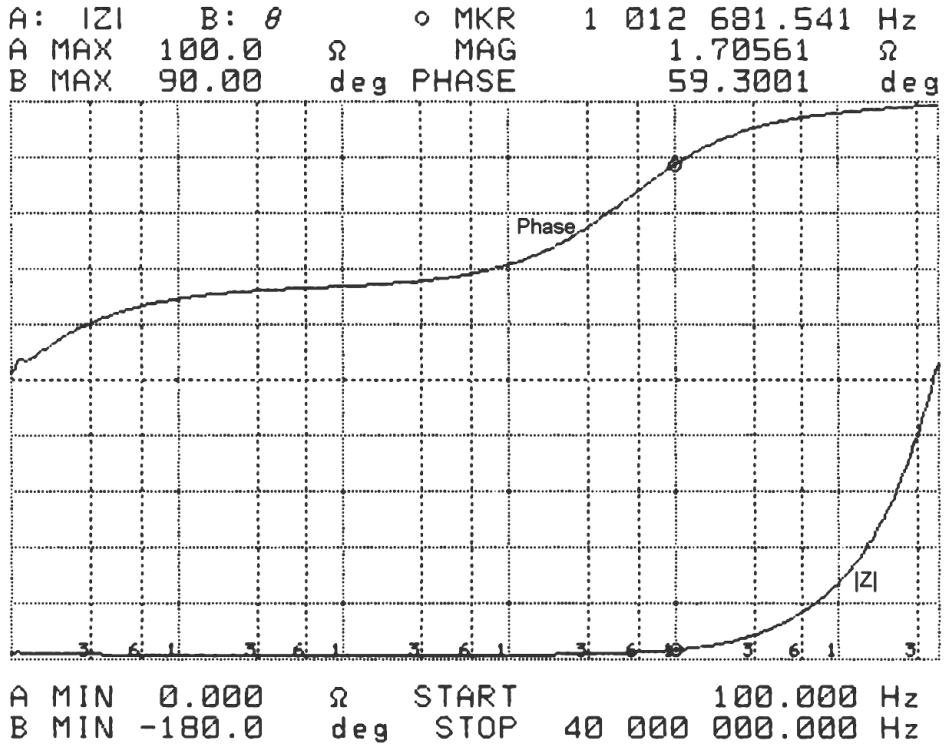

Figure B.2. Impedance of the input filter vs. frequency, measured from the output leads, input leads short. The impedance is low and approximately constant in the entire measurement range from 9 kHz –1 MHz. Parasitic inductance of the circuit and leads increases the impedance above 1 MHz.

APPENDIX B

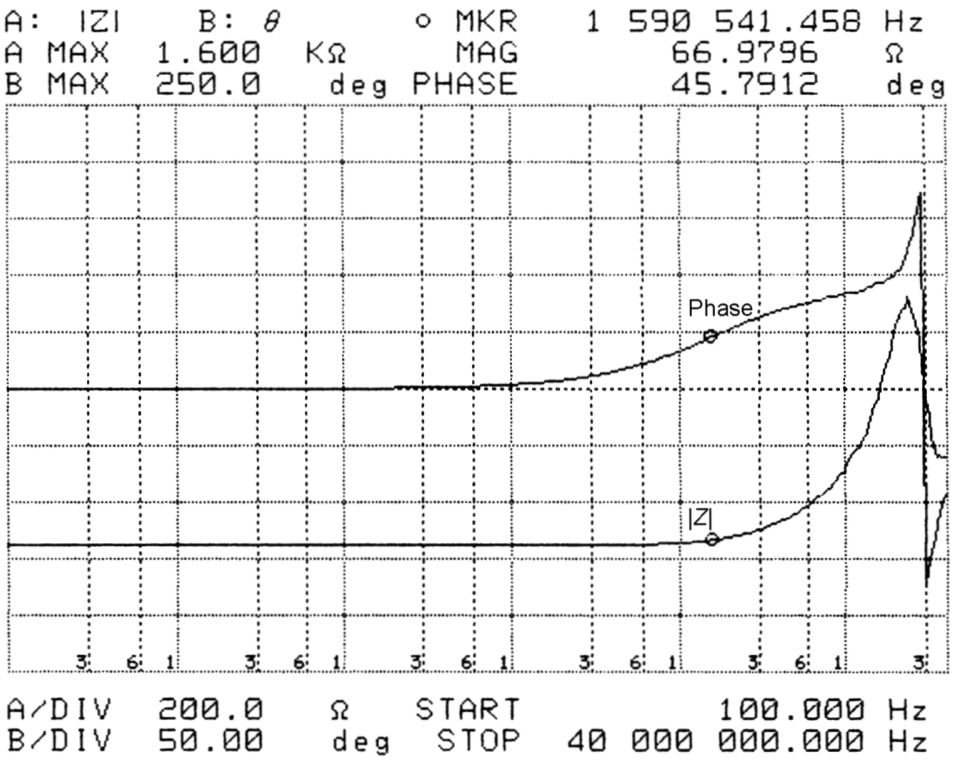

Figure B.3.Load impedance absolute value and phase angle versus frequency, including leads. The absolute value of the load impedance remains approximately constant at the whole test range (9 kHz – 1MHz). Frequency, where the phase shift of the impedance exceeds 45 degrees, is over 1.5 MHz. Horizontal axis: logarithmic frequency from 100 Hz to 40 MHz. Vertical axis: absolute value (200 Ω/div) and phase (50°/div, zero at center) of the impedance.

APPENDIX C

Component list, Shematic diagram and assembly drawing of the prototype

```
************************************************************
*                                                          *
* Component List (Generic)                                 *
*                                                          *
* C:\DRTHESIS\ORCADPROJ\SPREAD\PCB\SPREADBOOST12FINPDF.MAX  *
* Tue May 13 12:38:18 2003                                 *
*                                                          *
************************************************************
```

REF DES	VALUE	PACKAGE	FOOTPRINT
85			MTHOLE3
86			MTHOLE3
87			MTHOLE3
88			MTHOLE3
89			JUMPER300
90			JUMPER400
91			JUMPER500
95			JUMPER400
96			RAD/.300X.125/LS.200/.031
97			JUMPER400
C1	100N	C	RAD/.300X.125/LS.200/.031
C2	220U	C	CPCYL1/D.650/LS.325/.040
C3	470N	C	SM/C_1206
C4	1N	C	SM/C_0603
C5	1N	C	SM/C_0603
C6	2.2U	C	SM/CT_3528_12
C7	2.2U	C	SM/CT_3528_12
C8	2.2U	C	SM/CT_3528_12
C9	47N	C	SM/C_0603
C10	47N	C	SM/C_0603
C11	47N	C	SM/C_0603
C12	47N	C	SM/C_0603
C13	47N	C	SM/C_0603
C14	47N	C	SM/C_0603
C15	100N	C	SM/C_0603
C16	47N	C	SM/C_0603
C17	47N	C	SM/C_0603
C18	2.2U	C	SM/CT_3528_12
C19	2.2U	C	SM/CT_3528_12
C20	2.2U	C	SM/CT_3528_12
C21	2.2U	C	SM/CT_3528_12
C22	47N	C	SM/C_0603
C23	47N	C	SM/C_0603
C24	47N	C	SM/C_0603
C25	47N	C	SM/C_0603
C26	47N	C	SM/C_0603
C27	47N	C	SM/C_0603
C28	100N	C	SM/C_0603
D1	MUR820	MUR820	DO220HEATSINK
D2	D1N4148	D1N4148	SM/DO213AA_21
D3	D1N4148	D1N4148	SM/DO213AA_21
J1	CON2	CON2	BANSKU
J2	BNC	BNC	RF/BNC/R1.350
J3	BNC	BNC	RF/BNC/R1.350
J4	BNC	BNC	RF/BNC/R1.350
J5	BNC	BNC	RF/BNC/R1.350
J6	CON3	CON3	BLKCON.156/RH/TM1SQS/W.585/3
L1	100UH	L	ETD34
M1	IRF530	IRF530	TO220HEATSINK

APPENDIX C

R1	510K	R	SM/R_0603
R2	10K	R	SM/R_0603
R3	10K	R	SM/R_0603
R4	820	R	SM/R_0603
R5	10K	R	SM/R_0603
R6	820	R	SM/R_0603
R7	1K	POT	VRES16
R9	44	R	BANSKU
R10	10K	R	SM/R_0603
R11	100MEG	R	AX/.400X.100/.034
R12	100MEG	R	AX/.400X.100/.034
R13	1	R	SM/R_1206
R14	100MEG	R	AX/.400X.100/.034
R15	1	R	AX/.400X.100/.034
R16	100MEG	R	SM/R_1206
R17	100MEG	R	AX/.400X.100/.034
R18	10K	R	SM/R_0603
R19	10	R	AX/.400X.100/.034
R20	1K	R	AX/.400X.100/.034
R21	1	R	AX/.400X.100/.034
R22	100MEG	R	SM/R_1206
R23	.01	R	SM/DO214AB_12
R24	1K	R	SM/R_0603
R25	50K	R	SM/R_0603
R26	50	R	AX/.400X.100/.034
R27	220	R	AX/.400X.100/.034
R28	10K	R	SM/R_0603
R29	1K	R	SM/R_0603
R30	1K	R	SM/R_0603
R31	1K	R	SM/R_0603
R32	10K	R	SM/R_0603
R33	1K	R	SM/R_0603
R34	1K	R	SM/R_0603
R35	10K	R	SM/R_0603
R36	8.2K	R	SM/R_0603
U1	EL2244/EL	EL2244/EL	DIP.100/8/W.300/L.450
U2	74LS279A	74LS279A	DIP.100/16/W.300/L.900
U3	LM311/SO	LM311/SO	SOG.050/8/WG.244/L.175
U4	LM311/SO	LM311/SO	SOG.050/8/WG.244/L.175
U5	74LS14	74LS14	DIP.100/14/W.300/L.800
U6	INA118/BB	INA118/BB	DIP.100/8/W.300/L.450
U7	74LS74A	74LS74A	SOG.050/14/WG.244/L.325
U8	LM78L05ACZ	LM7805C_2	TO92/100

APPENDIX C

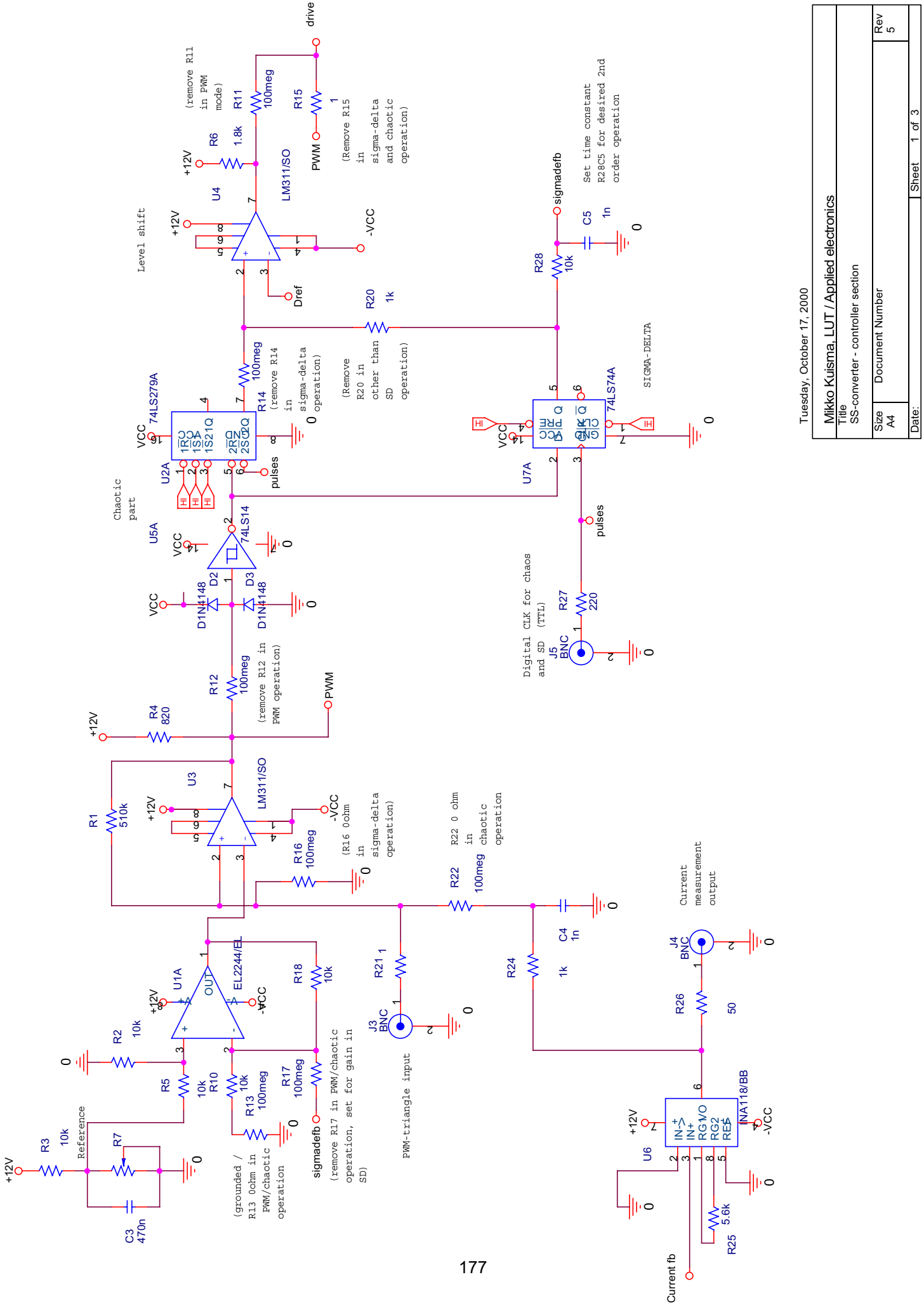
Tuesday, October 17, 2000
Mikko Kuisma, LUT / Applied electronics
Title
SS-converter - controller section
Size A4
Document Number
Rev 5
Date:
Sheet 1 of 3
drive
PWM
(remove R11 in PWM mode)
(Remove R15 in sigma-delta and chaotic operation)
LM311/SO
Level shift
Dref
-VCC
+12V
R6 1.8k
R11 100meg
R15 1
R20 1k
(Remove R20 in other than SD operation)
R14 100meg
(remove R14 in sigma-delta operation)
74LS279A
U2A
pulses
Chaotic part
74LS14
U5A
D1N4148
D2
D3
R12 100meg
(remove R12 in PWM operation)
R4 820
R1 510k
U3
R16 100meg
(R16 0ohm in sigma-delta operation)
R22 100meg
R22 0 ohm in chaotic operation
EL2244/EL
U1A
R18 10k
R21 1
R24 1k
C4 1n
J3 BNC
PWM-triangle input
R2 10k
R5 10k
R10 10k
R13 10k
R17 100meg
(grounded / R13 0ohm in PWM/chaotic operation
sigmadefb
(remove R17 in PWM/chaotic operation, set for gain in SD)
R3 10k
Reference
R7
C3 470n
sigmadefb
Set time constant R28C5 for desired 2nd order operation
R28 10k
C5 1n
74LS74A
U7A
SIGMA-DELTA
Digital CLK for chaos and SD (TTL)
R27 220
J5 BNC
Current measurement output
J4 BNC
R26 50
INA118/BB
U6
R25 5.6k
Current fb

APPENDIX C

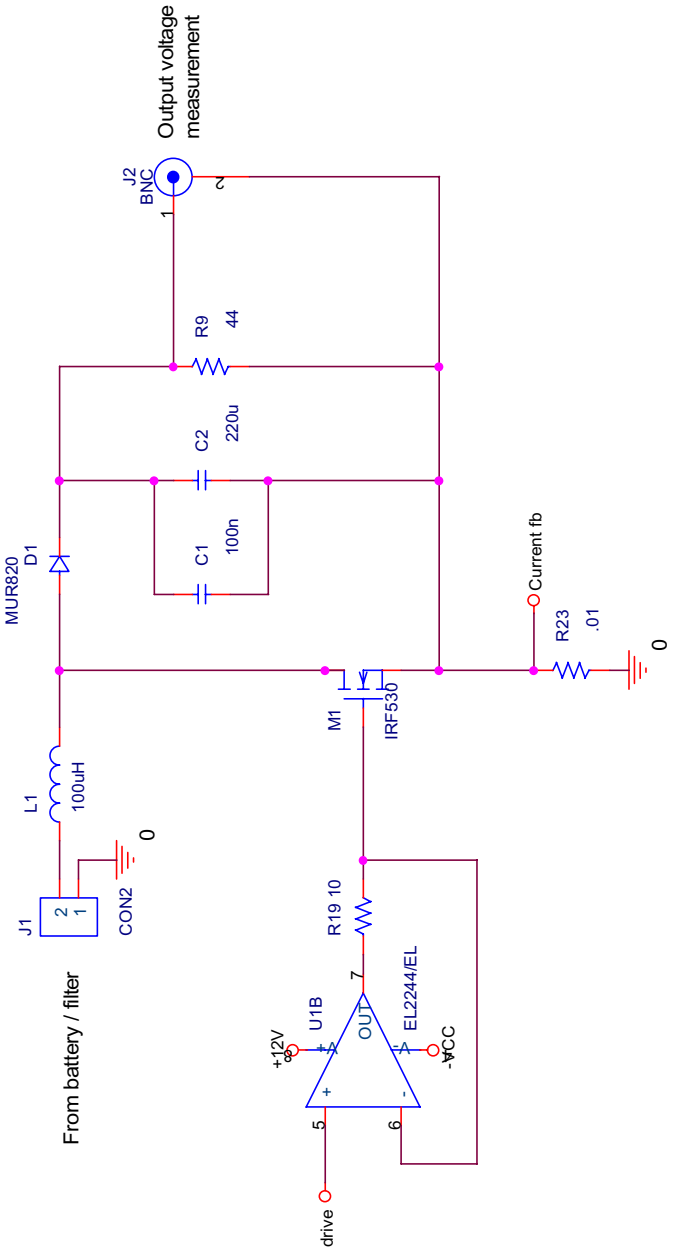

Tuesday, October 17, 2000

Mikko Kuisma, LUT / Applied electronics		
Title: SS-converter - Main power stage		
Size: A4	Document Number	Rev: 5
Date:	Sheet 2 of 3	

APPENDIX C

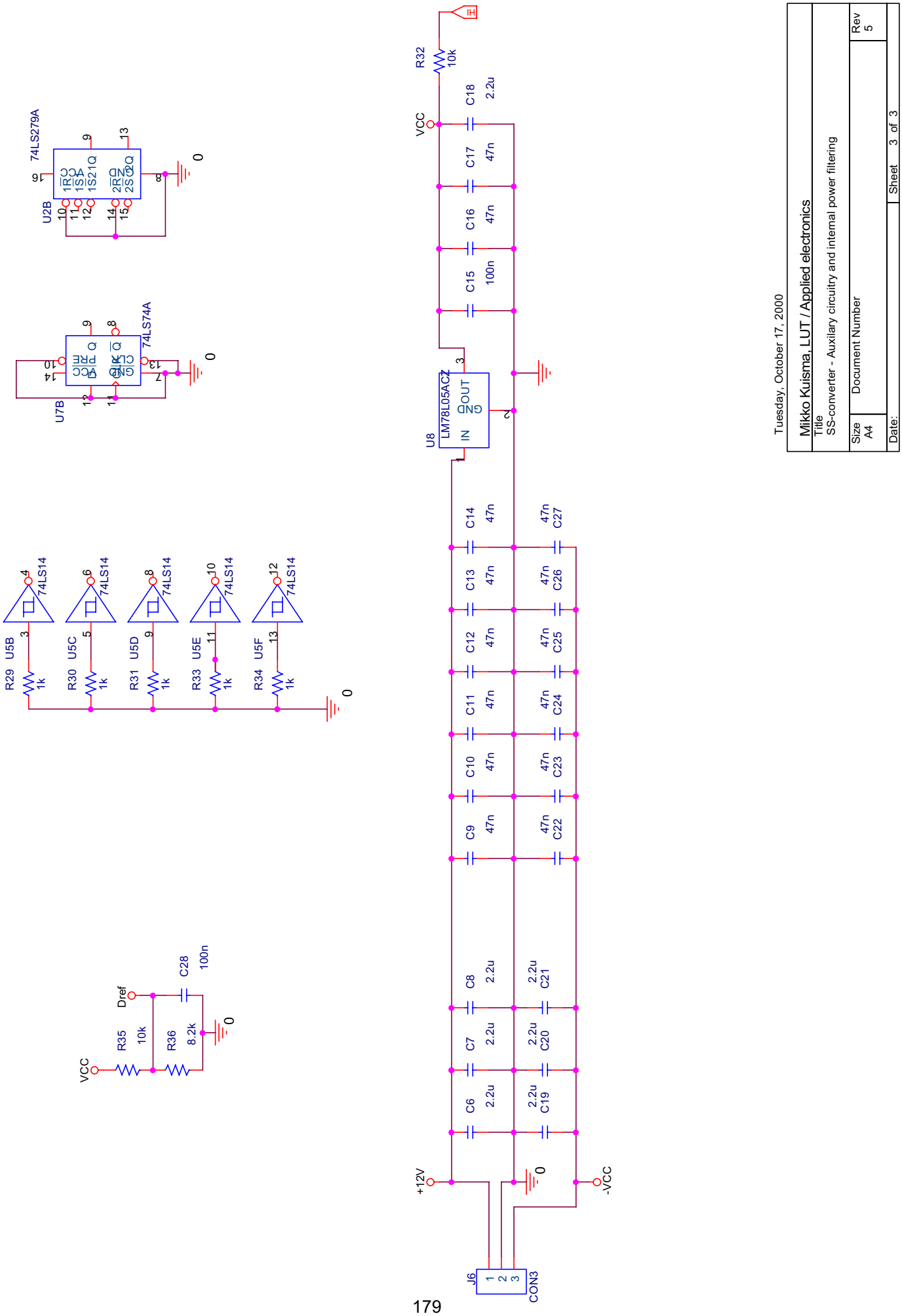

Tuesday, October 17, 2000

Mikko Kuisma, LUT / Applied electronics		
Title: SS-converter - Auxilary circuitry and internal power filtering		
Size: A4	Document Number	Rev: 5
Date:	Sheet 3 of 3	

APPENDIX C

PCB layout, top layer

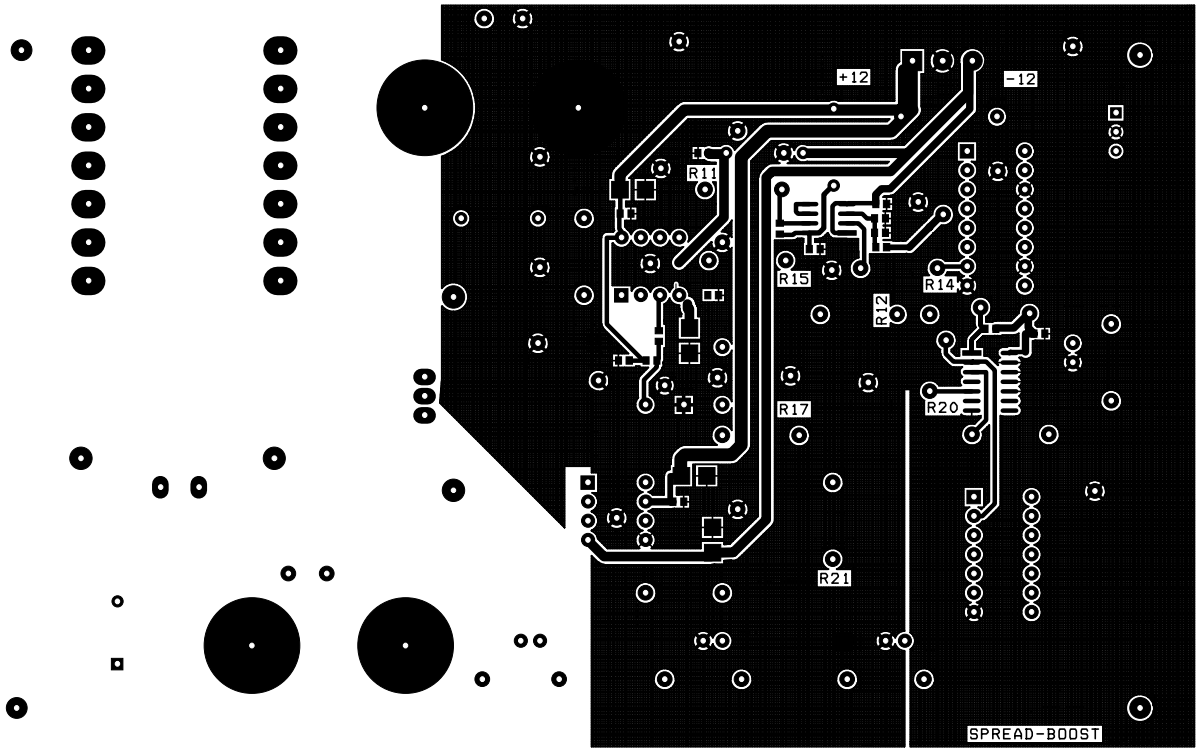

PCB layout, bottom layer

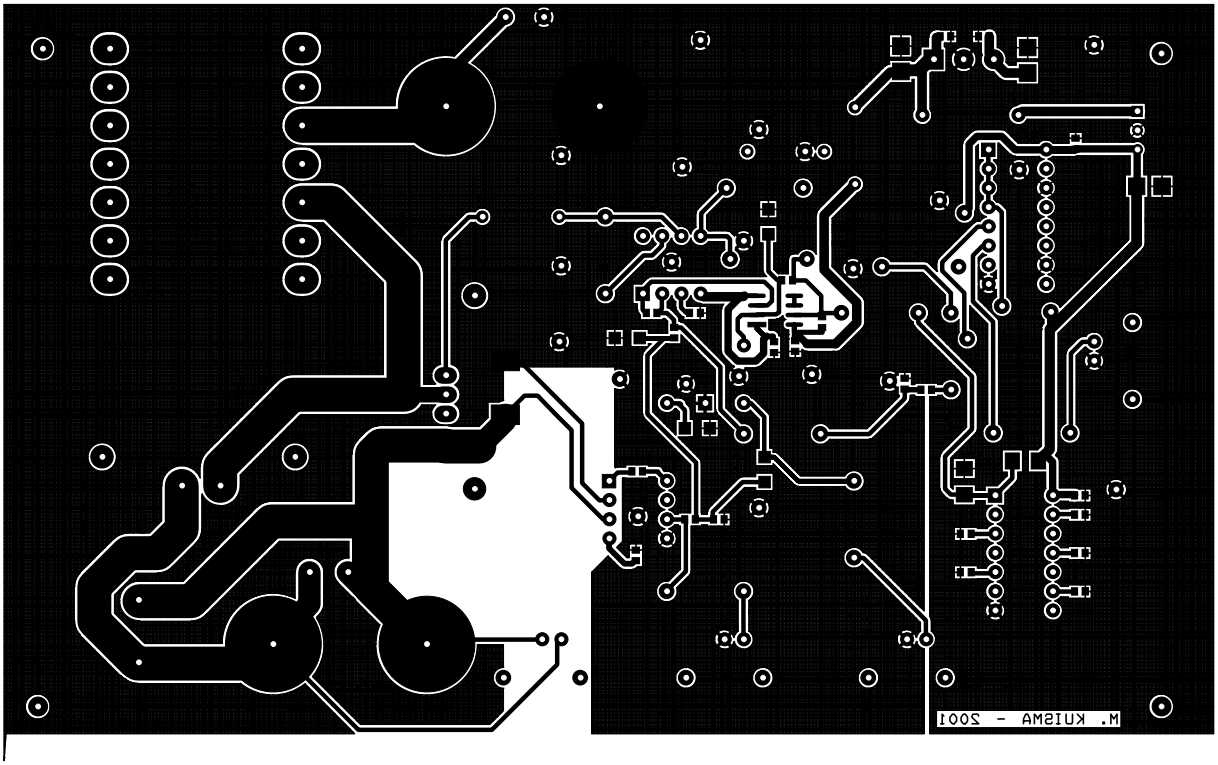

APPENDIX C

Assembly drawing, top layer

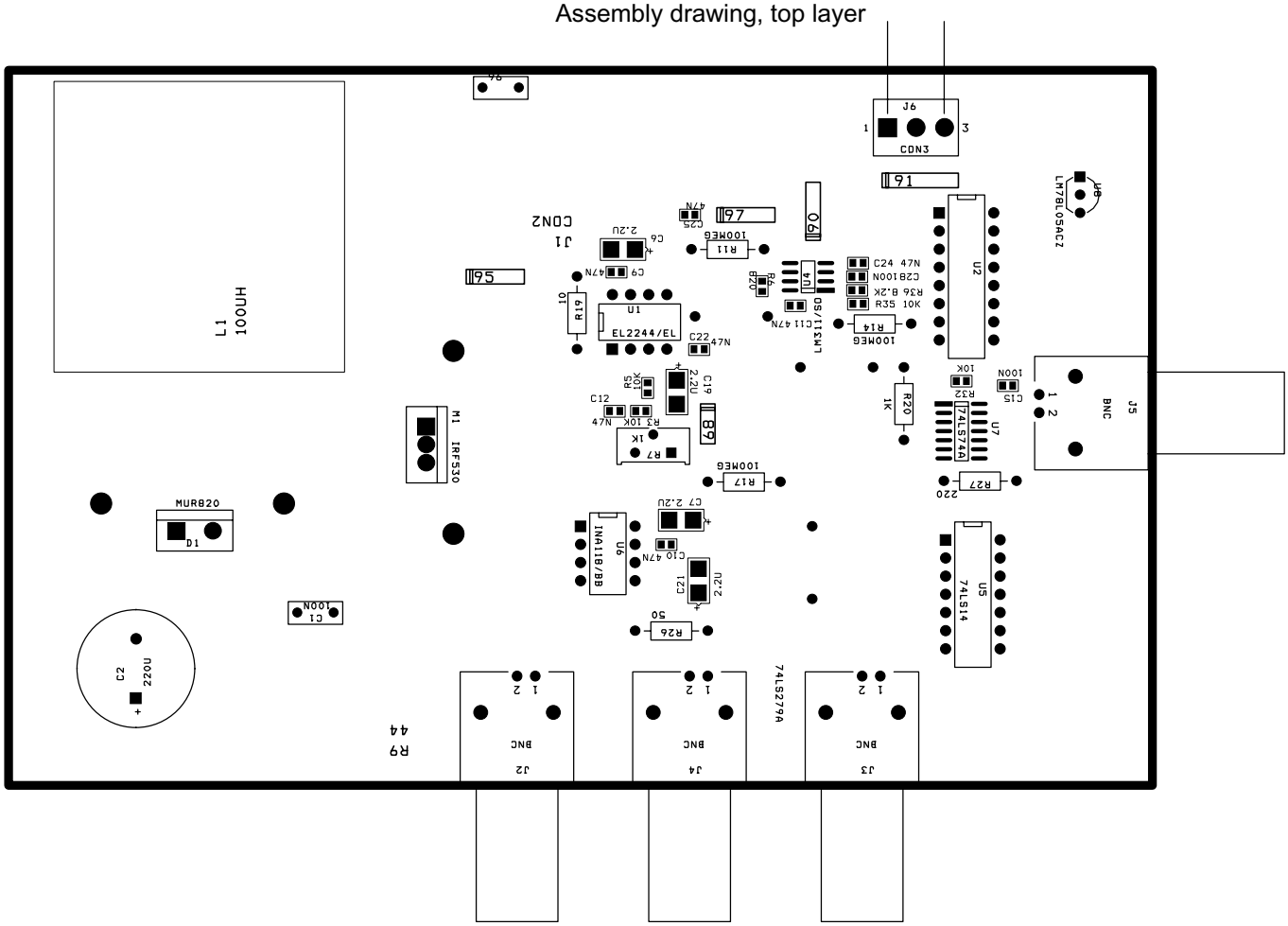

Assembly drawing, bottom layer

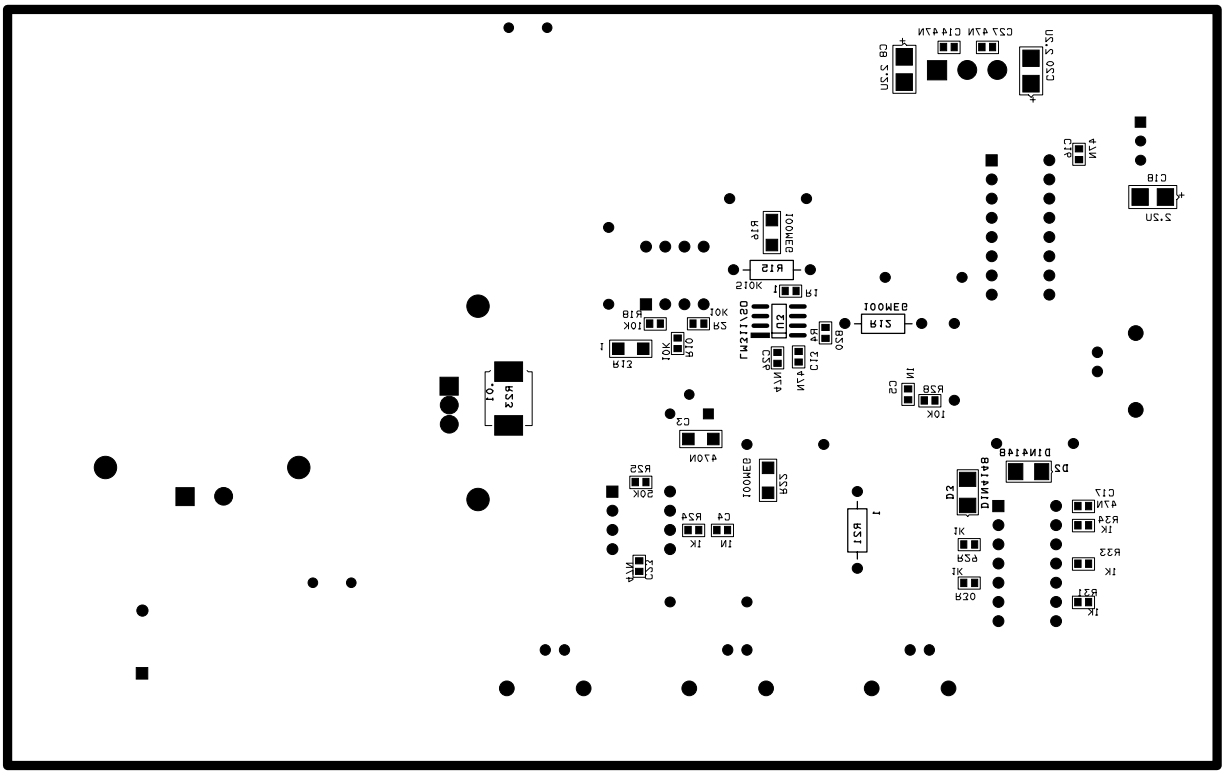

APPENDIX D

Background noise measured from the test setup, all instruments and power on, converter switching disabled.

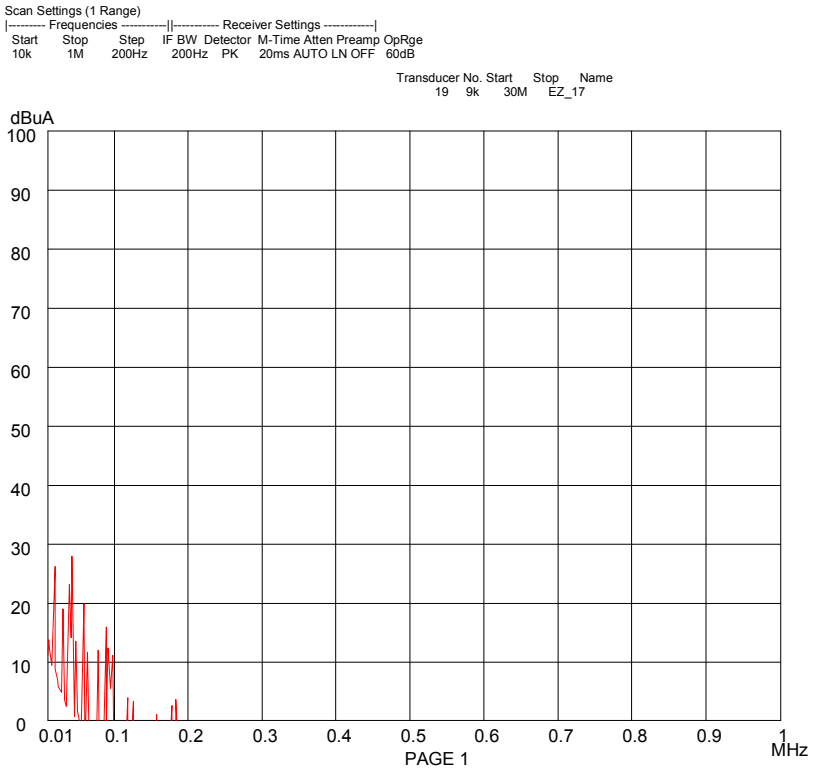

Figure D.1 Measured background noise 9 kHz – 1 MHz. IFBW 200 Hz, measuring time 20 ms/IFBW.

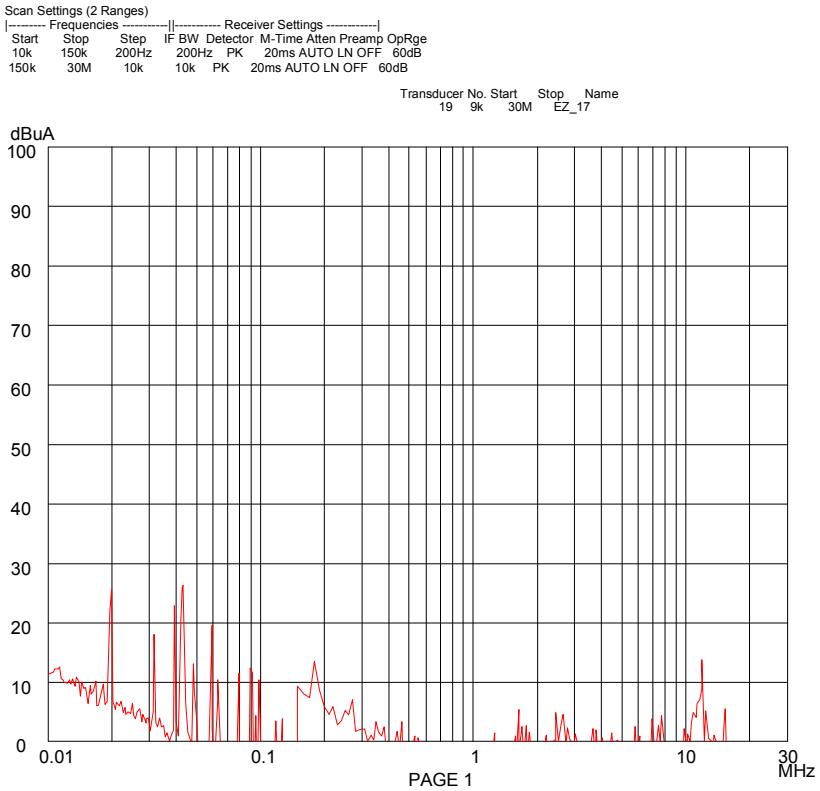

Figure D.2 Measured background noise 9 kHz – 30 MHz. IFBW 200 Hz from 9 kHz to 150 kHz, IFBW 10 kHz from 150 kHz to 30 MHz, measuring time 20 ms/IFBW.

APPENDIX E

Measured EMI Current Spectrum from 9 kHz to 30 MHz

Measured EMI-spectrum in different SS-cases in frequency range from 9kHz to 30 MHz. IF bandwidth of the receiver is 200 Hz below 150 kHz and 10 kHz from 150 kHz to 30 MHz. Frequency axis is in logarithmic scale, peak detector mode.

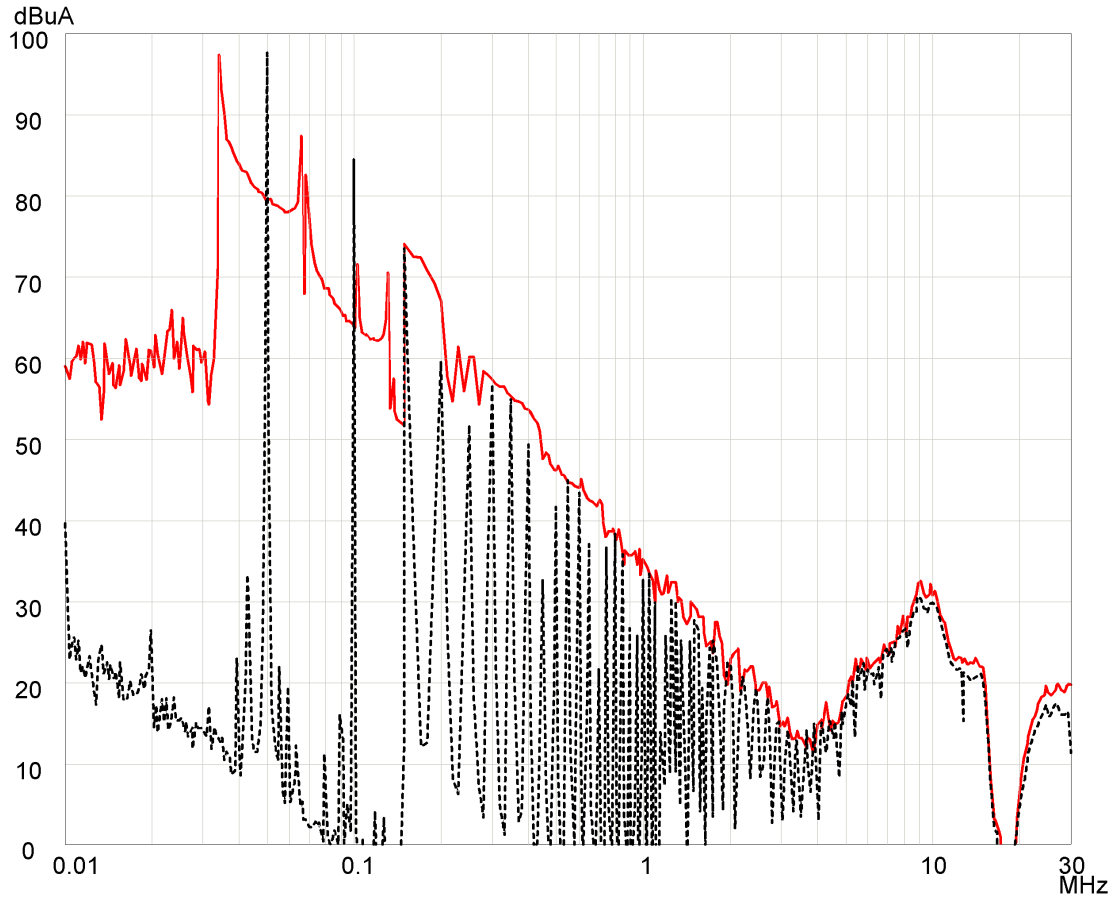

Figure E.1. Measured input current spectrum from 9 kHz to 30 MHz, peak detector. Case 1: solid, PWM-reference: dotted. Below 150 kHz some reduction can be achieved, but over 150 kHz curve is descending almost at same level as PWM-reference. IF bandwidth of the receiver is 200 Hz below 150 kHz and from 150 kHz to 30 MHz IFBW is 10 kHz.

APPENDIX E

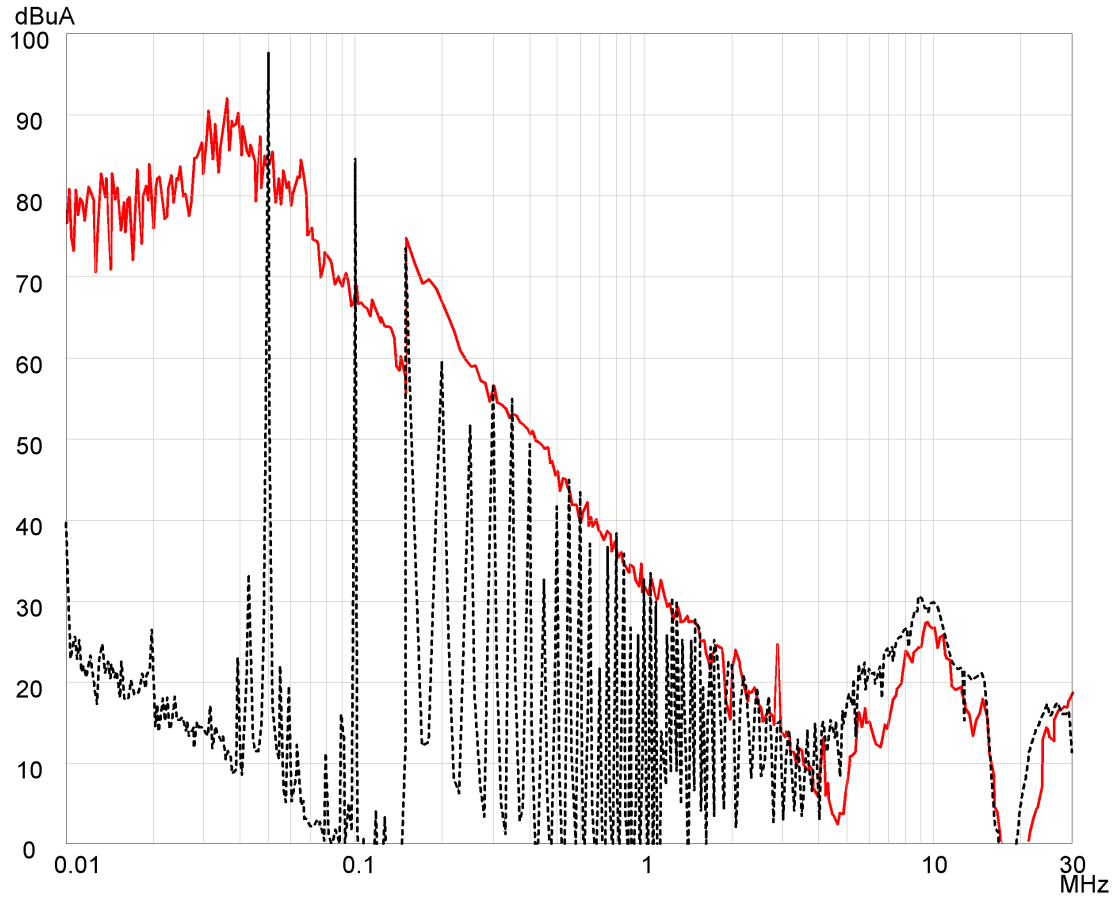

Figure E.2. Measured input current spectrum from 9 kHz to 30 MHz, peak detector. Case 2: solid, PWM-reference: dotted. Below 150 kHz spectral curve of the modulated converter is lowered and clear spikes have been vanished, but over 150 kHz curve is descending at same level as PWM-reference.

APPENDIX E

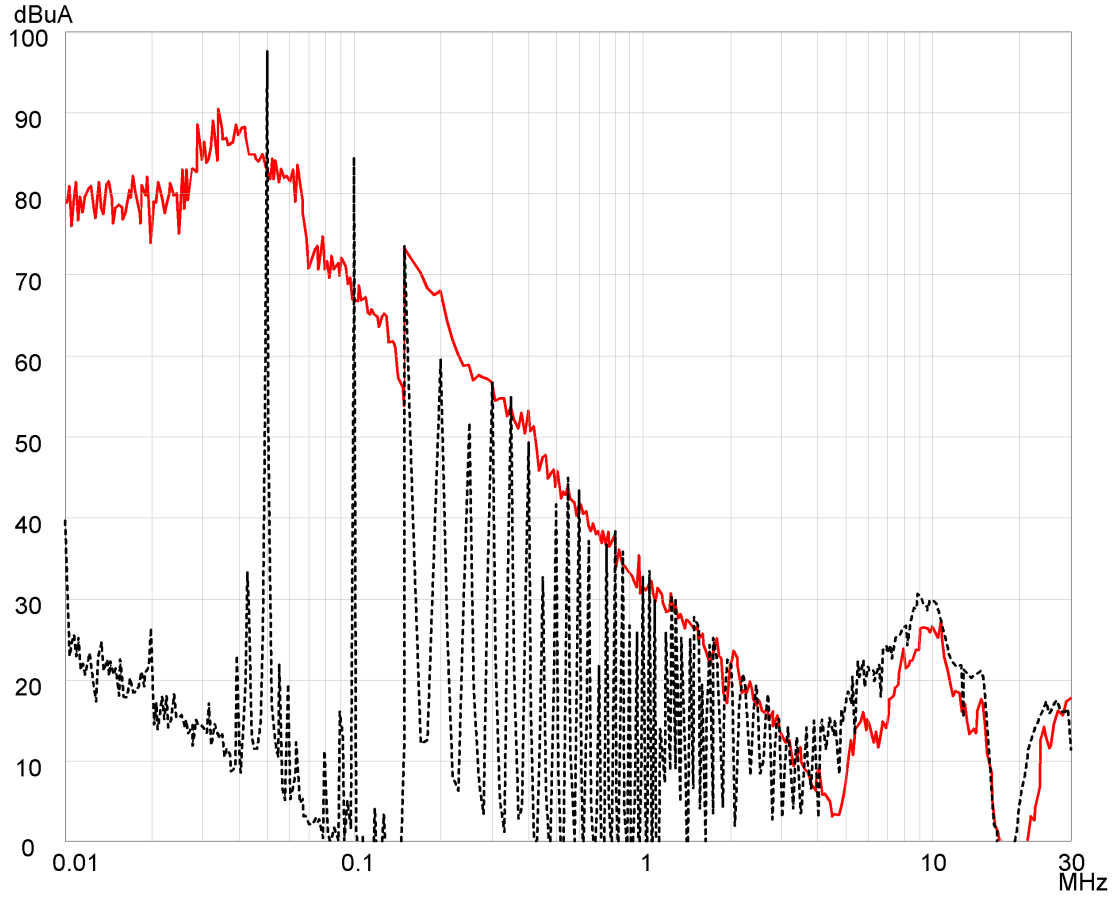

Figure E.3. Measured input current spectrum from 9 kHz to 30 MHz, peak detector. Case 3: solid, PWM-reference: dotted. Spectral curve is smoother compared to other frequency modulated converters and there are no single tone spikes in the spectrum. Again, over 150 kHz curve is descending almost at same level as PWM-reference.

APPENDIX E

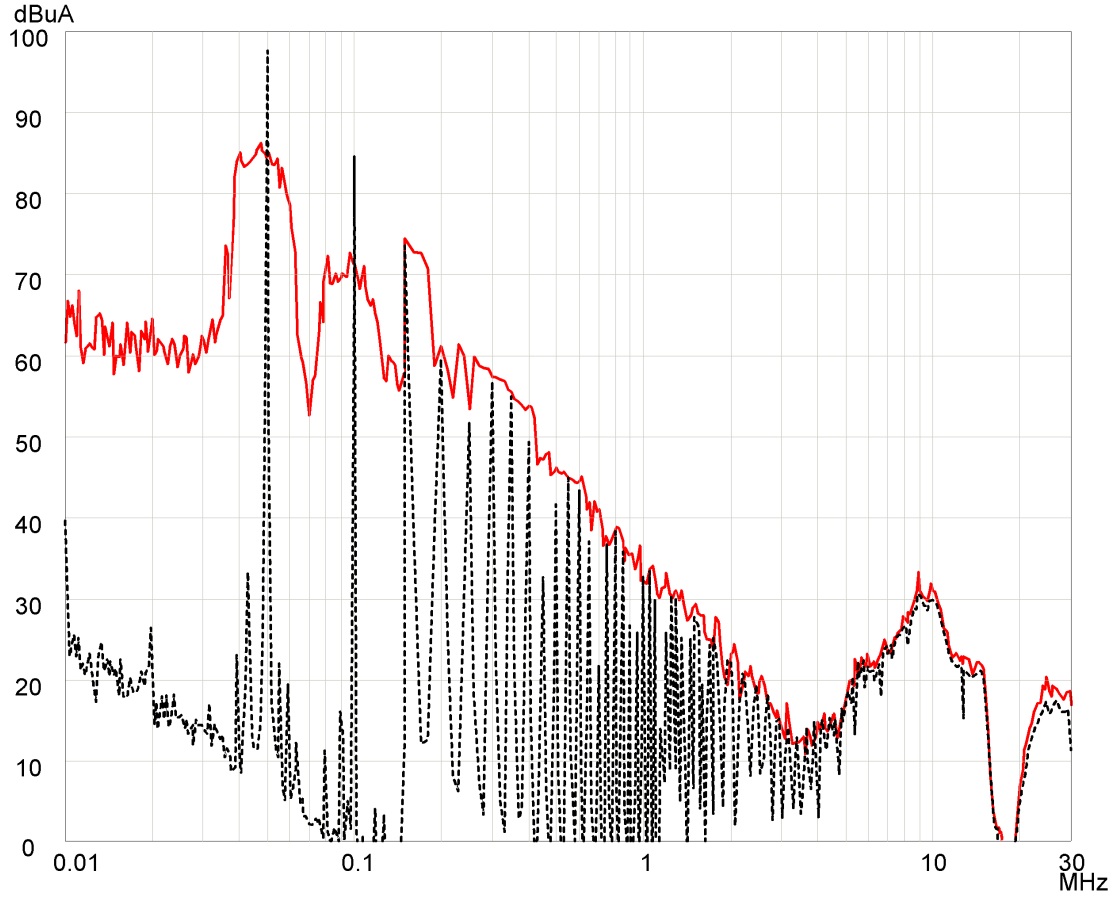

Figure E.1. Measured input current spectrum from 9 kHz to 30 MHz, peak detector. Case 4: solid, PWM-reference: dotted. Spectral curve has jumps around the nominal switching frequency and harmonics although there are no single tone spikes in the spectrum. Again, over 150 kHz curve is descending almost at same level as PWM-reference.

APPENDIX E

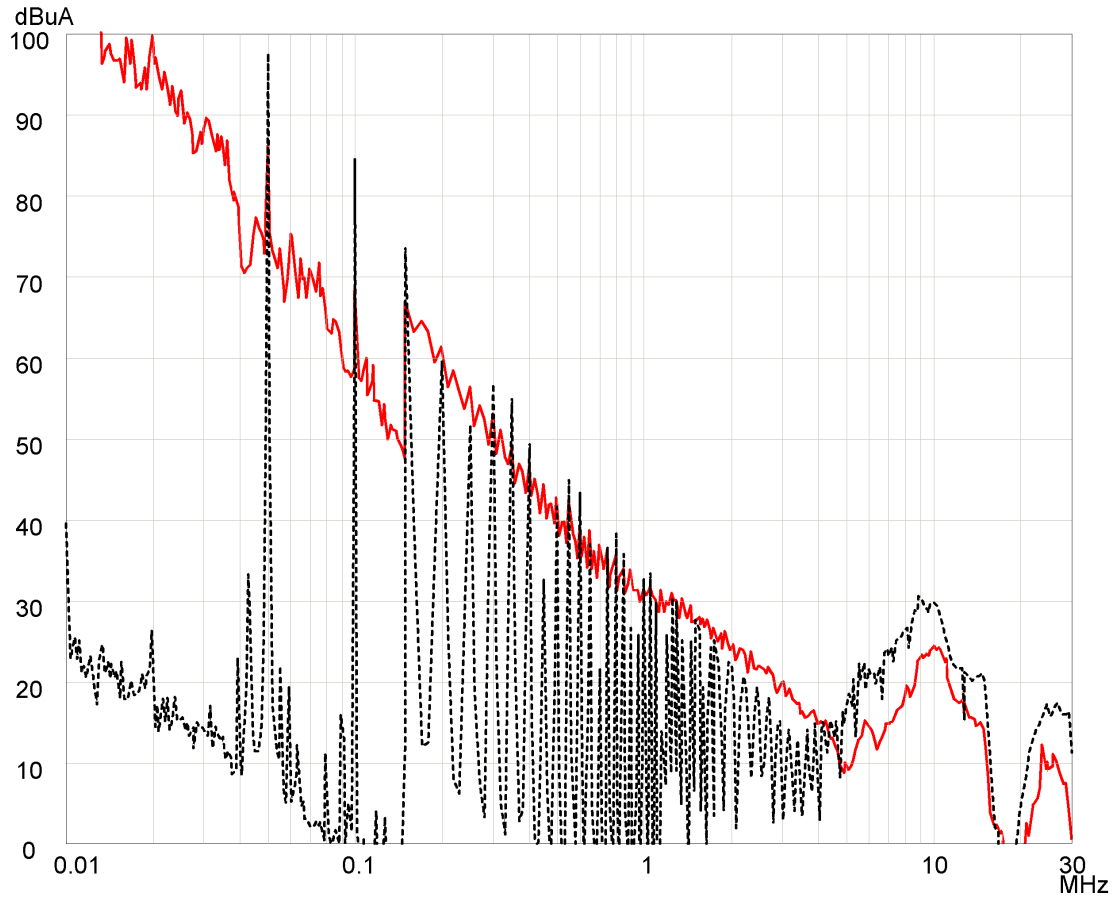

Figure E.5. Measured input current spectrum from 9 kHz to 30 MHz, peak detector. Case 5: solid, PWM-reference: dotted. Large portion of the signal power is concentrated at low frequency range. This has also effect on the high frequency range, where some reduction can be noted even with peak detector mode.

APPENDIX E

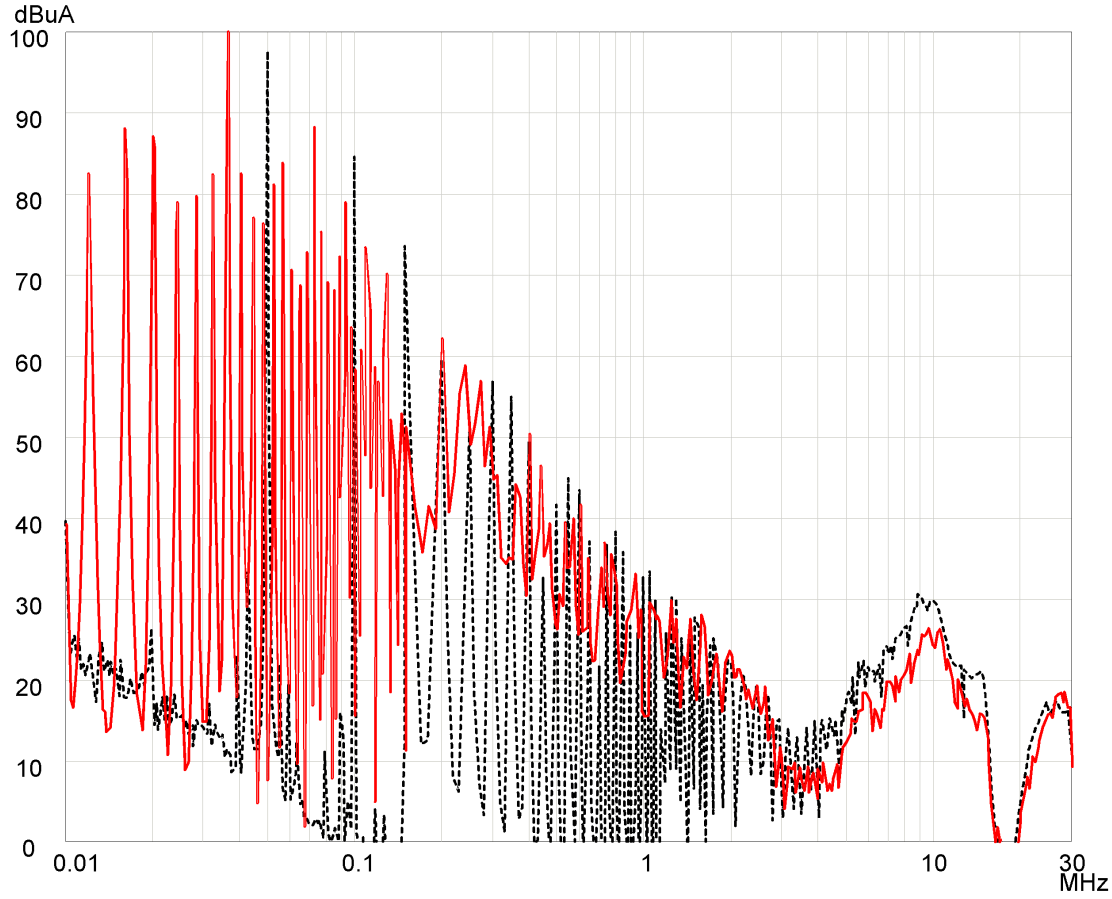

Figure E.6. Measured input current spectrum from 9 kHz to 30 MHz, peak detector. Case 6: solid, PWM-reference: dotted. Spectral curve has many "sinusoidal-like" spikes, and there is no noticeable reduction to the emission level with this particular sigma-delta configuration.

APPENDIX F

Measurement uncertainty

Measurement uncertainties in RF-measurements, such as in EMI-measurements, are usually quite large. However, uncertainty with current clamp measurement is much easier to control than in case of radiated emission measurement. There are several guides concerning about evaluating uncertainties in EMC-measurement, including [Taylor 1994], [Bronaugh 1996], [Stecher 1997], [Stecher 2001], [Krattenmacher 1999]. Minimum EMC test setup comprises a transducer, a signal cable, a test receiver or a spectrum analyzer and an operator. Uncertainty caused by apparatus involved in the test setup is easy to evaluate and track compared to the human factor. For example, manual reading made for table comparison added a great deal of systematic error.

The measurement uncertainty is often classified in two different categories, [Taylor 1994]

A. Those which are evaluated by statistical methods, and
B. Those which are evaluated by other means.

Type A uncertainty is not applicable here, because statistical values cannot be calculated from limited test result. Type B uncertainty evaluation is based on specifications from the instrument manufacturers and on estimations made based on common guidelines and experience. Combined standard uncertainty u_{tot} is then calculated as a root-sum-square of individual (independent) uncertainty components u_n:

$$u_{\text{tot}} = \sqrt{u_1^{\,2} + u_2^{\,2} + u_3^{\,2} + \ldots + u_n^{\,2}} \qquad \text{(F.1)}$$

Above equation is valid if individual uncertainty is expressed as a standard uncertainty for normal distribution. For a rectangular distribution, the “accuracy” is divided by square-root of three to get standard uncertainty *u(y)*, before calculating combined uncertainty, [Taylor 1994] :

$$u(y) = \frac{e}{\sqrt{3}}, \qquad \text{(F.2)}$$

where *e* is error, expressed for example as $\pm$ *x* % or $\pm$ *x*.

If the uncertainty components are taken in dB instead of linear values, dB values must be converted to linear scale before calculating combined uncertainty. It would be against mathematical principles to deal with squares of quantities in dB, [Stecher 2001]. Although Stecher [Stecher 2001] mention this logarithmic notation, example calculations made in his paper are calculated as a sum of square logarithms.

Estimated main factors affecting on the uncertainty of the test setup is collected in Repeatability of the EMI-receiver (R&S ESHS-30) was examined with a signal generator (HP ESG-2000A) and a spectrum analyzer (Agilent E7402A). The signal generator output was sinusoidal wave at 500 kHz and the amplitude was 40 dBmV. The output was monitored with the spectrum

analyzer. Measurement was made 17 times with the EMI-receiver and the test lasted nine days. The receiver turned off and on arbitrarily during the test. Before the measurement, the receiver was turned on at least half an hour before. The receiver was manually tuned to record the maximum value. According to this test, calculated standard deviation of the EMI-receiver repeatability is 0.06 dB.

The most important factor in this work is the repeatability of the EMI-receiver. The nature of the test system is comparative, and therefore if the repeatability sets the practical uncertainty limit for this setup. Other uncertainties that were taken into consideration in this setup are the estimated system repeatability and reading accuracy. Overall system repeatability including cable joints, current probe positioning etc. was not included in the repeatability test. Reading accuracy of the test results were also estimated. This human factor ads the largest part of uncertainty to the test setup.
Table F-. Repeatability of the EMI-receiver (R&S ESHS-30) was examined with a signal generator (HP ESG-2000A) and a spectrum analyzer (Agilent E7402A). The signal generator output was sinusoidal wave at 500 kHz and the amplitude was 40 dBmV. The output was monitored with the spectrum analyzer. Measurement was made 17 times with the EMI-receiver and the test lasted nine days. The receiver turned off and on arbitrarily during the test. Before the measurement, the receiver was turned on at least half an hour before. The receiver was manually tuned to record the maximum value. According to this test, calculated standard deviation of the EMI-receiver repeatability is 0.06 dB.

The most important factor in this work is the repeatability of the EMI-receiver. The nature of the test system is comparative, and therefore if the repeatability sets the practical uncertainty limit for this setup. Other uncertainties that were taken into consideration in this setup are the estimated system repeatability and reading accuracy. Overall system repeatability including cable joints, current probe positioning etc. was not included in the repeatability test. Reading accuracy of the test results were also estimated. This human factor ads the largest part of uncertainty to the test setup.

Table F-1. Uncertainty budged for amplitude measurement.

Factor	Distribution	Value	Uncertainty in linear scale
Receiver repeatability	Normal	0.06 dB	1.006
Reading accuracy (operator)	Rectangular	2 dB	1.259
System repeatability	Rectangular	0.3 dB	1.035
Combined standard uncertainty		2.8 dB	1.378
Expanded measurement uncertainty, k = 2		8.8 dB	2.756

Uncertainty values expressed in dB are first converted to linear scale in Table F-1. Combined standard uncertainty is the calculated from Equation (F.3):

APPENDIX F

$$
\begin{aligned}
u_{\text{tot}} &= \sqrt{1.006^2 + \frac{1.259^2}{3} + \frac{1.035^2}{3}} \\
&= 1.378 \qquad \text{(F.3)} \\
u_{\text{tot,dB}} &= 20 \log 1.378 \\
&= 2.8 \text{ dB}
\end{aligned}
$$

Combined standard uncertainty $u_{\text{tot,dB}}$ (2.8 dB) and expanded uncertainty U (8.8 dB), k = 2, is calculated from the values presented in Table F-1.

ACTA UNIVERSITATIS LAPPEENRANTAENSIS

132. TORKKELI, MARKO, Technology selection and group decision support systems: Case studies on supporting strategic technology selection processes. 2002. U.s. Diss.

133. KYRKI, VILLE. Local and global feature extraction for invariant object recognition. 2002. 115 s. Diss.

134. HEIKKILÄ, TANJA. Permanent magnet synchronous motor for industrial inverter applications-analysis and design. 2002. 109 s. Diss.

135. HUTTUNEN, PENTTI. Data-parallel computation in parallel and distributed environments. 2002. U.s. Diss.

136. LIU, YONG. On sliding mode control of hydraulic servo systems and a manipulator. 2002. U.s. Diss.

137. JUHANTILA, OLLI-PEKKA. Establishing intercompany relationships: Motives and methods for successful collaborative engagement. 2002. 281 s. Diss.

138. PREIS, SERGEI. Practical applications of a systematic approach to the chemical abatement of pollutants in water and air. 2002. 234 s. Diss.

139. TIIHONEN, JARI. Influence of stationary phase and eluent properties on chromatographic separation of carbohydrates. 2002. U.s. Diss.

140. KILKKI, JUHA. Automated formulation of optimisation models for steel beam structures. 2002. 85 s., liitt. Diss.

141. LENSU, LASSE. Photoelectric properties of bacteriorhodopsin films for photosensing and information processing. 2002. 114 s. Diss.

142. KAURANNE, TUOMO. Introducing parallel computers into operational weather forecasting. 2002. U.s. Diss.

143. PUUMALAINEN, KAISU. Global diffusion of innovations in telecommunications: Effects of data aggregation and market environment. 2002. 153 s. Diss.

144. SARRETTE, CHRISTINE. Effect of noncondensable gases on circulation of primary coolant in nuclear power plants in abnormal situations. 2003. 114 s. Diss.

145. SAARENKETO, SAMI. Born globals – internationalization of small and medium-sized knowledge-intensive firms. 2002. 247 s. Diss.

146. IKONEN, KIRSI. Metal surface and subsurface inspection using nondestructive optical methods. 2002. U.s. Diss.

147. OLLIKAINEN, Mikael. Origins of production errors and significance of employee empowerment in reducing production error amount in sheet metal fabricating industry. 2003. 153 s. Diss.

148. KOUVO, PETRI. Formation and control of trace metal emissions in co-firing of biomass, peat and wastes in fluidised bed combustors. 2003. U.s. Diss.

149. MOOSAVI, ALI. Transport properties of multi-phase composite materials. 2003. U.s. Diss.

150. SMOLANDER, KARI. On the role of architecture in systems development. 2003. U.s. Diss.

151. VERENICH, SVETLANA. Wet oxidation of concentrated wastewaters: process combination and reaction kinetic modeling. 2003. U.s. Diss.

152. STÅHLE, PIRJO, STÅHLE, STEN & PÖYHÖNEN, AINO. Analyzing dynamic intellectual capital: System-based theory and application. 2003. 191 s.

153. HAATAJA, JORMA. A comparative performance study of four-pole induction motors and synchronous reluctance motors in variable speed drives. 2003. 135 s. Diss.

154. KURRONEN, PANU. Torque vibration model of axial-flux surface-mounted permanent magnet synchronous machine. 2003. 123 s. Diss.

156. KUIVALAINEN, OLLI. Knowledge-based view of internationalisation – studies on small and medium-sized information and communication technology firms. 2003. U.s. Diss.

157. AHOLA, JERO. Applicability of power-line communications to data transfer of on-line condition monitoring of electrical drives. 2003. 141 s. Diss.

158. 1st Workshop on Applications of Wireless Communications. Edited by Jari Porras, Jouni Ikonen and Pekka Jäppinen. 2003. 67 s.

159. TUUTTI, VEIKKO. Ikkunoiden lasirakenteet ja niiden valintaan vaikuttavat tekijät. 2003. 294 s. Diss.

160. METSÄMUURONEN, SARI. Critical flux and fouling in ultrafiltration of proteins. 2003. U.s. Diss.

161. TUIMALA, JARNO. Aiding the strategic purchasing benchmarking process by decision support systems. 2003. U.s. Diss.

162. SORSA, TIA. The interaction of the calcium sensitiser levosimendan with cardiac troponin C. 2003. U.s. Diss.

163. KOVANEN, JANNE. Improving dynamic characteristics of open-loop controlled log crane. 2003. 97 s. Diss.

164. KURTTILA, HEIKKI. Isentropic exergy and pressure of the shock wave caused by the explosion of a pressure vessel. 2003. 114 s., liitt. Diss.

165. KÄMÄRÄINEN, JONI-KRISTIAN. Feature extraction using Gabor filters. 2003. U.s. Diss.

167. MIELIKÄINEN, JARNO. Lossless compression of hyperspectral images. 2003. U.s. Diss.

168. LI, XIAOYAN. Effect of mechanical and geometric mismatching on fatigue and damage of welded joints. 2003. U.s. Diss.

169. OJANEN, VILLE. R&D performance analysis: case studies on the challenges and promotion of the evaluation and measurement of R&D. 2003. U.s. Diss.

170. PÖLLÄNEN, RIKU. Converter-flux-based current control of voltage source PWM rectifiers – analysis and implementation. 2003. 165 s. Diss.

171. FRANK, LAURI. Mobile communications within the European Union: the role of location in the evolution and forecasting of the diffusion process. 2003. U.s. Diss.

172. KOISTINEN, PETRI. Development and use of organizational memory in close and long-term cooperation between organizations. 2003. 170 s. Diss.

173. HALLIKAS, JUKKA. Managing risk in supplier networks: case studies in inter-firm collaboration. 2003. U.s. Diss.

174. LINDH, TUOMO. On the condition monitoring of induction machines. 2003. 146 s. Diss.

175. NIKKANEN, MARKKU. Railcarrier in intermodal freight transportation network. 2003. 217 s. Diss.

176. HUISKONEN, JANNE. Supply chain integration: studies on linking customer responsiveness and operational efficiency in logistics policy planning. 2004. 151 s. Diss.

Corrigenda (09.03.2004)

Mikko Kuisma “Minimizing Conducted RF-emissions in Switch Mode Power Supplies Using Spread-Spectrum Techniques”

- Page 112, Table 4-2 calculated with wrong parameters. Table 4-2 should be replaced by Table E-1.
- Page 141, Table 5-2 calculated with wrong parameters. Table 5-2 should be replaced by Table E-2.
- Page 143, Table 5-4 calculated with wrong parameters. Table 5-4 should be replaced by Table E-3. According to these new tables, the end of the paragraph starting with the sentence “The largest standard deviation…” should be deleted.

Table E-1. Calculated peak values of the Welch estimate of the switching function at different frequency ranges. The first row represents the peak values (in dB/Hz) of the constant frequency reference converter. Different cases are listed in different rows where peak values, attenuation to the reference converter and average attenuation (mean) are listed.

CASE ↓	Frequency band →	10 kHz - 100 kHz	101 kHz - 200 kHz	201 kHz - 300 kHz	301 kHz - 400 kHz	401 kHz - 500 kHz	501 kHz - 600 kHz	601 kHz - 700 kHz	701 kHz - 800 kHz	801 kHz - 900 kHz	901 kHz - 1 MHz
PWM reference	Peak [dB]	-29.0	-31.4	-47.4	-41.5	-47.4	-45.0	-47.4	-47.4	-47.4	-49.7
CASE 1 FM-sine	Peak [dB]	-38.0	-50.0	-59.8	-55.5	-59.2	-61.8	-68.9	-63.9	-65.9	-66.9
	Reduction [dB]	9.0	18.6	12.4	14	11.8	16.8	21.5	16.5	18.5	17.2
	Mean reduction	**15.6 dB**									
CASE 2 FM-sine + noise	Peak [dB]	-44.1	-58.4	-59.9	-64.6	-66.6	-67.7	-69.1	-69.9	-70.2	-70.5
	Reduction [dB]	15.1	27.0	12.5	23.1	19.2	22.7	21.7	22.5	22.8	20.8
	Mean reduction	**20.7 dB**									
CASE 3 FM-triangle + noise	Peak [dB]	-44.3	-58.7	-60.4	-64.3	-66.8	-68.1	-68.5	-69.7	-70.5	-71.2
	Reduction [dB]	15.3	27.3	13.0	22.8	19.4	23.1	21.1	22.3	23.1	21.5
	Mean reduction	**20.9 dB**									
CASE 4 Frequency-hopping	Peak [dB]	-40.9	-55.5	-61.1	-64.9	-65.1	-67.4	-68.7	-69.4	-70.0	-70.7
	Reduction [dB]	11.9	24.1	13.7	23.4	17.7	22.4	21.3	22.0	22.6	21.0
	Mean reduction	**20.0 dB**									
CASE 5 Chaotic Peak current	Peak [dB]	-39.1	-44.6	-50.7	-53.6	-56.0	-57.5	-58.5	-59.7	-59.9	-60.2
	Reduction [dB]	10.1	13.2	3.3	12.1	8.6	12.5	11.1	12.3	12.5	10.5
	Mean reduction	**10.6 dB**									
CASE 6 Chaotic $\Sigma\Delta$-modulation	Peak [dB]	-30.9	-38.4	-45.4	-47.1	-50.1	-50.8	-52.5	-52.8	-53.6	-53.6
	Reduction [dB]	1.9	7.0	-2.0	5.6	2.7	5.8	5.1	5.4	6.2	3.9
	Mean reduction	**4.2 dB**									

Table E-2. Calculated maximum values of the simulated input current Welch PSD at selected frequency bands. The highest value (in dB/Hz) of the PWM-reference converter in each frequency band is shown in the first row. The peak value and reduction compared to the reference at the same frequency band is listed in the following rows.

CASE ↓	Frequency band →	10 kHz - 100 kHz	101 kHz - 200 kHz	201 kHz - 300 kHz	301 kHz - 400 kHz	401 kHz - 500 kHz	501 kHz - 600 kHz	601 kHz - 700 kHz	701 kHz - 800 kHz	801 kHz - 900 kHz	901 kHz - 1 MHz
PWM reference	Peak [dB]	-31.2	-39.6	-62.1	-59.0	-67.7	-67.3	-70.4	-71.4	-71.9	-74.6
CASE 1 FM-sine	Peak [dB]	-40.7	-56.5	-73.6	-78.1	-80.9	-88.2	-88.5	-89.0	-94.7	-93.3
	Reduction [dB]	9.5	16.9	11.5	19.1	13.2	20.9	18.1	17.6	22.8	18.7
CASE 2 FM-sine + noise	Peak [dB]	-47.6	-62.5	-76.0	-82.5	-85.7	-89.7	-91.1	-93.5	-94.7	-95.3
	Reduction [dB]	16.4	22.9	13.9	23.5	18.0	22.4	20.7	22.1	22.8	20.7
CASE 3 FM-triangle + noise	Peak [dB]	-48.4	-61.8	-77.4	-81.7	-86.2	-90.2	-91.9	-93.5	-94.5	-95.1
	Reduction [dB]	17.2	22.2	15.3	22.7	18.5	22.9	21.5	22.1	22.6	20.5
CASE 4 Frequency-hopping	Peak [dB]	-46.9	-58.4	-79.5	-79.5	-85.8	-89.4	-91.0	-93.3	-93.5	-94.8
	Reduction [dB]	15.7	18.8	17.4	20.5	18.1	22.1	20.6	21.9	21.6	20.2
CASE 5 Chaotic peak current	Peak [dB]	-32.9	-52.3	-64.5	-71.5	-75.3	-78.9	-81.2	-82.8	-84.1	-84.8
	Reduction [dB]	1.7	12.7	2.4	12.5	7.6	11.6	10.8	11.4	12.2	10.2
CASE 6 Chaotic ΣΔ-modulation	Peak [dB]	-31.4	-46.4	-60.4	-63.9	-69.7	-71.3	-74.5	-75.2	-76.8	-76.9
	Reduction [dB]	0.2	6.8	-1.7	4.9	2.0	4.0	4.1	3.8	4.9	2.3

Table E-3. The average attenuation and standard deviation for each case calculated from the simulations and measurements analyzed in Tables 4-2, 5-2 and 5-3.

	Simulated *q*(*t*)		**Simulated current**		**Measured current**	
	Average Attenuation [db/Hz]	**Standard deviation [dB unit]**	**Average Attenuation [db/Hz]**	**Standard deviation [dB unit]**	**Average Attenuation [dbμA]**	**Standard deviation [dB unit]**
Case 1: FM-sin	**15.6 dB**	**3.8**	**16.8 dB**	**4.2**	**8.0 dB**	**5.0**
Case 2: FM-sin+noise	**20.7 dB**	**4.2**	**16.1 dB**	**3.2**	**10.9 dB**	**4.6**
Case 3: FM-triangle +noise	**20.9 dB**	**4.1**	**15.9 dB**	**2.6**	**11.5 dB**	**4.6**
Case 4: Frequency hopping	**20.0 dB**	**4.2**	**15.3 dB**	**2.1**	**11.6 dB**	**4.4**
Case 5: Chaotic modulation	**10.6 dB**	**10.6**	**9.2 dB**	**4.1**	**9.4 dB**	**5.1**
Case 6: ΣΔ-modulation	**4.2 dB**	**4.2**	**7.1 dB**	**2.4**	**1.1 dB**	**5.9**

- Pages 168 – 169, some parameters in the program script "*MATLAB-script for analysis of switching function q(t)*" are wrong causing erroneous results in original Tables 4-2 and 5-4. After the line "%Calculating maximum values of spectrum estimate, 10 frequency ranges" following lines should be replaced by:

```
pxx=pwelch(ScopeData(:,2),13000,6500,13000,2e6);
N=0;v=1;
dbmax(v)=max(10*log10(pxx(65:N+650)));
for v=2:10
        N=N+650;
        dbmax(v)=max(10*log10(pxx(N+1:N+650)));
end;
```

- Pages 170 – 171, some parameters in the program script "*MATLAB-script for analysis of simulated input current and output voltage*" are wrong and missing. In line 2 there is:

```
pwelch(ScopeData(:,2),13000,6500,13000,2e6);
```

It should be replaced by:

```
pwelch(I1(:,2),13000,6500,13000,2e6);
```

The following lines should be added to the end of the script to obtain correct results for Tables 5-2 and 5-4:

```
pxx=pwelch(I1(:,2),13000,6500,13000,2e6);
N=0;v=1;
dbmax(v)=max(10*log10(pxx(65:N+650)));
for v=2:10
        N=N+650;
        dbmax(v)=max(10*log10(pxx(N+1:N+650)));
end;
```